Università degli Studi di Cagliari

PhD Degree in Neuroscience

Cycle XXXII

Investigation on NAAA inhibitors, a novel class of medications that reduces nicotine reward and delays opioid tolerance.

BIO/14 Pharmacology

PhD Student:	Dr. Mauro Congiu
Coordinator of the PhD Programme	Prof. Paola Fadda
Supervisor	Prof. Marco Pistis
Co-supervisor	Dr. Anna Lisa Muntoni

Final exam. Academic Year 2018 – 2019

Thesis defence: January-February 2020 Session

1. INTRODUCTION

1.1 N-acylethanolamines: activities, targets and metabolism

N-acylethanolamines (NAEs) are ethanolamides of long-chain fatty acids and are present in both animals and plants. The most abundant NAEs in mammalian tissues are N-palmitoylethanolamine (PEA), N-oleoylethanolamine (OEA) and N-arachidonoylethanolamine (AEA) (Fig.1). They share the same basic scaffold but differ in length and unsaturation degree of the acyl chain. NAEs can bind to several different receptors and exert a plethora of biological effects.

AEA was first isolated in 1992 from porcine brain as an endogenous ligand of cannabinoid receptor and called anandamide (Devane et al., 1992). It is a partial agonist of type 1 cannabinoid receptor (CB1) while it remains much less active at the type 2 cannabinoid receptor (CB2) (Sugiura, Kishimoto, Oka, & Gokoh, 2006). Anandamide is also a ligand of vanilloid receptor (the transient receptor potential vanilloid type 1, TRPV1) (Van Der Stelt & Di Marzo, 2004) and G-protein-coupled receptor 18 (GPR18) (De Petrocellis et al., 2007; McHugh, Page, Dunn, & Bradshaw, 2012; O'Sullivan, 2016). Moreover, AEA has been reported as a peroxisome proliferator-activated receptor (PPAR) -α and -γ agonist, although studies have been carried out only through *in vitro* techniques (Sun et al., 2007). In general, AEA displays anti-inflammatory, analgesic, neuroprotective, anxiolytic, anti-depressive and cognitive effects (Iannotti, Di Marzo, & Petrosino, 2016).

PEA is known for more than 50 years (Bachur, Masek, Melmon, & Udenfriend, 1965). It was isolated from soybean lecithin, egg yolk and peanut meal and was shown to have anti-inflammatory properties (Lo Verme et al., 2005) as well as analgesic, anti-epileptic and neuroprotective actions (Mattace Raso, Russo, Calignano, & Meli, 2014; Petrosino & Di Marzo, 2017). Long after its discovery, it was revealed that PEA physiologically binds PPARα, but not PPAR-γ or -δ (Bouaboula et al., 2005; Lo Verme et al., 2005).

OEA is known for its anorectic activity in experimental animals (Serrano et al., 2011; Verme et al., 2005). Its administration leads to satiety and reduces body weight gain through the activation of PPARα (Fu et al., 2003). It is believed that OEA is produced from the digested dietary fat in the enterocytes of small intestine (Piomelli, 2003) and may be one actor mediating satiety after the intake of fatty food. Thus, OEA, its analogs or indirect agonists are considered as novel anti-obesity drugs. Binding studies demonstrated that OEA half-maximal concentration is higher for PPARβ/δ than α, being much more active on the latter, and showing no effect on PPARγ (Fu et al., 2003).

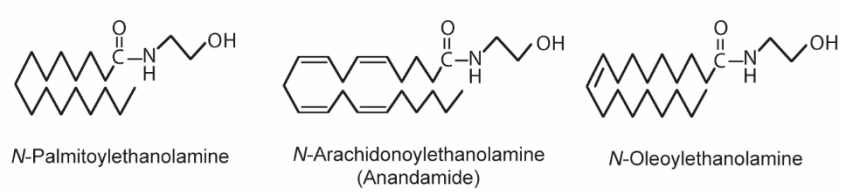

Figure 1. Structure of NAEs

Besides these well characterized NAEs, N-docosahexaenoylethanolamine (DHA) and N-eicosapentaenoylethanolamine (EPEA) were recently revealed to reduce macrophage activation and have anti-inflammatory properties *in vitro* and *in vivo* (M. Alhouayek, Bottemanne, Makriyannis, & Muccioli, 2017; Balvers et al., 2010; Meijerink et al., 2015; Park, Chen, Kevala, Lee, & Kim, 2016). These NAEs were reported to bind cannabinoid receptors, PPARs (Rovito et al., 2013) and the orphan receptor GPR110 (Lee et al., 2016).

PPARα, together with PPARγ and PPARβ/δ, form the subfamily of the peroxisome proliferator-activated receptors. PPARs function as transcription factors that, when activated by their ligand, regulate gene expression by binding to specific enhancer sites called peroxisome proliferator response elements (PPREs). Ligands allow PPAR to form heterodimers with retinoid X receptor (RXR), which recruit transcriptional coactivators leading to gene transcription. PPARγ has been shown to be involved in a wide range of events such as atherosclerotic plaque formation and stability, vascular tone, angiogenesis and inflammation. PPARβ/δ has been linked to myelinogenesis and glial cell maturation within the central nervous system (CNS) as well as embryo implantation and fertility (Berger & Moller, 2002).

PPARα is present in numerous tissues including liver, kidney, heart, skeletal muscle and brown fat (Auboeuf et al., 1997; Braissant, Foufelle, Scotto, Dauça, & Wahli, 1996). It is also present in monocytic (Chinetti et al., 1998), vascular endothelial (Inoue et al., 1998) and vascular smooth muscle cells (Staels et al., 1998). Activation of PPARα directly upregulates transcription of several enzymes involved in the peroxisomal-beta-oxidation pathway (Dreyer et al., 1992; Schoonjans, Staels, & Auwerx, 1996; Tugwood et al., 1992). Accordingly, it has been shown that PPARα plays a critical role in the regulation of cellular uptake, activation and beta-oxidation of fatty acids. Its activation induces expression of the fatty acid transport protein (FATP) (G. Martin, Schoonjans, Lefebvre, Staels, & Auwerx, 1997) and fatty acid translocase (FAT) (Motojima, Passilly, Peters, Gonzalez, & Latruffe, 1998), two proteins that transport fatty acids across the cell membrane.

PPARα has also an important role as a modulator of inflammation via multiple, distinct mechanisms (Bougarne et al., 2009; Cuzzocrea et al., 2008; Staels et al., 1998). *In vitro* and *in vivo* studies demonstrated that PPARα influences both acute and chronic inflammatory processes (Delerive et al., 1999; Delerive, Gervois, Fruchart, & Staels, 2000; Devchand et al., 1996; Paumelle et al., 2006; Pawlak

et al., 2014). At first, it was suggested that activation of PPARα inhibits the inflammatory action of eicosanoids by augmenting expression of hepatic enzymes involved in their metabolism. Then, evidence has emerged suggesting that PPARα anti-inflammatory properties involve a mechanism called trans-repression. Namely, PPARα inhibits the activity of proinflammatory mediators such as NF-kB, AP-1 and STAT, reducing the expression of proinflammatory genes (Lefebvre, Chinetti, Fruchart, & Staels, 2006). The mechanism of PPAR interference with NF-kB action involves a PPARα-mediated expression of the inhibitory protein IkBa. Moreover, PPARα activation inhibits cyclooxygenase-2 (COX-2) induction as a result of its interference with NF-kB and AP-1 signaling (Staels et al., 1998), a mechanism directly involving their interaction with p65 and c-jun, which are transcription factors involved in proinflammatory pathways.

In addition to downregulating the expression of proinflammatory genes, PPARα also suppresses the inflammatory response by direct upregulation of genes with anti-inflammatory actions. Transactivation and chromatin immunoprecipitation studies identified IL-1ra as a direct positive target gene of PPARα with a functional PPRE presents in the promoter (R. Stienstra et al., 2007). In the same setting, heme oxygenase-1, a PPARα target gene with a functional PPRE, is also directly upregulated by PPARα ligands and contributes to the anti-inflammatory effects in human vascular cells (Kronke et al., 2007).

While canonically associated with transcription regulation and gene expression control, PPARα can also act through rapid non-genomic ways that occur independently of transcriptional regulation.

Among these latter, a novel mechanism by which PPARα modulate the phosphorylation state of nicotinic acetylcholine receptors (nAChRs), and therefore their functionality, has been recently uncovered by our group (M. Melis et al., 2010; M. Melis et al., 2008; Miriam Melis & Pistis, 2014; M. Melis et al., 2013). In particular, we found that activation of PPARα by synthetic and endogenous (OEA and PEA) agonists triggers a rapid stimulation of tyrosine kinases, which in turn leads to phosphorylation and negative regulation of neuronal nAChRs. On these bases, a number of preclinical studies have been carried out to explore PPARα therapeutic potential in two disorders where nAChRs play a fundamental role, namely nicotine addiction (Mascia et al., 2011; M. Melis et al., 2010; Panlilio et al., 2012) and epilepsy (Puligheddu et al., 2013), leading to positive and very encouraging results. Notably, a clinical trial was also successfully conducted to test the efficacy of the PPARα agonist fenofibrate as adjunctive therapy in patients with nocturnal frontal lobe epilepsy (Puligheddu et al., 2017), a familial syndrome caused by several mutations in either α4 or β2 nAChR subunit genes which confer a gain of receptor function.

NAEs are produced on demand by cells, and their endogenous concentration is regulated by enzymes responsible for their metabolism. NAEs are biosynthesized starting from glycerophospholipids through distinct pathways including different steps and involving several

enzymes. A calcium-dependent N-acyltransferase (Ca-NAT) is responsible for the N-acylation of phosphatidylethanolamine (PE) generating N-acyl-PE (NAPE). Other actors mediating the formation of NAPE have been shown, such as the calcium-independent N-acyltransferase and the phospholipase A1/A2 (PLAAT) (Jin et al., 2007; Jin et al., 2009; Okamoto, Morishita, Tsuboi, Tonai, & Ueda, 2004; Uyama, Jin, Tsuboi, Tonai, & Ueda, 2009; Uyama, Morishita, et al., 2009). NAPE is then hydrolyzed to release N-acylethanolamines by a phospholipase D (PLD)-type enzyme (NAPE-PLD).

NAEs catabolism is mainly mediated by two enzymes, which differ in the selectivity of their action. Fatty acid amid hydrolase (FAAH) preferentially degrades AEA, whereas N-acylethanolamine-hydrolyzing acid amidase (NAAA) has a higher reactivity over PEA but less activity over AEA (Bonezzi et al., 2016; Petrosino et al., 2015; O. Sasso et al., 2018).

FAAH is a membrane bound serine hydrolase and it degrades NAEs by the hydrolysis to free fatty acids and ethanolamine (Cravatt et al., 1996). It is abundant in the brain and liver as the main degrading enzyme of all NAEs (Cravatt et al., 2001; Cravatt et al., 1996). On the other hand, NAAA is an enzyme localized in lysosomes that operates only at acidic pH (K. Tsuboi et al., 2007). It belongs to the cholylglycine hydrolase family and has no sequence similarity with FAAH. NAAA is present in macrophages, peripheral tissues (K. Tsuboi et al., 2007) and brain (Migliore et al., 2016). The assessment of its activity *in vitro* reveled that it has a significant preference for saturated NAEs, with PEA being the preferred substrate, although AEA and OEA can also be degraded by the enzyme (Kazuhito Tsuboi et al., 2005). Given that its substrates have been shown to be promising in various pathologic conditions, inhibition of NAAA has attracted attention as a potential innovative pharmacological strategy to augment endogenous levels of PEA (Bottemanne, Muccioli, & Alhouayek, 2018). In general, boosting the tissue bioavailability of an endogenous agonist represents a finer, safer and more effective way to activate a receptor as compared to act directly on it, since it complies with its temporal and spatial resolution. As described in the above section, principal enzymes responsible for degradation of NAEs are NAAA and FAAH. The latter has been explored as a possible therapeutic target in different investigations (Justinova et al., 2015; Luchicchi et al., 2010; Maria Scherma et al., 2008), but its clinical application is made difficult by the fact that its inhibition increases also the levels of AEA and its binding with CB1, leading to undesired side effects. In fact, given its interference with the canonical cannabinoid system, FAAA-inhibitors drugs have an abuse potential. On the contrary, NAAA does not show selectivity for AEA thus attracting the interest of the researchers. Different NAAA blockers have been developed and were mainly tested against inflammation, immune disorders and pain (Mireille Alhouayek et al., 2014; Bottemanne et al., 2018). It is important to point out that inhibition of NAAA can increase other NAE, typically OEA, depending on the animal model and tissue (Bottemanne et al., 2018). *In vitro*, NAAA inhibitors have been tested onto macrophages, inflammatory cells highly expressing NAAA. For example, the compound AM9053 showed efficacy on increasing the

levels of PEA and decreasing the expression of proinflammatory markers (M. Alhouayek et al., 2017; Li et al., 2012; Solorzano et al., 2009), but it also increased the levels of other NAEs (M. Alhouayek et al., 2017). On the other hand, the inhibitor called (S)-OOPP had no effect on AEA levels *in vitro* (Solorzano et al., 2009). *In vivo*, NAAA inhibitors have been also successfully tested in different disease models with an inflammatory component. For instance, AM9053 intraperitoneally administered to mice increased PEA levels in the colon and extensively decreased colon inflammation (Mireille Alhouayek et al., 2014). Interestingly, in several studies, these inhibitors were not effective in PPARα -/- mice, suggesting that the inhibition of NAAA was mediated by a NAE, probably PEA, acting on PPARα (Fiasella et al., 2014; O. Sasso et al., 2018; Solorzano et al., 2009). NAAA inhibitors were also assessed in a murine model of multiple sclerosis, a neurodegenerative disease with an important inflammatory component, leading to positive results. Indeed, a benzothiazole-piperazine derivative compound developed by Piomelli and co-workers, increased PEA and OEA levels in mouse brain, delayed disease onset and reduced symptoms in experimental autoimmune encephalomyelitis (Migliore et al., 2016). Moreover, given that PEA is known to have analgesic properties, NAAA inhibitors were assessed in several models of inflammatory or neuropathic pain. The compound called ARN077 applied topically reduced hyperalgesia in the carrageenan-induced model of inflammatory pain as well as mechanical allodynia in the chronic nerve ligation model of neuropathic pain in mice (O. Sasso et al., 2018). Notably, the effects were absent in PPARα -/- mice (Bonezzi et al., 2016; Yang et al., 2015). Other NAAA inhibitors were also tested in the same settings: intraperitoneal administration of diacerein increased PEA levels and decreased carrageenan-induced hyperalgesia (Petrosino et al., 2015), whereas ARN726 increased PEA and OEA levels and decreased paw edema and hyperalgesia induced by complete Freund's adjuvant (CFA) injection in the rat paw (Bonezzi et al., 2016).

Since NAAA has several substrates that activate different receptors, understanding how NAAA inhibition exerts its actions needs the quantification of its substrates in the specific model studied. In fact, NAAA inhibition in the same setting could have different effects on NAE levels (M. Alhouayek et al., 2017; Sun et al., 2005). However, limited amounts of data are available regarding this aspect, because most studies with NAAA inhibitors only report PEA levels, and sometimes OEA, but not the levels of the other NAEs. This happens because NAAA is classically considered as preferentially hydrolyzing PEA over other NAEs. However, in macrophages in culture NAAA inhibition has more effect on AEA levels than PEA levels, whereas the opposite is true for FAAH (M. Alhouayek et al., 2017; Sun et al., 2005). On the other hand, the situation is different *in vivo*. Indeed, studies reported that NAAA inhibition influenced the levels of PEA and occasionally OEA, but never AEA (Mireille Alhouayek et al., 2014; O. Sasso et al., 2018; Oscar Sasso et al., 2018; Solorzano et al., 2009). Thus, it is crucial to take into account that levels of NAEs and the expression of their metabolic enzymes can be altered depending on the tissue or the pathology considered.

To date, the studies outlined here suggest that NAAA could be an innovative potential therapeutic target especially in nicotine addiction, pain treatment and, more generally, in diseases with an inflammatory component.

1.2 N-acylethanolamines and nicotine addiction

Tobacco use and dependence is a global epidemic and it is the largest preventable cause of mortality and morbidity around the world. Globally, tobacco use causes nearly 6 million deaths per year, and it is predicted to reach 8 million deaths by 2030 (WHO, 2011). In chronic smokers, severe types of cancer (lungs, mouth, etc.), cardiovascular disease and respiratory problems (DHHS, 2014) have been reported. Pharmacotherapies for nicotine dependence can enhance quitting rates by about two–three-fold (Fiore et al., 2008). However, it is still very difficult for smokers to achieve permanent smoking cessation. For example, during 2015, 66.7 percent of male smokers were interested in quitting and 55.3 percent had made an attempt in that year but only 7.2 percent succeeded (Babb, 2017). Thus, considering that currently approved therapies increase the chance of remaining abstinent but lack high levels of efficacy and are associated with significant adverse side effects, there is a compelling unmet need for more effective antismoking medications.

Our group has discovered that NAEs might play a significant role in this context (Melis et al. 2013). In fact, NAEs are important regulators of neuronal nAChRs expressed in a brain structure which is centrally involved in addiction: the midbrain ventral tegmental area (VTA). The VTA contains cell bodies of dopamine (DA)-containing neurons densely projecting to both subcortical and cortical limbic regions (e.g. nucleus accumbens, amygdala, prefrontal cortex, hippocampus). Defined as the mesocorticolimbic dopamine system, these neurons are critically implicated in brain mechanisms of reward, reinforcement, and motivation (Solinas et al. 2019). As it will be more extensively described later, nAChRs are key modulators of dopaminergic neuronal activity and their activation within the VTA by nicotine ultimately leads to nicotine addiction (Benowitz 2010).

1.2.1 Drug addiction

In the past two decades, research advances have progressively sustained the idea of addiction as a brain disease (Volkow, Koob, & McLellan, 2016). In particular, addiction can be defined as a chronic, relapsing disorder of the brain reward and motivational system (American Society of Addiction Medicine, ASAM, 2011). Dysfunction in these pathways leads to a behavioral pathology characterized by compulsive drug seeking and use with progressive loss of control over consumption in spite of the emergence of significant negative or detrimental consequences (Volkow et al., 2016). In the fifth edition of the Diagnostic and Statistical Manual of Mental Disorders (DSM-5) (2013), the term addiction is synonymous with the most severe stage of substance use disorder (Volkow et al., 2016).

The development of drug addiction is a process characterized by a switch on the goal that drives drug consumption. In fact, the initial positive reinforcement is gradually substituted by a

negative reinforcement that is aimed to avoid the appearance of the withdrawal syndrome symptoms (Koob, 2004). The transition from the occasional use to drug addiction is determined by the instauration of plasticity that can begin from the very first drug consumption (Koob & Volkow, 2010). The initial common action of all addictive drugs is hypothesized to be an increased dopaminergic signaling from the midbrain VTA to the nucleus accumbens (NAc) (Lüscher & Ungless, 2006), two main components of the brain reward system. The resultant effect is a strong reinforcement which shapes behavior and leads to compulsive consumption in some individuals. This 'dopaminergic' hypothesis is based on direct measures of extracellular DA levels in the NAc (Di Chiara & Imperato, 1988) and on the observation that electrical activation of the medial forebrain bundle (which includes VTA-to-NAc axons) (Olds & Milner, 1954), or optogenetic excitation of VTA DA neurons in mice and rats (Ilango, Shumake, Wetzel, & Ohl, 2014; Pascoli, Terrier, Hiver, & Luscher, 2015; Witten et al., 2011), drive reinforcement. The activation of the brain reward system by drugs of abuse produces a wide array of short and long-term modifications (Koob & Volkow, 2010), ultimately leading to the development of addiction.

It is widely accepted that brain circuits that are responsible for natural (i.e. food, maternal behavior, social interaction, etc.) and non-natural rewards (i.e. drugs of abuse, gambling, etc.) primarily involve areas of the limbic system interconnected with each other, such as amygdala, dorsal and ventral striatum, hippocampus, limbic cortices (e.g. prefrontal cortex, PFC). Importantly, all these structures are strictly connected with VTA. DA neurons of VTA receive inputs from various regions representing the central relay of the reward system that plays a fundamental role in the valence, learning and motivated behaviors. VTA DA neurons massively project to the NAc but, importantly, they project also to PFC, amygdala and hippocampus (Beier et al., 2015; Björklund & Dunnett, 2007). These neurons can be considered as a crucial hub among regions that are important for sensorial, cognitive and motor information. *In vivo*, their firing rate and discharge pattern depend upon the balance between excitatory and inhibitory inputs, interacting with their intrinsic properties (Lobb, Wilson, & Paladini, 2010; Morikawa & Paladini, 2011). Bed nucleus of the stria terminalis (BNST) and PFC are two important areas releasing glutamate onto DA neurons. Pedunculus pontine nuclei and laterodorsal tegmental nucleus release acetylcholine together with glutamate (Marinelli, Rudick, Hu, White, & Disorders, 2006). GABAergic inputs come from interneurons (Bayer & Pickel, 1991; Anthony A Grace & Onn, 1989; Omelchenko & Sesack, 2009), basal ganglia (Marinelli et al., 2006; Morikawa & Paladini, 2011; Omelchenko & Sesack, 2009; Sesack & Grace, 2010) and from the rostromedial-tegmental nucleus (RMTg) (Jhou, Fields, Baxter, Saper, & Holland, 2009; Kaufling, Veinante, Pawlowski, Freund-Mercier, & Barrot, 2009; Lecca et al., 2011; Lecca, Melis, Luchicchi, Muntoni, & Pistis, 2012). *In vivo*, VTA DA neurons present different type of pattern discharge: regular, irregular (both characterized by action potentials that are fired singularly and temporally organized in a regular or irregular way) and

bursting (action potentials fired in trains). These different patterns are differently related to DA release in terminal areas (Floresco, West, Ash, Moore, & Grace, 2003). In fact, while phasic release of DA depends on bursting activity of the neurons (A. A. Grace, Floresco, Goto, & Lodge, 2007; Anthony A Grace & Onn, 1989), tonic release is dependent by tonic changes and by the number of cells spontaneously active in the VTA (Floresco et al., 2003). Burst firing or "phasic" activity is crucially dependent on afferent input (A. Grace & Bunney, 1984; Anthony A Grace & Onn, 1989) and is believed to be the functionally relevant signal sent to postsynaptic sites to indicate reward and modulate goal-directed behavior (K. C. Berridge & Robinson, 1998; Schultz, 1998).

1.2.2 Neurobiological basis of nicotine addiction: role of NAEs and PPARα

Inhalation of smoke from cigarettes distills nicotine from the tobacco. Smoke particles carry nicotine into the lungs, where it is rapidly absorbed into the pulmonary venous circulation. Then, nicotine enters the arterial circulation and quickly reaches the brain, where it binds nAChRs to produce its initial effects. In the CNS, nAChRs form ligand-gated ion channels in the plasma membranes of neurons and are made up of five subunits, organized symmetrically around a central pore (Itier & Bertrand, 2001). The neuronal subtypes are formed by various homomeric or heteromeric combinations of twelve different subunits: α2-α10 and β2-β4. Examples of the neuronal subtypes include the homomeric $(\alpha7)_5$ and the heteromeric $(\alpha4)_3(\beta2)_2$, $(\alpha4)_2(\beta2)_3$. While homomeric nAChRs show less affinity for agonists than those containing α4β2 subunits, they desensitize more rapidly (Changeux, 2010). The activation of nAChRs modifies neuronal state through two main mechanisms. First, the net flow of positively-charged ion depolarizes the membrane, resulting in an excitatory postsynaptic potential, and activates voltage-gated ion channels. Secondly, calcium entry acts either directly or indirectly on discrete intracellular cascades with consequent regulation of the activity of some genes and/or the release of neurotransmitters.

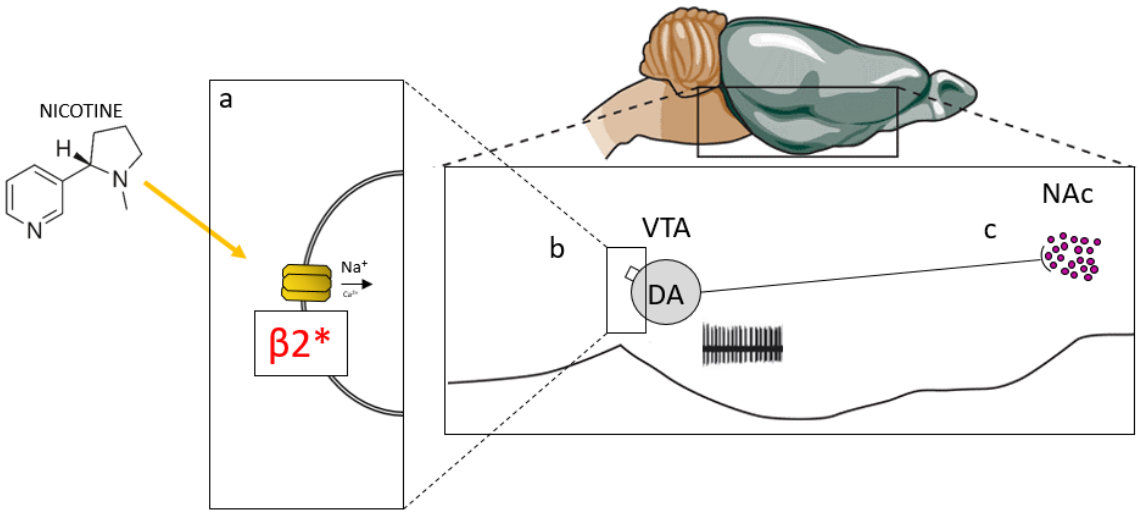

Figure 2. Hypothesized mechanism of action underlying nicotine rewarding properties. a) Nicotine binds nAChRs inducing a Na^+ and Ca^{2+} inward flow and depolarizing VTA DA cells; b) DA neurons projecting from the VTA to the NAc increase their firing rate and bursting activity; c) dopaminergic terminals in the NAc release a large amount of DA, responsible for the reinforcing properties of nicotine.

With regard to addiction, it is theorized that nicotine mainly exerts its reinforcing properties via nAChRs located in the VTA, which trigger an increase of DA levels in the NAc (Benowitz, 2010; Di Chiara & Imperato, 1988) (see Figure 2). In fact, a well-accepted hypothesis, confirmed also by studies in genetically modified mice, postulates a central function of β2- and α7-containing nAChRs in the modulation of nicotine reinforcing effects. In particular, the β2 subunit is considered as the subunit mainly involved in the neuron switching from a resting to an excited state, and the α7 as a fine regulator of the excited state after β2-containing receptors activation (Mameli-Engvall et al., 2006). Moreover, VTA DA neurons do not respond to nicotine injection (Picciotto et al., 1998) in genetically β2 ablated mice.

Our group discovered that α4β2-containing nAChRs are negatively regulated by PPARα receptors in VTA DA neurons (see Figure 3). In fact, as already mentioned, PPARα activation by both synthetic (i.e. WY14643) and endogenous (PEA, OEA) ligands rapidly leads to increased hydrogen peroxide production and consequent activation of tyrosine kinase(s) (M. Melis et al., 2010; M. Melis et al., 2008). In turn, these latter phosphorylate β2-containing nAChRs subunits on a tyrosine residue, inducing a reduction in functionality of these receptors (M. Melis et al., 2013). Hence, PPARα activation can prevent nicotine-induced neuronal responses. Moreover, direct activation of α7-nAChRs enhances intracellular NAE levels and prevents nicotine-induced effects on DA neuronal activity via phosphorylation of β2*nAChRs (M. Melis et al., 2013), thus mimicking the effects produced by PPARα agonists (Mascia et al., 2011; M. Melis et al., 2008; Panlilio et al., 2012).

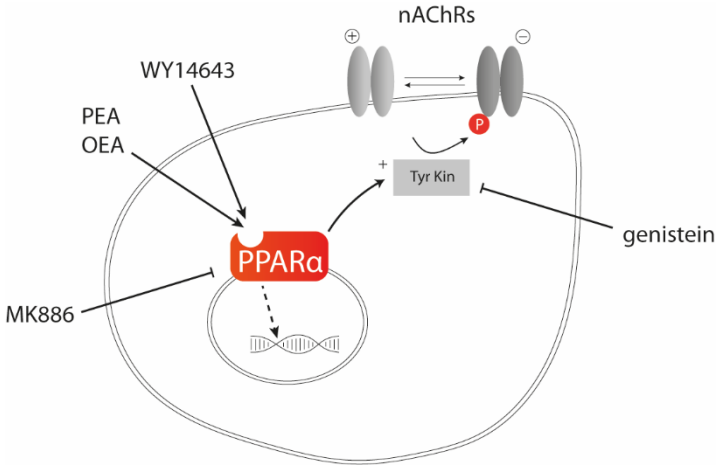

Figure 3. Schematic diagram illustrating the proposed mechanism of PPARα activation, and modulation of responses of DA neurons to nicotine, by the endogenous NAE OEA and PEA. Their action is mimicked by the synthetic PPARα agonist WY14643 and blocked by the PPARα antagonist MK886. It is proposed that activated PPARα stimulate the activity of tyrosine kinases (Tyr Kin) through a non-genomic mechanism. Tyrosine kinases, in turn, induce the phosphorylation (P) of nAChRs, which reduces their responses to agonists, or promotes rapid internalization. Genistein, a general tyrosine kinase inhibitor, blocks the effects of PPARα activation. ↑ activation; ⊥ inhibition (M. Melis et al., 2008).

On these bases, different strategies were adopted to take advantage of this mechanism in the context of potential treatments of nicotine addiction. Synthetic ligands of PPARα (e.g. fenofibrate), structurally-modified NAEs, or inhibitors of their degradation enzyme such as FAAH inhibitors, were utilized as pharmacological tools to modulate NAE/PPARα signaling and ultimately reduce the sensitivity of nAChRs to nicotine. PPARα agonists like WY14643 and methOEA (a long-lasting form of OEA) were tested in rats and monkeys and revealed the promising ability to counteract the electrophysiological, neurochemical, as well as behavioral effects of nicotine (Mascia et al., 2011). A following study employed synthetic PPARα ligands such as fibrates, which are lipid lowering medications long approved for human use. Fibrates prevented nicotine-induced electrophysiological and neurochemical effects responsible of nicotine acute rewarding properties (Panlilio et al., 2012). Moreover, fibrates decrease nicotine intake in rats and primates, and prevent reinstatement of nicotine seeking after a period of prolonged abstinence (Panlilio et al., 2012). In a similar setting, also FAAH inhibitors URB694 and URB597 successfully reduced nicotine rewarding properties and blocked nicotine reinstatement in squirrel monkeys (Justinova et al., 2015).

Thus, targeting PPARα represents a promising therapeutic approach in nicotine relapse prevention in humans and, ultimately, in nicotine cessation therapy. However, the bioactive lipids PEA and OEA are not suitable for drug development due to their lipophilic nature, which limits their solubility and bioavailability when given orally, while synthetic PPARα agonists did not show efficacy in preliminary clinical trials. On the other hand, the approach to inhibit NAE degrading enzymes represents a much finer strategy to activate PPARα via its physiological ligands. Importantly, pharmacological development and application of FAAH inhibitors has been slowed down by the fact that these drugs also increase AEA levels and therefore have potential for abuse. An alternative way would be to develop drugs to selectively target PPARα with PEA through inhibition of its key degrading enzyme: NAAA.

1.3 N-acylethanolamines and morphine analgesic effects

Opioids are the most effective drugs when considering the management of chronic pain. However, in the last years, opioid prescription increased exponentially, especially in the United States, and this has resulted in serious public health problems, such as diversion, overdose and addiction. Most notable are the fatalities from prescription opioid overdoses, which quadrupled between 1999 and 2015 in the United States from 2.2 to 9.3 deaths over 100,000 population (Fig.4) (Rudd, 2016; Skolnick, 2018).

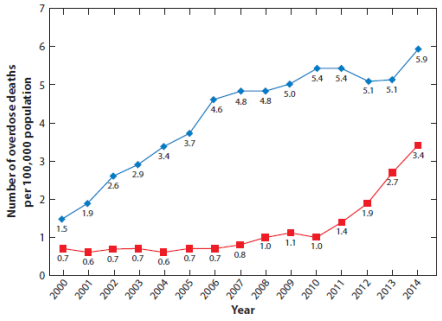

Figure 4. Age-adjusted rates of death related to prescription opioids (blue diamonds) and heroin drug poisoning (red squares) in the United States, 2000-2014 (Skolnick, 2018).

Besides dependence, one of the major problems of opioid use is the development of tolerance, a phenomenon consisting of a reduce effectiveness of drug following its repeated use. Consequently, the dosage needs to be increased leading to the exacerbation of drug side effects, such as constipation, addiction and respiratory depression, which undergo different degrees of tolerance. Lately, the scientific community is focusing on finding a strategy to counteract opioid tolerance. The mechanisms that underlies the development of opioid tolerance are diverse and extensively studied and involve receptor desensitization, phosphorylation, uncoupling with intracellular effectors and recycling (John T Williams et al., 2013). Intriguingly, among other mechanisms that are responsible for tolerance to opioids, their properties to activate microglia and mast cells has attracted attention. Indeed, exposure to opioids causes activation of these non-neuronal immune cell populations, thus contributing to an exacerbation of pro-inflammatory and pro-nociceptive processes and promoting, in the long-term, opioid-induced hyperalgesia and tolerance (Varrassi et al., 2018). Different groups have proposed to co-administer non-steroidal anti-inflammatory drugs or other molecules with anti-inflammatory properties and this approach revealed promising effects (Varrassi et al., 2018). Among these molecules, a growing body of preclinical studies demonstrates the ability of PEA to reduce inflammation and pain induced by various acute stimuli (Varrassi et al., 2018). Moreover, PEA could be a promising candidate also for minimizing the risks of chronic treatment with opioids mediated by activation of non-neuronal cells (Di Cesare Mannelli, Corti, Micheli, Zanardelli, & Ghelardini, 2015) (see next sections).

1.3.1 Pain

The International Association for the Study of Pain's defines pain as "an unpleasant sensory and emotional experience associated with actual or potential tissue damage or described in terms of such damage" (Bonica, 1979). Pain is the resultant of:

i) a perception component, defined as nociception, which is the neurobiological substrate of pain allowing the carriage of the harmful stimulus until the SNC;

ii) the experience, which is the psychic and emotional unpleasant internal state.

Acute pain is carried by fibers called nociceptors that constantly monitor the external environment. These neurons respond fast to mechanical, thermal and chemical stimuli, which have enough intensity to cause tissue damage. There are two principal type of fibers delivering noxious information: Aδ-fibers and C-fibers. The first ones are myelinic with high speed of conduction (20 m/s), and allow the perception of the noxious sensation immediately and precisely localized; the latter type of fibers are amyelinic with a slow conduction speed (2 m/s), and carry a less localized pain (Raja, Meyer, Ringkamp, & Campbell, 1999).

Afferent nociceptive fibers reach the dorsal horns (DH) of the spinal cord and connect with second order sensitive neurons, whose somas are located in the substantia gelatinosa (SG). These neurons form the lateral and anterior spinotalamic tracts, which finish in the reticular formation of the brainstem and in the thalamus. Thalamic afferents reach then the ventrobasal nucleus; here, third order neurons project to the somatosensory cortex, where the consciousness of the pain sensation takes place (Schnitzler & Ploner, 2000). Pain perception is the result of the combination of the centripetal impulses into the afferent fibers with the centrifuge impulses that go into the opposite way and negatively control nociceptive afferents (Fig. 5). These descending pathways integrate sensitive, cognitive, emotive and motivational information with the nociceptive afferents (Gebhart, 2004). One of the most important descending centers is the periaqueductal grey (PAG) of the mesencephalon. PAG receives afferents from hippocampus, cortex and thalamus and projects its axons to the rostral ventromedial medulla (RVM). This nucleus sends serotoninergic projections to the spinal cord, where serotonin modulates inhibitory interneurons in the SG. The serotoninergic system, together with the endogenous opioid system and the noradrenergic system, play a pivotal role in descending pain modulation (Fiorino & Garcia-Guzman, 2012; Guimaraes, Guimaraes, & Prado, 2000).

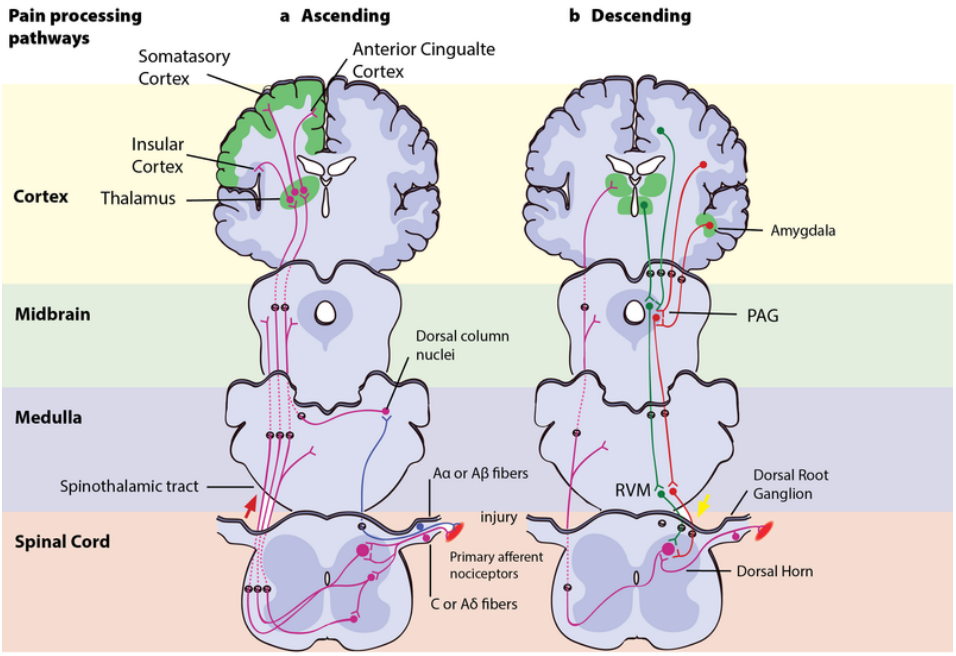

Figure 5. ***Pain processing pathways***

Left (a) - Ascending pain pathways: the C-pain and Aδ-fibers send pain information from nociceptors in the tissue or skin and transmit these signals to second order neurons in the dorsal horn (DH) of the spinal cord. The second order neurons then cross over to the opposite side, where they form the ascending spinothalamic tract. This tract projects signals to nuclei in the medulla and midbrain on the way up to the thalamus. The thalamus relays the information to the somatosensory and insular cortex, as well as cortical regions mediating different aspects of the pain experience such as affective responses in the cingulate cortex.
Right (b) - Descending pain modulation pathways: information from the environment and certain motivational states can activate this top–down pathway. Several areas in the limbic forebrain including the anterior cingulate and insular cortex, nuclei in the amygdala and the hypothalamus, project to the PAG, which then modulates ascending pain transmission from the afferent pain system indirectly through the RVM in the brainstem. This modulating system produces analgesia by the release of endogenous opioids and uses ON- and OFF-cells to exert either inhibitory (green) or facilitatory (red) control of nociceptive signals at the spinal DH (Loseth et al. 2019).

1.3.2 The locus coeruleus: a key structure where pain and opioids intersect

The noradrenergic system is crucial for several important functions in the body, including arousal, cognition, emotion, sensory and pain processing (Aston-Jones & Cohen, 2005; Llorca-Torralba, Borges, Neto, Mico, & Berrocoso, 2016; Pertovaara, 2013). Accordingly, disruption of noradrenaline (NE)-mediated signaling is associated with several psychiatric and neurological disorders in humans, emphasizing the clinical importance of this neuromodulatory system (C. W. Berridge & Waterhouse, 2003). As the major source of NE in the CNS, the Locus Coeruleus (LC) is a brainstem pontine nucleus that has been studied in numerous pain conditions, mostly due to its strategic location and network. In fact, beside from a well-known descending LC-spinal pathway which is critical for pain control, an ascending pathway passing through this structure appears to be responsible for the noradrenergic inputs to higher centers of the pain processing, such as the limbic system and frontal cortices (Fig. 6) (Llorca-Torralba et al., 2016).

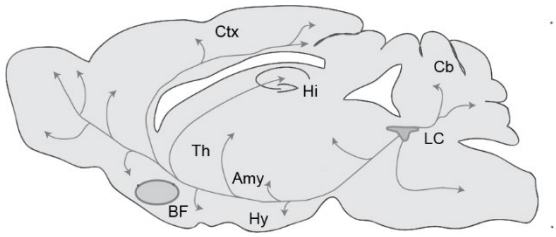

Figure 6. ***Locus coeruleus output connectivity.*** *LC: Locus coeruleus; Cb: Cerebellum; Hy: Hypothalamus; Amy: Amygdala; Th: Thalamus; Ctx: cortex; BF: Basal Forebrain.*

In addition, neurons of the LC receive a wide variety of afferent inputs from several sources. Forebrain afferents include, among others, glutamatergic inputs from the prefrontal and anterior cingulate cortices (Arnsten & Goldman-Rakic, 1984), amygdala (Pammer, Gorcs, & Palkovits, 1990) and posterior lateral hypothalamus (Downs et al., 2007). The LC also receives excitatory inputs from the C1 area of the RVM (Holloway et al., 2013) and is strongly interconnected with the dorsal raphe nucleus (Kim, Lee, Lee, & Waterhouse, 2004). Importantly, Lamina I of the DH provides nociceptive inputs to the LC (Westlund & Craig, 1996). Thus, the LC-NE system is well-positioned to affect different components of the pain experience and, accordingly, its modulation has different behavioral outcomes (Llorca-Torralba et al., 2016). For instance, NE ability to interfere with the cognitive-evaluative and the motivational-affective components of pain via LC ascending projections is recognized (Benarroch, 2018), as well as the therapeutic efficacy of pain relief medications that target the noradrenergic system (Obata, 2017). On the other hand, it should be pointed out that there are also some contradictions concerning the role of NA brain centers on nociception (Taylor & Westlund, 2017), with different studies indicating that the LC might have a minimal, or nonetheless unclear, impact in modulating both acute and chronic pain (Chandler et al., 2019; Llorca-Torralba et al., 2016; Pertovaara, 2013).

Historically, the LC-NE system has been implicated mainly in sensory processing and arousal (Aston-Jones & Cohen, 2005). In the early 80's, a seminal paper by Aston-Jones and Bloom (1981) showed that the LC-NE neuronal activity was positively correlated to the state of arousal: LC cells were most active during waking, while were silent during REM sleep (Aston-Jones & Bloom, 1981). This view was further supported by the consistent observation that highly salient and arousing stimuli cause a phasic activation of LC neurons (Aston-Jones & Bloom 1981b, Grant et al. 1988, Herve-Minvielle & Sara 1995, Rasmussen et al. 1986) and concomitant NE release in sensory brain areas (Abercrombie et al. 1988, Brun et al. 1993). In addition, selective LC stimulation triggers cortical arousal and, conversely, selective inhibition prevents cortical activation by stressors, thus corroborating the idea that this circuit plays a key role in the regulation of cortical arousal in response to stressors and other salient stimuli, such as nociceptive stimuli (C. W. Berridge & Foote, 1991; Page, Berridge, Foote, & Valentino, 1993). Importantly, the corticotropin-releasing factor (CRF) mediates stress-induced LC neuronal excitation, and endogenous opioids exert an opposite effect that probably serves to blunt excessive activation

and foster recovery after stress termination (Van Bockstaele, Reyes, & Valentino, 2010). Accordingly, acute administration of exogenous opioids, such as morphine, reduces the spontaneous activity of LC neurons (Torrecilla et al., 2002; J. T. Williams, Egan, & North, 1982), whereas repeated exposure leads, upon abrupt suspension, to an hyperactivity of LC NE neurons which greatly contributes to opioid withdrawal syndrome both in animals and humans (R Maldonado & Koob, 1993; Nestler, Alreja, & Aghajanian, 1994) and hyperalgesia (Alba-Delgado, Mico, Sánchez-Blázquez, & Berrocoso, 2012; M. Tsuruoka & W. D. Willis, Jr., 1996; M. Tsuruoka & W. D. J. B. r. Willis, 1996). Opioid tolerance is also postulated to increase stress-induced activation of the LC-NE system and promote drug seeking in order to 'calm down' the excessive neuronal response (Valentino & Volkow, 2019).

LC NE neurons consistently respond to noxious stimuli, such as paw pinch and foot-shock (FS) even in anesthetized animals (Alba-Delgado et al., 2012; Hirata & Aston-Jones, 1994), and this response represents a qualitative fingerprint of these cells (Cedarbaum & Aghajanian, 1977; Hirata & Aston-Jones, 1994; Muntoni et al., 2006). Electrophysiological studies carried out by Hirata and Aston-Jones (1994) have analyzed deeper the LC neuron response to FS, its origin and pharmacology. First, they showed a previously undescribed long-latency response, also called late response, which results from activation of nociceptive C-fibers in the sciatic nerve (Hirata and Aston-Jones 1994). Next, the same authors demonstrated that the LC response to FS, namely only the late phase, can be negatively modulated by an analgesic dose of morphine (Hirata & Aston-Jones, 1996). This last observation was not surprising considering that the LC was already known to be sensitive to both endogenous and exogenous opioids (Korf, Bunney, & Aghajanian, 1974; Pepper & Henderson, 1980). Thus, this nucleus seems to represent an ideal experimental target to explore the neurophysiological correlate of morphine antinociceptive properties and tolerance.

1.3.2 Opioid analgesia: the good and the bad side

Analgesic treatments aim to target different levels of the complex neural processes underlying pain (Fig. 7) (Schim & Stang, 2004). For instance, they can be used to inhibit the activity of afferent primary neurons or to hinder the transmission of painful stimuli in the spinal cord, to facilitate descending inhibitory pathways or to reduce inflammation of damaged tissues. Different aspects of pain perception, i.e. sensory and affective components, also explain why there is not just one single target structure for effective therapeutic approaches to pain. The most effective class of drugs available against pain is represented by opioids. However, while they are efficient in acute settings, their prolonged use is hindered because of a fast development of tolerance. One strategy to overcome the problem of prolonged opioid use may be the addition of another agent that effectively either reduces the development of tolerance or potentiates the drug efficacy, thus allowing the use of lower doses of opioids (Varrassi et al., 2018; Varrassi et al., 2017).

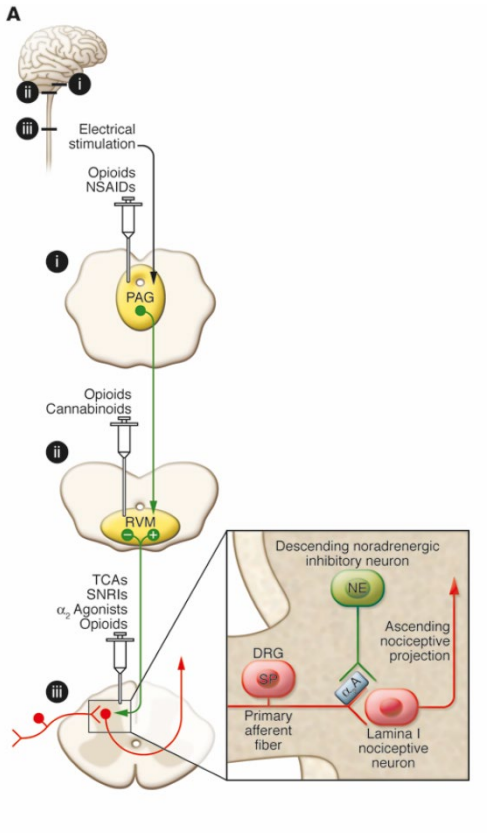

*Figure 7**. Schematic representation of bulbospinal pain inhibition and potential targets of analgesic activity**. (A) Descending pain inhibition from the PAG can be initiated by electrical stimulation or direct microinjection of opioids and nonsteroidal anti-inflammatory drug (NSAIDs). Opioids and cannabinoids inhibit pain by enhancing the baseline firing rate of OFF-cells and eliminating the OFF-cell pause in response to nociceptive stimuli. Inhibition of ON-cell activity may abolish enhanced pain states. The ON-cells and OFF-cells might correlate with pain facilitatory and inhibitory neurons in the RVM, respectively. At the level of the spinal cord, opioids can inhibit transmitter release from primary afferent terminals as well as activity of pain transmission neurons. NA release also inhibits pain transmission. Tricyclic antidepressants (TCAs) and other NE reuptake inhibitors enhance the antinociceptive effect of opioids by increasing the availability of spinal NE (box). Areas labeled "i–iii" in the small diagram correspond with labeled details of the larger diagram. α2A, α2-adrenergic receptor; DRG, dorsal root ganglion; SNRI, serotonin/NE reuptake inhibitor; SP, substance P (Ossipov, Dussor, & Porreca, 2010).*

The class of analgesic opioids includes 'weak' agonists (e.g. codein and tramadol) as well as 'strong' agonists (e.g. morphine and oxicodon). Opioids act through the interaction with opioid receptors μ, k and δ and relieve pain mainly by activating descending inhibitory circuits. The μ-opioid receptor (MOR) is the principal responsible for opioid-induced antinociception (Bobeck, McNeal, & Morgan, 2009; Fairbanks & Wilcox, 1997; Fang, Haws, Drasner, Williamson, & Fields, 1989; Morgan, Fossum, Levine, & Ingram, 2006; Tortorici, Morgan, & Vanegas, 2001). It is a G-protein coupled receptor that combines to inhibitory heterotrimeric G-proteins ($G_{i/o}$) leading to subsequent intracellular signaling and ion conductance (Gintzler & Chakrabarti, 2004; Goode & Raffa, 1997; Lueptow, Fakira, & Bobeck, 2018). MOR receptor are extensively expressed throughout the brain including areas involved in pain processing and descending nociception modulation (Mansour et al. 1995). Direct activation of the MOR results in the G_{α} subunit-mediated inhibition of the AC-cyclic adenosine monophosphate (cAMP)-protein kinase A (PKA) pathway (Guitart & Nestler, 1989; Hirst & Lambert, 1995; Sharma, Nirenberg, & Klee, 1975). In addition, $G_{\beta/\gamma}$ determines neuronal hyperpolarization through G protein-coupled inwardly-rectifying potassium (GIRK) channel. Opioid binding activates other signaling proteins, such as protein kinase C (PKC) and extracellular signal-regulated kinase 1 and 2 (ERK1/2) via β-arrestin pathways, which are independent of G-protein signaling. GABAergic neurons within the periaqueductal gray (PAG) are a critical site of action by opioids. Under normal conditions, these neurons have tonic activity but, upon binding of opioids to MOR, the activity of these neurons is

decreased, thus disinhibiting PAG projections to the RVM (Bobeck, Chen, Morgan, & Ingram, 2014; Stiller, Bergquist, Beck, Ekman, & Brodin, 1996; Vaughan, Ingram, Connor, & Christie, 1997). Recent studies support the hypothesis that this increase in PAG output to the RVM is a main contributor to the opioid-induced antinociception by demonstrating that either selective inhibition of GABAergic neurons, or activation of glutamatergic output neurons in the PAG, mimic the antinociceptive effects of opioids (Samineni et al., 2017).

An important feature of all opioids is that both the direct physical and perceptual effects of an initial administration diminish considerably with repeated administrations, resulting in tolerance, physical dependence, addiction, and hyperalgesia (Vokow et al. 2018). The underlying mechanisms of these adverse phenomena are not completely dissected but involve molecular- and circuit-level adaptations as well as counter-adaptations in opioid receptors and their intracellular signaling cascades (Roeckel, Le Coz, Gaveriaux-Ruff, & Simonin, 2016). Some of these unfavorable effects develop gradually, but some can emerge even after a few administrations (Kornetsky & Bain, 1968). Tolerance, physical dependence, and hyperalgesia in general resolve relatively rapidly after opioid discontinuation (Cortazzo, Copenhaver, & Fishman, 2013), while addiction does not resolve promptly. Importantly, tolerance to opioids does not develop to the same extent or at the same rate across all physiological responses. In particular, tolerance to analgesia and reward develops faster than tolerance to respiratory depression (Hill et al., 2016; Ling, Paul, Simantov, & Pasternak, 1989). This fact makes management of pain with opioids particularly challenging because the dose escalation necessary to maintain analgesic efficacy can increase the risk of overdose and, potentially, also the risk of addiction. Repeated exposure to opioids also results in the development of physical dependence, which it manifests as the emergence of withdrawal symptoms (e.g. insomnia, cramps, diarrhea, nausea, vomiting, aches, dysphoria, anxiety, irritability, etc.) upon abrupt discontinuation of the opioid analgesic. Moreover, chronic exposure to opioid analgesics can, in susceptible individuals, result in heightened pain sensitivity (hyperalgesia) (Arout, Edens, Petrakis, & Sofuoglu, 2015), which can lead to inappropriate increases in opioid doses that further exacerbate the pain.

Tolerance represents a significant impediment for adequate pain relief in approximately 60% of patients (Gulur, Williams, Chaudhary, Koury, & Jaff, 2014). However, the complex mechanisms causing the development of opioid tolerance are not completely elucidated, and the role of inflammation has been largely disregarded until relatively recently (Eidson & Murphy, 2019). One of the first and most studied mechanisms responsible for opioid tolerance involves regulation and signaling at the MOR (Mao, Price, & Mayer, 1995). Current research is further supporting the idea of MOR as key molecular player in the occurrence of antinociceptive tolerance. Indeed, several studies have demonstrated that tolerance greatly depends upon MOR desensitization and downregulation (Fig. 8) (Dang & Christie, 2012; John T Williams et al., 2013). In particular, the activated receptor first binds G_{α} and $G_{\beta/\delta}$ proteins

and subsequently is phosphorylated by G protein-coupled receptor kinases (GRKs). The phosphorylation uncouples the receptor from the G-proteins and allows the binding to β-arrestins. MOR is then internalized in vesicles, dephosphorylated and in part recycled. Importantly, morphine-activated MORs do not promote internalization, thus impairing the resensitization process. This is believed to be one of the reasons why morphine produces greater tolerance than other class of opioids (John T Williams et al., 2013).

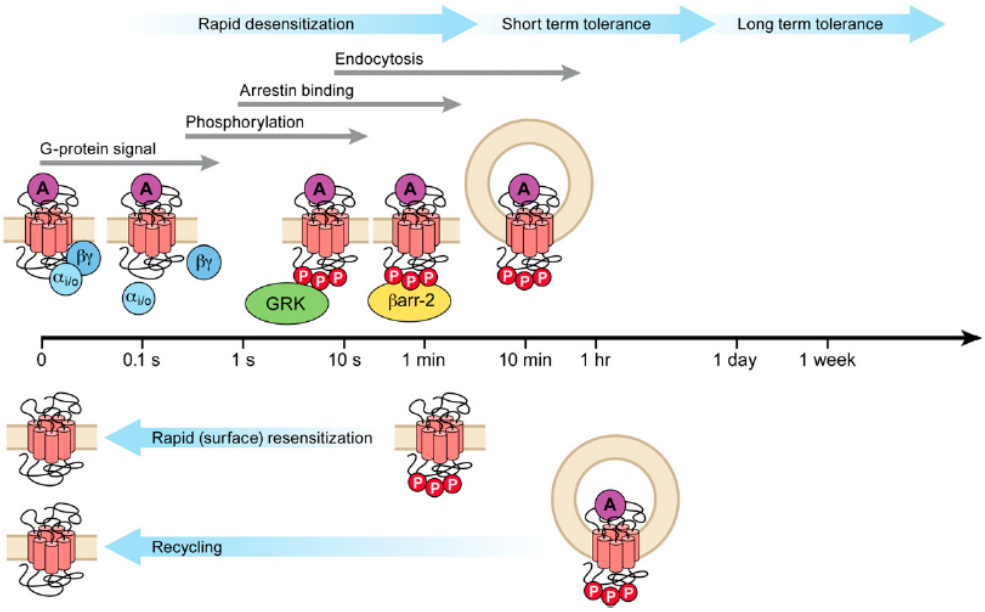

Figure 8. ***General scheme of MOR regulation following binding of an efficacious agonist such as [Met]5enkephalin.*** *The time scales for each process are shown (log scale). Phosphorylation by G protein receptor kinase (GRK) is very rapid, saturating in less than 20 seconds. Arrestin binding saturates in several minutes, and desensitization reaches steady state in approximately 5 minutes. The steady state of rapid desensitization represents the equilibrium between the forward desensitizing process, presumably phosphorylation and arrestin binding (other kinases may be involved) and dephosphorylation at the cell surface. Endocytosis reaches steady state in approximately 30 minutes and recycling over approximately 60 minutes, although this varies for different splice variants. Here, desensitization corresponds to the rapid process preceding significant endocytosis (approximately 2–5 minutes); short-term tolerance includes endocytosis and other mechanisms (up to 1 day); and long-term tolerance (greater than 1 day) presumably involves multiple regulatory processes (John T Williams et al., 2013).*

At neuronal level, evidence suggests that tolerance is also related to changes in the properties of MOR-containing GABAergic neurons in the PAG and DH (Bagley, Chieng, Christie, & Connor, 2005; Maher, Eisenach, Pan, Xiao, & Childers, 2001; Morgan, Clayton, & Lane, 2003; Ray, Gupta, & Gupta, 2004)
In addition, over the past few decades researchers have discovered that opioids are potent activators of immune cells within the CNS, and this inflammation seems to be another strong contributor to the development of opioid tolerance (Cahill & Taylor, 2017; Giron, Griffis, & Burkard, 2015). Specifically, it was shown that repeated administration of opioids, which leads to activation of glia within the PAG and spinal cord of the descending pain pathway, results in alterations in both intracellular signaling cascades and signaling properties of neurons. Furthermore, microglial inhibitors have been reported to attenuate morphine-induced tolerance (Y. Cui et al., 2008; Eidson & Murphy, 2013; Harada, Nakamoto, & Tokuyama, 2013; Raghavendra, Rutkowski, & DeLeo, 2002; Raghavendra, Tanga, & DeLeo, 2004; P. Song & Z. Q. Zhao, 2001). Though the precise mechanisms that underlie these changes

are only beginning to be uncovered, a few notable pathways which are likely significant contributors to the development of opioid tolerance have emerged. One prominent pro-inflammatory signaling cascade that has been implicated in opioid tolerance involves the immune receptor toll-like receptor 4 (TLR4), which triggers the activation of the p38-MAPK pathway, the PI3K/AKT pathway (cell survival/apoptosis), and the NFkB pathway (pro-inflammatory cytokine release) (Eidson & Murphy, 2013; Nakamoto et al., 2012; Ronnback & Hansson, 1988; Watkins, Hutchinson, Rice, & Maier, 2009). Consistently, in the spinal cord TLR4 is primarily expressed on microglial cells and is shown to be upregulated following morphine treatment (Wang et al., 2012). Notably, activation of TLR4 signaling can induce "naïve tolerance" to opioids (Eidson & Murphy, 2013; P. M. Grace, Maier, & Watkins, 2015). Furthermore, inhibition of TLR4 leads to attenuation of morphine tolerance, as well as decreased microglial activation, suggesting a prominent role for the TLR4 pathway in the development of opioid tolerance at the level of the spinal cord (M. R. Hutchinson et al., 2011; M. R. Hutchinson et al., 2010; Muscoli et al., 2010; Ndengele et al., 2009; Thomas, Mustafa, Johnson, Nicotra, & Hutchinson, 2015). Interestingly, it is also thought that TLR4 might be directly activated by opioids (P. M. Grace et al., 2015; M. R. Hutchinson et al., 2011; Wang et al., 2012).

How does the activation of glial cells determine alterations in neuronal signaling? One possibility is through modifications of neuronal excitability via increased release of glia-derived proinflammatory cytokines, including TNF (tumor necrosis factor) and IL-1b, which are known to increase neuronal AMPA and NMDA receptors, as well as down regulate GABA receptors (Stellwagen, Beattie, Seo, & Malenka, 2005; Valentinova et al., 2019; Viviani et al., 2003). This upregulation is concurrent with a downregulation of astrocyte glutamate transporters GLT-1 and GLAST, which are responsible for synaptic glutamate uptake. The overall effect is an increase in neuronal excitability, thereby lowering the ability of opioids to hyperpolarize MOR-containing GABAergic neurons. Within the PAG to RVM circuitry, this results in an inability for morphine to disinhibit output neurons to RVM (Eidson, Inoue, Young, Tansey, & Murphy, 2017; Eidson & Murphy, 2013) and, therefore, to reduce the activation of Lamina I nociceptive neurons.

Altogether, these data provide information about the mechanism by which inflammatory mediators and glia regulate morphine tolerance and indicate possible (pharmacological) approaches for the enhancement of opioid analgesic efficacy in the clinical management of pain.

PEA potential application in pain therapy in combination with opioids

Among NAEs, the most studied in the context of pain is PEA. In fact, PEA was already identified in the 1960s as a therapeutic with potent anti-inflammatory properties and, since the 1970s, its analgesic properties have been explored in a variety of chronic pain states (Hesselink, 2013). PEA is currently available worldwide as nutraceutical in different formulations (Hesselink, 2013). A large amount of preclinical and clinical evidence supports PEA potential role as an analgesic agent. For example, tissue

levels of PEA are increased on demand in brain areas involved in nociception and in the spinal cord following neuropathic pain induction, in human conditions associated with pain (Ghafouri et al., 2013; Sarchielli et al., 2007), as well as in settings associated with injury to nervous tissue (Esposito & Cuzzocrea, 2013; Skaper, Facci, & Giusti, 2014). The anti-inflammatory and analgesic effects of PEA have also been confirmed in models of chronic inflammation (De Filippis et al., 2011) and chronic or neuropathic pain (Bettoni et al., 2013; Costa, Comelli, Bettoni, Colleoni, & Giagnoni, 2008; Di Cesare Mannelli et al., 2013; Luongo et al., 2013). In these models, prolonged treatment with PEA reduced pain and preserved peripheral nerve morphology, reduced endoneural edema, the recruitment and activation of mast cells, and the production of pro-inflammatory mediators at the injury site (Bettoni et al., 2013; Costa et al., 2008; Luongo et al., 2013). Taken together, these data reveal that PEA, by regulating enduring inflammatory processes, can directly intervene in nervous tissue alterations causing pain to act as a disease-modifying agent (Di Cesare Mannelli et al., 2013).

Remarkably, antinociceptive and anti-inflammatory properties of PEA might result helpful against the development of opioid tolerance. The efficacy of a combination therapy of opioids with PEA has been successfully explored in some recent preclinical behavioral investigations (Di Cesare Mannelli, Corti, et al., 2015; Di Cesare Mannelli, Micheli, Lucarini, & Ghelardini, 2018). For example, it has been shown that PEA potentiates the antinociceptive effects of morphine and delays the development of tolerance in rats (Di Cesare Mannelli, Corti, et al., 2015). Importantly, this study also revealed that a PEA treatment is able to prevent astrocytes activation at the level of the DH. Notably, the same strategy proved to be effective in a rat model of oxaliplatin-induced neuropathy (Di Cesare Mannelli, Marcoli, et al., 2015).

1.4 Aims of the study

Based on this background, we took advantage of a novel, highly potent and brain permeable NAAA inhibitor, AM11095, to explore its ability, as indirect PPARα agonist, to:

1. Counteract nicotine neurobiological effects predictive of its abuse liability.
2. Enhance the effects of morphine in a neurophysiological correlate of analgesia and delay the onset of tolerance.

2. MATERIALS AND METHOD

2.1 Drugs

AM11095 was designed and synthesized at the Center for Drug Discovery, Northeastern University as described in US Patent 9,963,444 B2, 2018. AM11095 is a slowly reversible NAAA inhibitor with a halfmaximal inhibitory concentration (IC50) value of approximately 20 nM, while having no effect on FAAH and MGL activity at concentrations >10 μM. Nicotine ((−)-nicotine hydrogen tartrate) was purchased from Sigma (Italy), MK886 was purchased from Tocris (UK). AM11095 was dissolved in tween80, ethanol and saline (1:1:18) when injected i.p. or water and tween80 at 2% when administered p.o.; MK886 is dissolved in tween80, DMSO and saline (1:10:39); nicotine was diluted in saline (pH=7), morphine (S.A.L.A.R.S., Como, Italy) was dissolved in saline.

2.2 Animals and treatments

Male Sprague-Dawley rats weighing 200–350 g were group-housed and kept on a regular 12:12 h light/dark cycle, in temperature- and humidity-controlled facilities, with food and water available ad libitum. Rats were left to acclimatize at least 1 week after their arrival. The experimental protocols were conducted to minimize pain and suffering and to reduce the number of animals used. Experiments were approved by the Animal Ethics Committees of the University of Cagliari. Moreover, they were carried out in accordance with the European Directive on the protection of animals used for scientific purposes (2010/63/EU).

For electrophysiological experiments in VTA, animals received three injections of AM11095 (1 mg/kg or 5 mg/kg, i.p.), or vehicle, 24 h, 12 h and 2 h before the experimental procedures. The dose of 5 mg/kg was selected for subsequent experiments (N-acylethanolamine quantification, microdialysis, behavior), being the lower dose to prevent the excitatory effects of nicotine on DA neurons (see below). The treatment regimen was determined by pilot experiments and by comparison with NAAA inhibitors in different experimental setting (i.e. experimental inflammatory bowel disease) (Mireille Alhouayek et al., 2014). For behavioral studies, a different administration schedule was necessary, considering the protocol for CPP: for these experiments, rats received one AM11095 injection (5 mg/kg i.p.) daily during the conditioning session (see below). For electrophysiological experiments in LC, AM11095 (15 mg/kg i.p.) was administered 30 minutes before morphine (1 mg/kg i.v.) injection in acute experiments. For the experiments on morphine tolerance, each rat received AM11095 (15 mg/kg p.o.) or its vehicle once per day for 13 days included the day of the electrophysiological recording; moreover, 30 minutes after AM11095 administration, each rat received an injection of morphine (10 mg/kg s.c.) for 6 days before the electrophysiological recording.

2.3 N-acylethanolamine quantification ex vivo

A total number of 24 rats were utilized for these experiments. Three separate groups rats (n=8 per group) received the treatment with AM11095 as described above: three injections of AM11095 (5 mg/kg, i.p.), or vehicle, 24 h, 12 h and 2 h before sacrifice. One group of rats was sacrificed 2 h after last injection, whereas the second group was sacrificed 24 h after last administration. Control animals received vehicle injection. Rats were killed and brains were rapidly removed and dissected. Rat brain sections (midbrain, striatum, hippocampus and cortex) were rapidly frozen at −80 °C and sent to the Center for Drug Discovery for the analysis of various endocannabinoid levels metabolome. The samples were processed and analyzed by LC-MS/MS for endocannabinoid metabolome members: AEA, 2-arachidonoylglycerol (2-AG), PEA, OEA and docosahexaenoic acid (DHA).

Mixtures of the endocannabinoids and their deuterated analogs that had been stored at −80 °C were reconstituted in ethanol for further dilution in a 20 mg/mL solution of fatty acid free bovine serum albumin (BSA) to simulate analyte-free tissue and in ethanol to make the calibration standards, quality control (QC) samples and reference samples, as previously described (Williams et al., 2007). The calibration curves were constructed from the ratios of the peak areas of the analytes versus the internal standard.

Tissue samples were received on dry ice and immediately stored at −80 °C until they were processed and analyzed. The extraction procedure for the calibration standards, reference extraction and tissue samples were a modified version of the Folch extraction (Folch, Lees, & Sloane Stanley, 1957; J. Williams et al., 2007). Frozen brain sections were weighed prior to homogenization in ice cold acetone:PBS, pH 7.4 (3:1) and internal standard followed by centrifugation at 14,000 g for 5 min at 4 °C. The resulting supernatants were dried under nitrogen until the acetone was removed. To the remaining supernatant, 50 µL PBS, one volume of methanol and two volumes of chloroform were added for liquid-liquid phase extraction of the lipids. The two phases were separated by centrifugation and the bottom organic layer was evaporated to dryness under nitrogen. Samples were reconstituted in ethanol, vortexed and sonicated briefly and centrifuged prior to immediate analysis for the endocannabinoids.

Chromatographic separation was achieved using an Agilent Zorbax SB-CN column (2.1×50 mm, 5 mm) on a Finnigan TSQ Quantum Ultra triple quad mass spectrometer (Thermo Electron, San Jose CA) with an Agilent 1100 HPLC on the front end (Agilent Technologies, Wilmington DE) as previously described (Williams et al., 2007). The mobile phase consisted of 10mM ammonium acetate, pH 7.3 (A) and methanol (B) in a gradient to allow for the acids to elute first, while the mass spec was in negative ionization mode, followed by the ethanolamides and glycerol esters, while the mass spec was in positive ionization mode (flow rate=0.5 ml/min); the autosampler was kept at 4 °C to prevent analyte degradation. Eluted peaks were ionized via atmospheric pressure chemical ionization (APCI) in MRM

mode. Deuterated internal standards were used for each analyte's standard curves and their levels per gram tissue were determined. A one-way ANOVA calculation was used to determine if there was any statistical difference between the three groups for each of the detected endocannabinoid metabolome. The Dunnett's Test was used to determine the P-value, comparing groups A (sacrifice 2 h after last dose) and B (sacrifice 24 h after the last dose) to the control group (group C).

2.4 *In vivo* toxicological test battery

A total number of 66 rats were utilized for these experiments and divided into 3 groups (n=22 per group): vehicle, AM11095 (5 mg/kg) and AM11095 (25 mg/kg). Ten animals per group underwent the functional observation battery (FOB) procedure, which was adapted from Moscardo et al. (2007), 24 h before, 2 h and 24 h after random administration of AM11095 or its vehicle. Behavioral, neurologic and autonomic parameters (listed in Table 1) were observed for 1 min in the home cage and for 1 min in the open field (40×40×35 cm) for signs that did not require handling. Then rats were actively assessed by handling for a period lasting between 2 and 4 min. A complete observation session lasted for 4–6 min. The scoring was blind to the drug administration using objective scoring criteria (adapted from (Moscardo et al., 2007). Twelve animals per group were assessed for their resistance on the Rotarod (Rota-Rod Treadmill for rats Ugo Basile, Comerio, VA, Italy), which was performed to test for motor impairments, 24 h before, 2 h and 24 h after random administration of AM11095 (5 mg/kg and 25 mg/kg, i.p.) or its vehicle. Rats underwent training sessions once per day for 5 consecutive days, and only those that were competent in performing the protocol (constant rotation speed at 4 rpm for 5 min, constant acceleration over the following 4 min and finally held at 25 rpm for the final 5 min) were used for the experimental sessions. The rectal temperature and the body weight of each rat were measured at the end of each FOB or rotarod session.

2.5 *In vivo* single-unit extracellular recordings

2.5.1 Ventral Tegmental Area

A total number of 40 rats were utilized for these experiments and divided into 4 groups (n = 10 per group): vehicle, AM11095 (1 mg/kg), AM11095 (5 mg/kg), AM11095 (5 mg/kg) + MK886 (1 mg/kg). Rats were treated with AM11095 (1 mg/kg or 5 mg/kg, i.p.) or its vehicle 24 h, 12 h and 2 h before experiments. Then, rats were anaesthetized with urethane (1.3 g/kg, i.p.). For intravenous administration of pharmacological agents, a cannula was inserted into their femoral vein. Rats were placed in stereotaxic apparatus (Kopf, Tujunga, CA, USA) with their body temperature maintained at 37 ± 1 °C by a heating pad. The recording electrode (impedance 3-5 MΩ) was placed above the Parabrachial nucleus of the VTA (AP, −6.0 mm from bregma; L, 0.4–0.6 mm from midline; V, 7.0–8.0 mm from cortical surface), according to the stereotaxic rat brain atlas of Paxinos and Watson (2006). Single unit activity of neurons was recorded extracellularly (bandpass filter 0.1–10.000 Hz) with glass

micropipettes filled with 2% Pontamine sky blue dissolved in 0.5M sodium acetate. Individual action potentials were isolated and amplified by means of a window discriminator (Neurolog System, Digitimer, Hertfordshire, UK), and displayed on a digital storage oscilloscope (TDS 3012, Tektronics, Marlow, UK). Experiments were sampled on line and off line with Spike2 software by a computer connected to CED1401 interface (Cambridge Electronic Design, Cambridge, UK). DA neurons were isolated and identified according to already published criteria (Sagheddu et al., 2015) such as firing rate <10 Hz and duration of action potential > 2.5 ms. Bursts were defined as the occurrence of two spikes at interspike interval <80 ms and terminated when the interspike interval exceeded 160 ms.

2.5.2 Locus coeruleus

For electrophysiological single-unit recordings, the recording electrode (impedance 5-7 MΩ) was placed at these coordinates according to the stereotaxic rat brain atlas of Paxinos and Watson (2006): AP, -10 ± 0.5 mm from bregma; L, 1.3 ± 0.2 mm from midline; V, 5.5 – 6.5 mm from cerebellum cortical surface). NE neurons were isolated and identified according to already published criteria (Muntoni et al., 2006) such as (i) the presence just lateral to the LC of the mesencephalic nucleus of the V nerve, whose cells were activated by proprioceptive stimulation of the face (jaw stretch); (ii) a broad (3–4 ms in duration), often notched, biphasic waveform; (iii) slow spontaneous discharge (0.5–6.0 Hz); (iv) a typical response to noxious stimuli such as contralateral foot or tail pinch by an increase in activity followed by a quiescent interval; and (v) the inhibition by the a2-adrenoceptor agonist clonidine.

A total of 50 rats were used and divided into 4 groups: vehicle i.p. + morphine 1 (mg/kg i.v.), AM11095 (15 mg/kg i.p.) + morphine 1 (mg/kg i.v.), AM11095 (15 mg/kg p.o.) + morphine 10 (mg/kg s.c.) + morphine 1 (mg/kg i.v.), vehicle p.o. + morphine 10 (mg/kg s.c.) + morphine 1 (mg/kg i.v.). Basal activity was recorded for at least 3 min. Electrical pulses were generated by a stimulator (Digitimer, DS3 model) and they were applied using bipolar needle electrodes (26-gauge, 2-mm separation) connected to inserted subcutaneously into the medial-external surface of the left hind paw corresponding to the zone of innervation by the sciatic nerve and contralateral to the LC being recorded. Foot-shock stimuli (5.0 ms in duration, 10 mA in intensity) were delivered every 2 s using a Stimulator DS3 with a total of 50 repetitions per train.

At the end of recording sessions, DC current (15 mA for 15 min) was passed through the recording micropipette in order to eject PSB for marking the recording site. Brains were then rapidly removed and were frozen in isopentane cooled to -40 °C. The position of the electrodes was microscopically identified on serial 60 μm sections stained with Neutral Red.

2.6 *In vivo* microdialysis from freely moving rats

A total number of 10 rats were utilized for these experiments and divided into 2 groups (n = 5 per group): vehicle + nicotine, AM11095 (5 mg/kg) + nicotine. Apparatus and procedure were the same as described previously (M. Scherma et al., 2012). Sprague-Dawley rats were surgically implanted with a

concentric dialysis probe aimed at the shell of the NAc [anterior +2.0 mm and lateral 1.1 mm from bregma, vertical −7.9 mm from dura, according to the atlas by Paxinos and Watson (2006)] and dialysate samples were collected every 20 min and immediately analyzed by an HPLC system coupled to electrochemical detection. Rats were treated only after DA values (< 10% variability) were stable for at least three consecutive samples. AM11095 (5 mg/kg, i.p.) or its vehicle was injected 24 h, 12 h and 2 h min before saline or nicotine (0.4 mg/kg, s.c.). Only rats with correct probe placement were included in the study.

2.8 Conditioned place preference procedure

A total number of 60 rats were utilized for these experiments and divided into 6 groups (n = 10 per group): vehicle + saline; vehicle + nicotine; AM11095 + saline, AM11095 + nicotine, MK886 + nicotine, AM11095 + MK886 + nicotine. Apparatus and procedure were as described previously (M. Scherma et al., 2012; Maria Scherma et al., 2008). The general procedure consisted of three consecutive phases:
Rats were placed at the intersection of two compartments, with the guillotine door separating the two compartments raised to allow exploration of both sides for 15 min Time spent by the animal in each of the two compartments was recorded to monitor any initial preference for one side versus the other side. Animals showing a pronounced unconditioned preference for one compartment (more than 600 s spent in one compartment) were excluded from the subsequent (conditioning) phase of the experiment.

Conditioning sessions were conducted over 3 consecutive days, with two sessions per day. In the morning, all rats received an injection of saline before being placed in one of the two compartments for 20 min, with the door separating the two compartments closed. Four hours later, the rats received an injection of saline or nicotine (0.4 mg/kg) and were placed in the opposite compartment for 20 min. AM11095 (5 mg/kg) or its vehicle were injected i.p., in the home cage, 1.5 h before saline or nicotine injection. The PPARα antagonist MK886 (1 mg/kg, i.p.) was injected 1 h after AM11095 and 30 min before nicotine.

On the day after the last conditioning day, a test session was conducted using the same 15 min procedure as the pretest Time spent by the animal in each of the compartments was recorded.

2.9 Statistical analysis

Data obtained from the FOB measurements included binary, ordinal and continuous values. Normal scores from variables such as body weight, temperature, resistance on the rotarod, time of immobility, number of rears, are expressed as mean ± SEM. The difference between each dosed group vs controls was estimated with the Fisher's test or the analysis of variance (ANOVA) test as appropriate. Incidence data from variables such as posture, piloerection and vocalization are expressed as out of the total number of animals and the statistical significance decided upon Chi-squared test. Scores on observations from different behaviors are expressed ad median. The difference between each dosed

group vs controls was estimated using a non-parametric Mann-Whitney U test. Microdialysis data are mean ± S.E.M, of DA levels in 20 min dialysate samples, expressed as a percentage of basal values and were analyzed using one- or two-way ANOVA. CPP data are expressed as CPP score (mean ± S.E.M.) calculated as the time spent in the drug paired compartment during the test session minus the time spent in the drug-paired compartment during the pre-test session and were analyzed by one-way ANOVA. Post hoc comparisons, when appropriate, were performed by Tukey's multiple comparisons test or by Bonferroni's test. For *in vivo* electrophysiology, drug-induced changes in firing rate and regularity were calculated by averaging the effects of the drugs for the 2 min period following drug administration and comparing them to the mean of the pre-drug baseline. Changes in neurons response to foot-shock after morphine injection were calculated as the number of spikes evoked in the specific time window expressed in percentage compared with the spikes evoked during basal. All the numerical data are given as mean ± SEM. Statistical significance was assessed using two-way ANOVA for repeated measures, or one-way ANOVA or student's t-test when appropriate. Post-hoc multiple comparisons were made using either the Dunnett's test or Bonferroni's test. In all cases, $P < 0.05$ was considered significant and determined using the calculation software GraphPad Prism or IBM SPSS Statistics for non-parametric test.

Table 1. ***Components of FOB***

Observed parameter	Data type	Scale	Functional domain	Data display
Home cage observation				
Anormal posture	Binary	Present/absent	Physical	n° of rats
Awareness/fear				
Vocalizations	Binary	Present/absent	Affective	n° of rats
Ease of removal	Ordinal	(-2 to 2)	Behavioral	median
Ease of handling	Ordinal	(-2 to 2)	Behavioral	median
Arousal	Ordinal	(-2 to 2)	Affective	median
Finger approach	Ordinal	(-2 to 2)	Affective	median
Head touch	Ordinal	(-2 to 2)	Affective	median
Visual placing	Ordinal	(-3 to 0)	Sensorial	median
Motor activity				
Immobility	Continuous	Sec	Behavioral	mean ± SEM
Rears	Continuous	n°	Behavioral	mean ± SEM
Ataxic gait	Ordinal	(0 to 3)	Neurological	median
Central excitation				
Seizures	Ordinal	(0 to 4)	Neurological	median
Tail flick	Ordinal	(-2 to 2)	Sensorial	median
Finger snap	Ordinal	(-1 to 1)	Sensorial	median
Muscle tone				
Body tone	Ordinal	(-1 to 1)	Neurological	median
Reflexes				
Corneal reflex	Ordinal	(-1 to 1)	Sensorial	median
Righting reflex	Ordinal	(-4 to 0)	Sensorial	median
Air righting reflex	Ordinal	(-3 to 0)	Sensorial	median
Respiratory system				
Respiration	Ordinal	(-3 to 1)	Autonomic	median
Autonomic profile				
Salivation	Ordinal	(-1 to 1)	Autonomic	median
Larimation	Ordinal	(-1 to 1)	Autonomic	median
Piloerection	Binary	Present/absent	Autonomic	n° of rats
Feces	Continuous	n°	Affective	mean ± SEM
Urin	Continuous	n°	Affective	mean ± SEM
Miscellaneus observations				
Aggressiveness	Binary	Present/absent	Affective	n° of rats
Catalepsy	Binary	Present/absent	Physical	n° of rats
Tremors	Binary	Present/absent	Physical	n° of rats
Compulsive grooming	Binary	Present/absent	Affective	n° of rats
Death	Binary	Present/absent	Physical	n° of rats
Physiological measurements				
Body temperature	Continuous	C°	Autonomic	mean ± SEM
Body weight	Continuous	g	Physical	mean ± SEM

3. RESULTS

3.1 Safety and specificity of AM11095

The first fundamental objective of the study was to validate the safety, specificity and effectiveness of AM11095 as NAAA-inhibitor in behaving rodents. In order to achieve this purpose, we treated adult male rats with different doses of the drug and performed two different sets of experiments: we assessed a selection of autonomic, neurological, sensorial, affective and behavioral parameters and, in a different group of animals, we measured lipid levels in the central nervous system (CNS).

3.1.1 AM11095 does not show any sign of toxicity

Adult rats were treated with an intraperitoneal injection of AM11095 at 5 mg/kg or 25 mg/kg and the effects of the NAAA-inhibitor was investigated using a functional observational battery. A selection of autonomic, neurological, sensorial, affective and behavioral parameters was observed (Table 1) 24 h before, 2 and 24 h after the injection of AM11095 or its vehicle (n = 10 per group). The treatment with the NAAA-inhibitor at both doses did not affect any of the parameters evaluated, as summarized in Table 2 (n = 10 per group). Moreover, physiological parameters, such as weight and body temperature (Fig. 9A top and bottom, respectively) were not influenced by injection of AM11095 at both doses ($p > 0.05$). Finally, performance in the rotarod was not affected as compared to the control group (Fig. 9B), suggesting that AM11095 did not cause motor impairments ($p > 0.05$). The neurobehavioral observational battery indicates that AM11095 turned out to be devoid of side effects at 5 and 25 mg/kg in behaving adult male rats (table 2).

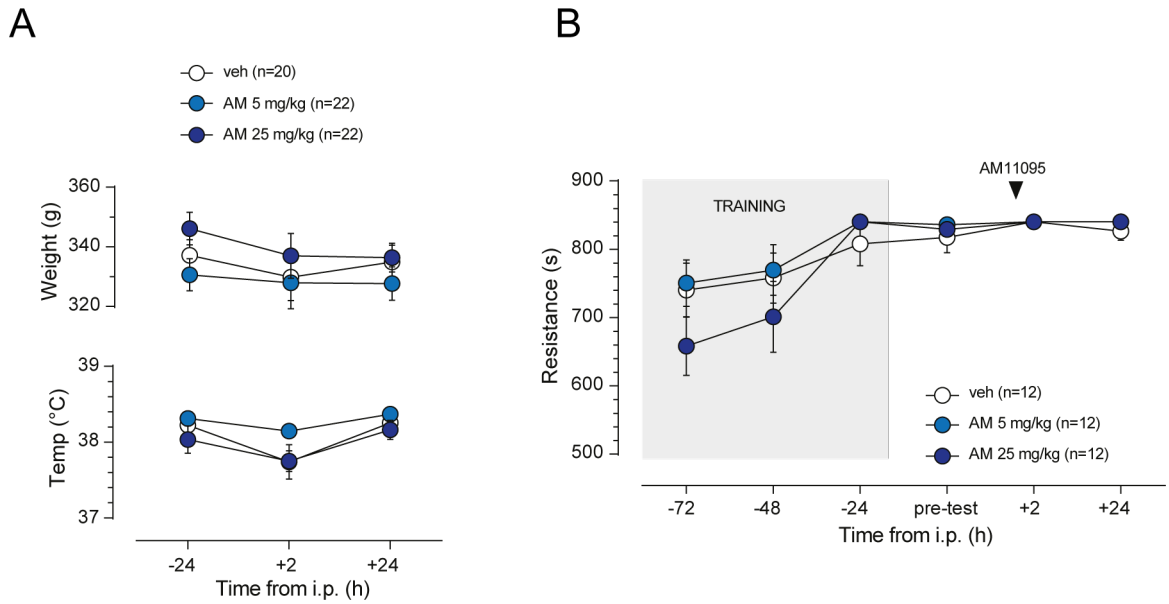

Figure 9 2. ***Effects of the NAAA inhibitor AM11095 on physiological parameters and motor test****. A) Weight (top) and body temperature (bottom) are not affected by injection of 5 mg/kg or 25 mg/kg i.p. of AM11095. Two-way ANOVA; P > 0.05. B) Performance of rats in the rotarod over different sessions is measured in total seconds of endurance. After five training sessions, the animals were challenged before (−24 h), 2 and 24 h after the injection of vehicle, AM11095 5 mg/kg or 25 mg/kg i.p., Two-way ANOVA did not show any significant effect among groups for time and treatment (P > 0.05). All data are expressed as mean ± SEM.*

AM11095 Functional Observational Battery									
	VEHICLE			5 mg/kg			25 mg/kg		
Observation	t=-24h	t=2h	t=24h	t=-24h	t=2h	t=24h	t=-24h	t=2h	t=24h
Home cage									
Anormal posture	0/10	0/10	0/10	0/10	2/10	0/10	0/10	4/10	2/10
Awareness/fear									
Vocalizations	0/10	0/10	0/10	0/10	0/10	0/10	0/10	0/10	0/10
Ease of removal (-2;2)	0	0	0	0	0	0	0	0	0
Ease of handling (-2;2)	0	0	0	0	0	0	0	0	0
Arousal (-2;2)	0	0	0	1	-0.25	-1	0	-1	-1
Finger approach (-2;2)	0	0	0	1	0	0	0	0	-1
Head touch (-2;2)	0	0	-0.5	0	0	0	0	0	-0.5
Visual placing (-3;0)	0	0	0	0	0	0	0	0	0
Motor activity									
Immobility (s)	3.2 ± 1.2	15.3 ± 4.3	17.3 ± 4.4	6.9 ± 2.5	17.2 ± 5.1	19.1 ± 3.7	6.75 ± 2.4	18.2 ± 4.9	24.2 ± 5.0
Rears (n°)	4.9 ± 0.9	3.4 ± 1.1	3.8 ± 0.9	5.2 ± 1.1	3.1 ± 0.9	2.0 ± 0.5	3.8 ± 0.9	3.1 ± 0.8	2.4 ± 0.6
Ataxic gait (0;3)	0	0	0	0	0	0	0	0	0
Central excitation									
Seizures (0;4)	0	0	0	0	0	0	0	0	0
Tail flick (-2;2)	0	0	0	0	0	0	0	0	0
Finger snap (-1;1)	0	0	0	0	0	0	0	0	0
Muscle tone									
Body tone (-1;1)	0	0	0	0	0	0	0	0	0
Reflexes									
Corneal reflex (-1;1)	0	0	0	0	0	0	0	0	0
Righting reflex (-4;0)	0	0	0	0	0	0	0	0	0
Air righting reflex (-3;0)	0	0	0	0	0	0	0	0	0
Respiratory system									
Respiration (-3;1)	0	0	0	0	0	0	0	0	0
Autonomic profile									
Salivation (-1;1)	0	0	0	0	0	0	0	0	0
Larimation (-1;1)	0	0	0	0	0	0	0	0	0
Piloerection	0/10	0/10	0/10	0/10	0/10	0/10	0/10	0/10	0/10
Feces (n°)	0.1 ± 0.1	0.3 ± 0.2	0.3 ± 0.2	0.1 ± 0.1	0	0.3 ± 0.3	0	0	0
Urin (n°)	0.1 ± 0.1	0	0	0	0		0	0	0
Miscellaneus									
Aggressiveness	0/10	0/10	0/10	0/10	0/10	0/10	0/10	0/10	0/10
Catalepsy	0/10	0/10	0/10	0/10	0/10	0/10	0/10	0/10	0/10
Tremors	0/10	0/10	0/10	0/10	0/10	0/10	0/10	0/10	0/10
Compulsive grooming	0/10	0/10	0/10	0/10	0/10	0/10	0/10	0/10	0/10
Death	0/10	0/10	0/10	0/10	0/10	0/10	0/10	0/10	0/10

Table 2. ***Results of the neurobehavioral observation battery****.*

3.1.2 NAAA-inhibition enhances brain N-acylethanolamine levels

After checked for potential adverse effects of AM11095, the next step was to verify whether *in vivo* administration of the drug was able to selectively augment brain NAE levels. For this aim, rats were treated intraperitoneally with AM11095 (5 mg/kg) or its vehicle 24 h, 12 h and 2 h before sacrifice (Fig. 10A). A second group of rats received the same treatment but were killed at 24 h after last AM11095 administration (n = 8). Control rats received vehicle injection and were sacrificed 2 h (n = 4) and 24 h (n = 4) after last injection. As no difference was found between the two control groups, data were merged. Endocannabinoids (AEA, 2-AG), NAEs (PEA, OEA) and DHA levels were assessed in the midbrain, striatum, hippocampus and cortex.

As shown in Fig. 10, lipid levels were affected by AM11095 and one-way ANOVA revealed significant effects. Specifically, increased PEA levels were found in hippocampus (Fig. 10D), and OEA levels in the hippocampus (Fig. 10E) and cortex (Fig. 10E), 2 h after AM11095 administration, compared to vehicle group. DHA levels were also significantly higher in cortex (Fig. 10F) and hippocampus (Fig. 10F) 2 h following AM11095 administration. OEA, PEA and DHA levels were similar to vehicle values 24 h later, indicating a transient effect of the NAAA inhibitor. Importantly, no changes were observed for AEA levels in all brain areas examined (Fig.10B), even though an increase in 2-AG level was detected at 24 h in the cortex (Fig. 10C).

To sum up, AM11095 administration at 5 mg/kg inhibited NAAA and this was sufficient to produce an increase of different lipid levels in the brain, including PEA and OEA. This increasing turned out to be transient since lipid levels returned to baseline after 24 h.

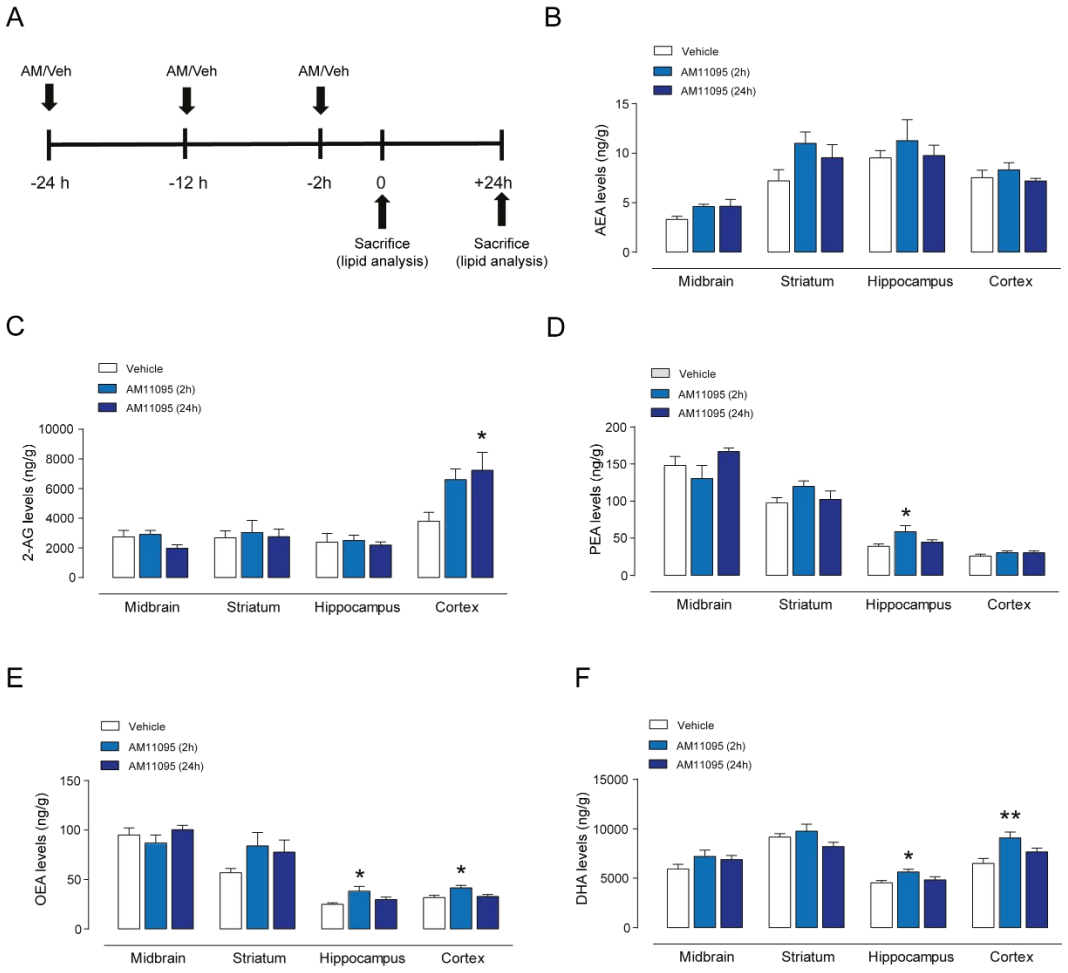

Figure 10. ***Effects of pretreatment with the NAAA inhibitor AM11095 on brain lipid levels****. A) Schematic representation of the protocol. Rats were killed and brain removed 2 h or 24 h after last AM11095 (AM, 5 mg/kg, i.p.) or vehicle (Veh) administration. B) Brain levels of the endocannabinoid AEA were not changed 2 or 24 h following AM11095 administration. One-way ANOVA: p > 0.05. C) Levels of the endocannabinoid 2-AG were increased in the cortex at 24 h following AM11095 administration. One-way ANOVA: $F_{(2, 21)} = 4.180$, *P < 0.05. D) PEA levels were increased in hippocampus at 2 h following AM11095 administration. One-way ANOVA: $F_{(2, 21)} = 3.687$, *p < 0.05. E) OEA levels were increased at 2 h following AM11095 administration in hippocampus (One-way ANOVA: $F_{(2, 21)} = 4.351$, *p < 0.05) and cortex (One-way ANOVA: $F_{(2, 21)} = 5.406$, *p < 0.05). F) DHA levels were increased in the cortex (One-way ANOVA: $F_{(2, 21)} = 6.665$, **P < 0.01) and hippocampus (One-way ANOVA: $F_{(2, 21)} = 4.114$, *p < 0.05) 2 h following AM11095 administration. N = 8 for each group. All data are shown as mean ± SEM.*

3.2 Effect of AM11095 on nicotine addictive properties

Given that PEA and OEA, through activation of PPARα receptors, are able to negatively modulate nicotinic receptors in VTA (M. Melis et al., 2010; M. Melis et al., 2008; M. Melis et al., 2013), we hypothesized that AM11095 might lead to the same result. Indeed, our group demonstrated that PPARα receptor activation-dependent negative modulation of nicotinic receptor is able to reduce nicotine potential for abuse in rodents and mammals. Therefore, we examined the potential ability of AM11095 in reducing nicotine-related effects in rat mesolimbic dopamine system, by inhibition of NAAA.

3.2.1 AM11095 prevents nicotine induced activation of mesolimbic dopamine neurons of the ventral tegmental area

First, we examined the possibility that NAAA inhibition was able to reduce DA neuron activation following intravenous injection of nicotine in anesthetized adult male rats. For this experiment, 40 rats were divided in 4 groups (n = 10 for each group): one group was administered AM11095 at 1 mg/kg i.p., one group AM11095 at 5 mg/kg i.p. and one vehicle 24, 12 and 2 h before the experiment (Fig 11A). The fourth group of rats received AM11095 (5 mg/kg i.p.) and the PPARα antagonist MK886 (1 mg/kg, i.p.) was administered 30 min after the last AM11095 dose. Importantly, *in vivo* single-unit electrophysiological recordings showed that a pretreatment with AM11095 at both doses did not change the spontaneous firing of VTA DA neurons (Fig. 11B), while it dose-dependently prevented nicotine-induced increase in discharge rate (Fig. 11E). Hence, two-way ANOVA shows a significant interaction between treatment and time; post-hoc analysis shows that AM11095 at 1 mg/kg has a significant effect at 2 min following nicotine injection, whereas the dose of 5 mg/kg has a significant effect at all time-points analyzed, when compared with vehicle. Post-hoc analysis also indicates that the effect of AM11095 + MK886 was not significant different from vehicle. Thus, the effect of AM11095 is fully reversed, namely the excitatory actions of nicotine are restored, upon administration of the PPARα antagonist MK886 (1 mg/kg, i.p.). AM11095 at 5 mg/kg also prevented nicotine-induced bursting of DA neurons: two-way ANOVA shows a significant interaction between treatment and time (Fig. 11D); post-hoc analysis shows that AM11095 at 1 mg/kg has not significant effects, whereas the dose of 5 mg/kg has a significant effect at all time-points analyzed, when compared with vehicle. Post-hoc analysis also indicates that the effect of AM11095 + MK886 was not significantly different from vehicle. Fig. 11F summarizes results on firing rate by illustrating the calculated areas under the curves (AUC); one-way ANOVA reveals a significant effect overall, whereas post-hoc analysis indicates that only the dose of 5 mg/kg i.v. significantly reversed the effects of nicotine. Therefore, for the following experiments we selected the dose of 5 mg/kg.

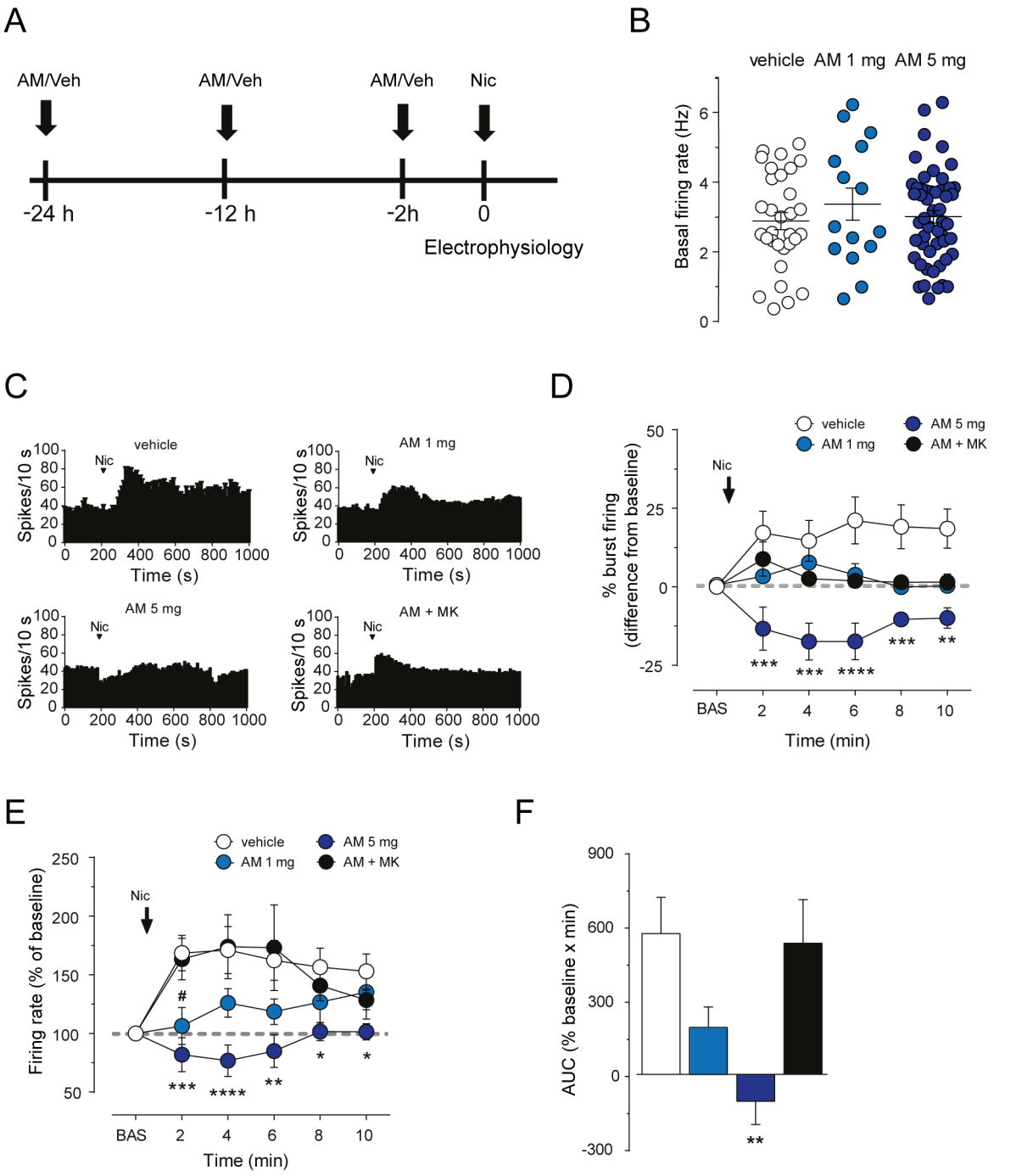

Figure 11. ***Effects of pretreatment with the NAAA inhibitor AM11095 on nicotine-related effects in the rat DA neurons of the VTA****. A) Schematic representation of the protocol. Experiment were carried out approximately 2 h after last AM11095 (AM, 1 or 5 mg/kg, i.p.) or vehicle (veh) administration. B) Graph showing that a pretreatment with 1 and 5 mg/kg AM11095 did not affect the spontaneous firing rate of VTA DA neurons (one-way ANOVA: $F_{(2,98)} = 0.604$, $p = 0.55$; vehicle n=31, AM 5 mg n=53, AM 1 mg n=15). C) Representative firing rate histograms of VTA DA neurons recorded from a rat pretreated with vehicle (top-left), AM11095 (5 mg/kg bottom-left; 1 mg/kg top-right) or AM11095 5 mg/kg + MK886 1 mg/kg (bottom-right). Arrows indicate the times of nicotine (0.2 mg/kg i.v.) injection. D) Pretreatment with 5 mg/kg AM11095 prevented nicotine-induced increase of bursting activity (two-way ANOVA: interaction treatment x time $F_{(15, 125)} = 3.63$, $p < 0.0001$; Bonferroni test, $^{**}p < 0.01$; $^{***}p < 0.001$; $^{****}p < 0.0001$; vehicle n = 10; AM 1 mg n = 6; AM 5 mg n = 7; AM +MK n=6) of VTA dopamine neurons. E) Pretreatment with 5 mg/kg AM11095 prevented nicotine-induced increase of the firing rate (two-way ANOVA: interaction treatment x time $F_{(15, 125)} = 3.07$, $P < 0.001$; Bonferroni test, $^{\#}p < 0.05$, $^{*}p < 0.05$, $^{**}p < 0.01$, $^{***}p < 0.001$; $^{****}p < 0.0001$; vehicle n=10; AM 1 mg n=6; AM 5 mg n=7; AM+MK n=6). F) Histogram summarizing results on firing rate calculated as areas under the curves (AUC; one-way ANOVA: $F_{(4,30)} = 6.39$, $p < 0.01$; post hoc: $^{**}p < 0.01$). All data are shown as mean ± SEM.

3.2.2 AM11095 treatment fully blocks nicotine induced increase of dopamine in the nucleus accumbens shell

For *in vivo* microdialysis experiments 10 rats were divided into two groups (n = 5 each group): one group was administered AM11095 (5 mg/kg, i.p. as in Fig. 12A) and the other group was administered vehicle. Dialysate collection was started 1 h before the last AM11095 administration and about 80 min before nicotine injection, to allow the detection of possible effect on baseline DA levels (Fig. 12B). One experiment in each group was discarded due to incorrect probe placement. Results showed that in vehicle-treated rats, nicotine (0.4 mg/kg s.c.) increased extracellular levels of DA in the NAc shell by about 80%, compared with basal levels ($p < 0.0001$). Pretreatment with AM11905 did not affect baseline DA levels but reduced nicotine-induced elevations (Fig. 121B). Two-way ANOVA showed a very significant effect of AM11905 treatment ($p < 0.0001$).

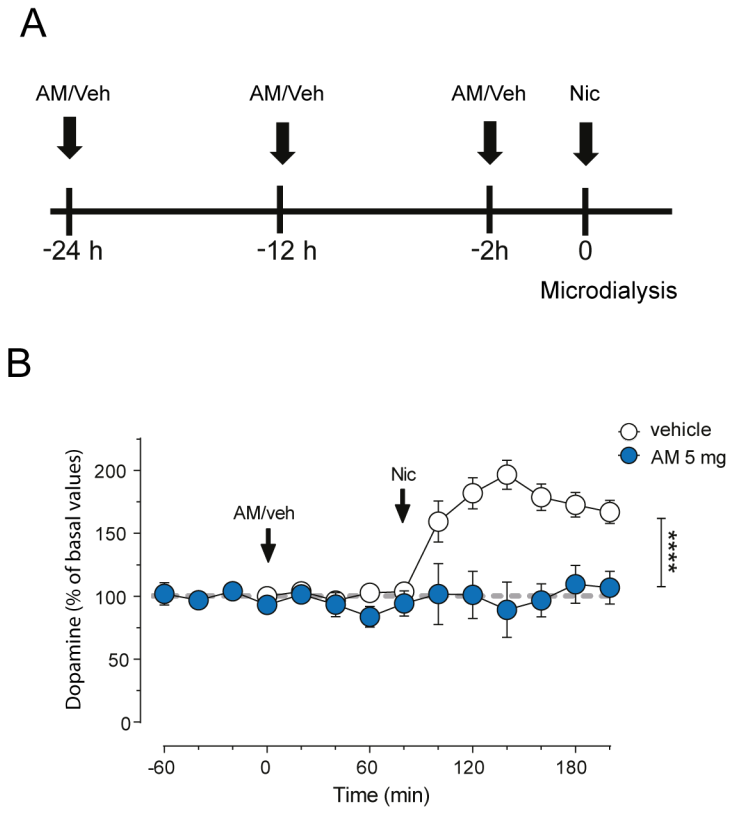

Figure 12. ***Effects of pretreatment with the NAAA inhibitor AM11095 on nicotine-dependent elevations of DA in the NAc.*** *A) Schematic representation of the protocol. B) Nicotine induces increasing of DA compared to baseline in vehicle group (one-way ANOVA: $F_{(13,42)} = 17.79$, $p < 0.0001$); AM11095 (5 mg/kg) prevented the increase in extracellular dopamine levels induced by nicotine (0.4 mg/kg, s.c.) in the shell of the nucleus accumbens (two-way ANOVA: treatment effect $F_{(13,78)} = 7.61$, $****_P < 0.0001$; vehicle and AM 5 mg n = 4) Data are expressed as mean ± SEM.*

3.2.3 AM11095 prevents the development of nicotine-induced CPP

Given the efficacy of AM11095 on counteracting nicotine-dependent stimulation of DA mesolimbic system, we explored the possibility that it could be also effective on preventing, or at least reduced, nicotine-dependent conditioning properties. For this purpose, we performed a nicotine conditioned place preference (CPP) in adult male rats. This behavioral paradigm allows to assess the conditioning properties of nicotine and whatever can interfere with this phenomenon. In our protocol the conditioning phase lasted 3 days, and AM11095 with or without MK886 was administered 30 min before the subcutaneous nicotine injection. After the conditioning phase, the rats were placed free to express their preference for one or another chamber.

Significant treatment effects were found between subjects when CPP score was compared ($p < 0.0001$). Post-hoc analysis showed that in vehicle-pretreated rats, a nicotine dose of 0.4 mg/kg induced a significant increase in the CPP score in comparison to the vehicle-saline group ($P < 0.01$, Fig. 13). However, when rats were pretreated with a 5 mg/kg dose of AM11905 before each nicotine conditioning session, the CPP score was reduced and was not significant when compared with vehicle + nicotine ($P > 0.05$, Fig. 13). On the other hand, AM11095 given before each saline conditioning session did not induced neither aversion nor preference (Fig. 13). The PPARα antagonist MK886 at the dose of 1 mg/kg, given after AM11905 and before each nicotine conditioning session, blocked the effect of AM11905 since a significant increase in the CPP score in comparison to the vehicle-saline group was found ($P < 0.001$, Fig. 13). Post-hoc analysis also showed that MK886 given alone before each nicotine conditioning session, did not affect the capacity of nicotine to induce CPP when compared to the vehicle-saline group ($P < 0.01$, Fig. 13).

In conclusion, our findings indicate that in rats NAAA inhibition can counteract the reward-related effects of nicotine on the brain and behavior. Hence, a pretreatment with the brain permeable NAAA inhibitor AM11095 prevented nicotine-induced excitation of dopaminergic transmission in reward-related areas of the brain. Specifically, the NAAA inhibitor prevented nicotine-induced increases in firing rate and burst firing in DA neurons in the VTA and nicotine-induced elevations of dopamine levels in the shell of the NAc. Consistent with the ability to prevent nicotine's effects in reward-related brain areas, AM11095 significantly decreased nicotine-induced CPP. These effects were abolished by the PPARα antagonist MK886.

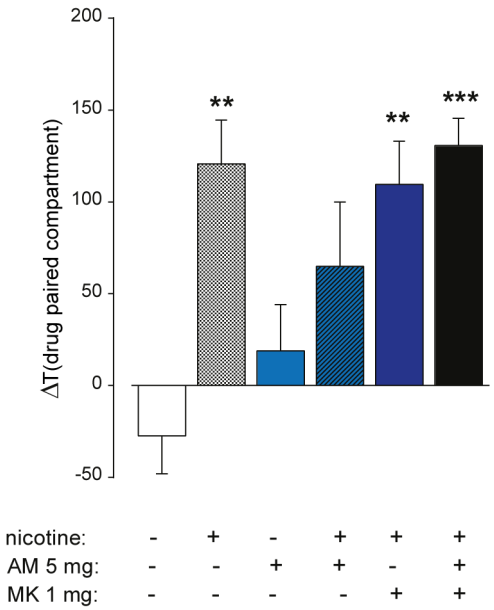

Figure 33. ***Effect of pretreatment with AM11095 on nicotine-induced expression of CPP****. AM11095 (5 mg/kg) or vehicle were injected i.p. 1.5 h before the animal was placed into the apparatus. MK886 (1 mg/kg) was injected 1 h after vehicle or AM11095 and 30 min before nicotine administration. Nicotine (0.4 mg/kg) or saline were injected s.c. right before the conditioning session. Data are expressed as mean ± SEM of ΔT (s) spent in the drug-paired compartment during the pre-test and the test (one-way ANOVA treatment effect: $F_{(5,47)} = 6.477$, $p < 0.0001$; Tukey's test, **P < 0.01, ***P < 0.001; n = 8–10 animals per group).*

3.3 Effect of AM11095 on the development of morphine antinociceptive tolerance

This part of the thesis was dedicated to explore the potential effect of AM11095 on morphine antinocicepetive effects. Our hypothesis is based on the evidence collected by Di Cesare Mannelli and colleagues (2015; 2018) that demonstrates how PEA can potentiate morphine analgesic effects and can delay the development of tolerance as assessed through behavioral paradigms. Thus, our strategy was to take advantage of AM11095, which increases brain levels of PEA and OEA via NAAA inhibition. We performed single-unit electrophysiological recordings from anesthetized rats and assessed AM11095 effects on LC NE neurons. This brain nucleus is implicated in pain processing (Pertovaara, 2013), opiate withdrawal and it is very sensitive to opioids as it expresses MOR (Aghajanian, 1978; Andrade, Vandermaelen, & Aghajanian, 1983). Moreover, it responds to noxious stimuli such as FS, even when the animal is anesthetized (Hirata & Aston-Jones, 1994), and morphine is able to diminish the late response of the neurons to FS (Hirata & Aston-Jones, 1996). These are the reason why LC represents a perfect candidate to study an electrophysiological correlate of pain and, therefore, to be used as a readout to assess AM11095 and morphine properties.

The experimental strategy was designed in order to assess whether sub-chronic treatment with morphine can affect i) LC basal electrophysiological properties, ii) its response to morphine injection, iii) its response to FS and iv) the ability of morphine to reduce the late phase of FS-evoked response. The following step was to evaluate the effect of AM11095 on the same parameters. Therefore, we divided the animals in 4 experimental groups: one group received a single injection of vehicle the same

day of the experiment, one group received an injection of AM11095 right before the experiment, one group was treated for 5 days prior the experiment with a subcutaneous injection of morphine (10 mg/kg, one injection per day) and the last group received the same sub-chronic treatment with morphine plus a treatment with the NAAA inhibitor, including the day of the electrophysiological experiment.

3.3.1. Basal electrophysiological features of LC neurons: spontaneous activity and response to morphine

We performed single-unit electrophysiological recordings from adult male rats anesthetized with urethane (Fig. 14A and B) and collected the spontaneous electrophysiological properties of LC NE neurons after the different pre-treatments as well as their response to a subsequent injection of morphine. Two-Way ANOVA and Bonferroni multiple's comparison statistical analysis reveal how spontaneous firing rate, bursting activity and coefficient of variation are unaffected by 5 days of morphine treatment (Fig 15B) (firing rate: veh 2.70±0.16 Hz vs chronic-mor 3.1±0.2 Hz; burst firing: veh 3.7±0.8 % vs chronic-mor 4.5±1.1 %; CV: veh 46.6±1.6 % vs chronic-mor 48.3±1.7 %; statistics shown in figure 15B legend), and that the administration of AM11095 did not alter the basal spontaneous activity of LC NE neurons neither acutely (firing rate: veh 2.7±0.2 vs AM11095 2.7±0.1 Hz; burst firing: veh 3.7±0. 8 % vs AM11905 6.3±1.5 %; CV: 46.6±1.6 % vs AM11095 52.7±2.5 %; statistics shown in figure 15B legend), nor when it was administered in co-treatment with morphine (firing rate: chronic-mor 3.1±0.2 Hz vs AM11095+chronic-mor 2.9±0.3 Hz; burst firing: chronic-mor 4.5±1.1 %; vs AM11095+chronic-mor 7.8±1.2 %; CV: chronic-mor 48.3±1.7 % vs AM11095+chronic-mor 53.1±3.1 %; statistics shown in figure 15B legend). Next, we assessed whether LC NA neurons response to morphine can be affected by AM11095 or by sub-chronic treatments (veh + morphine and AM11095 + morphine). As shown in figure 15C (right panel), the firing rate reduction after morphine i.v. administration was comparable among groups. This result was confirmed by two-way ANOVA and multiple comparison test (% of baseline: veh 67.2±8.4 % vs AM11905 57.8±8.5 % vs chronic-mor 78.1±5.67 % vs AM11095+chronic-mor 71.0±5.5 %; statistics shown in figure 15C legend).

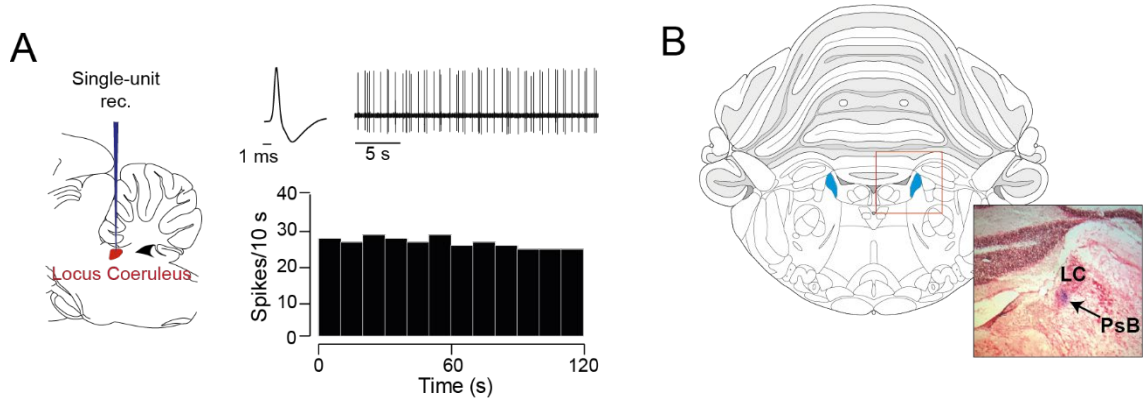

Figure 14. ***Example of electrophysiological recording and location of NE neuron of LC****. A) Left, schematic of the experimental technique; right, example of a typical action potential waveform, sample trace and rate histogram from a LC neuron. B) Left, coronal section of rat brain atlas (Paxinos & Watson, 2006); right, example of a recording location of a LC neuron (arrow, pontamine sky blue (PsB) dye.*

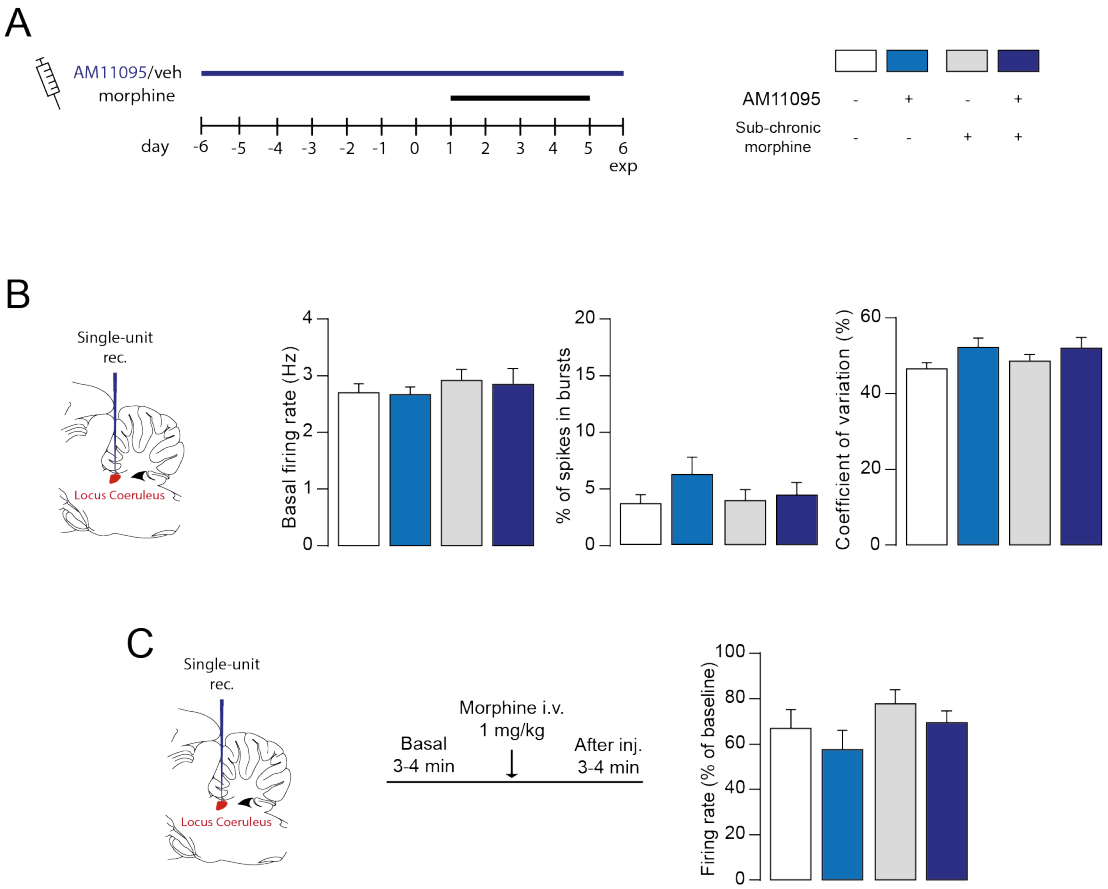

Figure 15. ***Basal electrophysiological features of LC NE neurons and their response to morphine are unaffected by AM11095 and sub-chronic morphine treatment****. A) Left, schematic of the treatment plan; right, schematic of the experimental groups. B) left, schematic of the experimental technique; right, bar graph rapresenting firing rate (Two-way ANOVA, bonferroni's multiple comparisons test: veh vs AM11095 acute effect t147=0.127 p=0.99; veh vs sub-chronic morphine: t147=1.433 p=0.308; veh+sub-chronic morphine vs AM1109+sub-chronic morphine: t147=0.74 p=0.915), bursting activity (Two-way ANOVA, bonferroni's multiple comparisons test: veh vs AM11095 acute effect t109=1.28 p=0.36; veh vs sub-chronic morphine: t109=0.269 p=0.955; veh+sub-chronic morphine vs AM1109+sub-chronic morphine: t109=0.135 p=0.988) and CV (Two-way ANOVA, bonferroni's multiple comparisons test: veh vs AM11095 acute effect t112=1.683 p=0.181; veh vs sub-chronic morphine: t112=0.022 p=0.999; veh+sub-chronic morphine vs AM1109+sub-chronic morphine: t112=0.361 p=0.921). C) left, schematic of the experimental technique; centre, schematic of the experimental protocol; right, bar graph rapresenting the firing rate change upon morphine i.v. injection (Two-way ANOVA, bonferroni's multiple comparisons test: veh vs AM11095 acute effect t28=0.922 p=0.595; veh vs sub-chronic morphine: t28=1.077 p=0.4969; veh+sub-chronic morphine vs AM1109+sub-chronic morphine: t28=0.922 p=0.660). (n veh=52; n AM11095 acute=42; n sub-chronic morphine=32; n AM11095+sub chronic morphine=27). Data are expressed as mean ± SEM.*

3.3.2 Locus coeruleus noradrenergic neurons respond to a noxious stimulus

We recorded from NE neurons of the LC while delivering a noxious stimulus. When the contralateral paw was connected with bipolar electrodes and an electric shock was delivered with an intensity of 10 mA and a duration of 5 ms (Fig. 16A), the neurons responded with a fast excitation followed by an inhibition. The neurons underwent a set of 50 FS with a frequency of 0.5 Hz. In figure 16B is illustrated an example of raster plot, superimposed traces and peristimulus time histogram (PSTH) of an LC NE neuron responding to the FS. The red superimposed line represents the mean response from 19 neurons belonging to the control group that received a complete set of FS. Overall, NE neurons respond with a triphasic excitation as represented by the three peaks resembling the response

obtained by Hirata and Aston-Jones (1994). We have identified three phases and, importantly, the late one coincides with the morphine-sensitive phase described by Hirata and Aston-Jones (1996). We then asked ourselves whether acute AM11095, or a sub-chronic morphine treatment, can influence FS response of LC neurons. As illustrated in figure 16D, we did not detect any difference in the number of spikes evoked in all the three phases as indexed by Two-way ANOVA (1^{st} phase: veh 52.8±5.2 vs AM11905 50.5±4.1 vs chronic-mor 56.6±4.1 vs AM11095+chronic-mor 51.2±4.5; statistics shown in figure 16D legend. 2^{nd} phase: veh 59.5±4.4 vs AM11905 52.5±5.2 vs chronic-mor 64.9±7.5 vs AM11095+chronic-mor 76.0±7.1; statistics shown in figure 16D legend. 3^{rd} phase: veh 53.7±6.6 vs AM11905 50.4±5.8 vs chronic-mor 67.9±9.0 vs AM11095+chronic-mor 64.7±8.8; statistics shown in figure 16D legend).

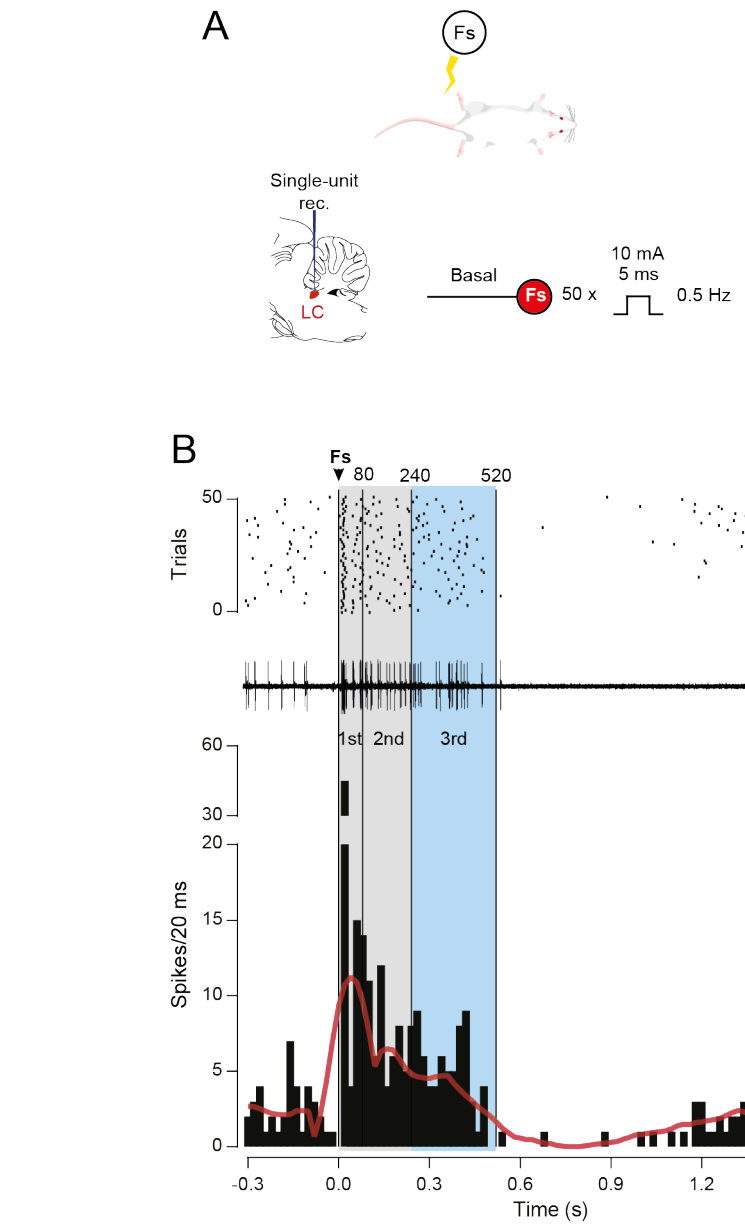
A
Fs
Single-unit
rec.
LC
Basal
Fs
50 x
10 mA
5 ms
0.5 Hz
B
Fs
80
240
520
Trials
50
0
1st
2nd
3rd
60
30
20
15
10
5
0
Spikes/20 ms
-0.3
0.0
0.3
0.6
0.9
1.2
1.5
Time (s)
C
AM11095/veh
morphine
day
-6
-5
-4
-3
-2
-1
0
1
2
3
4
5
6
exp
AM11095
Sub-chronic
morphine
D
n spikes 0-80 ms
n spikes 80-240 ms
n spikes 240-520 ms
100
80
60
40
20
0

Figure 16. ***FS-evoked response of LC neurons are unaffected by AM11095 and sub-chronic morphine treatment.*** *A) Schematic of the experimental protocol. B) Raster plot (above), example trace (middle) and peristimulus time histogram of a typical LC neuron after 50 footshocks; the red line represents the mean smoothed of 19 neurons. C) Left, schematic of the experimental protocol; right, schematic of the experimental groups. D) Bar graph rapresenting the number of spikes evoked by FS in basal condition; left (1st phase): Two-way ANOVA, bonferroni's multiple comparisons test: veh vs AM11095 acute effect t74=0.384 p=0.911; veh vs sub-chronic morphine: t74=0.600 p=0.797; veh+sub-chronic morphine vs AM1109+sub-chronic morphine: t74=0.384 p=0.633; centre (2nd phase): Two-way ANOVA, bonferroni's multiple comparisons test: veh vs AM11095 acute effect t74=0.794 p=0.674; veh vs sub-chronic morphine: t74=0.606 p*=0.09; veh+sub-chronic morphine vs AM1109+sub-chronic morphine: t74=0.795 p=0.378; right (3rd phase): Two-way ANOVA, bonferroni's multiple comparisons test: veh vs AM11095 acute effect t74=0.318 p=0.938; veh vs sub-chronic morphine: t74=1.308 p=0.3517; veh+sub-chronic morphine vs AM1109+sub-chronic morphine: t74=0.299 p=0.948. n veh=19; n AM11095 acute=20; n sub-chronic morphine=20; n AM11095+sub chronic morphine=19. Data are expressed as mean ± SEM*

3.3.3 Morphine reduces the response to foot-shock of neurons in the locus coeruleus

Given the evidence from Hirata and Aston-Jones (1996) that morphine can reduce the response to FS of NE neurons only in the late (or 3rd) phase, we sought to replicate this result in order to assess first the influence of AM11095 and then whether a sub-chronic treatment with the opioid can blunt this effect. Therefore, after the acquisition of a basal response to FS, we injected morphine (1 mg/kg i.v.) and delivered another train of FS while recording the same neuron (n = 9; Fig. 17A). As shown in figure 17B, morphine injection reduced the number of spikes evoked only in the 3rd phase (240-520 ms) (n spikes: 3rd basal 67.8 ± 11.8 vs 3rd morphine 1 mg/kg 30.2 ± 7.1) (***p<0.0001), while leaving unaffected the 1st and 2nd phase (n spikes: 1st basal 48.9 ± 8.7 vs 1st morphine 1 mg/kg 48.3 ± 10.3; 2nd basal 43.4 ± 5.9 vs 2nd morphine 1 mg/kg 32.8 ± 4.6; statistics shown in fig 17B legend).

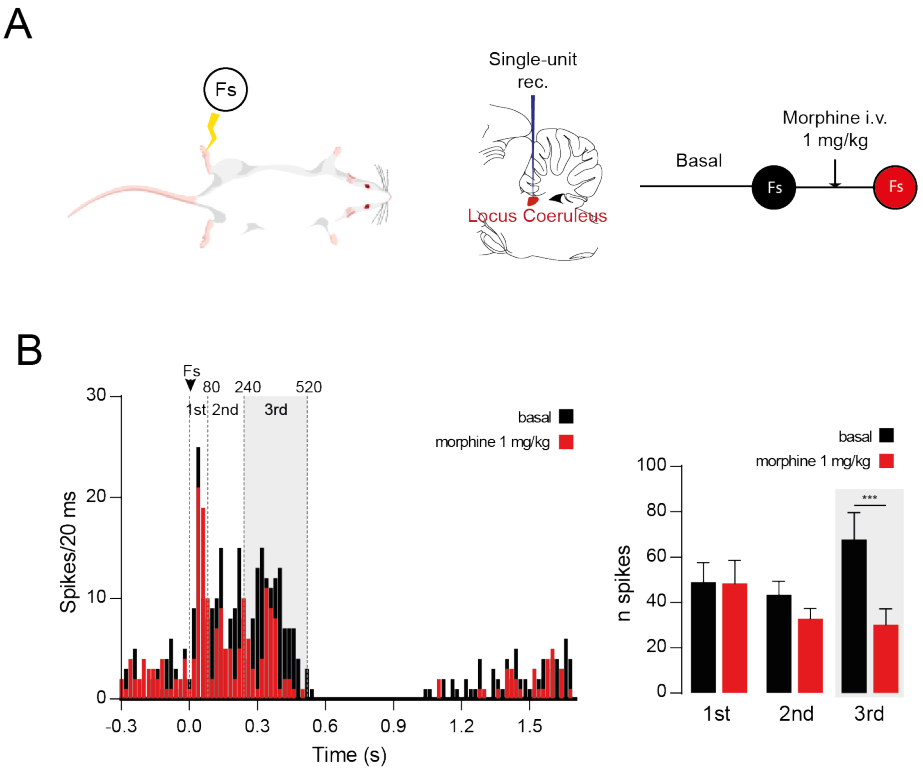

Figure 17. ***FS-evoked late response of LC neurons is attenuated by morphine****. A) Schematic of the experimental protocol. B) Left, single example PSTH before (black) and after (red) injection of morphine; right, bar graph rapresenting the number of spikes evoked in the three phases before-after morphine. Two-way ANOVA morphine effect: $F_{(1,24)}$ p < 0.0001; Bonferroni's tests 1st before vs 1st after: t24 = 0.10, p > 0.999; 2nd before vs 2nd after: t24 = 1.94, p = 0.193; 3rd before vs 3rd after: t24 = 6.83, ***p<0.0001 (n=9). Data are expressed as mean ± SEM.*

3.3.4 AM11095 potentiates morphine analgesic properties

Having established that morphine reduces LC neurons late (or 3rd) response to FS, we asked ourselves whether AM11095 could modulate morphine effects. Rats were treated with AM11095 at 15 mg/kg or its vehicle i.p. 30 minutes before the experiment (Fig. 18A). In vehicle treated rats, morphine reduced the number of spikes evoked in the 3rd phase to 55.8± 6.0 %, while in AM11095-treated-rats morphine further reduced about 76.9±5.2 % (Fig. 18B left). Statistical analysis revealed that the NAAA inhibitor potentiates morphine antinociceptive effects (*p < 0.05).

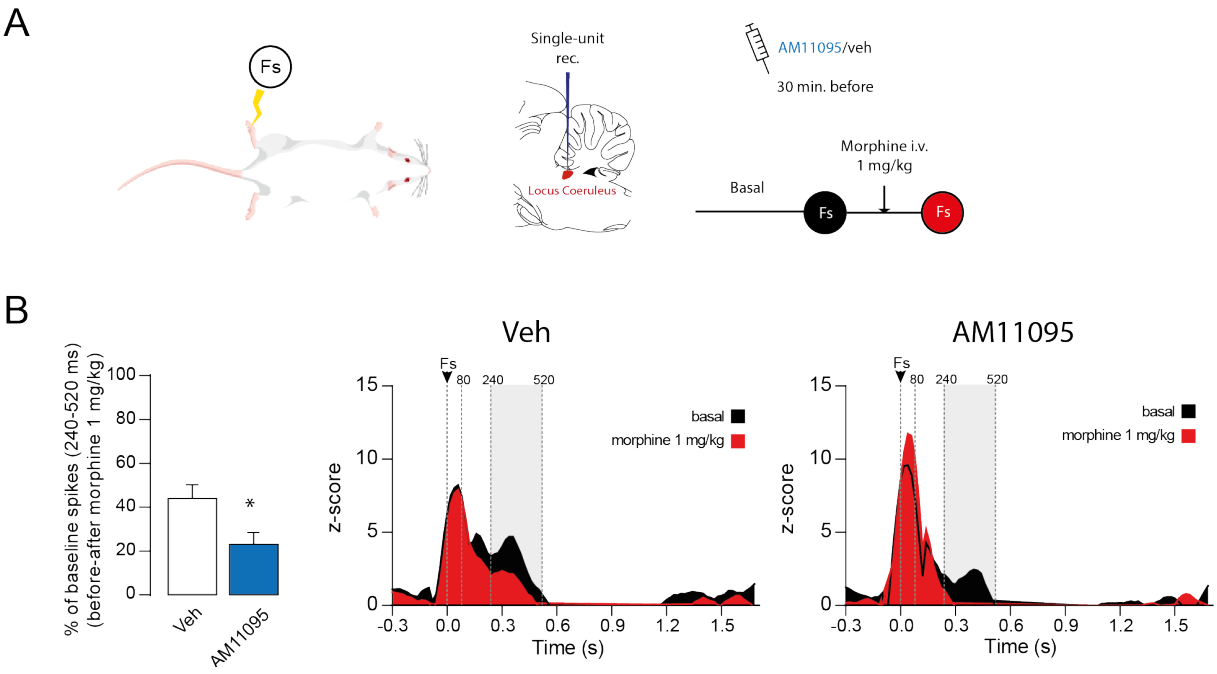

Figure 18. ***AM11095 treatment potentiates antinociceptive properties of morphine in LC neurons****. A) Schematic of the experimental protocol. B) Left, bar graph rapresenting the percentage of reduction of the number of spikes in the 3rd phase produced by morphine injection (unpaired t test: t_{10} = 2.50, *p = 0.031); centre (veh, n=7), right (AM11095, n=5): mean smoothed PSTH of the response before-after morphine injection calculated as the z score. Data are expressed as mean ± SEM.*

3.3.5 AM11095 delays the development of morphine tolerance

Finally, after establishing that the NAAA inhibitor acutely potentiates morphine effects in our paradigm, we investigated whether AM11095 could delay the development of morphine tolerance.

To this purpose, rats received once per day AM11095 (15 mg/kg p.o.) or its vehicle for 14 days, including the day of the experiment. Both groups were also treated once per day (30 min after the administration of AM/veh) with morphine (10 mg/kg s.c.) for 5 days before the experiment in order to induce morphine tolerance. The day of the experiment, each rat was treated with the last dose of AM11095 or its vehicle right before the administration of the anesthetic (Fig. 19A). The experiments were conducted in order to evaluate morphine effects on the response to FS in both groups.

As shown in figure 19B, morphine was able to reduce the spikes evoked in the late phase only in AM11095 treated rats. In fact, while in the latter group the reduction was of 48.2±8.7 %, in vehicle-

treated rats the 3rd phase was reduced only by 16.3±7.0%. Statistical analysis indicates that AM11095 significantly reduced the development of morphine tolerance (*p = 0.016).

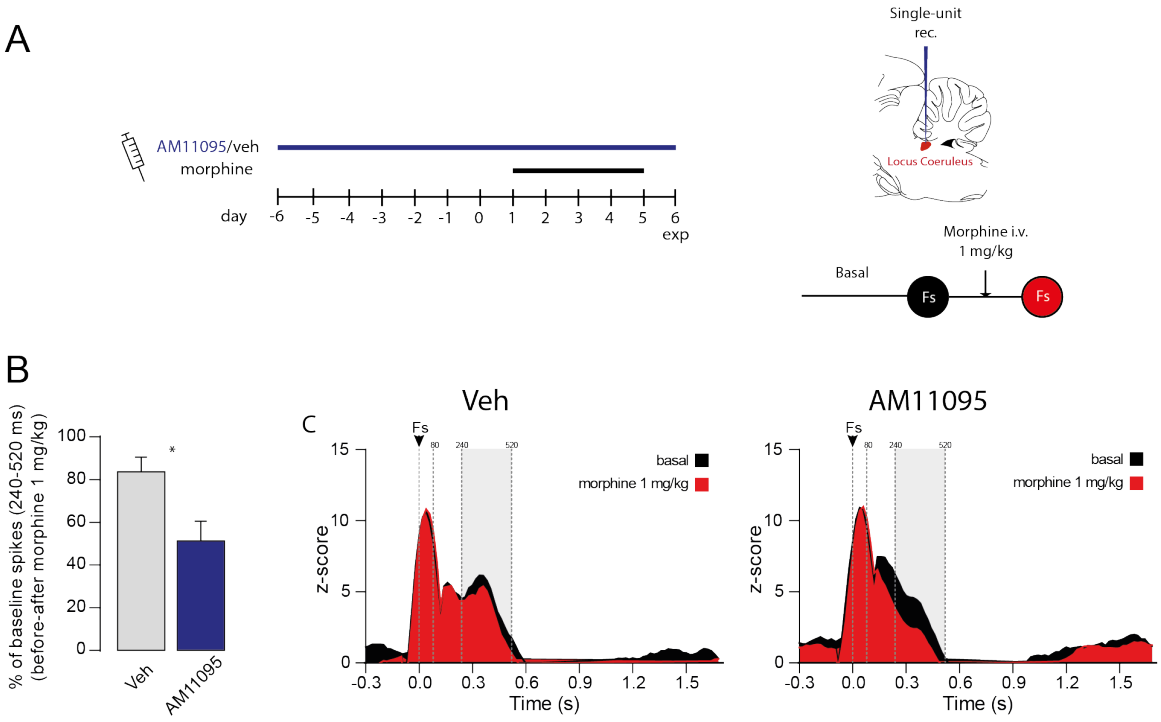

Figure 19. ***AM11095 reduces the development of morphine tolerance****. A) Schematic of the experimental protocol. B) Left, bar graph rapresenting the percentage of reduction of the number of spikes in the 3rd phase produced by morphine injection (unpaired t test: t_{14} = 2.732, *p = 0.016); centre (veh, n=7), right (AM11095, n=9): mean smoothed PSTH of the response before-after morphine injection calculated as the z score. Data are expressed as mean ± SEM.*

In summary, the obtained results demonstrate that electrophysiological properties of LC NE neurons, their response to morphine and to FS are unaffected either by AM11095 or by a sub-chronic morphine treatment. On the other hand, they also indicate that AM11095 potentiates morphine's ability to blunt the response of LC neurons to FS and it reduces the development of morphine tolerance after a sub-chronic treatment.

4. DISCUSSION

The findings described in this thesis highlight the therapeutic potential of NAAA inhibitors. The first important achievement of our research is the evidence that the NAAA inhibitor AM11095 increases NAEs' levels in the brain by inhibiting one of their major degrading enzymes, NAAA. Secondarily, we described its ability to reduce nicotine-induced neurobiological and behavioral effects and to potentiate and prolong morphine antinociceptive properties. These two effects might appear unrelated, but they share PPARα activation by the endogenous ligands PEA or OEA as common molecular substrate. Indeed, the pharmacological approach that we employed was aimed to increase the bioavailability of PPARα endogenous agonists (namely PEA and OEA), without affecting AEA which binds the CB1 receptors. Evidence suggests that NAAA is involved only in the degradation of PEA and OEA but not AEA, even though there are contrasting evidence between *in vivo* and *in vitro* studies (Bottemanne et al., 2018). To date, different pharmacological tools to activate PPARα are available: direct synthetic agonist (fibrates or WY14643), indirect agonists (FAAH inhibitors) or chemically modified endogenous agonists (methOEA, ultramicronized PEA). Employing an indirect agonist might offer several advantages to activate PPARα, when compared to direct agonists, since it follows the spatial and temporal resolution of action of its agonist. Additionally, an advantage of NAAA inhibitors over FAAH inhibitors is that increases in AEA levels, and consequent activation of CB1 receptors, are not expected.

In the next sections, I will discuss separately the key points of our study. I have divided the chapter in three parts: i) in the first part I will discuss the specificity and safety assessment of AM11095, then ii) I will address the part of the study that investigate how the NAAA inhibitor can influence the rewarding properties of nicotine and iii) I will discuss the findings related with its activity on morphine's antinociceptive effects.

Part I – Safety and specificity of AM11095

In the first part of the study, our aim was to assess whether this novel synthetized NAAA inhibitor was devoid of overt side effects. We administered the compound to adult male rats at two different doses: 5 and 25 mg/kg. We have opted to use 5 mg/kg i.p. being the dose effective on preventing nicotine-induced activation of VTA DA neurons. On the other hand, the dose of 25 mg/kg was chosen on the basis of different toxicological studies that suggested to increase the putative effective dose by 5- to 100-fold in order to maximize the probability to reveal side effects (Gauvin, Zimmermann, Dalton, & Baird, 2017; Moscardo et al., 2007). The toxicological evaluation covered a multitude of parameters including autonomic, vegetative and behavioral ones. Given the anorectic nature of OEA (a potential product of NAAA inhibition), one of the most important parameters to carefully observe was the variation in weight of the animal upon the treatment. Importantly, in our experimental conditions

AM11095 did not affect the weight of the animal, although we cannot exclude that a chronic regimen can instead reduce food consumptions. In fact, it has been reported that a different NAAA inhibitor is able to affect body weight in mice but only after more than 12 days of treatment (Migliore et al., 2016). A crucial step of our research was the validation of AM11095 as i) a brain permeable NAAA inhibitor therefore capable to determine increases of NAEs brain levels and ii) a compound specifically inducing PEA and/or OEA increases but not AEA. Accordingly, in rats treated with AM11095 2 h before sacrifice, a selective increase of OEA and PEA, but not of AEA, in the hippocampus together with an augment of OEA in the cortex were observed, suggesting that this hydrolytic enzyme is expressed in the brain and contributes to the regulation of N-acylethanolamines levels.

To date there are no direct evidence of the expression of NAAA in the brain, therefore our finding adds up to other indirect proofs provided by Migliore and collegues (2016). A further indirect indication of PPARα activation in the brain by its endogenous ligands is the increase in DHA detected in cortex and hippocampus, the same regions where we observed increased OEA and/or PEA levels. Hence, it has been shown that DHA biosynthesis requires a peroxisomal β-oxidation step (Ferdinandusse, Denis, Dacremont, & Wanders, 2003), which is enhanced by PPARα activation (Rakhshandehroo, Knoch, Muller, & Kersten, 2010). Consequently, PPARα activation may promote DHA biosynthesis, as it has been recently suggested in humans, where an elevated PPARα gene expression was associated to an increase in circulating DHA (Murru et al., 2018). Therefore, the finding of augmented DHA biosynthesis may imply that AM11095 induces peroxisomal β-oxidation.

The reason why we were unable to detect increases in OEA, PEA or DHA levels in other brain areas, such as the midbrain or striatum is unknown. One possibility is that NAE signalling, which is "on demand" and presumably spatially restricted, is not robust enough, or rises in NAEs levels are transient and difficult to detect within the time window between drug administration and sacrifice. On the other hand, specifically in the hippocampus, a robust NAE signalling and PPARα expression has been demonstrated in previous studies (Rivera et al., 2014). High levels of PPARα and NAPE-PLD expression and co-localization in several cell types might be the reason why transient boosts in NAE levels are easier to detect in this brain region. Moreover, our results highlight that these compounds do not induce general increases in the levels of endogenous endocannabinoids active at CB1/CB2 receptors. This property might be valuable in several conditions in which activation of cannabinoid receptors is not desired. Consistently, AM11095 is devoid of overt behavioral effects when assessed within the FOB and does not evoke CPP per se. Although no behavioral effects correlated with CB1 activation were present, an increase in 2-AG was observed in the cortex. Interestingly, Petrosino et al. (2015) reported that administration of PEA in humans and dogs induces an increase in 2-AG *in vitro* and *in vivo* through an unidentified mechanism.

These results point out to three important findings: AM11095 is devoid of overt side effects, it is brain permeable and selectively inhibits NAAA, leading to a temporally restricted increase of PEA and OEA.

Part II – Effect of AM11095 on nicotine-induced activation of mesolimbic DA system and place preference

The second part of the study was based on the hypothesis that NAAA inhibition could negatively modulate nicotine effects in the mesolimbic DA system and its rewarding properties. Our findings indicate that, when the brain permeable NAAA inhibitor AM11095 was administered in rats, it prevented nicotine-induced activation of DA neurons in the VTA and nicotine-induced elevations of DA levels in the NAcSh. In line with the ability to block nicotine's effects in reward-related brain areas, AM11095 significantly decreased nicotine-induced CPP. All these effects were abolished by the PPARα antagonist MK886, suggesting that AM11095 effects depend upon the activation of this receptor.

The effects of NAAA inhibitors observed in the present study on nicotine-related behavioral, electrophysiological, and neurochemical actions are comparable to those of PPARα agonists and the FAAH inhibitor URB597 (Luchicchi et al., 2010; Mascia et al., 2011; Panlilio et al., 2012). These results converge to suggest that the NAAA inhibitor modulates the rewarding effects of nicotine by increasing levels of the endogenous PPARα ligands, OEA and PEA. This is supported by the finding that the PPARα antagonist MK886 completely suppressed the effects of AM11095 in electrophysiological and behavioral settings.

The mechanism by which direct or indirect PPARα agonists and NAAA inhibition exert these anti-addictive actions is mostly understood (M. Melis et al., 2010; M. Melis et al., 2008; Miriam Melis & Pistis, 2014). The mesolimbic DA system plays a major role in nicotine addiction, being the VTA and NAcSh critical brain areas responsible for nicotine's rewarding effects (Corrigall, Coen, & Adamson, 1994; Nisell, Nomikos, Svensson, & toxicology, 1994). Nicotine enhances mesolimbic DA transmission directly through stimulation of somatodendritic nAChRs in DA neurons, and indirectly through stimulation of glutamate release in the VTA or in the NAc; both these mechanisms lead, in turn, to stimulation of DA neuron firing and/or DA release in the NAcSh (Mansvelder, Keath, & McGehee, 2002). Our data show that activation of PPARα, either indirectly through NAAA inhibition (present study) or directly by administration of PPARα agonists as in our previous studies (Mascia et al., 2011; M. Melis et al., 2010; M. Melis et al., 2008; Miriam Melis & Pistis, 2014), blocks nicotine-induced increases in firing rate and burst firing of DA neurons in the VTA and consequently prevents nicotine-induced elevations of DA levels in the NAcSh. Consistently, other groups have confirmed that PPARα signalling might reduce nicotine reward and decrease the severity of nicotine-induced withdrawal (Donvito et al., 2018; Jackson et al., 2017). The mechanism underlying these effects was elucidated by

our previous *in vitro* experiments, showing that activation of PPARα induces a rapid non-genomic phosphorylation of β2-containing nAChRs on VTA dopamine neurons (M. Melis et al., 2010; M. Melis et al., 2008). Phosphorylated nAChRs show diminished ionic conductance (Charpantier et al., 2005) and are rapidly internalized (Cho et al., 2005), thus reducing or abolishing the responses of DA neurons to nicotine. This downregulation of nAChRs is presumably the mechanism by which experimental drugs targeting PPARα directly (Mascia et al., 2011; M. Melis et al., 2010; M. Melis et al., 2008; Miriam Melis & Pistis, 2014; Panlilio et al., 2012) or indirectly (i.e. the FAAH inhibitor URB597 or the NAAA inhibitor AM11095) (Forget, Coen, & Le Foll, 2009; Luchicchi & Pistis, 2012; Maria Scherma et al., 2008) block the effects of nicotine in the VTA and NAcSh that are believed (Corrigall et al., 1994; Gotti et al., 2010) to underlie nicotine reward. The electrophysiological, neurochemical, and behavioral experiments of the present study extend these findings to the NAAA inhibitors.

Even though we were unable to detect increases in PEA or OEA levels in the VTA or NAc for the reasons explained above, yet the increase in the hippocampus and cortex are relevant for nicotine addiction. In fact, both hippocampus and cortex receive a rich cholinergic innervation and express a wide variety of nAChR subtypes (Dani & Bertrand, 2007). In the hippocampus, nicotine induces long-term potentiation (LTP) in the medial perforant path dentate gyrus synapses, the mossy fiber CA3 synapses, and the Schaffer collateral CA1 synapses (Gould, Leach, & memory, 2014). In several cortical areas, particularly in the insular cortex, nicotine was also shown to modulate long-term form of synaptic plasticity via β*nAChRs (Sato, Kawano, Yin, Kato, & Toyoda, 2017), or to induce dendritic remodeling (Ehlinger, Bergstrom, McDonald, & Smith, 2012). These nicotine-evoked forms of synaptic plasticity might play a role in addiction-related processing of contextual information associated with nicotine use. Thus, increased PPARα signalling in the hippocampus and the cortex, and consequent modulation of nAChRs, might underlie the potential effect of NAAA inhibitors in nicotine addiction.

Addiction, or rather drug use disorder, is a complex disease that is characterized by different temporally discrete phases equally contributing to the definition of the pathology. Koob and Volkow (2010) hypothesized that drug addiction features three pivotal stages: binge/intoxication, withdrawal/negative affect, and preoccupation/anticipation (craving). Each of these phases depend upon different brain areas that undergo profound plasticity and adaptations. Animal models of addiction proved to be very useful to unravel the neurobiology that lies behind this complex disorder. There are plenty of behavioral approaches suitable to investigate the basic mechanism of drug addiction as well as testing approaches to ameliorate it. In the present study, we employed a behavioral paradigm called CPP commonly used to assess reinforcing and/or aversive properties of stimuli, including drugs of abuse (Tzschentke, 2007). CPP takes advantage of a Pavlovian conditioning where the animal passively receives a drug (nicotine in our case) and is placed in one of two chambers

of the CPP apparatus. This apparatus consists of two compartments that differs with visual and tactile cues. The rodent will associate the cues with the stimulus and the test day it will be free to explore both chambers. The time spent in the drug-paired compartment will be used as an indirect measure of how the stimulus has been reinforcing (and therefore rewarding). In our specific case, we sought to assess whether NAAA inhibition could counteract the rewarding properties of nicotine. Consistent with neurochemical and electrophysiological results, AM11095 reduced the expression of nicotine-induced CPP, without inducing CPP *per se*.

Part III – NAAA inhibition reduces the development of morphine antinociceptive tolerance

In the third part of the thesis we examined the influence of AM11095 on the acute and chronic effects of morphine on the LC. This nucleus is very sensitive to endogenous and exogenous opioids as it expresses high density of MOR (Aghajanian, 1978; Andrade et al., 1983), and consistently responds to noxious stimuli (Cedarbaum & Aghajanian, 1977; Hirata & Aston-Jones, 1994; Muntoni et al., 2006). Besides, LC neurons have been widely implicated in opioid dependence and withdrawal, and acute opioid exposure dampens the firing rate of rodent LC neurons and their cAMP-mediated signaling.

We first replicated the finding that morphine blunts the late response of the LC to Fs (Hirata & Aston-Jones, 1996); then, we tested whether AM11095 administration could influence acute and chronic morphine effects on these neurons. Intriguingly, acute administration of the NAAA inhibitor potentiated morphine-mediated inhibition of the LC neuron late response to the noxious stimulus (i.e. Fs), suggesting that AM11095 might indeed enhance morphine antinociceptive effects. Moreover, whereas LC NE cells recorded from animals treated with vehicle and morphine became tolerant to this opioid after 5 day, a sub-chronic treatment of AM11095 in combination with morphine preserved the inhibitory effect of morphine on the response to Fs. Importantly, AM11095 did not have any effect *per se* since it did not affect either the nociceptive response of LC NE neurons, or their basal spontaneous activity, or its reduction upon morphine injection. Overall, our study demonstrates that AM11095 administration i) acutely potentiates morphine antinociceptive properties and ii) delays the development of antinociceptive tolerance.

Although it is well established the therapeutic efficacy of pain relief medications that target the noradrenergic system (Obata, 2017), it is still not clear the physiological role of NE brain centers on nociception (Taylor & Westlund, 2017). Different studies suggest that LC has a minimal role in conditions of “no pain” (i.e. in modulating acute pain) (Hayashida, Peters, Gutierrez, & Eisenach, 2012; Jasmin, Boudah, & Ohara, 2003; W. J. Martin, Gupta, Loo, Rohde, & Basbaum, 1999; Pertovaara, 2013; West, Yeomans, & Proudfit, 1993), while there are contrasting evidence regarding its implication in chronic pain (Llorca-Torralba et al., 2016). It has been suggested that in this condition, descending NE

projections to the spinal cord show a reduction of the ability to suppress nociceptive transmission (Tsuruoka, Matsutani, & Inoue, 2003; M. Tsuruoka & W. D. Willis, 1996; M. Tsuruoka & W. D. Willis, Jr., 1996; Wei, Dubner, & Ren, 1999), ability that can be restored by drugs activating NE receptors (Obata, 2017). By contrast, Martin et al. (1999) and Taylor et al. (2000) found that the selective destruction of NE neurons reduced, rather than increase, formalin-induced nociception. A possible explanation for these results can be rely on the fact that there is growing evidence to suggest that descending and ascending projections from the LC might contribute to an opposing facilitation of neuropathic pain, particularly at later time points after nerve injury (Brightwell & Taylor, 2009; Kaushal et al., 2016). Moreover, activation of ascending projection to cortical areas such as PFC can instead facilitate pain sensitivity (Kaushal et al., 2016). Within this framework, Pickering and colleagues hypothesized that the pro-nociceptive actions of the LC may be mediated by a subset of neurons that are also responsible for promoting arousal, wakefulness and attention (Carter et al., 2010), as part of a system to focus cognitive resources (Aston-Jones & Cohen, 2005; Hickey et al., 2014).

On the other hand, it seems clearer the role of LC NA neurons in opiate physical dependence and withdrawal. In fact, it is well known that acute binding of opioids to the MOR decreases the pacemaker activity of LC neurons (Torrecilla et al., 2002; J. T. Williams et al., 1982), thus promoting cellular adaptations that after chronic opiate administration result in an increased LC neuronal activity due, among other mechanisms, to an upregulation of the cAMP pathway (Akaoka & Aston-Jones, 1991; Rasmussen, Beitner-Johnson, Krystal, Aghajanian, & Nestler, 1990). These cellular maladaptations are responsible for contributing to dependence and physical symptoms of withdrawal, including hyperalgesia (Aghajanian, 1978; Lane-Ladd et al., 1997; R. Maldonado, Stinus, Gold, & Koob, 1992; Punch, Self, Nestler, & Taylor, 1997; Rasmussen et al., 1990; M. Tsuruoka & W. D. Willis, Jr., 1996; M. Tsuruoka & W. D. J. B. r. Willis, 1996).

In our hands, acute morphine administration reduced the spontaneous discharge rate of LC NE neurons in control rats as previously reported in the literature. On the other hand, in chronically morphine-treated rats (5 days) we did not observe changes in the spontaneous activity, response to FS nor to morphine-induced inhibition of firing rate. Contrarily to other findings, our results suggest that our treatment schedule was not sufficient to induce cellular adaptations in LC neurons. For example, Abdollahi and collegues (2016) reported that a 6-day treatment (with our same dose and route of administration) was effective in increasing the basal spontaneous activity of LC neurons and affected the ability of a subsequent injection of morphine to acutely reduce their firing rate. Other studies reported similar results (Fakhari, Azizi, & Semnanian, 2017; Oh, Eun, Kwon, Cho, & Kim, 2007), however they used different treatment schedules and took advantage of dissimilar readouts to measure morphine's effects.

Importantly, we found that the only parameter affected by chronic morphine treatment was the ability of the drug to reduce the response of LC neurons to the nociceptive stimulus generated by the FS. Two studies carried out by Hirata and Aston-Jones (1994;1996) have thoroughly characterized the response of the LC to the FS in anesthetized rats employing single-unit electrophysiological recordings. Their findings highlight how NA neurons phasically respond to the FS with an excitation, and how the duration of the excitation is positively correlated to the duration of the stimulus. Thus, a FS lasting 5 ms evokes a longer response compared to a FS lasting 0.2 or 2 ms. Importantly, they demonstrated that the response evoked at 5 ms, also called late response, is mediated by the slow nociceptive C-fibers of the sciatic nerve (Hirata & Aston-Jones, 1994). In the following study, it was also shown that the response of LC to the FS can be negatively modulated by morphine (Hirata & Aston-Jones, 1996). In particular, the authors evidenced that an analgesic dose of morphine (1 mg/kg i.v.) successfully attenuated only the late phase, namely the one depending on the noxious information carried by peripheral C-fibers (Hirata & Aston-Jones, 1994). In our experimental setting we were able to replicate the finding on morphine effectiveness in blunting the LC late response to FS, even though we observed a small time shift probably because of the different anesthetic used (urethane vs. alothane).

Even though we did not observe a difference in basal spontaneous discharge, response to FS or morphine property to inhibit the firing rate of LC neurons in chronically morphine-treated rats, we found that in these animals the opioid lost its ability to reduce the late phase. An interpretation of this result might be that LC *per se* did not undergo to profound cellular adaptation while, on the other hand, upstream relay areas, such as the DH in the spinal cord might be responsible for tolerance to morphine. Indeed, a study conducted by Di Cesare Mannelli and collegues (2015) reveals how a similar treatment schedule (morphine 10 mg/kg s.c.) profoundly affects glial cells in the DH and might, therefore, be responsible for the development of tolerance to morphine's antinociceptive effects. It is also plausible that chronic exposure to morphine impacts brain structures at different stages, as suggested by the fact that tolerance to analgesia and reward develops faster than tolerance to respiratory depression (Hill et al., 2016; Ling et al., 1989).

These findings support the LC as an ideal target to study the potential efficacy of the NAAA inhibitor , in enhancing the effects of morphine in a neurophysiological correlate of analgesia and delay the onset of tolerance. Our principal hypothesis is based on the evidence collected by Di Cesare Mannelli and colleagues (2015;2018) that suggested how PEA is able to delay the development of tolerance to morphine antinociception and potentiate its acute analgesic effects in the paw-pressure test. Thus, our strategy took advantage of the NAAA inhibitor to increase PEA brain levels; we evaluated both its acute properties and after a chronic co-administration with morphine.

We found that acute inhibition of NAAA did not alter the spontaneous properties of LC as well as its response to morphine injection or the response to FS. Moreover, when AM11095 was co-administered with morphine during the 5 day treatment, it did not display any influence on the basal properties of NE neurons. These findings are comparable to those obtained by previous studies showing that PEA lacked of antinociceptive effect *per se* (Di Cesare Mannelli, Corti, et al., 2015; Di Cesare Mannelli et al., 2018). In fact, it is well established how this NAE can exert analgesic effects in chronic inflammation (De Filippis et al., 2011), and chronic or neuropathic pain (Bettoni et al., 2013; Costa et al., 2008; Di Cesare Mannelli et al., 2013; Luongo et al., 2013). Therefore, it is plausible that, in our conditions, an indirect agonism of PEA functions (via the NAAA inhibitor AM11095) could not display antinociceptive properties because it mostly acts via regulation of persistent inflammatory processes (Di Cesare Mannelli et al., 2013).

Importantly, AM11095 acutely increased the ability of the opioid to reduce the late phase evoked by the FS and revealed to be effective on reducing the development of antinociceptive tolerance to morphine after 5 days of treatment. It is not known why NAAA inhibition influences only morphine's effects on the response to FS, but not the basal electrophysiological properties of LC. One hypothesis is that PPARα might regulate intracellular pathways downstream to MOR activation. Indeed, evidence suggests that PPARα is expressed in brain areas important for the antinociceptive effects of morphine, such as spinal cord (Benani, Heurtaux, Netter, & Minn, 2004; Lo Verme et al., 2005) and PAG (de Novellis et al., 2012), while there are no studies reporting its presence in the LC, even though we cannot exclude it.

Indeed, we can speculate that PPARα could directly interact with MOR function or with neurons expressing the receptors. It is plausible that NAAA inhibition might lead to PPARα-mediated genomic or non-genomic effects that influence MOR density, its interaction with G-proteins, or also desensitization-initiating proteins such as GSKs, β-arrestins or PKA.

A similar mechanism could account also for the delay of tolerance development. Morphine is defined as a non-internalizing opioid in contrast to the internalizing ones belonging, for example, to the family of fentanyl (John T Williams et al., 2013). In fact, morphine act as a biased-ligand to the MOR and does not activate its internalization and recycle, leading to the assumption that this is the reason behind the more rapid tolerance (Dang & Christie, 2012; Keith et al., 1996). Therefore, it is possible that PPARα activation could facilitate MOR recycling, therefore leaving more receptors ready to respond to a subsequent morphine administration. However, the precise mechanism remains to be elucidated.

Another possible explanation could be related to the idea that tolerance might also lie on the activation of glial cells. Astrocytes and microglia cells are activated by opioids and this ultimately leads to increase excitability of PAG and DH neurons, a mechanism that opposes opioid acute and chronic antinociceptive properties (Yu Cui et al., 2006; Y. Cui et al., 2008; Di Cesare Mannelli, Corti, et al., 2015;

Di Cesare Mannelli, Marcoli, et al., 2015; Mark R Hutchinson et al., 2008; P. Song & Z.-Q. J. N. r. Zhao, 2001). It has been shown that opioid exposure produces the activation of p38-MAPK, PI3k and NfKB causing the release of proinflammatory cytokine from glial cells (Eidson et al., 2017; Hansson & Rönnbäck, 1995; Nakamoto et al., 2012; Watkins et al., 2009). For example, they secrete large cytokines such as interleukin-1β (IL-1β), IL-6, and TNF-α, ATP, and nitric oxide (NO), contributing to the development of tolerance (Berrios, Castro, & Kuffler, 2008). This event seems to be primed by TLR4 activation in the spinal cord (Wang et al., 2012), and activation of TLR4 signaling can induce "naïve tolerance" to opioids (Eidson & Murphy, 2013; Peter M Grace, Maier, Watkins, & Pain, 2015). The importance of glia involvement is highlighted by the evidence that the reduction of the antinociceptive effect of morphine can be reversed by inhibition of glial metabolism, antagonism of IL-1 receptors, and induction of anti-inflammatory cytokine IL-10 expression (Johnston et al., 2004). PPARα controls transcriptional programs involved in the development of inflammation through mechanisms that include direct interactions with the proinflammatory transcription factors NF-kB and AP1 and modulation of IkB function (Glass & Ogawa, 2006; Lefebvre et al., 2006). PPARα activation can also upregulate the expression of IL-1 receptor antagonist (IL-1ra), an inhibitor of cytokine signaling (Stienstra, Duval, Müller, & Kersten, 2007). Therefore, we can speculate that the NAAA inhibitor acts through enhancing PEA/PPARα signaling and activating its anti-inflammatory properties which, in turn, might dampen the activation of glial cells. Studies from di Cesare Mannelli (Di Cesare Mannelli, Corti, et al., 2015; Di Cesare Mannelli et al., 2018; Di Cesare Mannelli, Pacini, et al., 2015) have highlighted the ability of PEA to reduce morphine tolerance and to reduce microglia-mediated inflammation in the spinal cord. The effect of PPARα could lie on reducing the expression of NFkB or IL-1, two pathways that are oppositely regulated by PPARα and opiates.

In summary, even though we must consider the possibility that PPARα activation can influence MOR directly, different clues encourage us to speculate that a deactivation of glial cells on the DH might be responsible for the AM11095 effects.

In alternative, we cannot exclude that our results can be also explained by the "entourage effect hypothesis". This theory has been proposed to justify pharmacological actions of PEA (Di Cesare Mannelli, Corti, et al., 2015) and it is based on an enhancement of AEA activity (Calignano, La Rana, Giuffrida, & Piomelli, 1998). PEA could have indirect effects on TRPV1 and CB1 receptors (Skaper, Facci, & Giusti, 2013) through potentiating AEA affinity, or by inhibiting its metabolic degradation (Smart, Jonsson, Vandevoorde, Lambert, & Fowler, 2002). There is evidence that cannabinoids can have a role on morphine tolerance and dependence (Navarro et al., 1998; Viganò et al., 2004) by reducing its development (Smith, Selley, Sim-Selley, & Welch, 2007). It is also believed that AEA reduces the release of proinflammatory molecules, including IL-1β, TNF-α, and NO (Cabral & Griffin-Thomas, 2009; Molina-Holgado, Lledó, & Guaza, 1997), and enhances the release of the anti-inflammatory cytokines IL-4 and

IL-10 (Klein et al. 2000). In addition, AEA can reduce the release of TNF-α from astrocytes (Molina-Holgado et al., 1997) and, by CB2 receptor stimulation, it attenuates morphine-induced microglial proinflammatory mediator increases, interfering with morphine effect by acting on the Akt-ERK1/2 signalling pathway (Merighi et al., 2012).

5. CONCLUSION

In conclusion, the results of this thesis show that NAAA inhibition by AM11095, via increasing brain PEA and OEA levels, is able to reduce nicotine rewarding properties and to ameliorate morphine antinociceptive effects.

The studies carried out for my thesis belongs to a research line that originated with the discovery that PPARα negatively modulates nAChRs (Melis et al 2008). Since then, different studies were conducted in order to take advantage of this mechanism and to reduce nicotine rewarding properties employing different pharmacological approaches (Justinova et al., 2015; Luchicchi et al., 2010; Mascia et al., 2011; M. Melis et al., 2010; Panlilio et al., 2012). The novelty of the present research relies on the fact that we employed a different pharmacological strategy, which targeted NAAA in order to increase brain levels of OEA and PEA, without affecting AEA levels. We believe that this approach represents a finer and more effective way to activate PPARα as compared with direct agonists, since it conforms with temporal and spatial resolution of endogenous NAE signalling. Moreover, given that PPARα has diverse short-and long effects, involving non genomic regulations of synaptic transmission or gene transcription, respectively, our studies have explored its potential also in other conditions such as depression (Scheggi et al., 2016), epilepsy (Puligheddu et al., 2017; Sagheddu et al., 2015) and neurodevelopmental disorders (De Felice et al., 2019).

In the second part of the present doctoral project, in view of the recent data suggesting that PEA can reduce glia activation upon morphine administration, we have investigated the potential effects of the NAEs/PPARα system on the antinociceptive properties of morphine.

Overall, the general take home message of my thesis is that a fine modulation of PPARα and NAEs activity is a promising pharmacological approach that can be further explored in order to reach therapeutic applications. We have collected evidence that these novel compounds might be effective for nicotine dependence and as add on medications in opioid analgesia. In fact, although behavioral and pharmacological options for smoking cessation are available, the rate of success is still poor and there is a need for novel treatments. Moreover, while opioids are very efficacious to manage pain, their long-term use is hampered by a rapid development of tolerance.

Despite the cellular mechanisms by which NAEs/PPARα interact with nAChRs has been very well characterized, how this signaling system affects opioids' actions has not been determined yet.

Nevertheless, NAAA inhibitors represent a novel class of medications that show promise as therapeutic options in neuropsychiatric disorders.

6. ACKNOWLEDGMENTS

I gratefully acknowledge Sardinian Regional Government for the financial support of the PhD scholarship (P.O.R. Sardegna F.S.E. - Operational Programme of the Autonomous Region of Sardinia, European Social Fund 2014-2020 - Axis III Education and training, Thematic goal 10, Investment Priority 10ii). I wish to thank all the people that participated to this project, starting from the group of Prof. Alexandros Makriyannis, who synthetized the compound and carried out precious experiments.
I would like to thank also the group of Prof. Paola Fadda for providing crucial neurochemical and behavioral data. A special thank goes to Claudia Sagheddu and Michele Santoni, who contributed greatly with experimental, technical and daily emotional support throughout all my doctoral period. Thanks also to Prof. Miriam Melis and Valeria Serra, friendly companions during my PhD journey.
I want to thank my co-supervisor Anna Lisa Muntoni, whose precious help and support never faded. Finally, I wish to thank my supervisor Prof. Marco Pistis, who welcomed me in his laboratory and gave me the opportunity to work on this project. Under his wing, I have matured and grown up.

7. BIBLIOGRAPHY

Abdollahi, H., Ghaemi-Jandabi, M., Azizi, H., & Semnanian, S. (2016). The role of orexin type-1 receptors in the development of morphine tolerance in locus coeruleus neurons: An electrophysiological perspective. *Brain Res, 1646*, 91-97. doi:10.1016/j.brainres.2016.05.043

Aghajanian, G. K. (1978). Tolerance of locus coeruleus neurones to morphine and suppression of withdrawal response by clonidine. *Nature, 276*(5684), 186-188. doi:10.1038/276186a0

Akaoka, H., & Aston-Jones, G. (1991). Opiate withdrawal-induced hyperactivity of locus coeruleus neurons is substantially mediated by augmented excitatory amino acid input. *J Neurosci, 11*(12), 3830-3839.

Alba-Delgado, C., Mico, J. A., Sánchez-Blázquez, P., & Berrocoso, E. J. P. (2012). Analgesic antidepressants promote the responsiveness of locus coeruleus neurons to noxious stimulation: implications for neuropathic pain. *153*(7), 1438-1449.

Alhouayek, M., Bottemanne, P., Makriyannis, A., & Muccioli, G. G. (2017). N-acylethanolamine-hydrolyzing acid amidase and fatty acid amide hydrolase inhibition differentially affect N-acylethanolamine levels and macrophage activation. *Biochim Biophys Acta Mol Cell Biol Lipids, 1862*(5), 474-484. doi:10.1016/j.bbalip.2017.01.001

Alhouayek, M., Bottemanne, P., Subramanian, K. V., Lambert, D. M., Makriyannis, A., Cani, P. D., & Muccioli, G. G. J. T. F. J. (2014). N-Acylethanolamine-hydrolyzing acid amidase inhibition increases colon N-palmitoylethanolamine levels and counteracts murine colitis. *29*(2), 650-661.

Andrade, R., Vandermaelen, C. P., & Aghajanian, G. K. (1983). Morphine tolerance and dependence in the locus coeruleus: single cell studies in brain slices. *Eur J Pharmacol, 91*(2-3), 161-169. doi:10.1016/0014-2999(83)90461-2

Arnsten, A. F., & Goldman-Rakic, P. S. (1984). Selective prefrontal cortical projections to the region of the locus coeruleus and raphe nuclei in the rhesus monkey. *Brain Res, 306*(1-2), 9-18. doi:10.1016/0006-8993(84)90351-2

Arout, C. A., Edens, E., Petrakis, I. L., & Sofuoglu, M. J. C. d. (2015). Targeting opioid-induced hyperalgesia in clinical treatment: neurobiological considerations. *29*(6), 465-486.

Aston-Jones, G., & Bloom, F. E. (1981). Activity of norepinephrine-containing locus coeruleus neurons in behaving rats anticipates fluctuations in the sleep-waking cycle. *J Neurosci, 1*(8), 876-886.

Aston-Jones, G., & Cohen, J. D. (2005). An integrative theory of locus coeruleus-norepinephrine function: adaptive gain and optimal performance. *Annu Rev Neurosci, 28*, 403-450. doi:10.1146/annurev.neuro.28.061604.135709

Auboeuf, D., Rieusset, J., Fajas, L., Vallier, P., Frering, V., Riou, J. P., . . . Vidal, H. J. D. (1997). Tissue distribution and quantification of the expression of mRNAs of peroxisome proliferator–activated receptors and liver X receptor-α in humans: no alteration in adipose tissue of obese and NIDDM patients. *46*(8), 1319-1327.

Babb, S. (2017). Quitting smoking among adults—United States, 2000–2015. *65*.

Bachur, N. R., Masek, K., Melmon, K. L., & Udenfriend, S. (1965). FATTY ACID AMIDES OF ETHANOLAMINE IN MAMMALIAN TISSUES. *J Biol Chem, 240*, 1019-1024.

Bagley, E. E., Chieng, B. C., Christie, M. J., & Connor, M. (2005). Opioid tolerance in periaqueductal gray neurons isolated from mice chronically treated with morphine. *Br J Pharmacol, 146*(1), 68-76. doi:10.1038/sj.bjp.0706315

Balvers, M. G., Verhoeckx, K. C., Plastina, P., Wortelboer, H. M., Meijerink, J., & Witkamp, R. F. (2010). Docosahexaenoic acid and eicosapentaenoic acid are converted by 3T3-

L1 adipocytes to N-acyl ethanolamines with anti-inflammatory properties. *Biochim Biophys Acta, 1801*(10), 1107-1114. doi:10.1016/j.bbalip.2010.06.006
Bayer, V. E., & Pickel, V. M. J. B. r. (1991). GABA-labeled terminals form proportionally more synapses with dopaminergic neurons containing low densities of tyrosine hydroxylase-immunoreactivity in rat ventral tegmental area. *559*(1), 44-55.
Beier, K. T., Steinberg, E. E., DeLoach, K. E., Xie, S., Miyamichi, K., Schwarz, L., . . . Luo, L. J. C. (2015). Circuit architecture of VTA dopamine neurons revealed by systematic input-output mapping. *162*(3), 622-634.
Benani, A., Heurtaux, T., Netter, P., & Minn, A. J. N. l. (2004). Activation of peroxisome proliferator-activated receptor alpha in rat spinal cord after peripheral noxious stimulation. *369*(1), 59-63.
Benarroch, E. (2018). Locus coeruleus. *373*(1), 221-232.
Benowitz, N. L. (2010). Nicotine addiction. *N Engl J Med, 362*(24), 2295-2303. doi:10.1056/NEJMra0809890
Berger, J., & Moller, D. E. (2002). The mechanisms of action of PPARs. *Annu Rev Med, 53*, 409-435. doi:10.1146/annurev.med.53.082901.104018
Berridge, C. W., & Foote, S. L. (1991). Effects of locus coeruleus activation on electroencephalographic activity in neocortex and hippocampus. *J Neurosci, 11*(10), 3135-3145.
Berridge, C. W., & Waterhouse, B. D. (2003). The locus coeruleus-noradrenergic system: modulation of behavioral state and state-dependent cognitive processes. *Brain Res Brain Res Rev, 42*(1), 33-84.
Berridge, K. C., & Robinson, T. E. (1998). What is the role of dopamine in reward: hedonic impact, reward learning, or incentive salience? *Brain Res Brain Res Rev, 28*(3), 309-369.
Berrios, I., Castro, C., & Kuffler, D. P. J. P. R. h. s. j. (2008). Morphine: axon regeneration, neuroprotection, neurotoxicity, tolerance, and neuropathic pain. *27*(2).
Bettoni, I., Comelli, F., Colombo, A., Bonfanti, P., Costa, B. J. C., & Targets, N. D.-D. (2013). Non-neuronal cell modulation relieves neuropathic pain: efficacy of the endogenous lipid palmitoylethanolamide. *12*(1), 34-44.
Björklund, A., & Dunnett, S. B. J. T. i. n. (2007). Dopamine neuron systems in the brain: an update. *30*(5), 194-202.
Bobeck, E. N., Chen, Q., Morgan, M. M., & Ingram, S. L. (2014). Contribution of adenylyl cyclase modulation of pre- and postsynaptic GABA neurotransmission to morphine antinociception and tolerance. *Neuropsychopharmacology, 39*(9), 2142-2152. doi:10.1038/npp.2014.62
Bobeck, E. N., McNeal, A. L., & Morgan, M. M. (2009). Drug dependent sex-differences in periaqueducatal gray mediated antinociception in the rat. *Pain, 147*(1-3), 210-216. doi:10.1016/j.pain.2009.09.008
Bonezzi, F. T., Sasso, O., Pontis, S., Realini, N., Romeo, E., Ponzano, S., . . . Piomelli, D. (2016). An Important Role for N-Acylethanolamine Acid Amidase in the Complete Freund's Adjuvant Rat Model of Arthritis. *J Pharmacol Exp Ther, 356*(3), 656-663. doi:10.1124/jpet.115.230516
Bonica, J. J. (1979). The need of a taxonomy. *Pain, 6*(3), 247-248.
Bottemanne, P., Muccioli, G. G., & Alhouayek, M. J. D. d. t. (2018). N-acylethanolamine hydrolyzing acid amidase inhibition: Tools and potential therapeutic opportunities. *23*(8), 1520-1529.
Bouaboula, M., Hilairet, S., Marchand, J., Fajas, L., Le Fur, G., & Casellas, P. (2005). Anandamide induced PPARgamma transcriptional activation and 3T3-L1 preadipocyte differentiation. *Eur J Pharmacol, 517*(3), 174-181. doi:10.1016/j.ejphar.2005.05.032

Bougarne, N., Paumelle, R., Caron, S., Hennuyer, N., Mansouri, R., Gervois, P., . . . De Bosscher, K. (2009). PPARalpha blocks glucocorticoid receptor alpha-mediated transactivation but cooperates with the activated glucocorticoid receptor alpha for transrepression on NF-kappaB. *Proc Natl Acad Sci U S A, 106*(18), 7397-7402. doi:10.1073/pnas.0806742106

Braissant, O., Foufelle, F., Scotto, C., Dauça, M., & Wahli, W. J. E. (1996). Differential expression of peroxisome proliferator-activated receptors (PPARs): tissue distribution of PPAR-alpha,-beta, and-gamma in the adult rat. *137*(1), 354-366.

Brightwell, J. J., & Taylor, B. K. (2009). Noradrenergic neurons in the locus coeruleus contribute to neuropathic pain. *Neuroscience, 160*(1), 174-185. doi:10.1016/j.neuroscience.2009.02.023

Cabral, G. A., & Griffin-Thomas, L. J. E. r. i. m. m. (2009). Emerging role of the cannabinoid receptor CB 2 in immune regulation: therapeutic prospects for neuroinflammation. *11*.

Cahill, C. M., & Taylor, A. M. J. C. o. i. b. s. (2017). Neuroinflammation—a co-occurring phenomenon linking chronic pain and opioid dependence. *13*, 171-177.

Calignano, A., La Rana, G., Giuffrida, A., & Piomelli, D. J. N. (1998). Control of pain initiation by endogenous cannabinoids. *394*(6690), 277.

Carter, M. E., Yizhar, O., Chikahisa, S., Nguyen, H., Adamantidis, A., Nishino, S., . . . de Lecea, L. (2010). Tuning arousal with optogenetic modulation of locus coeruleus neurons. *Nat Neurosci, 13*(12), 1526-1533. doi:10.1038/nn.2682

Cedarbaum, J. M., & Aghajanian, G. K. (1977). Catecholamine receptors on locus coeruleus neurons: pharmacological characterization. *Eur J Pharmacol, 44*(4), 375-385. doi:10.1016/0014-2999(77)90312-0

Chandler, D. J., Jensen, P., McCall, J. G., Pickering, A. E., Schwarz, L. A., & Totah, N. K. (2019). Redefining Noradrenergic Neuromodulation of Behavior: Impacts of a Modular Locus Coeruleus Architecture. *J Neurosci, 39*(42), 8239-8249. doi:10.1523/jneurosci.1164-19.2019

Changeux, J. P. (2010). Nicotine addiction and nicotinic receptors: lessons from genetically modified mice. *Nat Rev Neurosci, 11*(6), 389-401. doi:10.1038/nrn2849

Charpantier, E., Wiesner, A., Huh, K.-H., Ogier, R., Hoda, J.-C., Allaman, G., . . . Fuhrer, C. J. J. o. N. (2005). α7 neuronal nicotinic acetylcholine receptors are negatively regulated by tyrosine phosphorylation and Src-family kinases. *25*(43), 9836-9849.

Chinetti, G., Griglio, S., Antonucci, M., Torra, I. P., Delerive, P., Majd, Z., . . . Staels, B. J. J. o. B. C. (1998). Activation of proliferator-activated receptors α and γ induces apoptosis of human monocyte-derived macrophages. *273*(40), 25573-25580.

Cho, C.-H., Song, W., Leitzell, K., Teo, E., Meleth, A. D., Quick, M. W., & Lester, R. A. J. J. o. N. (2005). Rapid upregulation of α7 nicotinic acetylcholine receptors by tyrosine dephosphorylation. *25*(14), 3712-3723.

Corrigall, W. A., Coen, K. M., & Adamson, K. L. J. B. r. (1994). Self-administered nicotine activates the mesolimbic dopamine system through the ventral tegmental area. *653*(1-2), 278-284.

Cortazzo, M. H., Copenhaver, D. J., & Fishman, S. M. (2013). Major opioids and chronic opioid therapy. In *Practical Management of Pain: Fifth Edition* (pp. 495-507): Elsevier Inc.

Costa, B., Comelli, F., Bettoni, I., Colleoni, M., & Giagnoni, G. J. P. (2008). The endogenous fatty acid amide, palmitoylethanolamide, has anti-allodynic and anti-hyperalgesic effects in a murine model of neuropathic pain: involvement of CB1, TRPV1 and PPARγ receptors and neurotrophic factors. *139*(3), 541-550.

Cravatt, B. F., Demarest, K., Patricelli, M. P., Bracey, M. H., Giang, D. K., Martin, B. R., & Lichtman, A. H. (2001). Supersensitivity to anandamide and enhanced endogenous

cannabinoid signaling in mice lacking fatty acid amide hydrolase. *Proc Natl Acad Sci U S A, 98*(16), 9371-9376. doi:10.1073/pnas.161191698

Cravatt, B. F., Giang, D. K., Mayfield, S. P., Boger, D. L., Lerner, R. A., & Gilula, N. B. (1996). Molecular characterization of an enzyme that degrades neuromodulatory fatty-acid amides. *Nature, 384*(6604), 83-87. doi:10.1038/384083a0

Cui, Y., Chen, Y., Zhi, J.-L., Guo, R.-X., Feng, J.-Q., & Chen, P.-X. J. B. r. (2006). Activation of p38 mitogen-activated protein kinase in spinal microglia mediates morphine antinociceptive tolerance. *1069*(1), 235-243.

Cui, Y., Liao, X. X., Liu, W., Guo, R. X., Wu, Z. Z., Zhao, C. M., . . . Feng, J. Q. (2008). A novel role of minocycline: attenuating morphine antinociceptive tolerance by inhibition of p38 MAPK in the activated spinal microglia. *Brain Behav Immun, 22*(1), 114-123. doi:10.1016/j.bbi.2007.07.014

Cuzzocrea, S., Bruscoli, S., Mazzon, E., Crisafulli, C., Donato, V., Di Paola, R., . . . Riccardi, C. (2008). Peroxisome proliferator-activated receptor-alpha contributes to the anti-inflammatory activity of glucocorticoids. *Mol Pharmacol, 73*(2), 323-337. doi:10.1124/mol.107.041475

Dang, V. C., & Christie, M. J. J. B. j. o. p. (2012). Mechanisms of rapid opioid receptor desensitization, resensitization and tolerance in brain neurons. *165*(6), 1704-1716.

Dani, J. A., & Bertrand, D. J. A. R. P. T. (2007). Nicotinic acetylcholine receptors and nicotinic cholinergic mechanisms of the central nervous system. *47*, 699-729.

De Felice, M., Melis, M., Aroni, S., Muntoni, A. L., Fanni, S., Frau, R., . . . Pistis, M. (2019). The PPARalpha agonist fenofibrate attenuates disruption of dopamine function in a maternal immune activation rat model of schizophrenia. *CNS Neurosci Ther, 25*(5), 549-561. doi:10.1111/cns.13087

De Filippis, D., Luongo, L., Cipriano, M., Palazzo, E., Cinelli, M. P., de Novellis, V., . . . Iuvone, T. J. M. p. (2011). Palmitoylethanolamide reduces granuloma-induced hyperalgesia by modulation of mast cell activation in rats. *7*(1), 3.

de Novellis, V., Luongo, L., Guida, F., Cristino, L., Palazzo, E., Russo, R., . . . Rossi, F. J. E. j. o. p. (2012). Effects of intra-ventrolateral periaqueductal grey palmitoylethanolamide on thermoceptive threshold and rostral ventromedial medulla cell activity. *676*(1-3), 41-50.

De Petrocellis, L., Starowicz, K., Moriello, A. S., Vivese, M., Orlando, P., & Di Marzo, V. (2007). Regulation of transient receptor potential channels of melastatin type 8 (TRPM8): effect of cAMP, cannabinoid CB(1) receptors and endovanilloids. *Exp Cell Res, 313*(9), 1911-1920. doi:10.1016/j.yexcr.2007.01.008

Delerive, P., De Bosscher, K., Besnard, S., Vanden Berghe, W., Peters, J. M., Gonzalez, F. J., . . . Staels, B. (1999). Peroxisome proliferator-activated receptor alpha negatively regulates the vascular inflammatory gene response by negative cross-talk with transcription factors NF-kappaB and AP-1. *J Biol Chem, 274*(45), 32048-32054. doi:10.1074/jbc.274.45.32048

Delerive, P., Gervois, P., Fruchart, J. C., & Staels, B. (2000). Induction of IkappaBalpha expression as a mechanism contributing to the anti-inflammatory activities of peroxisome proliferator-activated receptor-alpha activators. *J Biol Chem, 275*(47), 36703-36707. doi:10.1074/jbc.M004045200

Devane, W. A., Hanus, L., Breuer, A., Pertwee, R. G., Stevenson, L. A., Griffin, G., . . . Mechoulam, R. (1992). Isolation and structure of a brain constituent that binds to the cannabinoid receptor. *Science, 258*(5090), 1946-1949. doi:10.1126/science.1470919

Devchand, P. R., Keller, H., Peters, J. M., Vazquez, M., Gonzalez, F. J., & Wahli, W. (1996). The PPARalpha-leukotriene B4 pathway to inflammation control. *Nature, 384*(6604), 39-43. doi:10.1038/384039a0

DHHS. (2014). The health consequences of smoking—50 years of progress: a report of the Surgeon General. *17*.

Di Cesare Mannelli, L., Corti, F., Micheli, L., Zanardelli, M., & Ghelardini, C. (2015). Delay of morphine tolerance by palmitoylethanolamide. *Biomed Res Int, 2015*, 894732. doi:10.1155/2015/894732

Di Cesare Mannelli, L., D'Agostino, G., Pacini, A., Russo, R., Zanardelli, M., Ghelardini, C., & Calignano, A. (2013). Palmitoylethanolamide is a disease-modifying agent in peripheral neuropathy: pain relief and neuroprotection share a PPAR-alpha-mediated mechanism. *Mediators Inflamm, 2013*, 328797. doi:10.1155/2013/328797

Di Cesare Mannelli, L., Marcoli, M., Micheli, L., Zanardelli, M., Maura, G., Ghelardini, C., & Cervetto, C. (2015). Oxaliplatin evokes P2X7-dependent glutamate release in the cerebral cortex: A pain mechanism mediated by Pannexin 1. *Neuropharmacology, 97*, 133-141. doi:10.1016/j.neuropharm.2015.05.037

Di Cesare Mannelli, L., Micheli, L., Lucarini, E., & Ghelardini, C. (2018). Ultramicronized N-Palmitoylethanolamine Supplementation for Long-Lasting, Low-Dosed Morphine Antinociception. *Front Pharmacol, 9*, 473. doi:10.3389/fphar.2018.00473

Di Cesare Mannelli, L., Pacini, A., Corti, F., Boccella, S., Luongo, L., Esposito, E., . . . Ghelardini, C. (2015). Antineuropathic profile of N-palmitoylethanolamine in a rat model of oxaliplatin-induced neurotoxicity. *PLoS One, 10*(6), e0128080. doi:10.1371/journal.pone.0128080

Di Chiara, G., & Imperato, A. (1988). Drugs abused by humans preferentially increase synaptic dopamine concentrations in the mesolimbic system of freely moving rats. *Proc Natl Acad Sci U S A, 85*(14), 5274-5278. doi:10.1073/pnas.85.14.5274

Donvito, G., Nass, S. R., Wilkerson, J. L., Curry, Z. A., Schurman, L. D., Kinsey, S. G., & Lichtman, A. H. J. N. (2018). The endogenous cannabinoid system: a budding source of targets for treating inflammatory and neuropathic pain. *43*(1), 52.

Downs, J. L., Dunn, M. R., Borok, E., Shanabrough, M., Horvath, T. L., Kohama, S. G., & Urbanski, H. F. (2007). Orexin neuronal changes in the locus coeruleus of the aging rhesus macaque. *Neurobiol Aging, 28*(8), 1286-1295. doi:10.1016/j.neurobiolaging.2006.05.025

Dreyer, C., Krey, G., Keller, H., Givel, F., Helftenbein, G., & Wahli, W. J. C. (1992). Control of the peroxisomal β-oxidation pathway by a novel family of nuclear hormone receptors. *68*(5), 879-887.

DSM-V. (2013). *Diagnostic and statistical manual of mental disorders (DSM-5®)*: American Psychiatric Pub.

Ehlinger, D. G., Bergstrom, H. C., McDonald, C. G., & Smith, R. F. J. N. l. (2012). Nicotine-induced dendritic remodeling in the insular cortex. *516*(1), 89-93.

Eidson, L. N., Inoue, K., Young, L. J., Tansey, M. G., & Murphy, A. Z. (2017). Toll-like Receptor 4 Mediates Morphine-Induced Neuroinflammation and Tolerance via Soluble Tumor Necrosis Factor Signaling. *Neuropsychopharmacology, 42*(3), 661-670. doi:10.1038/npp.2016.131

Eidson, L. N., & Murphy, A. Z. (2013). Blockade of Toll-like receptor 4 attenuates morphine tolerance and facilitates the pain relieving properties of morphine. *J Neurosci, 33*(40), 15952-15963. doi:10.1523/jneurosci.1609-13.2013

Eidson, L. N., & Murphy, A. Z. (2019). Inflammatory mediators of opioid tolerance: Implications for dependency and addiction. *Peptides, 115*, 51-58. doi:10.1016/j.peptides.2019.01.003

Esposito, E., & Cuzzocrea, S. J. M. r. i. m. c. (2013). Palmitoylethanolamide is a new possible pharmacological treatment for the inflammation associated with trauma. *13*(2), 237-255.

Fairbanks, C. A., & Wilcox, G. L. (1997). Acute tolerance to spinally administered morphine compares mechanistically with chronically induced morphine tolerance. *J Pharmacol Exp Ther, 282*(3), 1408-1417.
Fakhari, M., Azizi, H., & Semnanian, S. (2017). Central antagonism of orexin type-1 receptors attenuates the development of morphine dependence in rat locus coeruleus neurons. *Neuroscience, 363*, 1-10. doi:10.1016/j.neuroscience.2017.08.054
Fang, F. G., Haws, C. M., Drasner, K., Williamson, A., & Fields, H. L. (1989). Opioid peptides (DAGO-enkephalin, dynorphin A(1-13), BAM 22P) microinjected into the rat brainstem: comparison of their antinociceptive effect and their effect on neuronal firing in the rostral ventromedial medulla. *Brain Res, 501*(1), 116-128. doi:10.1016/0006-8993(89)91033-0
Ferdinandusse, S., Denis, S., Dacremont, G., & Wanders, R. J. J. J. o. l. r. (2003). Studies on the metabolic fate of n-3 polyunsaturated fatty acids. *44*(10), 1992-1997.
Fiasella, A., Nuzzi, A., Summa, M., Armirotti, A., Tarozzo, G., Tarzia, G., . . . Piomelli, D. J. C. (2014). 3-Aminoazetidin-2-one Derivatives as N-Acylethanolamine Acid Amidase (NAAA) Inhibitors Suitable for Systemic Administration. *9*(7), 1602-1614.
Fiore, M. C., Jaén, C. R., Baker, T. B., Bailey, W. C., Benowitz, N. L., Curry, S. J., . . . Services, H. (2008). Treating tobacco use and dependence: 2008 update.
Fiorino, D. F., & Garcia-Guzman, M. (2012). Muscarinic pain pharmacology: realizing the promise of novel analgesics by overcoming old challenges. *Handb Exp Pharmacol*(208), 191-221. doi:10.1007/978-3-642-23274-9_9
Floresco, S. B., West, A. R., Ash, B., Moore, H., & Grace, A. A. (2003). Afferent modulation of dopamine neuron firing differentially regulates tonic and phasic dopamine transmission. *Nat Neurosci, 6*(9), 968-973. doi:10.1038/nn1103
Folch, J., Lees, M., & Sloane Stanley, G. H. (1957). A simple method for the isolation and purification of total lipides from animal tissues. *J Biol Chem, 226*(1), 497-509.
Forget, B., Coen, K. M., & Le Foll, B. J. P. (2009). Inhibition of fatty acid amide hydrolase reduces reinstatement of nicotine seeking but not break point for nicotine self-administration—comparison with CB 1 receptor blockade. *205*(4), 613-624.
Fu, J., Gaetani, S., Oveisi, F., Lo Verme, J., Serrano, A., Rodriguez De Fonseca, F., . . . Piomelli, D. (2003). Oleylethanolamide regulates feeding and body weight through activation of the nuclear receptor PPAR-alpha. *Nature, 425*(6953), 90-93. doi:10.1038/nature01921
Gauvin, D. V., Zimmermann, Z. J., Dalton, J. A., & Baird, T. J. (2017). Repeated "Day 1" FOB testing in ICH S7A safety assessment protocols: The influence of within- and between-session learning. *J Pharmacol Toxicol Methods, 85*, 61-72. doi:10.1016/j.vascn.2017.02.018
Gebhart, G. F. (2004). Descending modulation of pain. *Neurosci Biobehav Rev, 27*(8), 729-737. doi:10.1016/j.neubiorev.2003.11.008
Ghafouri, N., Ghafouri, B., Larsson, B., Stensson, N., Fowler, C. J., & Gerdle, B. J. P. (2013). Palmitoylethanolamide and stearoylethanolamide levels in the interstitium of the trapezius muscle of women with chronic widespread pain and chronic neck-shoulder pain correlate with pain intensity and sensitivity. *154*(9), 1649-1658.
Gintzler, A. R., & Chakrabarti, S. (2004). Chronic morphine-induced plasticity among signalling molecules. *Novartis Found Symp, 261*, 167-176; discussion 176-180, 191-163.
Giron, S. E., Griffis, C. A., & Burkard, J. F. (2015). Chronic Pain and Decreased Opioid Efficacy: An Inflammatory Link. *Pain Manag Nurs, 16*(5), 819-831. doi:10.1016/j.pmn.2015.04.001
Glass, C. K., & Ogawa, S. J. N. R. I. (2006). Combinatorial roles of nuclear receptors in inflammation and immunity. *6*(1), 44.

Goode, T. L., & Raffa, R. B. (1997). An examination of the relationship between mu-opioid antinociceptive efficacy and G-protein coupling using pertussis and cholera toxins. *Life Sci, 60*(7), Pl107-113. doi:10.1016/s0024-3205(96)00684-4

Gotti, C., Guiducci, S., Tedesco, V., Corbioli, S., Zanetti, L., Moretti, M., . . . Clementi, F. J. J. o. N. (2010). Nicotinic acetylcholine receptors in the mesolimbic pathway: primary role of ventral tegmental area α6β2* receptors in mediating systemic nicotine effects on dopamine release, locomotion, and reinforcement. *30*(15), 5311-5325.

Gould, T. J., Leach, P. T. J. N. o. l., & memory. (2014). Cellular, molecular, and genetic substrates underlying the impact of nicotine on learning. *107*, 108-132.

Grace, A., & Bunney, B. (1984). The control of firing pattern in nigral dopamine neurons: burst firing. *J Journal of neuroscience, 4*(11), 2877-2890.

Grace, A. A., Floresco, S. B., Goto, Y., & Lodge, D. J. (2007). Regulation of firing of dopaminergic neurons and control of goal-directed behaviors. *Trends Neurosci, 30*(5), 220-227. doi:10.1016/j.tins.2007.03.003

Grace, A. A., & Onn, S. (1989). Morphology and electrophysiological properties of immunocytochemically identified rat dopamine neurons recorded in vitro. *Journal of Neuroscience, 9*(10), 3463-3481.

Grace, P. M., Maier, S. F., & Watkins, L. R. (2015). Opioid-induced central immune signaling: implications for opioid analgesia. *Headache, 55*(4), 475-489. doi:10.1111/head.12552

Grace, P. M., Maier, S. F., Watkins, L. R. J. H. T. J. o. H., & Pain, F. (2015). Opioid-induced central immune signaling: implications for opioid analgesia. *55*(4), 475-489.

Guimaraes, A. P., Guimaraes, F. S., & Prado, W. A. (2000). Modulation of carbachol-induced antinociception from the rat periaqueductal gray. *Brain Res Bull, 51*(6), 471-478. doi:10.1016/s0361-9230(99)00266-x

Gulur, P., Williams, L., Chaudhary, S., Koury, K., & Jaff, M. (2014). Opioid tolerance--a predictor of increased length of stay and higher readmission rates. *Pain Physician, 17*(4), E503-507.

Hansson, E., & Rönnbäck, L. J. T. F. j. (1995). Astrocytes in glutamate neurotransmission. *9*(5), 343-350.

Harada, S., Nakamoto, K., & Tokuyama, S. (2013). The involvement of midbrain astrocyte in the development of morphine tolerance. *Life Sci, 93*(16), 573-578. doi:10.1016/j.lfs.2013.08.009

Hayashida, K., Peters, C. M., Gutierrez, S., & Eisenach, J. C. (2012). Depletion of endogenous noradrenaline does not prevent spinal cord plasticity following peripheral nerve injury. *J Pain, 13*(1), 49-57. doi:10.1016/j.jpain.2011.09.009

Hesselink, J. M. (2013). Evolution in pharmacologic thinking around the natural analgesic palmitoylethanolamide: from nonspecific resistance to PPAR-alpha agonist and effective nutraceutical. *J Pain Res, 6*, 625-634. doi:10.2147/jpr.S48653

Hickey, L., Li, Y., Fyson, S. J., Watson, T. C., Perrins, R., Hewinson, J., . . . Pickering, A. E. (2014). Optoactivation of locus ceruleus neurons evokes bidirectional changes in thermal nociception in rats. *J Neurosci, 34*(12), 4148-4160. doi:10.1523/jneurosci.4835-13.2014

Hill, R., Lyndon, A., Withey, S., Roberts, J., Kershaw, Y., MacLachlan, J., . . . Hickman, M. J. N. (2016). Ethanol reversal of tolerance to the respiratory depressant effects of morphine. *41*(3), 762.

Hirata, H., & Aston-Jones, G. J. B. r. (1996). Long-latency responses of brain noradrenergic neurons to noxious stimuli are preferentially attenuated by intravenous morphine. *714*(1-2), 9-18.

Hirata, H., & Aston-Jones, G. J. J. o. n. (1994). A novel long-latency response of locus coeruleus neurons to noxious stimuli: mediation by peripheral C-fibers. *71*(5), 1752-1761.

Holloway, B. B., Stornetta, R. L., Bochorishvili, G., Erisir, A., Viar, K. E., & Guyenet, P. G. (2013). Monosynaptic glutamatergic activation of locus coeruleus and other lower brainstem noradrenergic neurons by the C1 cells in mice. *J Neurosci, 33*(48), 18792-18805. doi:10.1523/jneurosci.2916-13.2013

Hutchinson, M. R., Northcutt, A. L., Chao, L. W., Kearney, J. J., Zhang, Y., Berkelhammer, D. L., . . . immunity. (2008). Minocycline suppresses morphine-induced respiratory depression, suppresses morphine-induced reward, and enhances systemic morphine-induced analgesia. *22*(8), 1248-1256.

Hutchinson, M. R., Shavit, Y., Grace, P. M., Rice, K. C., Maier, S. F., & Watkins, L. R. (2011). Exploring the neuroimmunopharmacology of opioids: an integrative review of mechanisms of central immune signaling and their implications for opioid analgesia. *Pharmacol Rev, 63*(3), 772-810. doi:10.1124/pr.110.004135

Hutchinson, M. R., Zhang, Y., Shridhar, M., Evans, J. H., Buchanan, M. M., Zhao, T. X., . . . Watkins, L. R. (2010). Evidence that opioids may have toll-like receptor 4 and MD-2 effects. *Brain Behav Immun, 24*(1), 83-95. doi:10.1016/j.bbi.2009.08.004

Iannotti, F. A., Di Marzo, V., & Petrosino, S. (2016). Endocannabinoids and endocannabinoid-related mediators: Targets, metabolism and role in neurological disorders. *Prog Lipid Res, 62*, 107-128. doi:10.1016/j.plipres.2016.02.002

Ilango, A., Shumake, J., Wetzel, W., & Ohl, F. W. (2014). Contribution of emotional and motivational neurocircuitry to cue-signaled active avoidance learning. *Front Behav Neurosci, 8*, 372. doi:10.3389/fnbeh.2014.00372

Inoue, I., Shino, K., Noji, S., Awata, T., Katayama, S. J. B., & communications, b. r. (1998). Expression of peroxisome proliferator-activated receptor α (PPARα) in primary cultures of human vascular endothelial cells. *246*(2), 370-374.

Itier, V., & Bertrand, D. (2001). Neuronal nicotinic receptors: from protein structure to function. *FEBS Lett, 504*(3), 118-125. doi:10.1016/s0014-5793(01)02702-8

Jackson, A., Bagdas, D., Muldoon, P. P., Lichtman, A. H., Carroll, F. I., Greenwald, M., . . . Damaj, M. I. J. N. (2017). In vivo interactions between α7 nicotinic acetylcholine receptor and nuclear peroxisome proliferator-activated receptor-α: Implication for nicotine dependence. *118*, 38-45.

Jasmin, L., Boudah, A., & Ohara, P. T. (2003). Long-term effects of decreased noradrenergic central nervous system innervation on pain behavior and opioid antinociception. *J Comp Neurol, 460*(1), 38-55. doi:10.1002/cne.10633

Jhou, T. C., Fields, H. L., Baxter, M. G., Saper, C. B., & Holland, P. C. (2009). The rostromedial tegmental nucleus (RMTg), a GABAergic afferent to midbrain dopamine neurons, encodes aversive stimuli and inhibits motor responses. *Neuron, 61*(5), 786-800. doi:10.1016/j.neuron.2009.02.001

Jin, X. H., Okamoto, Y., Morishita, J., Tsuboi, K., Tonai, T., & Ueda, N. (2007). Discovery and characterization of a Ca2+-independent phosphatidylethanolamine N-acyltransferase generating the anandamide precursor and its congeners. *J Biol Chem, 282*(6), 3614-3623. doi:10.1074/jbc.M606369200

Jin, X. H., Uyama, T., Wang, J., Okamoto, Y., Tonai, T., & Ueda, N. (2009). cDNA cloning and characterization of human and mouse Ca(2+)-independent phosphatidylethanolamine N-acyltransferases. *Biochim Biophys Acta, 1791*(1), 32-38. doi:10.1016/j.bbalip.2008.09.006

Johnston, I. N., Milligan, E. D., Wieseler-Frank, J., Frank, M. G., Zapata, V., Campisi, J., . . . Fleshner, M. J. J. o. N. (2004). A role for proinflammatory cytokines and fractalkine

in analgesia, tolerance, and subsequent pain facilitation induced by chronic intrathecal morphine. *24*(33), 7353-7365.

Justinova, Z., Panlilio, L. V., Moreno-Sanz, G., Redhi, G. H., Auber, A., Secci, M. E., . . . Goldberg, S. R. (2015). Effects of Fatty Acid Amide Hydrolase (FAAH) Inhibitors in Non-Human Primate Models of Nicotine Reward and Relapse. *Neuropsychopharmacology, 40*(9), 2185-2197. doi:10.1038/npp.2015.62

Kaufling, J., Veinante, P., Pawlowski, S. A., Freund-Mercier, M. J., & Barrot, M. (2009). Afferents to the GABAergic tail of the ventral tegmental area in the rat. *J Comp Neurol, 513*(6), 597-621. doi:10.1002/cne.21983

Kaushal, R., Taylor, B. K., Jamal, A. B., Zhang, L., Ma, F., Donahue, R., & Westlund, K. N. (2016). GABA-A receptor activity in the noradrenergic locus coeruleus drives trigeminal neuropathic pain in the rat; contribution of NAalpha1 receptors in the medial prefrontal cortex. *Neuroscience, 334*, 148-159. doi:10.1016/j.neuroscience.2016.08.005

Keith, D. E., Murray, S. R., Zaki, P. A., Chu, P. C., Lissin, D. V., Kang, L., . . . von Zastrow, M. J. J. o. B. C. (1996). Morphine activates opioid receptors without causing their rapid internalization. *271*(32), 19021-19024.

Kim, M. A., Lee, H. S., Lee, B. Y., & Waterhouse, B. D. (2004). Reciprocal connections between subdivisions of the dorsal raphe and the nuclear core of the locus coeruleus in the rat. *Brain Res, 1026*(1), 56-67. doi:10.1016/j.brainres.2004.08.022

Koob, G. F. (2004). Allostatic view of motivation: implications for psychopathology. *Nebr Symp Motiv, 50*, 1-18.

Koob, G. F., & Volkow, N. D. (2010). Neurocircuitry of addiction. *Neuropsychopharmacology, 35*(1), 217-238. doi:10.1038/npp.2009.110

Kornetsky, C., & Bain, G. (1968). Morphine: single-dose tolerance. *Science, 162*(3857), 1011-1012. doi:10.1126/science.162.3857.1011

Kronke, G., Kadl, A., Ikonomu, E., Bluml, S., Furnkranz, A., Sarembock, I. J., . . . Leitinger, N. (2007). Expression of heme oxygenase-1 in human vascular cells is regulated by peroxisome proliferator-activated receptors. *Arterioscler Thromb Vasc Biol, 27*(6), 1276-1282. doi:10.1161/atvbaha.107.142638

Lane-Ladd, S. B., Pineda, J., Boundy, V. A., Pfeuffer, T., Krupinski, J., Aghajanian, G. K., & Nestler, E. J. (1997). CREB (cAMP response element-binding protein) in the locus coeruleus: biochemical, physiological, and behavioral evidence for a role in opiate dependence. *J Neurosci, 17*(20), 7890-7901.

Lecca, S., Melis, M., Luchicchi, A., Ennas, M. G., Castelli, M. P., Muntoni, A. L., & Pistis, M. (2011). Effects of drugs of abuse on putative rostromedial tegmental neurons, inhibitory afferents to midbrain dopamine cells. *Neuropsychopharmacology, 36*(3), 589-602. doi:10.1038/npp.2010.190

Lecca, S., Melis, M., Luchicchi, A., Muntoni, A. L., & Pistis, M. (2012). Inhibitory inputs from rostromedial tegmental neurons regulate spontaneous activity of midbrain dopamine cells and their responses to drugs of abuse. *Neuropsychopharmacology, 37*(5), 1164-1176. doi:10.1038/npp.2011.302

Lee, J. W., Huang, B. X., Kwon, H., Rashid, M. A., Kharebava, G., Desai, A., . . . Kim, H. Y. (2016). Orphan GPR110 (ADGRF1) targeted by N-docosahexaenoylethanolamine in development of neurons and cognitive function. *Nat Commun, 7*, 13123. doi:10.1038/ncomms13123

Lefebvre, P., Chinetti, G., Fruchart, J. C., & Staels, B. (2006). Sorting out the roles of PPAR alpha in energy metabolism and vascular homeostasis. *J Clin Invest, 116*(3), 571-580. doi:10.1172/jci27989

Li, Y., Yang, L., Chen, L., Zhu, C., Huang, R., Zheng, X., . . . Fu, J. J. P. O. (2012). Design and synthesis of potent N-acylethanolamine-hydrolyzing acid amidase (NAAA) inhibitor as anti-inflammatory compounds. *7*(8), e43023.

Ling, G. S., Paul, D., Simantov, R., & Pasternak, G. W. J. L. s. (1989). Differential development of acute tolerance to analgesia, respiratory depression, gastrointestinal transit and hormone release in a morphine infusion model. *45*(18), 1627-1636.

Llorca-Torralba, M., Borges, G., Neto, F., Mico, J. A., & Berrocoso, E. J. N. (2016). Noradrenergic Locus Coeruleus pathways in pain modulation. *338*, 93-113.

Lo Verme, J., Fu, J., Astarita, G., La Rana, G., Russo, R., Calignano, A., & Piomelli, D. (2005). The nuclear receptor peroxisome proliferator-activated receptor-alpha mediates the anti-inflammatory actions of palmitoylethanolamide. *Mol Pharmacol, 67*(1), 15-19. doi:10.1124/mol.104.006353

Lobb, C. J., Wilson, C. J., & Paladini, C. A. J. J. o. n. (2010). A dynamic role for GABA receptors on the firing pattern of midbrain dopaminergic neurons. *104*(1), 403-413.

Luchicchi, A., Lecca, S., Carta, S., Pillolla, G., Muntoni, A. L., Yasar, S., . . . Pistis, M. J. A. b. (2010). Effects of fatty acid amide hydrolase inhibition on neuronal responses to nicotine, cocaine and morphine in the nucleus accumbens shell and ventral tegmental area: involvement of PPAR-α nuclear receptors. *15*(3), 277.

Luchicchi, A., & Pistis, M. J. M. n. (2012). Anandamide and 2-arachidonoylglycerol: pharmacological properties, functional features, and emerging specificities of the two major endocannabinoids. *46*(2), 374-392.

Lueptow, L. M., Fakira, A. K., & Bobeck, E. N. (2018). The Contribution of the Descending Pain Modulatory Pathway in Opioid Tolerance. *Front Neurosci, 12*, 886. doi:10.3389/fnins.2018.00886

Luongo, L., Guida, F., Boccella, S., Bellini, G., Gatta, L., Rossi, F., . . . Targets, N. D.-D. (2013). Palmitoylethanolamide reduces formalin-induced neuropathic-like behaviour through spinal glial/microglial phenotypical changes in mice. *12*(1), 45-54.

Lüscher, C., & Ungless, M. A. J. P. m. (2006). The mechanistic classification of addictive drugs. *3*(11), e437.

Maher, C. E., Eisenach, J. C., Pan, H. L., Xiao, R., & Childers, S. R. (2001). Chronic intrathecal morphine administration produces homologous mu receptor/G-protein desensitization specifically in spinal cord. *Brain Res, 895*(1-2), 1-8. doi:10.1016/s0006-8993(00)03093-6

Maldonado, R., & Koob, G. F. J. B. r. (1993). Destruction of the locus coeruleus decreases physical signs of opiate withdrawal. *605*(1), 128-138.

Maldonado, R., Stinus, L., Gold, L. H., & Koob, G. F. (1992). Role of different brain structures in the expression of the physical morphine withdrawal syndrome. *J Pharmacol Exp Ther, 261*(2), 669-677.

Mameli-Engvall, M., Evrard, A., Pons, S., Maskos, U., Svensson, T. H., Changeux, J. P., & Faure, P. (2006). Hierarchical control of dopamine neuron-firing patterns by nicotinic receptors. *Neuron, 50*(6), 911-921. doi:10.1016/j.neuron.2006.05.007

Mansvelder, H. D., Keath, J. R., & McGehee, D. S. J. N. (2002). Synaptic mechanisms underlie nicotine-induced excitability of brain reward areas. *33*(6), 905-919.

Mao, J., Price, D. D., & Mayer, D. J. (1995). Mechanisms of hyperalgesia and morphine tolerance: a current view of their possible interactions. *Pain, 62*(3), 259-274. doi:10.1016/0304-3959(95)00073-2

Marinelli, M., Rudick, C., Hu, X.-T., White, F. J. C. D. T.-C., & Disorders, N. (2006). Excitability of dopamine neurons: modulation and physiological consequences. *5*(1), 79-97.

Martin, G., Schoonjans, K., Lefebvre, A.-M., Staels, B., & Auwerx, J. J. J. o. B. C. (1997). Coordinate regulation of the expression of the fatty acid transport protein and acyl-CoA synthetase genes by PPARα and PPARγ activators. *272*(45), 28210-28217.

Martin, W. J., Gupta, N. K., Loo, C. M., Rohde, D. S., & Basbaum, A. I. (1999). Differential effects of neurotoxic destruction of descending noradrenergic pathways on acute and persistent nociceptive processing. *Pain, 80*(1-2), 57-65. doi:10.1016/s0304-3959(98)00194-8

Mascia, P., Pistis, M., Justinova, Z., Panlilio, L. V., Luchicchi, A., Lecca, S., . . . Goldberg, S. R. (2011). Blockade of nicotine reward and reinstatement by activation of alpha-type peroxisome proliferator-activated receptors. *Biol Psychiatry, 69*(7), 633-641. doi:10.1016/j.biopsych.2010.07.009

Mattace Raso, G., Russo, R., Calignano, A., & Meli, R. (2014). Palmitoylethanolamide in CNS health and disease. *Pharmacol Res, 86*, 32-41. doi:10.1016/j.phrs.2014.05.006

McHugh, D., Page, J., Dunn, E., & Bradshaw, H. B. (2012). Delta(9) -Tetrahydrocannabinol and N-arachidonyl glycine are full agonists at GPR18 receptors and induce migration in human endometrial HEC-1B cells. *Br J Pharmacol, 165*(8), 2414-2424. doi:10.1111/j.1476-5381.2011.01497.x

Meijerink, J., Poland, M., Balvers, M. G., Plastina, P., Lute, C., Dwarkasing, J., . . . Witkamp, R. F. (2015). Inhibition of COX-2-mediated eicosanoid production plays a major role in the anti-inflammatory effects of the endocannabinoid N-docosahexaenoylethanolamine (DHEA) in macrophages. *Br J Pharmacol, 172*(1), 24-37. doi:10.1111/bph.12747

Melis, M., Carta, S., Fattore, L., Tolu, S., Yasar, S., Goldberg, S. R., . . . Pistis, M. (2010). Peroxisome proliferator-activated receptors-alpha modulate dopamine cell activity through nicotinic receptors. *Biol Psychiatry, 68*(3), 256-264. doi:10.1016/j.biopsych.2010.04.016

Melis, M., Pillolla, G., Luchicchi, A., Muntoni, A. L., Yasar, S., Goldberg, S. R., & Pistis, M. (2008). Endogenous fatty acid ethanolamides suppress nicotine-induced activation of mesolimbic dopamine neurons through nuclear receptors. *J Neurosci, 28*(51), 13985-13994. doi:10.1523/jneurosci.3221-08.2008

Melis, M., & Pistis, M. J. P. r. (2014). Targeting the interaction between fatty acid ethanolamides and nicotinic receptors: therapeutic perspectives. *86*, 42-49.

Melis, M., Scheggi, S., Carta, G., Madeddu, C., Lecca, S., Luchicchi, A., . . . Pistis, M. (2013). PPARalpha regulates cholinergic-driven activity of midbrain dopamine neurons via a novel mechanism involving alpha7 nicotinic acetylcholine receptors. *J Neurosci, 33*(14), 6203-6211. doi:10.1523/jneurosci.4647-12.2013

Merighi, S., Gessi, S., Varani, K., Fazzi, D., Mirandola, P., & Borea, P. A. J. B. j. o. p. (2012). Cannabinoid CB2 receptor attenuates morphine-induced inflammatory responses in activated microglial cells. *166*(8), 2371-2385.

Migliore, M., Pontis, S., Fuentes de Arriba, A. L., Realini, N., Torrente, E., Armirotti, A., . . . Pizzirani, D. J. A. C. (2016). Second-Generation Non-Covalent NAAA Inhibitors are Protective in a Model of Multiple Sclerosis. *128*(37), 11359-11363.

Molina-Holgado, F., Lledó, A., & Guaza, C. J. N. (1997). Anandamide suppresses nitric oxide and TNF-α responses to Theiler's virus or endotoxin in astrocytes. *8*(8), 1929-1933.

Morgan, M. M., Clayton, C. C., & Lane, D. A. (2003). Behavioral evidence linking opioid-sensitive GABAergic neurons in the ventrolateral periaqueductal gray to morphine tolerance. *Neuroscience, 118*(1), 227-232. doi:10.1016/s0306-4522(02)00822-9

Morgan, M. M., Fossum, E. N., Levine, C. S., & Ingram, S. L. (2006). Antinociceptive tolerance revealed by cumulative intracranial microinjections of morphine into the periaqueductal gray in the rat. *Pharmacol Biochem Behav, 85*(1), 214-219. doi:10.1016/j.pbb.2006.08.003

Morikawa, H., & Paladini, C. A. J. N. (2011). Dynamic regulation of midbrain dopamine neuron activity: intrinsic, synaptic, and plasticity mechanisms. *198*, 95-111.
Moscardo, E., Maurin, A., Dorigatti, R., Champeroux, P., Richard, S. J. J. o. p., & methods, t. (2007). An optimised methodology for the neurobehavioural assessment in rodents. *56*(2), 239-255.
Motojima, K., Passilly, P., Peters, J. M., Gonzalez, F. J., & Latruffe, N. J. J. o. B. C. (1998). Expression of putative fatty acid transporter genes are regulated by peroxisome proliferator-activated receptor α and γ activators in a tissue-and inducer-specific manner. *273*(27), 16710-16714.
Muntoni, A. L., Pillolla, G., Melis, M., Perra, S., Gessa, G. L., & Pistis, M. J. E. J. o. N. (2006). Cannabinoids modulate spontaneous neuronal activity and evoked inhibition of locus coeruleus noradrenergic neurons. *23*(9), 2385-2394.
Murru, E., Carta, G., Cordeddu, L., Melis, M., Desogus, E., Ansar, H., . . . Coakley, M. J. I. j. o. m. s. (2018). Dietary conjugated linoleic acid-enriched cheeses influence the levels of circulating n-3 highly unsaturated fatty acids in humans. *19*(6), 1730.
Muscoli, C., Doyle, T., Dagostino, C., Bryant, L., Chen, Z., Watkins, L. R., . . . Salvemini, D. (2010). Counter-regulation of opioid analgesia by glial-derived bioactive sphingolipids. *J Neurosci, 30*(46), 15400-15408. doi:10.1523/jneurosci.2391-10.2010
Nakamoto, K., Kawasaki, S., Kobori, T., Fujita-Hamabe, W., Mizoguchi, H., Yamada, K., . . . Tokuyama, S. (2012). Involvement of matrix metalloproteinase-9 in the development of morphine tolerance. *Eur J Pharmacol, 683*(1-3), 86-92. doi:10.1016/j.ejphar.2012.03.006
Navarro, M., Chowen, J., Carrera, M. R. A., del Arco, I., Villanúa, M. A., Martin, Y., . . . de Fonseca, F. R. J. N. (1998). CB1 cannabinoid receptor antagonist-induced opiate withdrawal in morphine-dependent rats. *9*(15), 3397-3402.
Ndengele, M. M., Cuzzocrea, S., Masini, E., Vinci, M. C., Esposito, E., Muscoli, C., . . . Salvemini, D. (2009). Spinal ceramide modulates the development of morphine antinociceptive tolerance via peroxynitrite-mediated nitroxidative stress and neuroimmune activation. *J Pharmacol Exp Ther, 329*(1), 64-75. doi:10.1124/jpet.108.146290
Nestler, E. J., Alreja, M., & Aghajanian, G. K. J. B. r. b. (1994). Molecular and cellular mechanisms of opiate action: studies in the rat locus coeruleus. *35*(5-6), 521-528.
Nisell, M., Nomikos, G. G., Svensson, T. H. J. P., & toxicology. (1994). Infusion of nicotine in the ventral tegmental area or the nucleus accumbens of the rat differentially affects accumbal dopamine release. *75*(6), 348-352.
O'Sullivan, S. E. (2016). An update on PPAR activation by cannabinoids. *Br J Pharmacol, 173*(12), 1899-1910. doi:10.1111/bph.13497
Obata, H. (2017). Analgesic Mechanisms of Antidepressants for Neuropathic Pain. *Int J Mol Sci, 18*(11). doi:10.3390/ijms18112483
Oh, K. W., Eun, J. S., Kwon, H. N., Cho, E. Y., & Kim, K. M. (2007). Effects of (-)-epigallocatechin gallate on the development of morphine-induced physical dependence. *Arch Pharm Res, 30*(9), 1111-1115. doi:10.1007/bf02980245
Okamoto, Y., Morishita, J., Tsuboi, K., Tonai, T., & Ueda, N. (2004). Molecular characterization of a phospholipase D generating anandamide and its congeners. *J Biol Chem, 279*(7), 5298-5305. doi:10.1074/jbc.M306642200
Olds, J., & Milner, P. (1954). Positive reinforcement produced by electrical stimulation of septal area and other regions of rat brain. *J Comp Physiol Psychol, 47*(6), 419-427.
Omelchenko, N., & Sesack, S. R. J. S. (2009). Ultrastructural analysis of local collaterals of rat ventral tegmental area neurons: GABA phenotype and synapses onto dopamine and GABA cells. *63*(10), 895-906.

Ossipov, M. H., Dussor, G. O., & Porreca, F. J. T. J. o. c. i. (2010). Central modulation of pain. *120*(11), 3779-3787.

Page, M. E., Berridge, C. W., Foote, S. L., & Valentino, R. J. J. N. l. (1993). Corticotropin-releasing factor in the locus coeruleus mediates EEG activation associated with hypotensive stress. *164*(1-2), 81-84.

Pammer, C., Gorcs, T., & Palkovits, M. (1990). Peptidergic innervation of the locus coeruleus cells in the human brain. *Brain Res, 515*(1-2), 247-255. doi:10.1016/0006-8993(90)90603-9

Panlilio, L. V., Justinova, Z., Mascia, P., Pistis, M., Luchicchi, A., Lecca, S., . . . Goldberg, S. R. (2012). Novel use of a lipid-lowering fibrate medication to prevent nicotine reward and relapse: preclinical findings. *Neuropsychopharmacology, 37*(8), 1838-1847. doi:10.1038/npp.2012.31

Park, T., Chen, H., Kevala, K., Lee, J. W., & Kim, H. Y. (2016). N-Docosahexaenoylethanolamine ameliorates LPS-induced neuroinflammation via cAMP/PKA-dependent signaling. *J Neuroinflammation, 13*(1), 284. doi:10.1186/s12974-016-0751-z

Pascoli, V., Terrier, J., Hiver, A., & Luscher, C. (2015). Sufficiency of Mesolimbic Dopamine Neuron Stimulation for the Progression to Addiction. *Neuron, 88*(5), 1054-1066. doi:10.1016/j.neuron.2015.10.017

Paumelle, R., Blanquart, C., Briand, O., Barbier, O., Duhem, C., Woerly, G., . . . Staels, B. (2006). Acute antiinflammatory properties of statins involve peroxisome proliferator-activated receptor-alpha via inhibition of the protein kinase C signaling pathway. *Circ Res, 98*(3), 361-369. doi:10.1161/01.Res.0000202706.70992.95

Pawlak, M., Bauge, E., Bourguet, W., De Bosscher, K., Lalloyer, F., Tailleux, A., . . . Staels, B. (2014). The transrepressive activity of peroxisome proliferator-activated receptor alpha is necessary and sufficient to prevent liver fibrosis in mice. *Hepatology, 60*(5), 1593-1606. doi:10.1002/hep.27297

Paxinos, G., & Watson, C. (2006). *The rat brain in stereotaxic coordinates: hard cover edition*: Elsevier.

Pertovaara, A. (2013). The noradrenergic pain regulation system: a potential target for pain therapy. *Eur J Pharmacol, 716*(1-3), 2-7. doi:10.1016/j.ejphar.2013.01.067

Petrosino, S., Ahmad, A., Marcolongo, G., Esposito, E., Allara, M., Verde, R., . . . Di Marzo, V. (2015). Diacerein is a potent and selective inhibitor of palmitoylethanolamide inactivation with analgesic activity in a rat model of acute inflammatory pain. *Pharmacol Res, 91*, 9-14. doi:10.1016/j.phrs.2014.10.008

Petrosino, S., & Di Marzo, V. (2017). The pharmacology of palmitoylethanolamide and first data on the therapeutic efficacy of some of its new formulations. *Br J Pharmacol, 174*(11), 1349-1365. doi:10.1111/bph.13580

Picciotto, M. R., Zoli, M., Rimondini, R., Lena, C., Marubio, L. M., Pich, E. M., . . . Changeux, J. P. (1998). Acetylcholine receptors containing the beta2 subunit are involved in the reinforcing properties of nicotine. *Nature, 391*(6663), 173-177. doi:10.1038/34413

Piomelli, D. (2003). The molecular logic of endocannabinoid signalling. *Nat Rev Neurosci, 4*(11), 873-884. doi:10.1038/nrn1247

Puligheddu, M., Melis, M., Pillolla, G., Milioli, G., Parrino, L., Terzano, G. M., . . . Pistis, M. J. E. (2017). Rationale for an adjunctive therapy with fenofibrate in pharmacoresistant nocturnal frontal lobe epilepsy. *58*(10), 1762-1770.

Puligheddu, M., Pillolla, G., Melis, M., Lecca, S., Marrosu, F., De Montis, M. G., . . . Aroni, S. J. P. O. (2013). PPAR-alpha agonists as novel antiepileptic drugs: preclinical findings. *8*(5), e64541.

Punch, L. J., Self, D. W., Nestler, E. J., & Taylor, J. R. (1997). Opposite modulation of opiate withdrawal behaviors on microinfusion of a protein kinase A inhibitor versus activator into the locus coeruleus or periaqueductal gray. *J Neurosci, 17*(21), 8520-8527.

Raghavendra, V., Rutkowski, M. D., & DeLeo, J. A. (2002). The role of spinal neuroimmune activation in morphine tolerance/hyperalgesia in neuropathic and sham-operated rats. *J Neurosci, 22*(22), 9980-9989.

Raghavendra, V., Tanga, F. Y., & DeLeo, J. A. (2004). Attenuation of morphine tolerance, withdrawal-induced hyperalgesia, and associated spinal inflammatory immune responses by propentofylline in rats. *Neuropsychopharmacology, 29*(2), 327-334. doi:10.1038/sj.npp.1300315

Raja, S. N., Meyer, R., Ringkamp, M., & Campbell, J. (1999). Peripheral mechanisms of nociception. 11-57.

Rakhshandehroo, M., Knoch, B., Muller, M., & Kersten, S. (2010). Peroxisome proliferator-activated receptor alpha target genes. *PPAR Res, 2010*. doi:10.1155/2010/612089

Rasmussen, K., Beitner-Johnson, D. B., Krystal, J. H., Aghajanian, G. K., & Nestler, E. J. J. J. o. N. (1990). Opiate withdrawal and the rat locus coeruleus: behavioral, electrophysiological, and biochemical correlates. *10*(7), 2308-2317.

Ray, S. B., Gupta, H., & Gupta, Y. K. (2004). Up-regulation of mu-opioid receptors in the spinal cord of morphine-tolerant rats. *J Biosci, 29*(1), 51-56. doi:10.1007/bf02702561

Rivera, P., Arrabal, S., Vargas, A., Blanco Calvo, E., Serrano, A., Pavon, F. J., . . . Suárez, J. J. F. i. n. (2014). Localization of peroxisome proliferator-activated receptor alpha (PPARα) and N-acyl phosphatidylethanolamine phospholipase D (NAPE-PLD) in cells expressing the Ca2+-binding proteins calbindin, calretinin, and parvalbumin in the adult rat hippocampus. *8*, 12.

Roeckel, L. A., Le Coz, G. M., Gaveriaux-Ruff, C., & Simonin, F. (2016). Opioid-induced hyperalgesia: Cellular and molecular mechanisms. *Neuroscience, 338*, 160-182. doi:10.1016/j.neuroscience.2016.06.029

Ronnback, L., & Hansson, E. (1988). Modulation of astrocyte activity--one way to reinforce morphine effects? *Cell Mol Biol, 34*(4), 337-349.

Rovito, D., Giordano, C., Vizza, D., Plastina, P., Barone, I., Casaburi, I., . . . Ando, S. (2013). Omega-3 PUFA ethanolamides DHEA and EPEA induce autophagy through PPARgamma activation in MCF-7 breast cancer cells. *J Cell Physiol, 228*(6), 1314-1322. doi:10.1002/jcp.24288

Rudd, R. A. (2016). Increases in drug and opioid-involved overdose deaths—United States, 2010–2015. *65*.

Sagheddu, C., Aroni, S., De Felice, M., Lecca, S., Luchicchi, A., Melis, M., . . . Pistis, M. (2015). Enhanced serotonin and mesolimbic dopamine transmissions in a rat model of neuropathic pain. *Neuropharmacology, 97*, 383-393. doi:10.1016/j.neuropharm.2015.06.003

Samineni, V. K., Grajales-Reyes, J. G., Copits, B. A., O'Brien, D. E., Trigg, S. L., Gomez, A. M., . . . Gereau, R. W. t. (2017). Divergent Modulation of Nociception by Glutamatergic and GABAergic Neuronal Subpopulations in the Periaqueductal Gray. *eNeuro, 4*(2). doi:10.1523/eneuro.0129-16.2017

Sarchielli, P., Pini, L. A., Coppola, F., Rossi, C., Baldi, A., Mancini, M. L., & Calabresi, P. J. N. (2007). Endocannabinoids in chronic migraine: CSF findings suggest a system failure. *32*(6), 1384.

Sasso, O., Summa, M., Armirotti, A., Pontis, S., De Mei, C., & Piomelli, D. (2018). The N-Acylethanolamine Acid Amidase Inhibitor ARN077 Suppresses Inflammation and Pruritus in a Mouse Model of Allergic Dermatitis. *J Invest Dermatol, 138*(3), 562-569. doi:10.1016/j.jid.2017.07.853

Sasso, O., Summa, M., Armirotti, A., Pontis, S., De Mei, C., & Piomelli, D. J. J. o. I. D. (2018). The N-acylethanolamine acid amidase inhibitor ARN077 suppresses inflammation and pruritus in a mouse model of allergic dermatitis. *138*(3), 562-569.

Sato, H., Kawano, T., Yin, D. X., Kato, T., & Toyoda, H. J. N. (2017). Nicotinic activity depresses synaptic potentiation in layer V pyramidal neurons of mouse insular cortex. *358*, 13-27.

Scheggi, S., Melis, M., De Felice, M., Aroni, S., Muntoni, A. L., Pelliccia, T., . . . Pistis, M. (2016). PPARalpha modulation of mesolimbic dopamine transmission rescues depression-related behaviors. *Neuropharmacology, 110*(Pt A), 251-259. doi:10.1016/j.neuropharm.2016.07.024

Scherma, M., Justinova, Z., Zanettini, C., Panlilio, L. V., Mascia, P., Fadda, P., . . . Goldberg, S. R. (2012). The anandamide transport inhibitor AM404 reduces the rewarding effects of nicotine and nicotine-induced dopamine elevations in the nucleus accumbens shell in rats. *Br J Pharmacol, 165*(8), 2539-2548. doi:10.1111/j.1476-5381.2011.01467.x

Scherma, M., Medalie, J., Fratta, W., Vadivel, S. K., Makriyannis, A., Piomelli, D., . . . Tanda, G. J. N. (2008). The endogenous cannabinoid anandamide has effects on motivation and anxiety that are revealed by fatty acid amide hydrolase (FAAH) inhibition. *54*(1), 129-140.

Schim, J. D., & Stang, P. (2004). Overview of pain management. *Pain Pract, 4 Suppl 1*, S4-18. doi:10.1111/j.1533-2500.2004.04010.x

Schnitzler, A., & Ploner, M. (2000). Neurophysiology and functional neuroanatomy of pain perception. *J Clin Neurophysiol, 17*(6), 592-603.

Schoonjans, K., Staels, B., & Auwerx, J. J. J. o. l. r. (1996). Role of the peroxisome proliferator-activated receptor (PPAR) in mediating the effects of fibrates and fatty acids on gene expression. *37*(5), 907-925.

Schultz, W. (1998). Predictive reward signal of dopamine neurons. *J Neurophysiol, 80*(1), 1-27. doi:10.1152/jn.1998.80.1.1

Serrano, A., Pavon, F. J., Tovar, S., Casanueva, F., Senaris, R., Dieguez, C., & de Fonseca, F. R. (2011). Oleoylethanolamide: effects on hypothalamic transmitters and gut peptides regulating food intake. *Neuropharmacology, 60*(4), 593-601. doi:10.1016/j.neuropharm.2010.12.007

Sesack, S. R., & Grace, A. A. J. N. (2010). Cortico-basal ganglia reward network: microcircuitry. *35*(1), 27.

Skaper, S. D., Facci, L., & Giusti, P. J. I. (2014). Mast cells, glia and neuroinflammation: partners in crime? *, 141*(3), 314-327.

Skaper, S. D., Facci, L., & Giusti, P. J. M. n. (2013). Glia and mast cells as targets for palmitoylethanolamide, an anti-inflammatory and neuroprotective lipid mediator. *48*(2), 340-352.

Skolnick, P. (2018). The Opioid Epidemic: Crisis and Solutions. *Annu Rev Pharmacol Toxicol, 58*, 143-159. doi:10.1146/annurev-pharmtox-010617-052534

Smart, D., Jonsson, K. O., Vandevoorde, S., Lambert, D. M., & Fowler, C. J. J. B. j. o. p. (2002). 'Entourage'effects of N-acyl ethanolamines at human vanilloid receptors. Comparison of effects upon anandamide-induced vanilloid receptor activation and upon anandamide metabolism. *136*(3), 452-458.

Smith, P. A., Selley, D. E., Sim-Selley, L. J., & Welch, S. P. J. E. j. o. p. (2007). Low dose combination of morphine and Δ9-tetrahydrocannabinol circumvents antinociceptive tolerance and apparent desensitization of receptors. *571*(2-3), 129-137.

Solorzano, C., Zhu, C., Battista, N., Astarita, G., Lodola, A., Rivara, S., . . . Antonietti, F. J. P. o. t. N. A. o. S. (2009). Selective N-acylethanolamine-hydrolyzing acid amidase

inhibition reveals a key role for endogenous palmitoylethanolamide in inflammation. *106*(49), 20966-20971.
Song, P., & Zhao, Z.-Q. J. N. r. (2001). The involvement of glial cells in the development of morphine tolerance. *39*(3), 281-286.
Song, P., & Zhao, Z. Q. (2001). The involvement of glial cells in the development of morphine tolerance. *Neurosci Res, 39*(3), 281-286.
Staels, B., Koenig, W., Habib, A., Merval, R., Lebret, M., Torra, I. P., . . . Tedgui, A. (1998). Activation of human aortic smooth-muscle cells is inhibited by PPARalpha but not by PPARgamma activators. *Nature, 393*(6687), 790-793. doi:10.1038/31701
Stellwagen, D., Beattie, E. C., Seo, J. Y., & Malenka, R. C. (2005). Differential regulation of AMPA receptor and GABA receptor trafficking by tumor necrosis factor-alpha. *J Neurosci, 25*(12), 3219-3228. doi:10.1523/jneurosci.4486-04.2005
Stienstra, R., Duval, C., Müller, M., & Kersten, S. J. P. r. (2007). PPARs, obesity, and inflammation. *2007*.
Stienstra, R., Mandard, S., Tan, N. S., Wahli, W., Trautwein, C., Richardson, T. A., . . . Muller, M. (2007). The Interleukin-1 receptor antagonist is a direct target gene of PPARalpha in liver. *J Hepatol, 46*(5), 869-877. doi:10.1016/j.jhep.2006.11.019
Stiller, C. O., Bergquist, J., Beck, O., Ekman, R., & Brodin, E. (1996). Local administration of morphine decreases the extracellular level of GABA in the periaqueductal gray matter of freely moving rats. *Neurosci Lett, 209*(3), 165-168. doi:10.1016/0304-3940(96)12638-0
Sugiura, T., Kishimoto, S., Oka, S., & Gokoh, M. (2006). Biochemistry, pharmacology and physiology of 2-arachidonoylglycerol, an endogenous cannabinoid receptor ligand. *Prog Lipid Res, 45*(5), 405-446. doi:10.1016/j.plipres.2006.03.003
Sun, Y.-X., Tsuboi, K., Zhao, L.-Y., Okamoto, Y., Lambert, D. M., Ueda, N. J. B. e. B. A.-M., & Lipids, C. B. o. (2005). Involvement of N-acylethanolamine-hydrolyzing acid amidase in the degradation of anandamide and other N-acylethanolamines in macrophages. *1736*(3), 211-220.
Taylor, B. K., Roderick, R. E., & Basbaum, A. I. (2000). Brainstem noradrenergic control of nociception is abnormal in the spontaneously hypertensive rat. *Neurosci Lett, 291*(3), 139-142. doi:10.1016/s0304-3940(00)01389-6
Taylor, B. K., & Westlund, K. N. (2017). The noradrenergic locus coeruleus as a chronic pain generator. *J Neurosci Res, 95*(6), 1336-1346. doi:10.1002/jnr.23956
Thomas, J., Mustafa, S., Johnson, J., Nicotra, L., & Hutchinson, M. (2015). The relationship between opioids and immune signalling in the spinal cord. *Handb Exp Pharmacol, 227*, 207-238. doi:10.1007/978-3-662-46450-2_11
Torrecilla, M., Marker, C. L., Cintora, S. C., Stoffel, M., Williams, J. T., & Wickman, K. (2002). G-protein-gated potassium channels containing Kir3.2 and Kir3.3 subunits mediate the acute inhibitory effects of opioids on locus ceruleus neurons. *J Neurosci, 22*(11), 4328-4334. doi:20026414
Tortorici, V., Morgan, M. M., & Vanegas, H. (2001). Tolerance to repeated microinjection of morphine into the periaqueductal gray is associated with changes in the behavior of off- and on-cells in the rostral ventromedial medulla of rats. *Pain, 89*(2-3), 237-244.
Tsuboi, K., Sun, Y.-X., Okamoto, Y., Araki, N., Tonai, T., & Ueda, N. J. J. o. B. C. (2005). Molecular characterization of N-acylethanolamine-hydrolyzing acid amidase, a novel member of the choloylglycine hydrolase family with structural and functional similarity to acid ceramidase. *280*(12), 11082-11092.
Tsuboi, K., Zhao, L. Y., Okamoto, Y., Araki, N., Ueno, M., Sakamoto, H., & Ueda, N. (2007). Predominant expression of lysosomal N-acylethanolamine-hydrolyzing acid amidase in macrophages revealed by immunochemical studies. *Biochim Biophys Acta, 1771*(5), 623-632. doi:10.1016/j.bbalip.2007.03.005

Tsuruoka, M., Matsutani, K., & Inoue, T. (2003). Coeruleospinal inhibition of nociceptive processing in the dorsal horn during unilateral hindpaw inflammation in the rat. *Pain, 104*(1-2), 353-361. doi:10.1016/s0304-3959(03)00042-3

Tsuruoka, M., & Willis, W. D. (1996). Descending modulation from the region of the locus coeruleus on nociceptive sensitivity in a rat model of inflammatory hyperalgesia. *Brain Res, 743*(1-2), 86-92. doi:10.1016/s0006-8993(96)01025-6

Tsuruoka, M., & Willis, W. D., Jr. (1996). Bilateral lesions in the area of the nucleus locus coeruleus affect the development of hyperalgesia during carrageenan-induced inflammation. *Brain Res, 726*(1-2), 233-236.

Tsuruoka, M., & Willis, W. D. J. B. r. (1996). Descending modulation from the region of the locus coeruleus on nociceptive sensitivity in a rat model of inflammatory hyperalgesia. *743*(1-2), 86-92.

Tugwood, J. D., Issemann, I., Anderson, R. G., Bundell, K. R., McPheat, W., & Green, S. J. T. E. j. (1992). The mouse peroxisome proliferator activated receptor recognizes a response element in the 5′ flanking sequence of the rat acyl CoA oxidase gene. *11*(2), 433-439.

Tzschentke, T. M. (2007). Measuring reward with the conditioned place preference (CPP) paradigm: update of the last decade. *Addict Biol, 12*(3-4), 227-462. doi:10.1111/j.1369-1600.2007.00070.x

Uyama, T., Jin, X. H., Tsuboi, K., Tonai, T., & Ueda, N. (2009). Characterization of the human tumor suppressors TIG3 and HRASLS2 as phospholipid-metabolizing enzymes. *Biochim Biophys Acta, 1791*(12), 1114-1124. doi:10.1016/j.bbalip.2009.07.001

Uyama, T., Morishita, J., Jin, X. H., Okamoto, Y., Tsuboi, K., & Ueda, N. (2009). The tumor suppressor gene H-Rev107 functions as a novel Ca2+-independent cytosolic phospholipase A1/2 of the thiol hydrolase type. *J Lipid Res, 50*(4), 685-693. doi:10.1194/jlr.M800453-JLR200

Valentino, R. J., & Volkow, N. D. (2019). Drugs, sleep, and the addicted brain. *Neuropsychopharmacology*. doi:10.1038/s41386-019-0465-x

Valentinova, K., Tchenio, A., Trusel, M., Clerke, J. A., Lalive, A. L., Tzanoulinou, S., . . . Mameli, M. (2019). Morphine withdrawal recruits lateral habenula cytokine signaling to reduce synaptic excitation and sociability. *Nat Neurosci, 22*(7), 1053-1056. doi:10.1038/s41593-019-0421-4

Van Bockstaele, E. J., Reyes, B. A., & Valentino, R. J. (2010). The locus coeruleus: A key nucleus where stress and opioids intersect to mediate vulnerability to opiate abuse. *Brain Res, 1314*, 162-174. doi:10.1016/j.brainres.2009.09.036

Van Der Stelt, M., & Di Marzo, V. (2004). Endovanilloids. Putative endogenous ligands of transient receptor potential vanilloid 1 channels. *Eur J Biochem, 271*(10), 1827-1834. doi:10.1111/j.1432-1033.2004.04081.x

Varrassi, G., Fusco, M., Skaper, S. D., Battelli, D., Zis, P., Coaccioli, S., . . . Paladini, A. (2018). A Pharmacological Rationale to Reduce the Incidence of Opioid Induced Tolerance and Hyperalgesia: A Review. *Pain Ther, 7*(1), 59-75. doi:10.1007/s40122-018-0094-9

Varrassi, G., Hanna, M., Macheras, G., Montero, A., Montes Perez, A., Meissner, W., . . . Scarpignato, C. (2017). Multimodal analgesia in moderate-to-severe pain: a role for a new fixed combination of dexketoprofen and tramadol. *Curr Med Res Opin, 33*(6), 1165-1173. doi:10.1080/03007995.2017.1310092

Vaughan, C. W., Ingram, S. L., Connor, M. A., & Christie, M. J. (1997). How opioids inhibit GABA-mediated neurotransmission. *Nature, 390*(6660), 611-614. doi:10.1038/37610

Verme, J. L., Gaetani, S., Fu, J., Oveisi, F., Burton, K., Piomelli, D. J. C., & sciences, m. l. (2005). Regulation of food intake by oleoylethanolamide. *62*(6), 708.

Viganò, D., Valenti, M., Grazia Cascio, M., Di Marzo, V., Parolaro, D., & Rubino, T. J. E. J. o. N. (2004). Changes in endocannabinoid levels in a rat model of behavioural sensitization to morphine. *20*(7), 1849-1857.

Viviani, B., Bartesaghi, S., Gardoni, F., Vezzani, A., Behrens, M. M., Bartfai, T., . . . Marinovich, M. (2003). Interleukin-1beta enhances NMDA receptor-mediated intracellular calcium increase through activation of the Src family of kinases. *J Neurosci, 23*(25), 8692-8700.

Volkow, N. D., Koob, G. F., & McLellan, A. T. J. N. E. J. o. M. (2016). Neurobiologic advances from the brain disease model of addiction. *374*(4), 363-371.

Wang, X., Loram, L. C., Ramos, K., de Jesus, A. J., Thomas, J., Cheng, K., . . . Yin, H. (2012). Morphine activates neuroinflammation in a manner parallel to endotoxin. *Proc Natl Acad Sci U S A, 109*(16), 6325-6330. doi:10.1073/pnas.1200130109

Watkins, L. R., Hutchinson, M. R., Rice, K. C., & Maier, S. F. (2009). The "toll" of opioid-induced glial activation: improving the clinical efficacy of opioids by targeting glia. *Trends Pharmacol Sci, 30*(11), 581-591. doi:10.1016/j.tips.2009.08.002

Wei, F., Dubner, R., & Ren, K. (1999). Laminar-selective noradrenergic and serotoninergic modulation includes spinoparabrachial cells after inflammation. *Neuroreport, 10*(8), 1757-1761. doi:10.1097/00001756-199906030-00024

West, W. L., Yeomans, D. C., & Proudfit, H. K. (1993). The function of noradrenergic neurons in mediating antinociception induced by electrical stimulation of the locus coeruleus in two different sources of Sprague-Dawley rats. *Brain Res, 626*(1-2), 127-135. doi:10.1016/0006-8993(93)90571-4

Westlund, K. N., & Craig, A. D. (1996). Association of spinal lamina I projections with brainstem catecholamine neurons in the monkey. *Exp Brain Res, 110*(2), 151-162. doi:10.1007/bf00228547

WHO. (2011). *World Heath Organization report on the global tobacco epidemic, 2011: warning about the dangers of tobacco*: Geneva: World Health Organization.

Williams, J., Wood, J., Pandarinathan, L., Karanian, D. A., Bahr, B. A., Vouros, P., & Makriyannis, A. (2007). Quantitative method for the profiling of the endocannabinoid metabolome by LC-atmospheric pressure chemical ionization-MS. *Anal Chem, 79*(15), 5582-5593. doi:10.1021/ac0624086

Williams, J. T., Egan, T. M., & North, R. A. (1982). Enkephalin opens potassium channels on mammalian central neurones. *Nature, 299*(5878), 74-77. doi:10.1038/299074a0

Williams, J. T., Ingram, S. L., Henderson, G., Chavkin, C., von Zastrow, M., Schulz, S., . . . Christie, M. J. J. P. r. (2013). Regulation of μ-opioid receptors: desensitization, phosphorylation, internalization, and tolerance. *65*(1), 223-254.

Witten, I. B., Steinberg, E. E., Lee, S. Y., Davidson, T. J., Zalocusky, K. A., Brodsky, M., . . . Deisseroth, K. (2011). Recombinase-driver rat lines: tools, techniques, and optogenetic application to dopamine-mediated reinforcement. *Neuron, 72*(5), 721-733. doi:10.1016/j.neuron.2011.10.028

Yang, L., Li, L., Chen, L., Li, Y., Chen, H., Li, Y., . . . Qiu, Y. J. S. r. (2015). Potential analgesic effects of a novel N-acylethanolamine acid amidase inhibitor F96 through PPAR-α. *5*, 13565.

Neuropharmacology 144 (2019) 327–336

Contents lists available at ScienceDirect

Neuropharmacology

journal homepage: www.elsevier.com/locate/neuropharm

Inhibition of N-acylethanolamine acid amidase reduces nicotine-induced dopamine activation and reward

Claudia Sagheddu[a], Maria Scherma[a], Mauro Congiu[a], Paola Fadda[a,c], Gianfranca Carta[a], Sebastiano Banni[a], JodiAnne T. Wood[b], Alexandros Makriyannis[b], Michael S. Malamas[b], Marco Pistis[a,c,*]

[a] Department of Biomedical Sciences, University of Cagliari, 09042, Monserrato, Italy
[b] Center for Drug Discovery, Department of Pharmaceutical Sciences, Department of Chemistry and Chemical Biology, Northeastern University, Boston, MA 02115, USA
[c] Neuroscience Institute, National Research Council of Italy (CNR), Section of Cagliari, 09042, Monserrato, Italy

HIGHLIGHTS

- We synthetized the novel specific brain permeable NAAA inhibitor AM11095.
- Lipid analysis showed that AM11095 increased levels of PPARα endogenous ligands in discrete rat brain areas.
- AM11095 prevented nicotine-induced increase in dopamine transmission in rats.
- AM11095 decreased the expression of nicotine conditioned place preference in rats.

ARTICLE INFO

Keywords:
Nicotine
Dopamine
Microdialysis
Electrophysiology
NAAA inhibitor
PPARα
Conditioned place preference

ABSTRACT

Tobacco smoke is the leading preventable cause of death in the world and treatments aimed to increase success rate in smoking cessation by reducing nicotine dependence are sought. Activation of peroxisome proliferator-activated receptor-alpha (PPARα) by synthetic or endogenous agonists was shown to suppress nicotine-induced activation of mesolimbic dopamine system, one of the major neurobiological substrates of nicotine dependence, and nicotine-seeking behavior in rats and monkeys. An alternative indirect way to activate PPARα is inhibition of N-acylethanolamine acid amidase (NAAA), one of the major hydrolyzing enzyme for its endogenous agonists palmitoylethanolamide (PEA) and oleoylethanolamide (OEA). We synthetized a novel specific brain permeable NAAA inhibitor, AM11095. We administered AM11095 to rats and carried out brain lipid analysis, a functional observational battery (FOB) to assess toxicity, *in vivo* electrophysiological recording from dopamine cells in the ventral tegmental area, brain microdialysis in the nucleus accumbens shell and behavioral experiments to assess its effect on nicotine -induced conditioned place preference (CPP).

AM11095 (5 and 25 mg/kg, i.p.) was devoid of neurotoxic and behavioral effects and did not affect motor behavior and coordination. This NAAA inhibitor (5 mg/kg i.p.) increased OEA and PEA levels in the hippocampus and cortex, prevented nicotine-induced activation of mesolimbic dopamine neurons in the ventral tegmental area, nicotine-induced elevation of dopamine levels in the nucleus accumbens shell and decreased the expression of nicotine CPP.

Our results indicate that NAAA inhibitors represent a new class of pharmacological tools to modulate brain PEA/PPARα signalling and show potential in the treatment of nicotine dependence.

1. Introduction

Tobacco use and dependence is a global epidemic and it is the largest preventable cause of mortality and morbidity around the world. Globally, tobacco use causes nearly 6 million deaths per year, and it is estimated to reach 8 million deaths by 2030 (World Health Organization, 2011). Nicotine, the major addictive component of tobacco products, stimulates the activity of the mesolimbic dopamine

* Corresponding author. University of Cagliari, Department of Biomedical Sciences, Division of Neuroscience and Clinical Pharmacology, Cittadella Universitaria di Monserrato, 09042, Monserrato, CA, Italy.
E-mail address: mpistis@unica.it (M. Pistis).

https://doi.org/10.1016/j.neuropharm.2018.11.013
Received 20 June 2018; Received in revised form 5 October 2018; Accepted 9 November 2018
Available online 12 November 2018
0028-3908/

(DA) neurons in the brain and enhances dopamine release in terminal regions. This action is believed to lead to reinforcement and addiction and is shared by other addictive drugs and is concordant in humans and animals (Brody, 2006; Di Chiara and Imperato, 1988; Wise, 2004; Zhou et al., 2001).

It has recently been discovered (Melis et al., 2008, 2010; Pistis and Melis, 2010) that this nicotine-induced dopamine signalling is negatively modulated by α-type peroxisome proliferator-activated receptors (PPARα). PPARα are nuclear receptors that are highly expressed in many tissues including specific areas of the brain (Moreno et al., 2004), have anti-inflammatory and neuroprotective effects (Pistis and Melis, 2010), and regulate lipid metabolism (O'Sullivan, 2007; Pistis and O'Sullivan, 2017). We have shown that experimental drugs that activate PPARα and endogenous agonists, such as the N-acylethanolamines (NAEs) palmitoylethanolamide (PEA) and oleoylethanolamide (OEA), block nicotine-induced firing of dopamine neurons in the ventral tegmental area (VTA) and nicotine-induced elevations of extracellular dopamine levels in the nucleus accumbens shell of rats, and that they decrease nicotine-seeking behavior in rats and monkeys (Mascia et al., 2011; Melis et al., 2008, 2013; Panlilio et al., 2012).

Activation of PPARα triggers a non-genomic stimulation of tyrosine kinases, which leads to phosphorylation (Melis et al., 2010, 2013) and negative regulation of neuronal nAChRs (Charpantier et al., 2005). Importantly, PEA and OEA lack binding affinity for the cannabinoid receptors CB1 and CB2 (Lambert and Di Marzo, 1999) and lack the adverse psychoactive effects produced by medications which target cannabinoid type 1 receptors, thus positioning them as potential safer pharmacotherapies of choice for smoking cessation.

These preclinical findings suggest that PPARα could be an effective target for anti-smoking medications. However, the bioactive lipids PEA and OEA are not suitable for drug development due to their lipophilic nature, which limits their solubility and bioavailability when given orally and secondly the synthetic PPARα agonists although showed promise in animal models of nicotine addiction did not show efficacy in preliminary clinical trials. Thus, we sought to exploit alternative targets to activate PPARα. We pointed to *N*-acylethanolamine acid amidase (NAAA) (Tsuboi et al., 2007; Ueda et al., 2001), the lysosomal cysteine hydrolase mainly involved in PEA degradation (Tai et al., 2012), as a target for small molecule inhibitors to increase tissue levels of PEA (Ribeiro et al., 2015; Solorzano et al., 2009). NAAA is a key enzyme for the degradation of PEA; however, also oleoylethanolamide (OEA), stearoylethanolamide (SEA) are hydrolyzed by NAAA (Tai et al., 2012).

Therefore, we synthesized a novel highly potent and selective inhibitor of human NAAA (AM11095; IC_{50} = 20 nM) and tested its ability, as an indirect PPARα agonist, to suppress electrophysiological, neurochemical and behavioral effects of nicotine that are predictive of its abuse liability, namely, enhancement of dopamine neurons' firing rate and dopamine release in the shell of the nucleus accumbens and conditioned place preference (CPP) in rats.

2. Materials and methods

2.1. Drugs

AM11095 was designed and synthesized at the Center for Drug Discovery, Northeastern University as described in US Patent 9,963,444 B2, 2018. AM11095 is a slowly reversible NAAA inhibitor with a half-maximal inhibitory concentration (IC_{50}) value of approximately 20 nM, while having no effect on FAAH and MGL activity at concentrations > 10 μM. The pharmacokinetic profile in mice is provided as Supplemental Information. Nicotine ((−)-nicotine hydrogen tartrate) was purchased from Sigma (Italy), MK886 was purchased from Tocris (UK). AM11095 was dissolved in tween80, ethanol and saline (1:1:18), MK886 in tween80, DMSO and saline (1:10:39); nicotine was diluted in saline (pH = 7).

2.2. Animals and treatments

Male Sprague-Dawley rats (ENVIGO, Italy) weighing 250–350 g were group-housed and kept on a regular 12:12 h light/dark cycle, in temperature- and humidity-controlled facilities, with food and water available ad libitum. The experimental protocols were conducted to minimize pain and suffering and to reduce the number of animals used. Experiments were approved by the Animal Ethics Committees of the University of Cagliari and were carried out in accordance with the European Directive on the protection of animals used for scientific purposes (2010/63/EU). For electrophysiological experiments, animals received three injections of AM11095 (1 mg/kg or 5 mg/kg, i.p.), or vehicle, 24 h, 12 h and 2 h before the experimental procedures. The dose of 5 mg/kg was selected for subsequent experiments (N-acylethanolamine quantification, microdialysis, behavior), being the lower dose to prevent the excitatory effects of nicotine on dopamine neurons (see below). The treatment regimen was determined by pilot experiments and by comparison with NAAA inhibitors in different experimental setting (i.e. experimental inflammatory bowel disease) (Alhouayek et al., 2015).

For behavioral studies, a different administration schedule was necessary, considering the protocol for CPP: for these experiments rats received one AM11095 injection (5 mg/kg i.p.) daily during the conditioning session (see below).

2.3. N-acylethanolamine quantification ex vivo

A total number of 24 rats were utilized for these experiments. Three separate groups rats (n = 8 per group) received the treatment with AM11095 as described above: three injections of AM11095 (5 mg/kg, i.p.), or vehicle, 24 h, 12 h and 2 h. One group of rats was sacrificed 2 h after last injection, whereas the second group was sacrificed 24 h after last administration. Control animals received vehicle injection. Rats were killed and brains were rapidly removed and dissected. Rat brain sections (midbrain, striatum, hippocampus and cortex) were rapidly frozen at −80 °c and sent to the Center for Drug Discovery for the analysis of various endocannabinoid levels metabolome. The samples were processed and analyzed by LC-MS/MS for endocannabinoid metabolome members: anandamide (AEA), 2-arachidonoylglycerol (2-AG), palmitoylethanolamide (PEA), oleoylethanolamide (OEA) and docosahexaenoic acid (DHA).

2.3.1. Standard curve preparation

Mixtures of the endocannabinoids and their deuterated analogs that had been stored at −80 °C were reconstituted in ethanol for further dilution in a 20 mg/mL solution of fatty acid free bovine serum albumin (BSA) to simulate analyte-free tissue and in ethanol to make the calibration standards, quality control (QC) samples and reference samples, as previously described (Williams et al., 2007). The calibration curves were constructed from the ratios of the peak areas of the analytes versus the internal standard.

2.3.2. Sample extraction

Tissue samples were received on dry ice and immediately stored at −80 °C until they were processed and analyzed. The extraction procedure for the calibration standards, reference extraction and tissue samples was a modified version of the Folch extraction (Folch et al., 1957; Williams et al., 2007). Frozen brain sections were weighed prior to homogenization in ice cold acetone:PBS, pH 7.4 (3:1) and internal standard followed by centrifugation at 14,000 g for 5 min at 4 °C. The resulting supernatants were dried under nitrogen until the acetone was removed. To the remaining supernatant, 50 μL PBS, one volume of methanol and two volumes of chloroform were added for liquid-liquid phase extraction of the lipids. The two phases were separated by centrifugation and the bottom organic layer was evaporated to dryness under nitrogen. Samples were reconstituted in ethanol, vortexed and

sonicated briefly and centrifuged prior to immediate analysis for the endocannabinoids.

2.3.3. LC-MS analysis for N-Acylethanolaminess and endocannabinoids

Chromatographic separation was achieved using an Agilent Zorbax SB-CN column (2.1 × 50 mm, 5 mm) on a Finnigan TSQ Quantum Ultra triple quad mass spectrometer (Thermo Electron, San Jose CA) with an Agilent 1100 HPLC on the front end (Agilent Technologies, Wilmington DE) as previously described (Williams et al., 2007). The mobile phase consisted of 10 mM ammonium acetate, pH 7.3 (A) and methanol (B) in a gradient to allow for the acids to elute first, while the mass spec was in negative ionization mode, followed by the ethanolamides and glycerol esters, while the mass spec was in positive ionization mode (flow rate = 0.5 ml/min); the autosampler was kept at 4 °C to prevent analyte degradation. Eluted peaks were ionized via atmospheric pressure chemical ionization (APCI) in MRM mode. Deuterated internal standards were used for each analyte's standard curves and their levels per gram tissue were determined.

A one-way ANOVA calculation was used to determine if there was any statistical difference between the three groups for each of the detected endocannabinoid metabolome. The Dunnett's Test was used to determine the *P*-value, comparing groups A (sacrifice 2 h after last dose) and B (sacrifice 24 h after the last dose) to the control group (group C).

2.4. In vivo single unit recordings

A total number of 40 rats were utilized for these experiments and divided into 4 groups (n = 10 per group): vehicle + nicotine, AM11095 (1 mg/kg) +nicotine, AM11095 (5 mg/kg) +nicotine, AM11095 (5 mg/kg) + MK886 (1 mg/kg) + nicotine. Rats were treated with AM11095 (1 mg/kg or 5 mg/kg, i.p.) or its vehicle 24 h, 12 h and 2 h before experiments. Then, rats were anaesthetized with urethane (1.3 g/kg, i.p.). For intravenous administration of pharmacological agents, a cannula was inserted into their femoral vein. Rats were placed in stereotaxic apparatus (Kopf, Tujunga, CA, USA) with their body temperature maintained at 37 ± 1 °C by a heating pad. The recording electrode was placed above the Parabrachial nucleus of the VTA (AP, −6.0 mm from bregma; L, 0.4–0.6 mm from midline; V, 7.0–8.0 mm from cortical surface), according to the stereotaxic rat brain atlas of Paxinos and Watson (2007). Single unit activity of neurons was recorded extracellularly (bandpass filter 0.1–10.000 Hz) with glass micropipettes filled with 2% Pontamine sky blue dissolved in 0.5 M sodium acetate. Individual action potentials were isolated and amplified by means of a window discriminator (Neurolog System, Digitimer, Hertfordshire, UK) and displayed on a digital storage oscilloscope (TDS 3012, Tektronics, Marlow, UK). Experiments were sampled on line and off line with Spike2 software by a computer connected to CED1401 interface (Cambridge Electronic Design, Cambridge, UK). DA neurons were isolated and identified according to already published criteria (Sagheddu et al., 2015) such as firing rate < 10 Hz and duration of action potential > 2.5 ms. Bursts were defined as the occurrence of two spikes at interspike interval < 80 ms, and terminated when the interspike interval exceeded 160 ms.

2.5. In vivo microdialysis

A total number of 10 rats were utilized for these experiments and divided into 2 groups (n = 5 per group): vehicle + nicotine, AM11095 (5 mg/kg) +nicotine. Apparatus and procedure were the same as described previously (Scherma et al., 2012). Sprague-Dawley rats were surgically implanted with a concentric dialysis probe aimed at the shell of the nucleus accumbens [anterior +2.0 mm and lateral 1.1 mm from bregma, vertical −7.9 mm from dura, according to the atlas by Paxinos and Watson (2007)] and dialysate samples were collected every 20 min and immediately analyzed by an HPLC system coupled to electrochemical detection. Rats were treated only after dopamine values (< 10% variability) were stable for at least three consecutive samples. AM11095 (5 mg/kg, i.p.) or its vehicle was injected 24 h, 12 h and 2 h min before saline or nicotine (0.4 mg/kg, s.c.). Only rats with correct probe placement were included in the study.

2.6. Conditioned place preference (CPP) procedure

A total number of 60 rats were utilized for these experiments and divided into 6 groups (n = 10 per group): vehicle + saline; vehicle + nicotine; AM11095 + saline, AM11095 + nicotine, MK886 + nicotine, AM11095 + MK886 + nicotine. Apparatus and procedure were as described previously (Scherma et al., 2008, 2012). The general procedure consisted of three consecutive phases:

2.6.1. Pretest

Rats were placed at the intersection of two compartments, with the guillotine door separating the two compartments raised to allow exploration of both sides for 15 min Time spent by the animal in each of the two compartments was recorded to monitor any initial preference for one side versus the other side. Animals showing a pronounced unconditioned preference for one compartment (more than 600 s spent in one compartment) were excluded from the subsequent (conditioning) phase of the experiment.

2.6.2. Conditioning

Conditioning sessions were conducted over 3 consecutive days, with two sessions per day In the morning, all rats received an injection of saline before being placed in one of the two compartments for 20 min, with the door separating the two compartments closed. Four hours later, the rats received an injection of saline or nicotine (0.4 mg/kg) and were placed in the opposite compartment for 20 min. AM11095 (5 mg/kg) or its vehicle were injected i.p., in the home cage, 1.5 h before saline or nicotine injection. The PPARα antagonist MK886 (1 mg/kg, i.p.) was injected 1 h after AM11095 and 30 min before nicotine.

2.6.3. Test

On the day after the last conditioning day, a test session was conducted using the same 15 min procedure as the pretest Time spent by the animal in each of the compartments was recorded.

2.7. In vivo toxicological test battery

A total number of 66 rats were utilized for these experiments and divided into 3 groups (n = 22 per group): vehicle, AM11095 (5 mg/kg) and AM11095 (25 mg/kg). Ten animals per group underwent the functional observation battery (FOB) procedure, which was performed adapted from Moscardo et al. (2007), 24 h before, 2 h and 24 h after random administration of AM11095 or its vehicle. Behavioral, neurologic and autonomic parameters (listed in Table 1) were observed for 1 min in the home cage and for 1 min in the open field (40 × 40 × 35 cm) for signs that did not require handling. Then rats were actively assessed by handling for a period lasting between 2 and 4 min. A complete observation session lasted for 4–6 min. The scoring was blind to the drug administration using objective scoring criteria (adapted from Moscardo et al. (2007)).

Twelve animals per group were assessed for their resistance on the Rotarod (Rota-Rod Treadmill for rats Ugo Basile, Comerio, VA, Italy), which was performed to test for motor impairments, 24 h before, 2 h and 24 h after random administration of AM11095 (5 mg/kg and 25 mg/kg, i.p.) or its vehicle. Rats underwent training sessions once per day for 5 consecutive days, and only those that were competent in performing the protocol (constant rotation speed at 4 rpm for 5 min, constant acceleration over the following 4 min and finally held at 25 rpm for the final 5 min) were used for the experimental sessions. The rectal temperature and the body weight of each rat were measured at the end of each FOB or rotarod session.

Table 1
Components of FOB.

Observed parameter	Data type	Scale	Functional domain	Data display
Home cage observation				
Abnormal posture	Binary	Present/ absent	Physical	n° of rats
Awareness/fear				
Vocalizations	Binary	Present/ absent	Affective	n° of rats
Ease of removal	Ordinal	(-2 to 2)	Behavioral	median
Ease of handling	Ordinal	(-2 to 2)	Behavioral	median
Arousal	Ordinal	(-2 to 2)	Affective	median
Finger approach	Ordinal	(-2 to 2)	Affective	median
Head touch	Ordinal	(-2 to 2)	Affective	median
Visual placing	Ordinal	(-3 to 0)	Sensorial	median
Motor activity				
Immobility	Continuous	sec	Behavioral	mean ± SEM
Rears	Continuous	n°	Behavioral	mean ± SEM
Ataxic gait	Ordinal	(0–3)	Neurological	median
Central excitation				
Seizures	Ordinal	(0–4)	Neurological	median
Tail flick	Ordinal	(-2 to 2)	Sensorial	median
Finger snap	Ordinal	(-1 to 1)	Sensorial	median
Muscle tone				
Body tone	Ordinal	(-1 to 1)	Neurological	median
Reflexes				
Corneal reflex	Ordinal	(-1 to 1)	Sensorial	median
Righting reflex	Ordinal	(-4 to 0)	Sensorial	median
Air righting reflex	Ordinal	(-3 to 0)	Sensorial	median
Respiratory system				
Respiration	Ordinal	(-3 to 1)	Autonomic	median
Autonomic profile				
Salivation	Ordinal	(-1 to 1)	Autonomic	median
Lacrimation	Ordinal	(-1 to 1)	Autonomic	median
Piloerection	Binary	Present/ absent	Autonomic	n° of rats
Feces	Continuous	n°	Affective	mean ± SEM
Urine	Continuous	n°	Affective	mean ± SEM
Miscellaneus observations				
Aggressiveness	Binary	Present/ absent	Affective	n° of rats
Catalepsy	Binary	Present/ absent	Physical	n° of rats
Tremors	Binary	Present/ absent	Physical	n° of rats
Compulsive grooming	Binary	Present/ absent	Affective	n° of rats
Death	Binary	Present/ absent	Physical	n° of rats
Physiological measurements				
Body temperature	Continuous	C°	Autonomic	mean ± SEM
Body weight	Continuous	g	Physical	mean ± SEM

2.8. Statistical analysis

Data obtained from the FOB measurements included binary, ordinal and continuous values. Normal scores from variables such as body weight, temperature, resistance on the rotarod, time of immobility, number of rears, are expressed as mean ± SEM. The difference between each dosed group vs controls was estimated with the Fisher's test or the analysis of variance (ANOVA) test as appropriate. Incidence data from variables such as posture, piloerection and vocalization are expressed as out of the total number of animals and the statistical significance decided upon Chi-squared test. Scores on observations from different behaviors are expressed ad median. The difference between each dosed group vs controls was estimated using a non-parametric Mann-Whitney *U* test.

Microdialysis data are mean ± S.E.M, of dopamine levels in 20 min dialysate samples, expressed as a percentage of basal values and were analyzed using one- or two-way ANOVA. CPP data are expressed as CPP score (mean ± S.E.M.) calculated as the time spent in the drug paired compartment during the test session minus the time spent in the drug-paired compartment during the pre-test session and were analyzed by one-way ANOVA. Post hoc comparisons, when appropriate, were performed by Tukey's multiple comparisons test or by Bonferroni's test.

For *in vivo* electrophysiology, drug-induced changes in firing rate and regularity were calculated by averaging the effects of the drugs for the 2 min period following drug administration and comparing them to the mean of the pre-drug baseline. All the numerical data are given as mean ± SEM. Statistical significance was assessed using two-way ANOVA for repeated measures, or one-way ANOVA or student's t-test when appropriate. Post-hoc multiple comparisons were made using either the Dunnett's test or Bonferroni's test.

In all cases, $P < 0.05$ was considered significant and determined using the calculation software GraphPad Prism or IBM SPSS Statistics for non-parametric test.

3. Results

3.1. N-acylethanolamine quantification ex vivo

For these experiments, rats were treated with AM11095 (5 mg/kg, i.p.) or its vehicle 24 h, 12 h and 2 h before sacrifice (n = 8) (Fig. 1A). A second group of rats received the same treatment but were killed at 24 h after last AM11095 administration (n = 8). Control rats received vehicle injection and were sacrificed 2 h (n = 4) and 24 h (n = 4) after last injection. As no difference was found between the two control groups, data were merged. Endocannabinoids (AEA, 2-AG), NAEs (PEA, OEA) and docosahexaenoic acid (DHA) levels were assessed in the midbrain, striatum, hippocampus and cortex.

As shown in Fig. 1, lipid levels were affected by AM11095 and one-way ANOVA revealed significant effects. Specifically, increased PEA levels were found in hippocampus (Fig. 1D; $F_{(2, 21)} = 3.687$, $P < 0.05$), and OEA levels in the hippocampus (Fig. 1E; $F_{(2, 21)} = 4.351$, $P < 0.05$) and cortex (Fig. 1E; $F_{(2, 21)} = 5.406$, $P < 0.05$) 2 h after AM11095 administration, compared to vehicle group. DHA levels were also significantly higher in cortex (Fig. 1F; $F_{(2, 21)} = 6.665$, $P < 0.01$) and hippocampus (Fig. 1F; $F_{(2, 21)} = 4.114$, $P < 0.05$) 2 h following AM11095 administration. OEA, PEA and DHA levels were similar to vehicle values 24 h later, indicating a transient effect of the NAAA inhibitor. No changes were observed for AEA levels in all brain areas examined (Fig. 1B), however an increase in 2-AG level was detected at 24 h in the cortex (Fig. 1C; $F_{(2, 21)} = 4.180$, $P < 0.05$).

3.2. Effects of AM11905 on nicotine-related effects in the rat mesolimbic dopamine system

For these experiments, 40 rats were divided in four groups (n = 10 for each group): one group was administered AM11095 at 1 mg/kg i.p., one group 5 mg/kg i.p. and one vehicle according to the protocol described above (Fig. 2A). The fourth group of rats received AM11095 5 mg/kg i.p. and the PPARα antagonist MK886 (1 mg/kg, i.p.) was administered 30 min after the last AM11095 dose. As not all experiments could be completed for several reasons (i.e. death following anesthesia or cell lost after drug administration), the actual number of experiments utilized for statistical analysis is shown in Fig. 2 legend. *In vivo* single unit electrophysiological recordings showed that a pre-treatment with AM11095 at both doses did not change the spontaneous firing of VTA dopamine neurons (Fig. 2B; one-way ANOVA, $F_{(2,98)} = 0.604$, $P = 0.55$), while it dose dependently prevented nicotine-induced increase in discharge rate (Fig. 2C and D). Hence, two-way ANOVA shows a significant interaction between treatment and time ($F_{(15, 125)} = 3.07$, $P < 0.001$); post-hoc analysis (Bonferroni's test) shows that AM11095 1 mg/kg has a significant effect at 2 min following nicotine injection, whereas the dose of 5 mg/kg has a significant effect at all time-points analyzed, when compared with vehicle. Post-hoc analysis also indicates that the effect of AM11095 + MK886 was not significant different from vehicle. Thus, the effect of AM11095 is fully

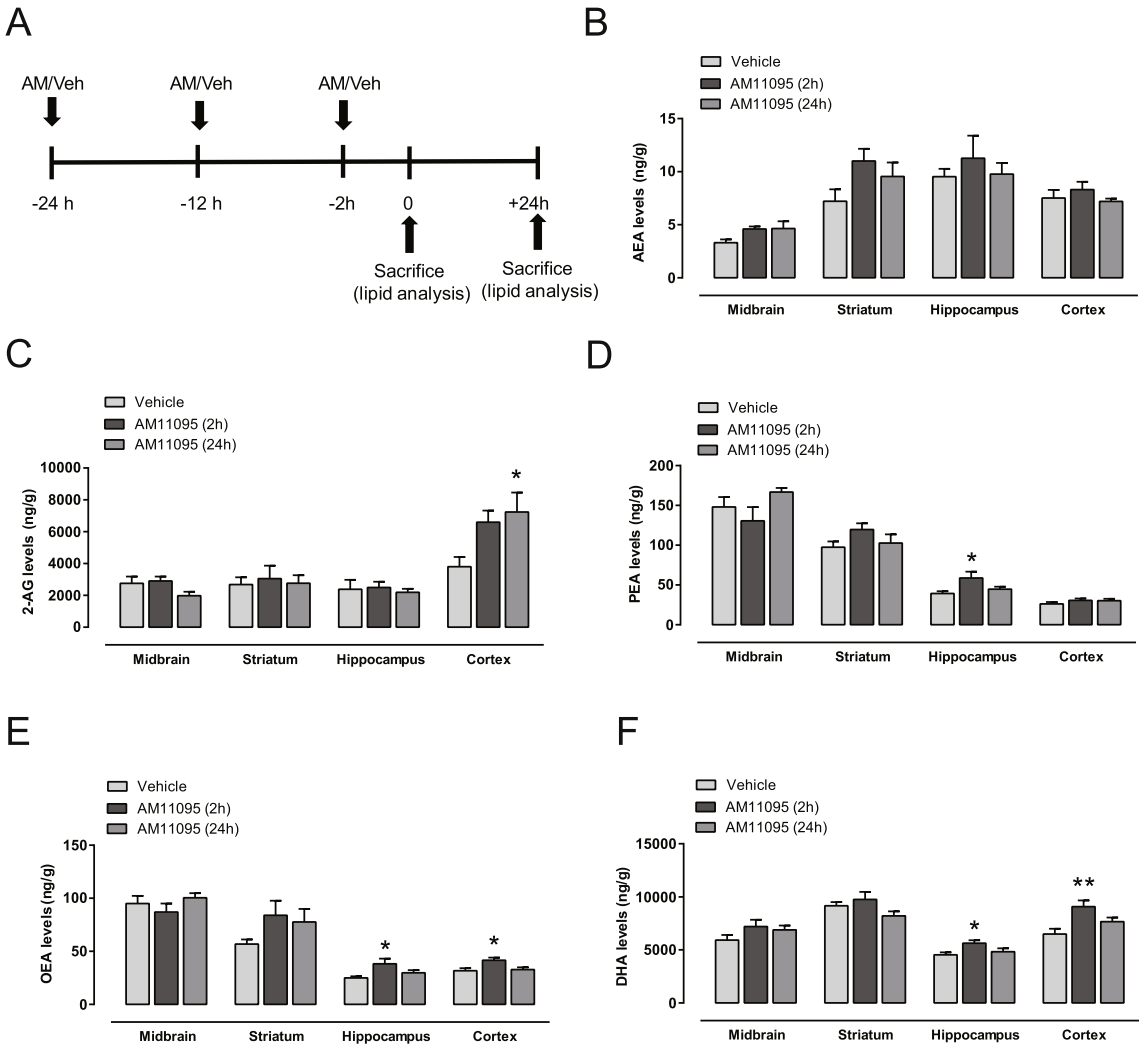

Fig. 1. Effects of pretreatment with the NAAA inhibitor AM11095 on brain lipid levels. A) Schematic representation of the protocol. Rats were killed and brain removed 2 h or 24 h after last AM11095 (AM, 5 mg/kg, i.p.) or vehicle (Veh) administration. B) Brain levels of the endocannabinoid anandamide (AEA) were not changed 2 or 24 h following AM11095 administration. One-way ANOVA; $P > 0.05$. C) Levels of the endocannabinoid 2-AG were increased in the cortex at 24 h following AM11095 administration. One-way ANOVA; *$P < 0.05$. D) PEA levels were increased in hippocampus at 2 h following AM11095 administration. One-way ANOVA; *$P < 0.05$. E) OEA levels were increased at 2 h following AM11095 administration in hippocampus (One-way ANOVA; *$P < 0.05$) and cortex (One-way ANOVA; *$P < 0.05$). F) DHA levels were increased in the cortex (One-way ANOVA; **$P < 0.01$) and hippocampus (One-way ANOVA; *$P < 0.05$) 2 h following AM11095 administration. $N = 8$ for each group. All data are shown as Mean ± SEM.

reversed, namely the excitatory actions of nicotine are restored, upon administration of the PPARα antagonist MK886 (1 mg/kg, i.p.). AM11095 at 5 mg/kg also prevented nicotine-induced bursting of dopamine neurons: two-way ANOVA shows a significant interaction between treatment and time (Fig. 2F; $F_{(15, 125)} = 3.63$, $P < 0.0001$); post-hoc analysis shows that AM11095 at 1 mg/kg has not significant effects, whereas the dose of 5 mg/kg has a significant effect at all time-points analyzed, when compared with vehicle. Post-hoc analysis also indicates that the effect of AM11095 + MK886 was not significant different from vehicle. Fig. 2E summarizes results on firing rate by illustrating the calculated areas under the curves (AUC); one-way ANOVA revealed a significant effect overall ($F_{(4,30)} = 6.39$, $p < 0.01$), whereas post-hoc analysis indicates that only the dose of 5 mg/kg i.v. significantly reversed the effects of nicotine. Therefore, for the following experiments we selected the dose of 5 mg/kg.

For in vivo microdialysis experiments 10 rats were divided into two groups ($N = 5$ each group): one group was administered AM11095 (5 mg/kg, i.p. as in Fig. 2A) and the other group was administered vehicle. Dialysate collection was started 1 h before the last AM11095 administration and about 80 min before nicotine injection, to allow the detection of possible effect on baseline dopamine levels (Fig. 2G). One experiment in each group was discarded due to incorrect probe placement. Results showed that in vehicle-treated rats nicotine (0.4 mg/kg s.c.) increased extracellular levels of dopamine in the nucleus accumbens shell by about 80%, compared with basal levels (one-way ANOVA $F_{(13,42)} = 17.79$, $P < 0.0001$). Pretreatment with AM11905 did not affect baseline dopamine levels but reduced nicotine-induced elevations (Fig. 2G). Two-way ANOVA showed a very significant effect of AM11905 treatment ($F_{(13,78)} = 7.61$, $P < 0.0001$).

3.3. Effects of AM11905 on development of nicotine-induced CPP

Significant treatment effects were found between subjects when CPP score was compared (one-way ANOVA $F_{(5,47)} = 6.477$, $P < 0.0001$). Post-hoc analysis showed that in vehicle-pretreated rats, a nicotine dose of 0.4 mg/kg induced a significant increase in the CPP score in comparison to the vehicle-saline group ($P < 0.01$, Fig. 3). However, when rats were pretreated with a 5 mg/kg dose of AM11905 before each nicotine conditioning session, the CPP score was reduced and was not significant when compared with vehicle + nicotine ($P > 0.05$, Fig. 3).

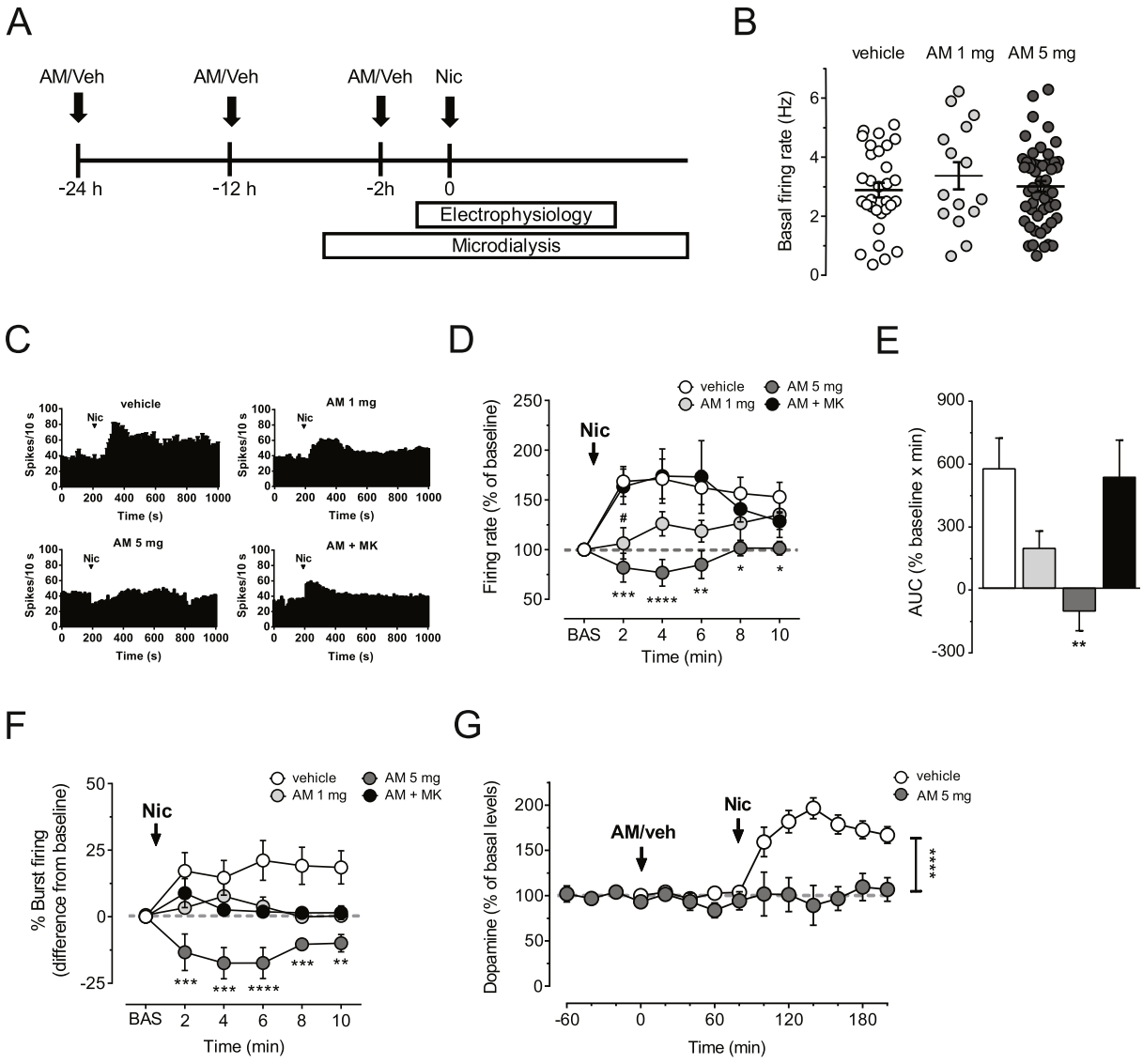

Fig. 2. Effects of pretreatment with the NAAA inhibitor AM11095 on nicotine-related effects in the rat mesolimbic dopamine system. A) Schematic representation of the protocol. Experiment were carried out approximately 2 h after last AM11095 (AM, 1 or 5 mg/kg, i.p.) or vehicle (veh) administration. B) Graph showing that a pretreatment with 1 and 5 mg/kg AM11095 did not affect the spontaneous firing rate of VTA dopamine neurons (one-way ANOVA; $P > 0.05$; vehicle n = 31, AM 5 mg n = 53, AM 1 mg n = 15). C) Representative firing rate histograms of VTA dopamine neurons recorded from a rat pretreated with vehicle (top-left), AM11095 (5 mg/kg bottom-left; 1 mg/kg top-right) or AM11095 5 mg/kg + MK886 1 mg/kg (bottom-right). Arrows indicate the times of nicotine (0.2 mg/kg i.v.) injection. D) Pretreatment with 5 mg/kg AM11095 prevented nicotine-induced increase of the firing rate (two-way ANOVA and Bonferroni test, $^{\#}P < 0.05$, $^{*}P < 0.05$, $^{**}P < 0.01$, $^{***}P < 0.001$; $^{****}P < 0.0001$; vehicle n = 10; AM 1 mg n = 6; AM 5 mg n = 7; AM + MK n = 6). E) Histogram summarizing results on firing rate calculated as areas under the curves (AUC; one-way ANOVA, $^{**}P < 0.01$). F) Pretreatment with 5 mg/kg AM11095 prevented nicotine-induced increase of bursting activity (two-way ANOVA and Bonferroni test, $^{**}P < 0.01$; $^{***}P < 0.001$; $^{****}P < 0.0001$; vehicle n = 10; AM 1 mg n = 6; AM 5 mg n = 7; AM + MK n = 6) of VTA dopamine neurons. G) AM11095 (5 mg/kg) prevented the increase in extracellular dopamine levels induced by nicotine (0.4 mg/kg, s.c.) in the shell of the nucleus accumbens (two-way ANOVA, $^{****}P < 0.0001$; vehicle and AM 5 mg n = 4). Data are expressed as Mean ± SEM.

On the other hand, AM11095 given before each saline conditioning session did not induced neither aversion nor preference (Fig. 3). The PPARα antagonist MK886 at the dose of 1 mg/kg, given after AM11905 and before each nicotine conditioning session, blocked the effect of AM11905 since a significant increase in the CPP score in comparison to the vehicle-saline group was found ($P < 0.001$, Fig. 3). Post-hoc analysis also showed that MK886 given alone before each nicotine conditioning session, did not affect the capacity of nicotine to induce CPP when compared to the vehicle-saline group ($P < 0.01$, Fig. 3).

3.4. Neurobehavioral observation battery for AM11095

In adult rats, the effect of AM11095 at 5 mg/kg or 25 mg/kg doses was investigated using a functional observational battery. A selection of autonomic, neurological, sensorial, affective and behavioral parameters was observed (Table 1) 24 h before, 120 min and 24 h after the injection of AM11095 or its vehicle (n = 10 per group). Rats did not show any significant effect, as summarized in Table 2 (n = 10 per group). Moreover, physiological parameters, such as weight and body temperature (Fig. 4A top and bottom, respectively) were not conditioned by injection of AM11095 at both doses (two-way ANOVA, $P > 0.05$). Performance in the rotarod was not affected as compared to the control group (Fig. 4B), suggesting that AM11095 did not cause motor impairments (two-way ANOVA, $P > 0.05$, n = 12 per group).

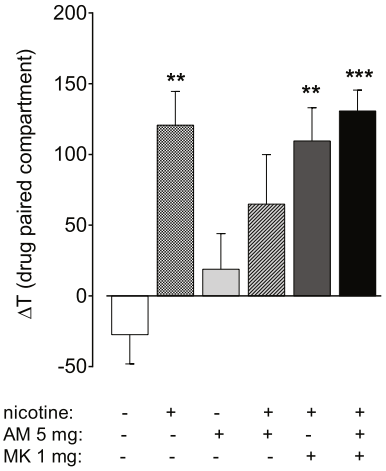

Fig. 3. Effect of pretreatment with AM11095 on nicotine-induced expression of CPP. AM11095 (5 mg/kg) or vehicle were injected i.p. 1.5 h before the animal was placed into the apparatus. MK886 (1 mg/kg) was injected 1 h after vehicle or AM11095 and 30 min before nicotine administration. Nicotine (0.4 mg/kg) or saline were injected s.c. right before the conditioning session. Data are expressed as mean ± SEM of ΔT (s) spent in the drug-paired compartment during the pre-test and the test (one-way ANOVA, Tukey's test, $^{**}P < 0.01$, $^{***}P < 0.001$; n = 8–10 animals per group).

4. Discussion

Our findings indicate that in rats NAAA inhibition induces increases in PEA and OEA levels in the hippocampus and OEA levels in the cortex and can counteract the reward-related effects of nicotine on the brain and behavior. Hence, a pretreatment with the brain permeable NAAA inhibitor AM11095 prevented nicotine-induced excitation of dopaminergic transmission in reward-related areas of the brain. Specifically, the NAAA inhibitor prevented nicotine-induced increases in firing rate and burst firing in dopamine neurons in the VTA and nicotine-induced elevations of dopamine levels in the shell of the nucleus accumbens. Consistent with the ability to prevent nicotine's effects in reward-related brain areas, AM11095 significantly decreased nicotine-induced CPP. These effects were abolished by the PPARα antagonist MK886. At the doses that produced these potentially beneficial effects with nicotine (5 mg/kg) or at a 5-fold higher dose (25 mg/kg) AM11095 was devoid of neurobehavioral or neurotoxic effects, as it did not impair motor coordination and did not affect neurovegetative parameters or rat spontaneous behavior in the home cage or in the observation arena.

In rats treated with AM11095 2 h before sacrifice, a selective increase of OEA and PEA, but not of AEA, was observed in the hippocampus and OEA in the cortex, suggesting that this hydrolytic enzyme is expressed in the brain and contributes to the regulation of N-acylethanolamines levels. An indirect evidence of PPARα activation in the brain by its endogenous ligands is the increase in DHA detected in cortex and hippocampus, the same regions where we observed increased OEA and/or PEA levels. Hence, it has been shown that DHA

Table 2
Results of the neurobehavioral observation battery.

Observation	vehicle			5 mg/kg			25 mg/kg		
	t = −24 h	t = 2 h	t = 24 h	t = −24 h	t = 2 h	t = 24 h	t = −24 h	t = 2 h	t = 24 h
Home cage									
Abnormal posture	0/10	0/10	0/10	0/10	2/10	0/10	0/10	4/10	2/10
Awareness/fear									
Vocalizations	0/10	0/10	0/10	0/10	0/10	0/10	0/10	0/10	0/10
Ease of removal	0	0	0	0	0	0	0	0	0
Ease of handling	0	0	0	0	0	0	0	0	0
Arousal	0	0	0	1	−0.25	−1	0	−1	−1
Finger approach	0	0	0	1	0	0	0	0	−1
Head touch	0	0	−0.5	0	0	0	0	0	−0.5
Visual placing	0	0	0	0	0	0	0	0	0
Motor activity									
Immobility	3.2 ± 1.2	15.3 ± 4.3	17.3 ± 4.4	6.9 ± 2.5	17.2 ± 5.1	19.1 ± 3.7	6.7 ± 2.4	18.2 ± 4.9	24. 2 ± 5.0
Rears	4.9 ± 0.9	3.8 ± 0.9	3.8 ± 0.9	5.2 ± 1.1	3.1 ± 0.9	2.0 ± 0.5	3.8 ± 0.9	3.1 ± 0.8	2.4 ± 0.6
Ataxic gait	0	0	0	0	0	0	0	0	0
Central excitation									
Seizures	0	0	0	0	0	0	0	0	0
Tail flick	0	0	0	0	0	0	0	0	0
Finger snap	0	0	0	0	0	0	0	0	0
Muscle tone									
Body tone	0	0	0	0	0	0	0	0	0
Reflexes									
Corneal reflex	0	0	0	0	0	0	0	0	0
Righting reflex	0	0	0	0	0	0	0	0	0
Air righting reflex	0	0	0	0	0	0	0	0	0
Respiratory system									
Respiration	0	0	0	0	0	0	0	0	0
Autonomic profile									
Salivation	0	0	0	0	0	0	0	0	0
Lacrimation	0	0	0	0	0	0	0	0	0
Piloerection	0/10	0/10	0/10	0/10	0/10	0/10	0/10	0/10	0/10
Feces	0.1 ± 0.1	0.3 ± 0.2	0.3 ± 0.2	0.1 ± 0.1	0	0.3 ± 0.3	0	0	0
Urine	0.1 ± 0.1	0	0	0	0	0	0	0	0
Miscellaneus									
Aggressiveness	0/10	0/10	0/10	0/10	0/10	0/10	0/10	0/10	0/10
Catalepsy	0/10	0/10	0/10	0/10	0/10	0/10	0/10	0/10	0/10
Tremors	0/10	0/10	0/10	0/10	0/10	0/10	0/10	0/10	0/10
Compulsive grooming	0/10	0/10	0/10	0/10	0/10	0/10	0/10	0/10	0/10
Death	0/10	0/10	0/10	0/10	0/10	0/10	0/10	0/10	0/10

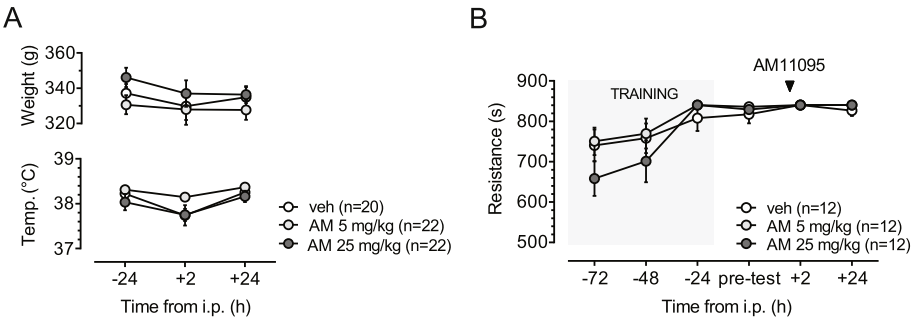

Fig. 4. Effects of the NAAA inhibitor AM11095 on physiological parameters and motor test. A) Weight (top) and body temperature (bottom) are not affected by injection of 5 mg/kg or 25 mg/kg i.p. of AM11095. Two-way ANOVA; $P > 0.05$. B) Performance of rats in the rotarod over different sessions is measured in total seconds of endurance. After five training sessions, the animals were challenged before (−24 h), 2 and 24 h after the injection of vehicle, AM11095 5 mg/kg or 25 mg/kg i.p., n = 12 animals per group. Two-way ANOVA did not show any significant effect among groups for time and treatment ($P > 0.05$). All data are expressed as Mean ± SEM.

biosynthesis requires a peroxisomal β-oxidation step (Ferdinandusse et al., 2003) which is enhanced by PPARα activation (Rakhshandehroo et al., 2010). Consequently, PPARα activation may enhance DHA biosynthesis, as it has been recently suggested in humans, where an elevated PPARα gene expression was associated to an increase in circulating DHA (Murru et al., 2018). Therefore, the finding of increased DHA biosynthesis may imply that AM11095 induces peroxisomal β-oxidation.

The reason why we were unable to detect increases in OEA, PEA or DHA levels in other brain areas, such as the midbrain or striatum is unknown, one possibility is that NAE signalling, which is "on demand" and presumably spatially restricted is not robust enough, or increases in NAEs levels are transient and difficult to detect within the time window between drug administration and sacrifice. On the other hand, specifically in the hippocampus a robust NAE signalling and PPARα expression has been demonstrated in previous studies (Rivera et al., 2014). High levels of PPARα and NAPE-PLD expression and colocalization in several cell types might be the reason why transient increases in NAE levels are easier to detect in this brain region. Moreover, both hippocampus and cortex receive a dense cholinergic innervation and express a wide variety of nAChR subtypes (Dani and Bertrand, 2007). In the hippocampus, nicotine induces LTP in the medial perforant path-dentate gyrus synapses, the mossy fiber CA3 synapses, and the Schaffer collateral CA1 synapses (Gould and Leach, 2014). In several cortical areas, particularly in the insular cortex, nicotine was also shown to modulate long-term form of synaptic plasticity via β*nAChRs (Sato et al., 2017) or to induce dendritic remodelling (Ehlinger et al., 2012). These nicotine-induced forms of synaptic plasticity might play a role in addiction-related processing of contextual information associated with nicotine use. Thus, increased PPARα signalling in the hippocampus and the cortex, and consequent modulation of nAChRs, might underlie the potential effect of NAAA inhibitors in nicotine addiction.

Our results are is in line with findings obtained in other studies with NAAA inhibitors (Migliore et al., 2016) and highlight that these compounds do not induce general increases in the levels of endogenous endocannabinoids active at CB1/CB2 receptors. This property might be an advantage in several conditions when activation of cannabinoid receptors is not required or desirable. Consistently, AM11095 is devoid of overt behavioral effects when assessed within the FOB and does not evoke CPP *per se*. Although no significant behavioral effect potentially correlated with CB1 activation was detected, an increase in 2-AG was observed in the cortex. Interestingly, Petrosino et al. (2016) reported that administration of PEA in humans and dogs induces an increase in 2-AG *in vitro* and *in vivo* with an unknown mechanism.

The effects of NAAA inhibitors in the present study on nicotine-related behavioral, electrophysiological, and neurochemical actions are comparable to those of PPARα agonists and the FAAH inhibitor URB597 (Luchicchi et al., 2010; Mascia et al., 2011; Panlilio et al., 2012). These findings converge to suggest that the NAAA inhibitor modulates the rewarding effects of nicotine by increasing levels of the endogenous PPARα ligands OEA and PEA. This is supported by the finding that the PPARα antagonist MK886 completely suppressed the effects of AM11095 in electrophysiological and behavioral settings.

The mechanism by which direct or indirect PPARα agonists and NAAA inhibition exert these anti-addictive actions is mostly understood (Melis et al., 2008, 2010; Melis and Pistis, 2014). Mesolimbic dopamine plays a major role in nicotine addiction, being the VTA and nucleus accumbens shell critical brain areas responsible for nicotine's rewarding effects (Corrigall et al., 1994; Nisell et al., 1994; Pontieri et al., 1996). Nicotine enhances dopamine transmission in the nucleus accumbens shell directly through stimulation of somatodendritic nicotinic receptors in dopamine neurons and indirectly through stimulation of glutamate release in the VTA or in the nucleus accumbens, which in turn stimulates dopamine neuron firing and dopamine release in the nucleus accumbens shell (Mansvelder et al., 2002). Our data show that activation of PPARα, either indirectly through NAAA inhibition (present study) or directly by administration of PPARα agonists as in our previous studies (Mascia et al., 2011; Melis et al., 2008, 2010; Melis and Pistis, 2014; Panlilio et al., 2012), prevents nicotine-induced increases in firing rate and burst firing in dopamine neurons in the VTA and consequently prevents nicotine-induced elevations of dopamine levels in the shell of the nucleus accumbens. Consistently, other groups have confirmed that PPARα signalling might reduce nicotine reward and decrease the severity of nicotine-induced withdrawal (Donvito et al., 2018; Jackson et al., 2017). The mechanism underlying these effects was elucidated by our previous *in vitro* experiments, showing that activation of PPARα induces a rapid non-genomic phosphorylation of β2-containing nicotinic receptors on VTA dopamine neurons (Melis et al., 2008, 2010). Phosphorylated nicotinic receptors show diminished ionic conductance (Charpantier et al., 2005) and are rapidly internalized (Cho et al., 2005), reducing or abolishing the responses of dopamine neurons to nicotine. This downregulation of nicotine receptors is presumably the mechanisms by which experimental drugs that activate PPARα directly (Mascia et al., 2011; Melis et al., 2008, 2010; Melis and Pistis, 2014; Panlilio et al., 2012) or indirectly (i.e. the FAAH inhibitor URB597 or the NAAA inhibitor AM11095) (Forget et al., 2009; Luchicchi and Pistis, 2012; Scherma et al., 2008) block effects of nicotine in the VTA and nucleus accumbens shell that are believed (Corrigall et al., 1994; Gotti et al., 2010) to underlie nicotine reward. The electrophysiology, microdialysis, and behavioral experiments of the present study extend these findings to the NAAA inhibitors.

In conclusion, NAAA inhibitors represent a new class of pharmacological tools to modulate PEA/PPARα signalling in the brain and reduce nicotine rewarding properties, showing promise as anti-smoking medications. Future studies are needed to confirm their potential by assessing their efficacy in animal models of nicotine dependence.

Funding and disclosure

This work was supported by Progetti di Rilevante Interesse Dipartimentale (PRID), University of Cagliari and Fondazione Banco Di Sardegna (Progetti cofinanziati Università di Cagliari, Bando, 2017).

Conflict of interest

The authors declare no conflict of interest.

Acknowledgments

We thank Marta Tuveri and Dr. Barbara Tuveri for their skillful assistance.

Appendix A. Supplementary data

Supplementary data to this article can be found online at https://doi.org/10.1016/j.neuropharm.2018.11.013.

References

Alhouayek, M., Bottemanne, P., Subramanian, K.V., Lambert, D.M., Makriyannis, A., Cani, P.D., Muccioli, G.G., 2015. N-Acylethanolamine-hydrolyzing acid amidase inhibition increases colon N-palmitoylethanolamine levels and counteracts murine colitis. FASEB J 29, 650–661. https://doi.org/10.1096/fj.14-255208.

Brody, A.L., 2006. Functional brain imaging of tobacco use and dependence. J. Psychiatr. Res. 40, 404–418. https://doi.org/10.1016/j.jpsychires.2005.04.012.

Charpantier, E., Wiesner, A., Huh, K.H., Ogier, R., Hoda, J.C., Allaman, G., Raggenbass, M., Feuerbach, D., Bertrand, D., Fuhrer, C., 2005. Alpha7 neuronal nicotinic acetylcholine receptors are negatively regulated by tyrosine phosphorylation and Src-family kinases. J. Neurosci. 25, 9836–9849.

Cho, C.H., Song, W., Leitzell, K., Teo, E., Meleth, A.D., Quick, M.W., Lester, R.A., 2005. Rapid upregulation of alpha7 nicotinic acetylcholine receptors by tyrosine dephosphorylation. J. Neurosci. 25, 3712–3723.

Corrigall, W.A., Coen, K.M., Adamson, K.L., 1994. Self-administered nicotine activates the mesolimbic dopamine system through the ventral tegmental area. Brain Res. 653, 278–284.

Dani, J.A., Bertrand, D., 2007. Nicotinic acetylcholine receptors and nicotinic cholinergic mechanisms of the central nervous system. Annu. Rev. Pharmacol. Toxicol. 47, 699–729. https://doi.org/10.1146/annurev.pharmtox.47.120505.105214.

Di Chiara, G., Imperato, A., 1988. Drugs abused by humans preferentially increase synaptic dopamine concentrations in the mesolimbic system of freely moving rats. Proc. Natl. Acad. Sci. U. S. A 85, 5274–5278.

Donvito, G., Piscitelli, F., Muldoon, P., Jackson, A., Vitale, R.M., D'Aniello, E., Giordano, C., Ignatowska-Jankowska, B.M., Mustafa, M.A., Guida, F., Petrie, G.N., Parker, L., Smoum, R., Sim-Selley, L., Maione, S., Lichtman, A.H., Damaj, M.I., Di Marzo, V., Mechoulam, R., 2018. N-Oleoyl-glycine reduces nicotine reward and withdrawal in mice. Neuropharmacology. https://doi.org/10.1016/j.neuropharm.2018.03.020.

Ehlinger, D.G., Bergstrom, H.C., McDonald, C.G., Smith, R.F., 2012. Nicotine-induced dendritic remodeling in the insular cortex. Neurosci. Lett. 516, 89–93. https://doi.org/10.1016/j.neulet.2012.03.064.

Ferdinandusse, S., Denis, S., Dacremont, G., Wanders, R.J.A., 2003. Studies on the metabolic fate of n-3 polyunsaturated fatty acids. J. Lipid Res. 44, 1992–1997. https://doi.org/10.1194/jlr.M300223-JLR200.

Folch, J., Lees, M., Sloane Stanley, G.H., 1957. A simple method for the isolation and purification of total lipides from animal tissues. J. Biol. Chem. 226, 497–509.

Forget, B., Coen, K.M., Le Foll, B., 2009. Inhibition of fatty acid amide hydrolase reduces reinstatement of nicotine seeking but not break point for nicotine self-administration–comparison with CB(1) receptor blockade. Psychopharmacology (Berl) 205, 613–624. https://doi.org/10.1007/s00213-009-1569-5.

Gotti, C., Guiducci, S., Tedesco, V., Corbioli, S., Zanetti, L., Moretti, M., Zanardi, A., Rimondini, R., Mugnaini, M., Clementi, F., Chiamulera, C., Zoli, M., 2010. Nicotinic acetylcholine receptors in the mesolimbic pathway: primary role of ventral tegmental area 6 2* receptors in mediating systemic nicotine effects on dopamine release, locomotion, and reinforcement. J. Neurosci. 30, 5311–5325. https://doi.org/10.1523/jneurosci.5095-09.2010.

Gould, T.J., Leach, P.T., 2014. Cellular, molecular, and genetic substrates underlying the impact of nicotine on learning. Neurobiol. Learn. Mem. 107, 108–132. https://doi.org/10.1016/j.nlm.2013.08.004.

Jackson, A., Bagdas, D., Muldoon, P.P., Lichtman, A.H., Carroll, F.I., Greenwald, M., Miles, M.F., Damaj, M.I., 2017. In vivo interactions between alpha7 nicotinic acetylcholine receptor and nuclear peroxisome proliferator-activated receptor-alpha: implication for nicotine dependence. Neuropharmacology 118, 38–45. https://doi.org/10.1016/j.neuropharm.2017.03.005.

Lambert, D.M., Di Marzo, V., 1999. The palmitoylethanolamide and oleamide enigmas : are these two fatty acid amides cannabimimetic? Curr. Med. Chem. 6, 757–773.

Luchicchi, A., Lecca, S., Carta, S., Pillolla, G., Muntoni, A.L., Yasar, S., Goldberg, S.R., Pistis, M., 2010. Effects of fatty acid amide hydrolase inhibition on neuronal responses to nicotine, cocaine and morphine in the nucleus accumbens shell and ventral tegmental area: involvement of PPAR-alpha nuclear receptors. Addict. Biol. 15, 277–288. https://doi.org/10.1111/j.1369-1600.2010.00222.x.

Luchicchi, A., Pistis, M., 2012. Anandamide and 2-arachidonoylglycerol: pharmacological properties, functional features, and emerging specificities of the two major endocannabinoids. Mol. Neurobiol. 46, 374–392. https://doi.org/10.1007/s12035-012-8299-0.

Mansvelder, H.D., Keath, J.R., McGehee, D.S., 2002. Synaptic mechanisms underlie nicotine-induced excitability of brain reward areas. Neuron 33, 905–919.

Mascia, P., Pistis, M., Justinova, Z., Panlilio, L.V., Luchicchi, A., Lecca, S., Scherma, M., Fratta, W., Fadda, P., Barnes, C., Redhi, G.H., Yasar, S., Le Foll, B., Tanda, G., Piomelli, D., Goldberg, S.R., 2011. Blockade of nicotine reward and reinstatement by activation of alpha-type peroxisome proliferator-activated receptors. Biol. Psychiatry 69, 633–641. https://doi.org/10.1016/j.biopsych.2010.07.009.

Melis, M., Carta, S., Fattore, L., Tolu, S., Yasar, S., Goldberg, S.R., Fratta, W., Maskos, U., Pistis, M., 2010. Peroxisome proliferator-activated receptors-alpha modulate dopamine cell activity through nicotinic receptors. Biol. Psychiatry 68, 256–264. https://doi.org/10.1016/j.biopsych.2010.04.016.

Melis, M., Pillolla, G., Luchicchi, A., Muntoni, A.L., Yasar, S., Goldberg, S.R., Pistis, M., 2008. Endogenous fatty acid ethanolamides suppress nicotine-induced activation of mesolimbic dopamine neurons through nuclear receptors. J. Neurosci. 28, 13985–13994.

Melis, M., Pistis, M., 2014. Targeting the interaction between fatty acid ethanolamides and nicotinic receptors: therapeutic perspectives. Pharmacol. Res. 86, 42–49. https://doi.org/10.1016/j.phrs.2014.03.009.

Melis, M., Scheggi, S., Carta, G., Madeddu, C., Lecca, S., Luchicchi, A., Cadeddu, F., Frau, R., Fattore, L., Fadda, P., Ennas, M.G., Castelli, M.P., Fratta, W., Schilstrom, B., Banni, S., De Montis, M.G., Pistis, M., 2013. PPARalpha regulates cholinergic-driven activity of midbrain dopamine neurons via a novel mechanism involving alpha7 nicotinic acetylcholine receptors. J. Neurosci. 33, 6203–6211. https://doi.org/10.1523/JNEUROSCI.4647-12.2013.

Migliore, M.D., Pontis, S.D., Fuentes de Arriba, A.L., Realini, N., Torrente, E., Armirotti, A., Romeo, E., Di Martino, S., Russo, D., Pizzirani, D., Summa, M., Lanfranco, M., Ottonello, G., Busquet, P., Jung, K.M., Garcia-Guzman, M., Heim, R., Scarpelli, R., Piomelli, D., 2016. Second-generation non-covalent NAAA inhibitors are protective in a model of multiple sclerosis. Angew. Chem., Int. Ed. Engl. 55, 11193–11197. https://doi.org/10.1002/anie.201603746.

Moreno, S., Farioli-Vecchioli, S., Ceru, M.P., 2004. Immunolocalization of peroxisome proliferator-activated receptors and retinoid X receptors in the adult rat. CNS Neurosci. 123, 131–145.

Moscardo, E., Maurin, A., Dorigatti, R., Champeroux, P., Richard, S., 2007. An optimised methodology for the neurobehavioural assessment in rodents. J. Pharmacol. Toxicol. Methods 56, 239–255. https://doi.org/10.1016/j.vascn.2007.03.007.

Murru, E., Carta, G., Cordeddu, L., Melis, M.P., Desogus, E., Ansar, H., Chilliard, Y., Ferlay, A., Stanton, C., Coakley, M., Ross, R.P., Piredda, G., Addis, M., Mele, M.C., Cannelli, G., Banni, S., Manca, C., 2018. Dietary conjugated linoleic acid-enriched cheeses influence the levels of circulating n-3 highly unsaturated fatty acids in humans. Int. J. Mol. Sci. 19. https://doi.org/10.3390/ijms19061730.

Nisell, M., Nomikos, G.G., Svensson, T.H., 1994. Systemic nicotine-induced dopamine release in the rat nucleus accumbens is regulated by nicotinic receptors in the ventral tegmental area. Synapse 16, 36–44. https://doi.org/10.1002/syn.890160105.

O'Sullivan, S.E., 2007. Cannabinoids go nuclear: evidence for activation of peroxisome proliferator-activated receptors. Br. J. Pharmacol. 152, 576–582.

Panlilio, L.V., Justinova, Z., Mascia, P., Pistis, M., Luchicchi, A., Lecca, S., Barnes, C., Redhi, G.H., Adair, J., Heishman, S.J., Yasar, S., Aliczki, M., Haller, J., Goldberg, S.R., 2012. Novel use of a lipid-lowering fibrate medication to prevent nicotine reward and relapse: preclinical findings. Neuropsychopharmacology 37, 1838–1847. https://doi.org/10.1038/npp.2012.31.

Paxinos, G., Watson, C., 2007. The Rat Brain in Stereotaxic Coordinates. Elsevier Academic Press, London.

Petrosino, S., Schiano Moriello, A., Cerrato, S., Fusco, M., Puigdemont, A., De Petrocellis, L., Di Marzo, V., 2016. The anti-inflammatory mediator palmitoylethanolamide enhances the levels of 2-arachidonoyl-glycerol and potentiates its actions at TRPV1 cation channels. Br. J. Pharmacol. 173, 1154–1162. https://doi.org/10.1111/bph.13084.

Pistis, M., Melis, M., 2010. From surface to nuclear receptors: the endocannabinoid family extends its assets. Curr. Med. Chem. 17, 1450–1467.

Pistis, M., O'Sullivan, S.E., 2017. The role of nuclear hormone receptors in cannabinoid function. Adv. Pharmacol. 80, 291–328. https://doi.org/10.1016/bs.apha.2017.03.008.

Pontieri, F.E., Tanda, G., Orzi, F., Di Chiara, G., 1996. Effects of nicotine on the nucleus accumbens and similarity to those of addictive drugs. Nature 382, 255–257. https://doi.org/10.1038/382255a0.

Rakhshandehroo, M., Knoch, B., Muller, M., Kersten, S., 2010. Peroxisome proliferator-activated receptor alpha target genes. PPAR Res. https://doi.org/10.1155/2010/612089. 2010.

Ribeiro, A., Pontis, S., Mengatto, L., Armirotti, A., Chiurchiu, V., Capurro, V., Fiasella, A., Nuzzi, A., Romeo, E., Moreno-Sanz, G., Maccarrone, M., Reggiani, A., Tarzia, G., Mor, M., Bertozzi, F., Bandiera, T., Piomelli, D., 2015. A potent systemically active N-acylethanolamine acid amidase inhibitor that suppresses inflammation and human macrophage activation. ACS Chem. Biol. 10, 1838–1846. https://doi.org/10.1021/acschembio.5b00114.

Rivera, P., Arrabal, S., Vargas, A., Blanco Calvo, E., Serrano, A., Pavon, F.J., Rodriguez de Fonseca, F., Suarez, J., 2014. Localization of peroxisome proliferator-activated receptor alpha (PPARα) and N-acyl phosphatidylethanolamine phospholipase D (NAPE-PLD) in cells expressing the Ca2+-binding proteins calbindin, calretinin, and parvalbumin in the adult rat hippocampus. Front. Neuroanat. 8. https://doi.org/10.3389/fnana.2014.00012.

Sagheddu, C., Aroni, S., De Felice, M., Lecca, S., Luchicchi, A., Melis, M., Muntoni, A.L., Romano, R., Palazzo, E., Guida, F., Maione, S., Pistis, M., 2015. Enhanced serotonin and mesolimbic dopamine transmissions in a rat model of neuropathic pain. Neuropharmacology 97, 383–393. https://doi.org/10.1016/j.neuropharm.2015.06.003.

Sato, H., Kawano, T., Yin, D.X., Kato, T., Toyoda, H., 2017. Nicotinic activity depresses

synaptic potentiation in layer V pyramidal neurons of mouse insular cortex. Neuroscience 358, 13–27. https://doi.org/10.1016/j.neuroscience.2017.06.031.

Scherma, M., Justinova, Z., Zanettini, C., Panlilio, L.V., Mascia, P., Fadda, P., Fratta, W., Makriyannis, A., Vadivel, S.K., Gamaleddin, I., Le Foll, B., Goldberg, S.R., 2012. The anandamide transport inhibitor AM404 reduces the rewarding effects of nicotine and nicotine-induced dopamine elevations in the nucleus accumbens shell in rats. Br. J. Pharmacol. 165, 2539–2548. https://doi.org/10.1111/j.1476-5381.2011.01467.x.

Scherma, M., Panlilio, L.V., Fadda, P., Fattore, L., Gamaleddin, I., Le Foll, B., Justinova, Z., Mikics, E., Haller, J., Medalie, J., Stroik, J., Barnes, C., Yasar, S., Tanda, G., Piomelli, D., Fratta, W., Goldberg, S.R., 2008. Inhibition of anandamide hydrolysis by URB597 reverses abuse-related behavioral and neurochemical effects of nicotine in rats. J. Pharmacol. Exp. Therapeut. https://doi.org/10.1124/jpet.108.142224.

Solorzano, C., Zhu, C., Battista, N., Astarita, G., Lodola, A., Rivara, S., Mor, M., Russo, R., Maccarrone, M., Antonietti, F., Duranti, A., Tontini, A., Cuzzocrea, S., Tarzia, G., Piomelli, D., 2009. Selective N-acylethanolamine-hydrolyzing acid amidase inhibition reveals a key role for endogenous palmitoylethanolamide in inflammation. Proc. Natl. Acad. Sci. U. S. A 106, 20966–20971. https://doi.org/10.1073/pnas.0907417106.

Tai, T., Tsuboi, K., Uyama, T., Masuda, K., Cravatt, B.F., Houchi, H., Ueda, N., 2012. Endogenous molecules stimulating N-acylethanolamine-hydrolyzing acid amidase (NAAA). ACS Chem. Neurosci. 3, 379–385. https://doi.org/10.1021/cn300007s.

Tsuboi, K., Takezaki, N., Ueda, N., 2007. The N-acylethanolamine-hydrolyzing acid amidase (NAAA). Chem. Biodivers. 4, 1914–1925. https://doi.org/10.1002/cbdv.200790159.

Ueda, N., Yamanaka, K., Yamamoto, S., 2001. Purification and characterization of an acid amidase selective for N-palmitoylethanolamine, a putative endogenous anti-inflammatory substance. J. Biol. Chem. 276, 35552–35557. https://doi.org/10.1074/jbc.M106261200.

Williams, J., Wood, J., Pandarinathan, L., Karanian, D.A., Bahr, B.A., Vouros, P., Makriyannis, A., 2007. Quantitative method for the profiling of the endocannabinoid metabolome by LC-atmospheric pressure chemical ionization-MS. Anal. Chem. 79, 5582–5593. https://doi.org/10.1021/ac0624086.

Wise, R.A., 2004. Dopamine, learning and motivation. Nat. Rev. Neurosci. 5, 483–494.

World Health Organization, 2011. Who report on the global tobacco epidemic, 2011. Warning About the Dangers of Tobacco (World Health Organization).

Zhou, F.M., Liang, Y., Dani, J.A., 2001. Endogenous nicotinic cholinergic activity regulates dopamine release in the striatum. Nat. Neurosci. 4, 1224–1229. https://doi.org/10.1038/nn769.

Received: 14 December 2018 | Revised: 14 February 2019 | Accepted: 5 March 2019

DOI: 10.1111/ejn.14400

SHORT COMMUNICATION

EJN European Journal of Neuroscience FENS WILEY

Opposite responses to aversive stimuli in lateral habenula neurons

Mauro Congiu[1,2,3] | **Massimo Trusel**[1] | **Marco Pistis**[2,3] | **Manuel Mameli**[1,4] | **Salvatore Lecca**[1]

[1]Department of Fundamental Neuroscience, University of Lausanne, Lausanne, Switzerland

[2]Department of Biomedical Science, University of Cagliari, Cagliari, Italy

[3]Section of Cagliari, Neuroscience Institute, National Research Council of Italy (CNR), Monserrato, Italy

[4]Institut national de la Santé et de la Recherche Médicale UMR-S 839, Paris, France

Correspondence
Salvatore Lecca, Department of Fundamental Neuroscience, University of Lausanne, Lausanne, Switzerland.
Email: salvatore.lecca@unil.ch

Funding information
Narsad Young Investigator, Grant/Award Number: 27089; Swiss National Science Foundation, Grant/Award Number: 31003A; European Research Council Starting Grant, Grant/Award Number: 335333

Abstract

Appropriate behavioural strategies to cope with unexpected salient stimuli require synergistic neuronal responses in diverse brain regions. Among them, the epithalamic lateral habenula (LHb) plays a pivotal role in processing salient stimuli of aversive valence. Integrated in the complex motivational circuit, LHb neurons are indeed excited by aversive stimuli, including footshock (Fs). However, whether such excitation is a common feature represented throughout the LHb remains unclear. Here, we combined single-unit extracellular recordings in anaesthetized mice with juxtacellular labelling to describe the nature, location and pharmacological properties of Fs-driven responses within the LHb. We find that, along with Fs-excited cells, about 10% of LHb neurons display Fs-mediated inhibitory responses. Such inhibited neuronal population, in contrast to Fs-excited neurons, display regular and high frequency activity at baseline and is clustered in the medial portion of the LHb. Juxtacellular labelling of Fs-excited and inhibited neurons unravels that both populations are of glutamatergic type, as they co-localized with the EAAC1 glutamatergic transporter but not with the GAD67 GABAergic marker. Moreover, while the excitatory responses to Fs require both AMPA and NMDA receptors, the inhibitory responses rely instead on $GABA_A$ channels. Taken together, our results indicate that two functionally and partly segregated LHb neuronal ensembles encode Fs in an opposite fashion. This highlights the neuronal complexity in the LHb for processing aversive external stimuli.

KEYWORDS

aversion, in vivo recordings, juxtacellular labelling, lateral habenula, pharmacology

1 | INTRODUCTION

Behavioural adaptations to unexpected harmful stimuli require, in both animals and humans, the coordination of diverse brain regions (Hu, 2016), including the lateral habenula (LHb). The LHb is an epithalamic nucleus, which lies within the neuronal circuits guiding motivated behaviours (Hikosaka, 2010; Lecca, Meye, & Mameli, 2014).

Neurons in the LHb exert inhibitory control over dopamine (DA)-containing cells in the midbrain (Christoph, Leonzio, & Wilcox, 1986; Ji & Shepard, 2007; Stamatakis & Stuber, 2012), mainly via a direct modulation of GABAergic neurons in the rostromedial tegmental nucleus (RMTg; Jhou, Geisler, Marinelli, Degarmo, & Zahm,

Edited by Michel Barrot. Reviewed by Thomas Jhou and Jennifer Kaufling.

All peer review communications can be found with the online version of the article.

TABLE 1 Mice and cells included in the study

Experiment	Fs-excited cells	Fs-inhibited cells	Fs-not responsive cells	Total of Cells per experiment (*n*)	Mice (*N*)
Distribution of cells (Figure 1d)	29	8	44	81	14
Juxtacellular labelling (Figure 2)	4	3		7	5
Pharmacology (Figure 3)	17	13		30	25
Total	50	24	44	118	44

2009; Kaufling, Veinante, Pawlowski, Freund-Mercier, & Barrot, 2009; Lecca et al., 2011). Accordingly, convergent evidence from non-human primates and rodents shows that LHb neurons process reward and aversion in an opposite fashion compared to DAergic cells of the ventral tegmental area (VTA)/substantia nigra (SN). Indeed, LHb cells display a phasic activation upon aversive stimuli (or cues predicting negative outcomes) and inhibition to rewarding events (and reward-associated stimuli) (Matsumoto & Hikosaka, 2007; Schultz, Dayan, & Montague, 1997; Tian & Uchida, 2015; Wang et al., 2017). Consistently, aversive stimuli including footshocks (Fs) predominantly recruit glutamatergic neurotransmission arising from several inputs (i.e. hypothalamus and/or entopeduncular nucleus; Shabel, Proulx, Trias, Murphy, & Malinow, 2012; Stephenson-Jones et al., 2016; Barker et al., 2017) to excite LHb neurons (Lecca et al., 2017). Yet, aversion-excited cells in the LHb represent only a portion of the entire neuronal population (Dong, Wilson, Skolnick, & Dafny, 1992; Gao, Hoffman, & Benabid, 1996; Lecca et al., 2017; Wang et al., 2017). Whether the remaining LHb neuronal subset is simply not involved in processing aversive stimuli or rather differently modulated is unknown.

2 | MATERIALS AND METHODS

2.1 | Experimental subjects

All experiments were carried out in 7- to 9-week-old C57Bl/6J male mice (Janvier Labs, France). Animals were used in accordance with the regulations of the Cantonal Veterinary Offices of Vaud and Zurich (Switzerland; License VD3171). Mice were housed five per cage with water and food ad libitum under a 12 h light/dark cycle (with lights on at 07:00 hr). The number of mice employed in this study as well the cells recorded is reported in table 1.

2.2 | In vivo electrophysiology

Mice were anaesthetized using isoflurane (Univentor, Malta. Induction: 2%; maintenance: 1–1.5%) and placed in the stereotaxic apparatus (Kopf, Germany). Their body temperature was maintained at 36 ± 1°C using a feedback-controlled heating pad (CMA 450 Temperature controller, USA). The scalp was retracted and one burr hole was drilled above the LHb (AP: −1.3 to −1.6 mm, L: 0.35–0.5 mm, V: −2.3 to −3.2 mm) for the placement of a recording electrode. Single-unit activity was recorded extracellularly using glass micropipettes filled with 2% Chicago sky blue dissolved in 0.5 M sodium acetate (impedance 5–15 MΩ). Signal was filtered (band-pass 500–5000 Hz), pre-amplified (DAM80, WPI, Germany), amplified (Neurolog System, Digitimer, UK) and displayed on a digital storage oscilloscope (OX 530, Metrix, USA). Experiments were sampled on- and offline by a computer connected to CED Power 1401 laboratory interface (Cambridge Electronic Design, Cambridge, UK) running the Spike2 software (Cambridge Electronic Design).

Single units were isolated and the spontaneous activity was recorded for a minimum of 3 min before starting the shock protocol. Spontaneous firing rate, percent of spikes in bursts and coefficient of variation (CV = standard deviation of inter-spike intervals/mean inter-spike interval; a measure of firing regularity) expressed as percentage were

FIGURE 1 Opposite responses to footshock in the Lateral Habenula. (a) Schematic of the experimental timeline, spike waveform and representative firing patterns of LHb neurons; (b) Representative trace, raster plot and peristimulus time histogram of an Fs-excited LHb neuron. For graphical simplification, only 15 trials out of 30 are reported in the raster plot. A representative trace is highlighted in the raster plot. (c) Same as B but for a Fs-Inhibited LHb neuron. (d) Pie chart for Fs-excited, inhibited and not responding LHb neurons; (e) Recording location of a LHb neuron (arrow, pontamine sky blue (PsB) dye); territorial distribution of all the Fs-excited and Fs-inhibited neurons recorded in this study. (f) Bar graph and scatter plot of Fs response latency (left), duration (centre) and firing rate$_{\text{shock-baseline}}$ (right) for excited (red) and inhibited (blue) cells. (g) Bar graph and scatter plot of % of spikes in burst (left), coefficient of variation (CV%, centre) and baseline firing rate (right), for Fs-excited (red) and Fs-inhibited (blue) cells. (h) Graph representing CV% versus basal firing rate of the single cells. DG: Dentate Gyrus; 3V: 3d Ventricle; MHb: medial habenula; sm: stria medullaris; fr: fasciculus retroflexus. [Colour figure can be viewed at wileyonlinelibrary.com]

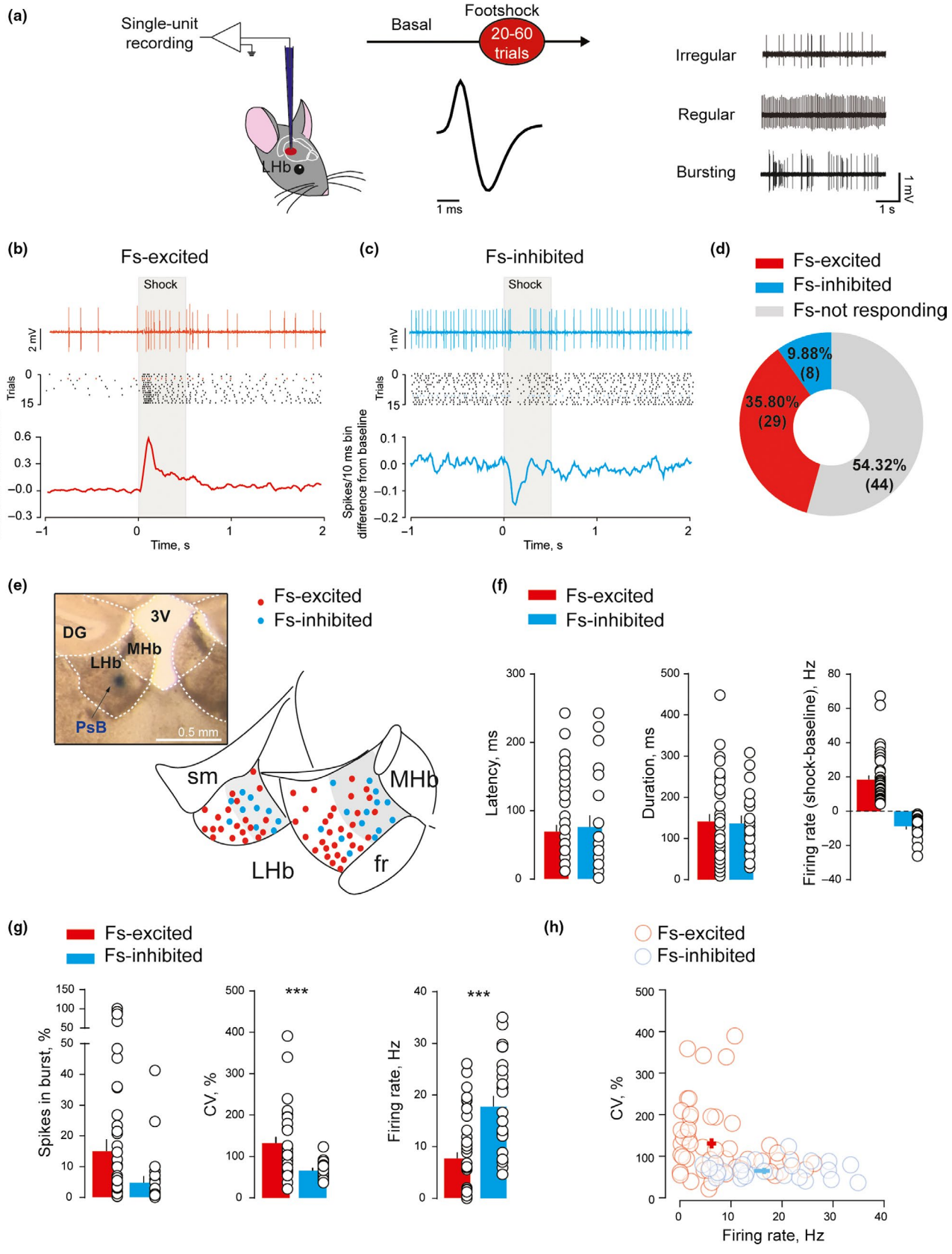

determined. Bursts were identified as the occurrence of two spikes at an inter-spike interval of <10 ms and terminated when the inter-spike interval exceeded 20 ms.

After recording baseline activity, each cell was tested for its response to repetitive (every 5 s) shocks (0.5 s, 1 mA) delivered to the hind paw contralateral to the recording side.

Peristimulus time histograms (PSTHs) and raster plots were built from 20 to 60 shocks and displayed using 10 ms bin width. A cell was considered excited when the mean number of action potentials/bin (bin length = 10 ms) in at least one of the four epochs (50 ms per epoch) after the shock inset was higher than the baseline (the average number of action potentials/bin in the 2-s period before the shock) plus two times the Standard Deviation (*SD*). The latency of the response was calculated as the first of at least two consecutive bin higher than the 2*SD* of the averaged baseline. The duration of the response was calculated from the latency to the first of at least five consecutive bins not different than the baseline +2*SD*.

Inhibition was defined as a period of at least three consecutive bins in which the mean count per bin dropped at least 35% below average baseline during Fs presentation (Tan et al., 2012). The duration of the inhibitory response was obtained subtracting the latency (represented by the first of at least three consecutive bins in which the average count was < 35% of the average baseline) from the last of at least two consecutive bins higher than the 35% of the baseline. The magnitude of the response in both cases was obtained subtracting the baseline firing rate to the firing during the duration of the shock response.

A double-barrel pipette assembly (injection tip, <50 μm in diameter attached ~100 μm above the recording tip) was used for recording LHb spike activity with simultaneous local microinjection of drugs (Lecca et al., 2017). The injection pipette was filled with one of the following: CGP 54626 (100 μM), Picrotoxin (PTX, 0.5 μM), AP5 (100 μM) and NBQX (100 μM) (Lecca et al., 2017; Root, Mejias-Aponte, Qi, & Morales, 2014; Root, Mejias-Aponte, Zhang, et al., 2014). Drugs were microinjected into the LHb, using brief

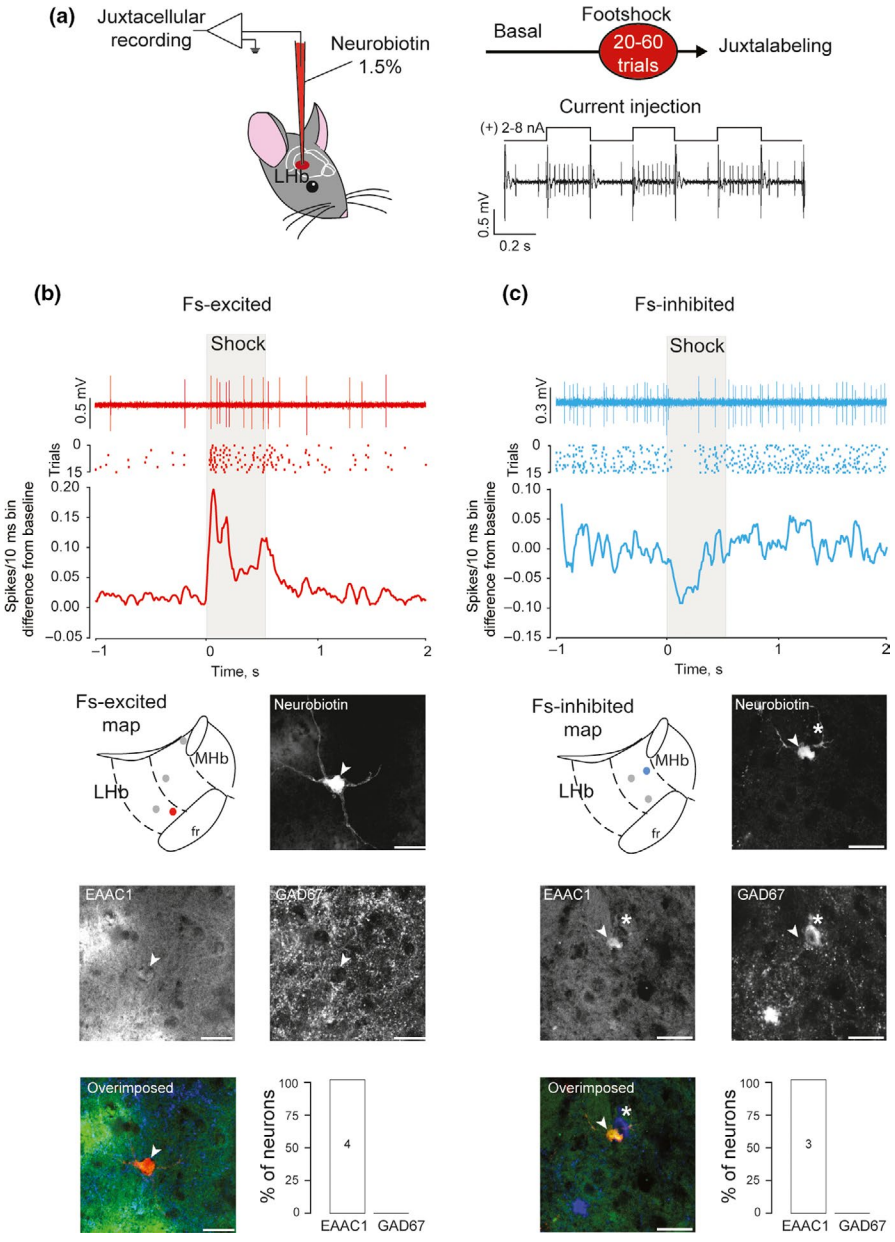

FIGURE 2 Fs-excited and Fs-inhibited cells are glutamatergic. (a) Schematic of the experiments, representative trace of an LHb neuron entrained to current injections during juxtacellular labelling trace. (b) Representative trace, raster plot and PSTH of an Fs-excited neuron. For graphical simplification, only 15 trials out of 30 are reported on the raster plot. Recording location of the labelled Fs-excited neurons shown. LHb neuron juxtacellularly labelled and immunohistochemically identified as EAAC1 positive (scale bar: 25 μm). Percentage of Fs-excited and Fs-inhibited neurons positive for EAAC1 and GAD67 staining. (c) Same as B but for Fs-inhibited neuron; * indicates a GAD67-positive neuron. [Colour figure can be viewed at wileyonlinelibrary.com]

pulses of pneumatic pressure (40 psi, 40 ms, Picospritzer, IM-300, Narishige, Japan). In all experiments, a total volume of 60–100 nl was infused over 30 s for each injection. Two injections maximum per animal were given at an interval >30 min.

At the end of each experiment, mice were euthanized (overdose of isoflurane prior to killing) and the electrode placement was determined with an iontophoretic deposit of pontamine sky blue dye (1 mA, continuous current for 5 min). Brains were then rapidly removed and fixed in 4% paraformaldehyde solution. The position of the electrodes was identified with a microscope in coronal sections (100 µm). Only recordings in the correct area were considered for analysis.

2.3 | Juxtacellular labelling and immunostaining

For this experiment, single units were isolated with glass microelectrodes (5–15 MΩ; filled with 1.5% neurobiotin (Vector Laboratories) in 0.5 M sodium acetate). The electrode was lowered in the LHb using a single axis Scientifica manipulator (IVM-1000). Signals were amplified (x 1000), filtered (band-pass 500–5000 Hz) with a Neurolog system (NL102G head-stage and DC preamplifier; Digitimer) and acquired online with a Micro1401 interface and Spike2 software (v8; Cambridge Electronic Design). After successful data collection, single neurons were labelled using the juxtacellular method (Pinault, 1996).Briefly, positive current pulses were applied through the microelectrode (200 ms, 50% duty cycle; 1–8 nA). The current was adjusted to entrain the neuron for 1 to 5 min and hence allow the uptake of neurobiotin (Vector Laboratories). After the entrainment, mice were kept for at least 30 min before being subjected to transcardial perfusion with 4% PFA. Brains were removed and kept in 4% PFA overnight, and then transferred to 30% sucrose solution. Coronal sections (30 µm) containing LHb were cut with a cryostat. Free-floating sections were rinsed in PBS + 0.1% Triton X-100 three times for 15 min and then incubated with Alexa Fluor 568-conjugated streptavidin (Invitrogen, 1:1000 in PBS + 0.1% Triton X-100; catalog number S11226) overnight at 4°C. Free-floating sections were rinsed in PBS three times for 15 min and they underwent an anti-gene retrieval with sodium citrate 50 mM in purified water at pH 9 for 30 min at 80°C. The sections were rinsed in PBS three times for 15 min and incubated with a blocking solution (PBS with 5% normal goat serum) for 1 hr before to be incubated with anti-GAD67 (host species mouse; dilution 1:500 in PBS with 5% normal goat serum; catalog number MAB5406, Chemicon) and anti-EAAC1 (host species goat; dilution 1:300 in PBS with 5% normal goat serum; catalog number AB1520, Chemicon) antibodies for 48 hr at 4°C. The slices were washed one time with high salt PBS (NaCl 600 mM), two times with PBS and incubated with secondary antibody anti-goat (host species donkey; dilution 1:500 in PBS with 5% normal goat serum, conjugated with Alexa Fluor 488; Invitrogen) 24 hr

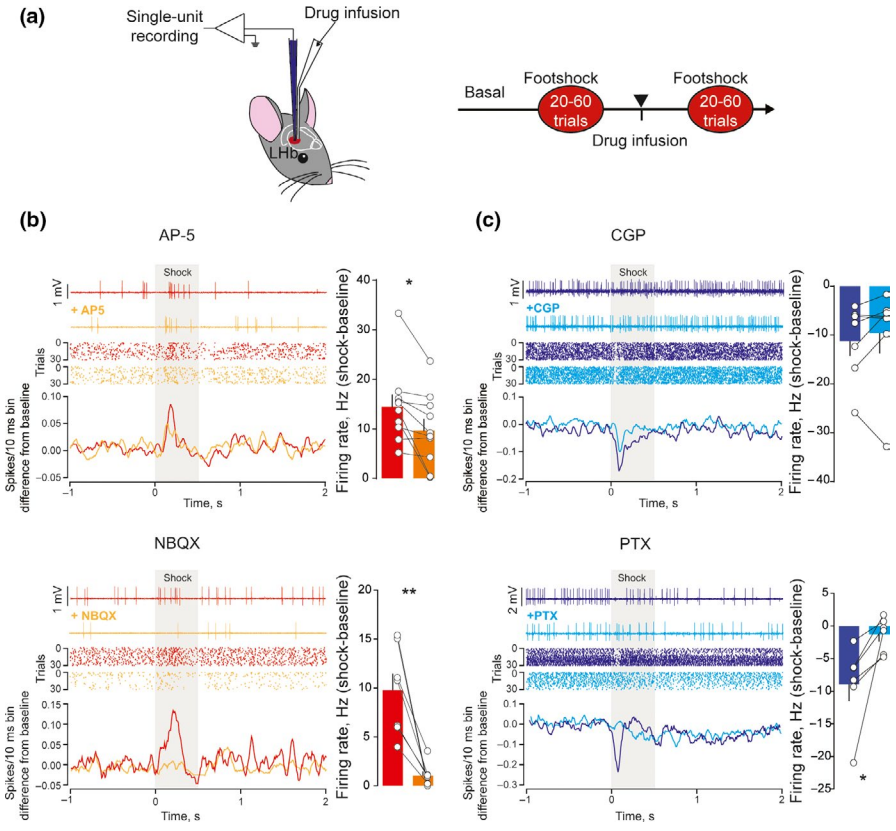

FIGURE 3 AMPA, NMDA and $GABA_A$ receptors mediation of Fs responses. (a) Schematic of the experiments. (b) Top panel: example trace, raster plot and PSTH before and after local infusion of NMDA receptor antagonist (AP-5 100 µM); right: bar graph and scatter plot of the firing $rate_{shock\text{-}baseline}$ before and after infusion of APV. Bottom panel: same as B top panel but for AMPA receptor antagonist (NBQX 100 µM). (c) Top panel: same as B top panel but for $GABA_B$ receptor antagonist (CGP 54626, 100 µM); on the right bar graph and scatter plot of the delta firing before and after infusion of CGP. Bottom panel: same as top panel but before and after infusion of $GABA_A$ antagonist (picrotoxin, PTX, 0.5 µM). [Colour figure can be viewed at wileyonlinelibrary.com]

at room temperature. The slices were rinsed one time with high salt PBS (NaCl 600 mM), two times with PBS and incubated with secondary antibody anti-mouse (host species goat; dilution 1:500 in PBS with 5% normal goat serum, conjugated with Alexa Fluor 647; Invitrogen) 24 hr at room temperature. The slices were rinsed one time with high salt PBS (NaCl 600 mM), two times with PBS and mounted on glass slides with Pro-Long antifade reagent (Invitrogen, p36931). Images were acquired using a confocal microscope (TCS SP5 AOBS TANDEM, Leica) with a 20X and a 63X immersion objective.

ImageJ software (version 1.6, http://rsb.info.nih.gov/ij/) was used for image processing.

2.4 | Drugs

The $GABA_A$ antagonist (picrotoxin), the $GABA_B$ antagonist (CGP 54626), the NMDA receptor antagonist (AP5) and the AMPA receptor antagonist (NBQX) were obtained from Tocris and Hello Bio (Bristol, UK). All drugs were dissolved in PBS, except for CGP54626 that was dissolved in DMSO.

2.5 | Statistical analysis

Online/offline analyses were performed using Spike2 (Cambridge Electronic Design) and Prism (Graphpad, USA). Data distribution was systematically tested with D'Agostino–Pearson and Shapiro–Wilk normality tests. Depending on the distribution, parametric or not parametric test was used. Single data points are always plotted. Sample size was pre-estimated from previously published research and from pilot experiments performed in the laboratory. Compiled data are expressed as mean ± *SEM*. Significance was set at $p < 0.05$ using two-sided unpaired and paired *t* test, Mann–Whitney test, Kolmogorov–Smirnov test or Wilcoxon matched-pairs signed rank test.

3 | RESULTS

3.1 | Distinct footshock responses within the LHb

We employed extracellular single-unit recordings in isoflurane-anaesthetized mice recording a total number of 118 cells in 44 mice (table 1). We first isolated the activity of 81 LHb neurons (from 14 mice) in an unbiased way to quantify and qualify their responses to footshocks (Fs, Figure 1a). In line with previous reports (Kowski, Veh, & Weiss, 2009; Lecca et al., 2017;Yang, Cui, et al., 2018; Yang, Wang, Hu, & Hu, 2018), LHb neurons fire spontaneously with a regular, irregular or burst pattern (Figure 1a). We found that 29 LHb cells displayed a phasic excitation upon Fs (Fs-excited cells). On the other hand, eight neurons showed a significant phasic inhibition time locked to Fs delivery (Fs-inhibited cells, Figure 1c,d). The remaining cells recorded were not responding to Fs (Fs-not responding).

Next, we sought to compare location and features of solely Fs-excited and Fs-inhibited cells. To this purpose, we analysed and compared all Fs-responsive cells recorded throughout the study (see Table 1; $n_{mice} = 44$, Fs-excited vs. Fs-inhibited: $n_{cells} = 50$ vs. 24). Interestingly, mapping the position of recorded neurons using post hoc histological analysis revealed that Fs-inhibited cells were mainly located in the medial portion of the LHb (Figure 1e). In contrast, Fs-excited neurons were found throughout the LHb without any apparent territorial preference (Lecca et al., 2017). Both inhibitory and excitatory responses to Fs shared similar properties including latency (Fs-excited vs. Fs-inhibited: 70.6 ± 8.38 ms vs. 77.08 ± 15.47 ms; Mann-Whitney test, U = 593.5, $p = 0.471$) and duration (Fs-excited vs. Fs-inhibited: 145.2 ± 15.12 ms vs. 137.9 ± 16.98 ms; Mann-Whitney test, U = 591, $p = 0.46$) of the response (Figure 1f). Furthermore, we also computed the overall Fs-driven modulation in firing for each recorded cell (Figure 1f): Fs-excited and Fs-inhibited LHb neurons displayed an increase of about 20 Hz and a decrease of about 10 Hz respectively (Firing $rate_{shock\text{-}baseline}$; Fs-excited: 18.63 ± 1.84 Hz; Fs-inhibited: −9.08 ± 1.22 Hz). We found that the baseline firing rate of Fs-inhibited cells was regular (% of spikes in burst; Fs-excited vs. Fs-inhibited: 14.87 ± 3.49% vs.: 4.84 ± 1.92%; Mann-Whitney test, U = 485 $p = 0.0901$. CV %; Fs-excited vs. Fs-inhibited: 131.4 ± 12.14% vs. 67.45 ± 4.04%; Mann-Whitney test, U = 247, $^{***}p < 0.0001$) and higher in frequency (Fs-excited vs. Fs-inhibited: 7.77 ± 1.02 Hz vs. 17.84 ± 1.91 Hz; Mann-Whitney test, U = 226, $^{***}p < 0.0001$) than Fs-excited neurons (Figure 1g). The dissimilar baseline firing pattern, together with the frequency of spontaneous action potential discharge and the partial territorial segregation, indicates the existence of two LHb neuronal subtypes with discernible electrophysiological features (Figure 1h).

3.2 | Fs-excited and Fs-inhibited LHb neurons are glutamatergic

Previous studies indicate that LHb neurons are morphologically heterogeneous, long-range projecting, and glutamate-containing (Aizawa, Kobayashi, Tanaka, Fukai, & Okamoto,2012; Li et al., 2011; Weiss & Veh, 2011). However, this assumption was recently challenged by evidence reporting the existence of a hybrid GABA/Glutamate-containing neuronal subtype (Zhang, Hernández, Vázquez-Juárez, Chay, & Barrio, 2016; Zhang, Hernánde, et al., 2018; Zhang, Shen, et al., 2018). This neuronal population represents a minority of LHb neurons, they display long-range axons, and may potentially act as local inhibitory interneurons, although their function remains still unknown. Importantly, similar to Fs-inhibited neurons, such GABAergic population

is located exclusively in the medial portion of the LHb. To test the neurochemical nature of Fs-excited and Fs-inhibited neurons, we examined the expression of glutamatergic and/or GABAergic markers (EAAC1, a non-vesicular glutamatergic transporter and GAD67, one of the main enzyme synthetizing GABA respectively). We isolated either Fs-excited or Fs-inhibited cells in the LHb and juxtacellular labelled them with neurobiotin (Figure 2a). We successfully neurobiotin-filled and recovered four Fs-excited and three Fs-inhibited neurons (Figure 2b–c). Notably, the location of the cells inhibited by footshock was again confined to the medial portion of the LHb, strengthening our previous observation (Figure 2c).

Immunolabelling of EAAC1 was found in both Fs-excited and Fs-inhibited cells (Figure 2b–c). In contrast, although we did observe GAD67 positive cells in the LHb (Figure 2c), neither excited nor inhibited neurons co-stained with this marker. This suggests that both LHb neurons modulated by Fs are of glutamatergic nature.

3.3 | Cellular substrates of Fs responses in LHb neurons

Fs-driven excitation of LHb neurons requires glutamatergic transmission from the lateral hypothalamus (Lecca et al., 2017). Yet, the exact contribution of the glutamatergic receptors subtype remains unexplored. We thereby tested the independent role of postsynaptic glutamate receptors in the Fs-induced excitation (Figure 3a–b). We used a double-barrel system allowing pharmacological infusion in close proximity of the recorded cell. After isolating LHb single units and acquiring Fs-induced excitation, we infused the NMDA receptor antagonist AP5 (100 μM; $n_{mice} = 7$; $n_{cells} = 10$). Blocking NMDA receptors reduced the Fs-induced excitation of LHb neurons (Firing $rate_{shock\text{-}baseline;}$ before vs. after: 14.43 ± 2.42 Hz vs. 9.61 ± 2.32 Hz; paired t-test, $t_9 = 3.069$, $^*p = 0.0134$) (Figure 3b). In a second set of mice, we tested the role of the AMPA receptor component in the Fs-induced excitation. NBQX infusion (AMPA receptor antagonist, 100 μM) ($n_{mice} = 5$; $n_{cells} = 7$) completely abolished Fs-driven excitation (Firing $rate_{shock\text{-}baseline;}$ before vs. after: 9.773 ± 1.71 Hz vs. 1.03 ± 0.48 Hz; paired *t*-test, $t_6 = 4.872$, $^{**}p = 0.0028$) (Figure 3b). Notably, the variance of the AP5 effect was larger, and the NBQX-mediated reduction higher than the one promoted by AP5 (% reduction from baseline Fs response; NBQX vs. AP5: $88.06 \pm 4.218\%$ vs. $33.38 \pm 11.7\%$; unpaired t-test, $t_{15} = 3.758$, $^{**}p = 0.0019$). Altogether, these data reveal the necessity of AMPAR and NMDA receptors for such Fs response.

Next, we tested whether GABA transmission underlies Fs-driven inhibition of LHb neurons. Notably, LHb neurons express both $GABA_A$ and $GABA_B$ receptors (Lecca et al., 2016; Wang, Gong, Luo, & Xu, 2006). We examined the role of $GABA_B$ receptors for Fs-evoked inhibitory responses in seven neurons ($n_{mice} = 7$; $n_{cells} = 7$). Local infusion of the $GABA_B$ receptors antagonist CGP54626 (100 μM) did not affect the Fs-inhibition (Firing $rate_{shock\text{-}baseline}$; before vs. after: -11.28 ± 2.96 Hz; vs. -9.70 ± 3.98 Hz; paired t-test, $t_6 = 0.8602$, $p = 0.4227$) (Figure 3c). Instead, picrotoxin (PTX) infusion ($n_{mice} = 6$, $n_{cells} = 6$) ($GABA_A$ antagonist, 0.5 μM) in six LHb neurons abolished Fs inhibitory responses (Firing $rate_{shock\text{-}baseline}$; before vs. after: -8.937 ± 2.60 Hz vs. -1.29 ± 1.10 Hz; paired *t* test, $t_5 = 2.913$, $^*p = 0.0333$) (Figure 3c). This suggests that $GABA_A$ but not $GABA_B$ receptors mediate the 'pause' produced by Fs in this LHb subpopulation.

4 | DISCUSSION

Here we provide evidence for the existence of two neuronal populations in the LHb, both encoding aversive stimuli in an opposite fashion, namely via excitation or inhibition. Indeed, in this study, alongside with a previously characterized aversion-excited population (Lecca et al., 2017; Matsumoto & Hikosaka, 2007; Trusel et al., 2019), we describe a territorially segregated, glutamate-containing LHb neuronal subtype inhibited by Fs. Interestingly, in the anaesthetized mouse, these Fs-inhibited cells preferentially fire more regularly and at a higher frequency (with a relatively rare occurrence of spikes in burst) compared to Fs-excited neurons. These dissimilar features may arise from a different inhibitory/excitatory-input balance and/or by specific intrinsic properties distinct in the two neuronal subtypes (Llinás, 2014; Valentinova & Mameli, 2016). The juxtacellular experiments indicate that these neurons are EAAC1-positive and GAD67-negative. However, given the low number of labelled cells we cannot rule out that a proportion of inhibited, or even excited cells, could be of GABAergic nature. Future studies, are therefore required to provide a systematic and comprehensive genetic atlas containing the identity of most LHb neurons (Proulx, Hikosaka, & Malinow, 2014).

The pharmacological approach revealed that both AMPA and NMDA receptors contribute for the Fs-induced excitation on LHb cells. However, AMPA receptors antagonism completely abolished the Fs-excitatory response. In contrast, blockade of NMDA receptors led to a less extent and variable Fs reduction (Figure 3b). This requires a better understanding of NMDA receptors function within the LHb, a process, which remains still elusive.

On the other hand, Fs-mediated phasic inhibition of LHb neuronal firing requires solely $GABA_A$ receptor activation without involving the slow component mediated by $GABA_B$ receptors (Tan, Nuno-Perez, Mameli, & Meye, 2018; Tchenio, Lecca, Valentinova, & Mameli, 2017). Altogether, these data provide a cellular logic underlying phasic Fs responses in the LHb.

Rabies-assisted cell-type-specific monosynaptic mapping revealed a hypothalamic-habenula-midbrain (GABA) circuit where the Fs-excited cells are embedded (Lecca et al., 2017). Are Fs-inhibited cells part of the same LHb circuit? LHb sends axons through the fasciculus retroflexus mostly innervating GABAergic cells in the rostromedial tegmental nucleus (RMTg or VTAtail, Jhou et al., 2009; Kaufling et al., 2009), a key inhibitory hub for the midbrain DA system (Ji & Shepard, 2007; Lecca et al., 2011; Stamatakis & Stuber, 2012). However, LHb neurons also send axons directly to VTA DA neurons (Lammel et al., 2012; Lecca et al., 2017; Meye et al., 2016), and 5HT cells of the raphe nuclei (Lecca et al., 2017; Pollak Dorocic et al., 2014). Intriguingly, such DA- and 5HT-projecting cells present an almost exclusive localization in the medial portion of the LHb (Lecca et al., 2017; Meye et al., 2016; Pollak Dorocic et al., 2014). Therefore, monoamine-projecting neurons and Fs-inhibited cells may represent an overlapping population. However, we cannot exclude that Fs-inhibited cells would project to alternative structures including the laterodorsal tegmentum or the hypothalamus (González, Iordanidou, Strom, Adamantidis, & Burdakov, 2016; Yang et al., 2016).

Fs-inhibition requires $GABA_A$ receptors. Therefore, Fs-inhibited cells are likely innervated by GABAergic inputs susceptible to respond to Fs with an excitation. Remarkably, the LHb receives afferents from diverse brain regions involved in aversion processing (Tan et al., 2012) and containing GABAergic cells (Meye, Lecca, Valentinova, & Mameli, 2013). Particularly, neurons in the VTA, Lateral hypothalamus (LH), Lateral Preoptic Area (LPO) and Ventral Pallidum (VP) project GABAergic axons to the medial portion of the LHb (Barker et al., 2017; Faget et al., 2018; Lammel et al., 2012; Root, Mejias-Aponte, Qi, & Morales, 2014; Root, Mejias-Aponte, Zhang, et al., 2014; Stamatakis et al., 2016). Therefore, any of these regions may drive Fs-mediated inhibition. Another possibility is that a recently described population of GABAergic interneurons in the medial LHb promotes the inhibition after shock, although such functional connectivity remains to be demonstrated (Zhang, Hernández, Vázquez-Juárez, Chay, & Barrio, 2016; Zhang, Hernánde, et al., 2018; Zhang, Shen, et al., 2018). Finally, the block of Fs-excitation or Fs-inhibition by pharmacological agents revealed pure excitatory or inhibitory responses. This is indicative of two independent LHb circuits for such aversion encoding.

Studies in rats reported inhibitory responses to painful stimuli other than Fs in LHb cells (Zhang, Zhang, Xu, Li, & Wang, 2013). This suggests that aversion-driven inhibition might generalize to aversive stimuli of different nature, which is also the case for excited neurons (Lecca et al., 2017; Matsumoto & Hikosaka, 2007). But, what is the behavioural function of such opposite aversion-driven responses?

Hypothalamic glutamatergic signal into the LHb is necessary to trigger LHb excitation and promotes innate escape behaviour (Lecca et al., 2017). Similarly, other glutamatergic inputs also drive aversive behaviours (Barker et al., 2017; Knowland et al., 2017; Shabel et al., 2012; Zhang, Hernánde, et al., 2018; Zhang, Shen, et al., 2018).

In contrast, the behavioural relevance of aversion-driven GABA-mediated inhibition in LHb cells remains unknown. Optogenetic activation of GABAergic terminals arising from different structures onto the LHb drives place preference (Barker et al., 2017; Root, Mejias-Aponte, Qi, & Morales, 2014; Root, Mejias-Aponte, Zhang, et al., 2014; Stamatakis et al., 2016; Zhang, Hernánde, et al., 2018; Zhang, Shen, et al., 2018). This is in line with a potential role of LHb inhibition in reward encoding (Matsumoto & Hikosaka, 2007). It is therefore surprising that Fs inhibits LHb neurons. Whether Fs-inhibited cells are part of a non-canonical LHb pathway for precise aspects of aversive behaviours needs further consideration.

Altogether, these data provide a dichotomy of Fs responses in the LHb that may be relevant for motivated states as well as for pathological condition characterized by LHb dysfunction including addiction and depression (Nuno-Perez, Tchenio, Mameli, & Lecca, 2018).

ACKNOWLEDGEMENTS

We thank the entire Mameli laboratory for discussions and comments on the manuscript. This work is supported by European Research Council Starting Grant SalienSy 335333, The Swiss National Science Foundation (31003A) to M.M. and the Narsad Young Investigator Grant (27089) to S.L.

CONFLICT OF INTEREST

The authors declare no conflict of interest.

DATA ACCESSIBILITY

Data can be obtained by contacting the corresponding author.

AUTHORS CONTRIBUTION

M.C., M.T., M.P, M.M. and S.L. designed the study. M.C. and S.L. performed electrophysiological recordings. M.C. and M.T. performed the juxtacellular recovery and the immunolabelling. M.C. and S.L. wrote the paper with the help of M.M., M.P. and M.T.

ORCID

Manuel Mameli https://orcid.org/0000-0002-0570-6964
Salvatore Lecca https://orcid.org/0000-0001-5411-5485

REFERENCES

Aizawa, H., Kobayashi, M., Tanaka, S., Fukai, T., & Okamoto, H. (2012). Molecular characterization of the subnuclei in rat habenula. *The Journal of Comparative Neurology*, *520*(18), 4051–4066. https://doi.org/ 10.1002/cne.23167

Barker, D. J., Miranda-Barrientos, J., Zhang, S., Root, D. H., Wang, H. L., Liu, B., … Morales, M. (2017). Lateral preoptic control of the lateral habenula through convergent glutamate and gaba transmission. *Cell Reports*, *21*(7), 1757–1769. https://doi.org/10.1016/j.celrep.2017.10.066

Christoph, G. R., Leonzio, R. J., & Wilcox, K. S. (1986). Stimulation of the lateral habenula inhibits dopamine-containing neurons in the substantia nigra and ventral tegmental area of the rat. *Journal of Neuroscience*, *6*(3), 613–619.

Dong, W. Q., Wilson, O. B., Skolnick, M. H., & Dafny, N. (1992). Hypothalamic, dorsal raphe and external electrical stimulation modulate noxious evoked responses of habenula neurons. *Neuroscience*, *48*(4), 933–940.

Faget, L., Zell, V., Souter, E., McPherson, A., Ressler, R., Gutierrez-Reed, N., … Hnasko, T. S. (2018). Opponent control of behavioral reinforcement by inhibitory and excitatory projections from the ventral pallidum. *Nature Communications*, *9*(1), 849. https://doi.org/10.1038/s41467-018-03125-y

Gao, D. M., Hoffman, D., & Benabid, A. L. (1996). Simultaneous recording of spontaneous activities and nociceptive responses from neurons in the pars compacta of substantia nigra and in the lateral habenula. *European Journal of Neuroscience*, *8*(7), 1474–1478.

González, J. A., Iordanidou, P., Strom, M., Adamantidis, A., & Burdakov, D. (2016). Awake dynamics and brain-wide direct inputs of hypothalamic MCH and orexin networks. *Nature Communications*, *7*, 11395. https://doi.org/10.1038/ncomms11395

Hikosaka, O. (2010). The habenula: from stress evasion to value-based decision-making. *Nature Reviews Neuroscience*, *11*(7), 503–513. https://doi.org/10.1038/nrn2866

Hu, H. (2016). Reward and aversion. *Annual Review of Neuroscience*, *39*, 297–324. https://doi.org/10.1146/annurev-neuro-070815-014106

Jhou, T. C., Geisler, S., Marinelli, M., Degarmo, B. A., & Zahm, D. S. (2009). The mesopontine rostromedial tegmental nucleus: A structure targeted by the lateral habenula that projects to the ventral tegmental area of Tsai and substantia nigra compacta. *The Journal of Comparative Neurology*, *513*(6), 566–596. https://doi.org/10.1002/cne.21891

Ji, H., & Shepard, P. D. (2007). Lateral habenula stimulation inhibits rat midbrain dopamine neurons through a GABAA receptor-mediated mechanism. *Journal of Neuroscience*, *27*, 6923–6930. https://doi.org/ 10.1523/JNEUROSCI.0958-07.2007

Kaufling, J., Veinante, P., Pawlowski, S. A., Freund-Mercier, M. J., & Barrot, M. (2009). Afferents to the GABAergic tail of the ventral tegmental area in the rat. *The Journal of Comparative Neurology*, *513*(6), 597–621. https://doi.org/10.1002/cne.21983

Knowland, D., Lilascharoen, V., Pacia, C. P., Shin, S., Wang, E. H., & Lim, B. K. (2017). Distinct ventral pallidal neural populations mediate separate symptoms of depression. *Cell*, *170*(2), 284–297. https://doi.org/10.1016/j.cell.2017.06.015

Kowski, A. B., Veh, R. W., & Weiss, T. (2009). Dopaminergic activation excites rat lateral habenular neurons in vivo. *Neuroscience*, *161*(4), 1154–1165. https://doi.org/10.1016/j.neuroscience.2009.04.026

Lammel, S., Lim, B. K., Ran, C., Huang, K. W., Betley, M. J., Tye, K. M., … Malenka, R. C. (2012). Input-specific control of reward and aversion in the ventral tegmental area. *Nature*, *491*(7423), 212–217. https://doi.org/10.1038/nature11527

Lecca, S., Melis, M., Luchicchi, A., Ennas, M. G., Castelli, M. P., Muntoni, A. L., & Pistis, M. (2011). Effects of drugs of abuse on putative rostromedial tegmental neurons, inhibitory afferents to midbrain dopamine cells. *Neuropsychopharmacology*, *36*(3), 589–602. https://doi.org/10.1038/npp.2010.190

Lecca, S., Meye, F. J., & Mameli, M. (2014). The lateral habenula in addiction and depression: an anatomical, synaptic and behavioral overview. *European Journal of Neuroscience*, *39*(7), 1170–1178. https://doi.org/10.1111/ejn.12480

Lecca, S., Meye, F. J., Trusel, M., Tchenio, A., Harris, J., Schwarz, M. K., … Mameli, M. (2017). Aversive stimuli drive hypothalamus-to-habenula excitation to promote escape behavior. *Elife*, *6*, pii e30697. https://doi.org/10.7554/eLife.30697

Lecca, S., Pelosi, A., Tchenio, A., Moutkine, I., Lujan, R., Hervé, D., & Mameli, M. (2016). Rescue of GABAB and GIRK function in the lateral habenula by protein phosphatase 2A inhibition ameliorates depression-like phenotypes in mice. *Nature Medicine*, (3), 254–261. https://doi.org/10.1038/nm.4037

Li, B., Piriz, J., Mirrione, M., Chung, C., Proulx, C. D., Schulz, D., … *22*Malinow, R. *(2011).* Synaptic potentiation onto habenula neurons in the learned helplessness model of depression. *Nature*, *470*(7335), 535–539. https://doi.org/10.1038/nature09742

Llinás, R. R. (2014). Intrinsic electrical properties of mammalian neurons and CNS function: A historical perspective. *Frontiers in Cellular Neuroscience*, *8*, 320. https://doi.org/10.3389/fncel.2014.00320

Matsumoto, M., & Hikosaka, O. (2007). Lateral habenula as a source of negative reward signals in dopamine neurons. *Nature*, *447*(7148), 1111–1115. https://doi.org/10.1038/nature05860

Meye, F. J., Lecca, S., Valentinova, K., & Mameli, M. (2013). Synaptic and cellular profile of neurons in the lateral habenula. *Frontiers in Human Neuroscience*, *16*(7), 860. https://doi.org/10.3389/fnhum.2013.00860

Meye, F. J., Soiza-Reilly, M., Smit, T., Diana, M. A., Schwarz, M. K., & Mameli, M. (2016). Shifted pallidal co-release of GABA and glutamate in habenula drives cocaine withdrawal and relapse. *Nature Neuroscience*, *19*(8), 1019–1024. https://doi.org/10.1038/nn.4334

Nuno-Perez, A., Tchenio, A., Mameli, M., & Lecca, S. (2018). Lateral habenula gone awry in depression: bridging cellular adaptations with therapeutics. *Frontiers in Neuroscience*, *12*, 485. https://doi.org/10.3389/fnins.2018.00485

Pinault, D. (1996). A novel single-cell staining procedure performed in vivo under electrophysiological control: morpho-functional features of juxtacellularly labeled thalamic cells and other central neurons with biocytin or Neurobiotin. *Journal of Neuroscience Methods*, *65*(2), 113–136.

Pollak Dorocic, I., Fürth, D., Xuan, Y., Johansson, Y., Pozzi, L., Silberberg, G., … Meletis, K. (2014). A whole-brain atlas of inputs to serotonergic neurons of the dorsal and median raphe nuclei. *Neuron*, *83*(3), 663–678. https://doi.org/10.1016/j.neuron.2014.07.002

Proulx, C. D., Hikosaka, O., & Malinow, R. (2014). Reward processing by the lateral habenula in normal and depressive behaviors. *Nature Neuroscience*, *17*(9), 1146–1152.

Root, D. H., Mejias-Aponte, C. A., Qi, J., & Morales, M. (2014). Role of glutamatergic projections from ventral tegmental area to lateral habenula in aversive conditioning. *Journal of*

Neuroscience, *34*(42), 13906–13910. https://doi.org/10.1523/JNEUROSCI.2029-14.2014

Root, D. H., Mejias-Aponte, C. A., Zhang, S., Wang, H. L., Hoffman, A. F., Lupica, C. R., & Morales, M. (2014). Single rodent mesohabenular axons release glutamate and GABA. *Nature Neuroscience*, *17*(11), 1543–1551. https://doi.org/10.1038/nn.3823

Schultz, W., Dayan, P., & Montague, P. R. (1997). A neural substrate of prediction and reward. *Science*, *275*(5306), 1593–1599. Review.

Shabel, S. J., Proulx, C. D., Trias, A., Murphy, R. T., & Malinow, R. (2012). Input to the lateral habenula from the basal ganglia is excitatory, aversive, and suppressed by serotonin. *Neuron*, *74*(3), 475–481. https://doi.org/10.1016/j.neuron.2012.02.037

Stamatakis, A. M., & Stuber, G. D. (2012). Activation of lateral habenula inputs to the ventral midbrain promotes behavioral avoidance. *Nature Neuroscience*, *15*(8), 1105–1107. https://doi.org/10.1038/nn.3145

Stamatakis, A. M., Van Swieten, M., Basiri, M. L., Blair, G. A., Kantak, P., & Stuber, G. D. (2016). Lateral hypothalamic area glutamatergic neurons and their projections to the lateral habenula regulate feeding and reward. *Journal of Neuroscience*, *36*(2), 302–311. https://doi.org/10.1523/JNEUROSCI.1202-15.2016

Stephenson-Jones, M., Yu, K., Ahrens, S., Tucciarone, J. M., van Huijstee, A. N., Mejia, L. A., … Li, B. (2016). A basal ganglia circuit for evaluating action outcomes. *Nature*, *539*(7628), 289–293. https://doi.org/10.1038/nature19845

Tan, D., Nuno-Perez, A., Mameli, M., & Meye, F. J. (2018). Cocaine withdrawal reduces GABA(B) R transmission at entopeduncular nucleus - lateral habenula synapses. *European Journal of Neuroscience*, *50*, 2124–2133. https://doi.org/10.1111/ejn.14120

Tan, K. R., Yvon, C., Turiault, M., Mirzabekov, J. J., Doehner, J., Labouèbe, G., … Lüscher, C. (2012). GABA neurons of the VTA drive conditioned place aversion. *Neuron*, *73*(6), 1173–1183. https://doi.org/10.1016/j.neuron.2012.02.015

Tchenio, A., Lecca, S., Valentinova, K., & Mameli, M. (2017). Limiting habenular hyperactivity ameliorates maternal separation-driven depressive-like symptoms. *Nature Communications*, *8*(1), 1135. https://doi.org/10.1038/s41467-017-01192-1

Tian, J., & Uchida, N. (2015). Habenula lesions reveal that multiple mechanisms underlie dopamine prediction errors. *Neuron*, *87*(6), 1304–1316. https://doi.org/10.1016/j.neuron.2015.08.028

Trusel, M., Nuno-Perez, A., Lecca, S., Harada, H., Lalive, A., Congiu, M., … Mameli, M. (2019). Punishment-predictive cues guide avoidance through potentiation of hypothalamus-to-habenula synapses. *Neuron*, *102*, 120–127. https://doi.org/10.1016/j.neuron.2019.01.025

Valentinova, K., & Mameli, M. (2016). mGluR-LTD at excitatory and inhibitory synapses in the lateral habenula tunes neuronal output. *Cell Reports*, *16*(9), 2298–2307. https://doi.org/10.1016/j.celrep.2016.07.064

Wang, D. G., Gong, N., Luo, B., & Xu, T. L. (2006). Absence of GABA type A signaling in adult medial habenular neurons. *Neuroscience*, *141*(1), 133–141. https://doi.org/10.1016/j.neuroscience.2006.03.045

Wang, D., Li, Y., Feng, Q., Guo, Q., Zhou, J., & Luo, M. (2017). Learning shapes the aversion and reward responses of lateral habenula neurons. *Elife*, *6*, pii e23045. https://doi.org/10.7554/eLife.23045

Weiss, T., & Veh, R. W. (2011). Morphological and electrophysiological characteristics of neurons within identified subnuclei of the lateral habenula in rat brain slices. *Neuroscience*, *172*, 74–93. https://doi.org/10.1016/j.neuroscience.2010.10.047

Yang, Y., Cui, Y., Sang, K., Dong, Y., Ni, Z., Ma, S., & Hu, H. (2018). Ketamine blocks bursting in the lateral habenula to rapidly relieve depression. *Nature*, *554*(7692), 317–322. https://doi.org/10.1038/nature25509

Yang, Y., Wang, H., Hu, J., & Hu, H. (2018). Lateral habenula in the pathophysiology of depression. *Current Opinion in Neurobiology*, *48*, 90–96. https://doi.org/10.1016/j.conb.2017.10.024

Yang, H., Yang, J., Xi, W., Hao, S., Luo, B., He, X., … Wang, H. (2016). Laterodorsal tegmentum interneuron subtypes oppositely regulate olfactory cue-induced innate fear. *Nature Neuroscience*, *19*(2), 283–289. https://doi.org/10.1038/nn.4208

Zhang, L., Hernández, V. S., Swinny, J. D., Verma, A. K., Giesecke, T., Emery, A. C., … Eiden, L. E. (2018). A GABAergic cell type in the lateral habenula links hypothalamic homeostatic and midbrain motivation circuits with sex steroid signaling. *Translational Psychiatry*, *8*(1), 50.

Zhang, L., Hernández, V. S., Vázquez-Juárez, E., Chay, F. K., & Barrio, R. A. (2016). Thirst is associated with suppression of habenula output and active stress coping: is there a role for a non-canonical vasopressin-glutamate pathway? *Frontiers in Neural Circuits*, *10*, 13. https://doi.org/10.3389/fncir.2016.00013

Zhang, G. W., Shen, L., Zhong, W., Xiong, Y., Zhang, L. I., & Tao, H. W. (2018). Transforming sensory cues into aversive emotion via septal-habenular pathway. *Neuron*, *99*(5), 1016–1028.e5. https://doi.org/10.1016/j.neuron.2018.07.023

Zhang, C. X., Zhang, H., Xu, H. Y., Li, M. X., & Wang, S. (2013). The lateral habenula is a common target of cocaine and dexamethasone. *Neuroscience Letters*, *555*, 12–17. https://doi.org/10.1016/j.neulet.2013.09.019

SUPPORTING INFORMATION

Additional supporting information may be found online in the Supporting Information section at the end of the article.

How to cite this article: Congiu M, Trusel M, Pistis M, Mameli M, Lecca S. Opposite responses to aversive stimuli in lateral habenula neurons. *Eur J Neurosci*. 2019;50:2921–2930. https://doi.org/10.1111/ejn.14400

Report

Neuron

Punishment-Predictive Cues Guide Avoidance through Potentiation of Hypothalamus-to-Habenula Synapses

Highlights

- Punishments and punishment-predictive cues excite LHb neurons
- Avoidance learning strengthens hypothalamus-to-LHb excitation
- Hypothalamic inputs and AMPAR potentiation underlie avoidance

Authors

Massimo Trusel, Alvaro Nuno-Perez, Salvatore Lecca, ..., Takuya Takahashi, Francesco Ferraguti, Manuel Mameli

Correspondence

manuel.mameli@unil.ch

In Brief

Learning to predict a threat is crucial for survival. Trusel et al. identify the plasticity of neural circuit elements within the lateral habenula as a mechanism instrumental in guiding anticipation and avoidance of external aversive events.

Trusel et al., 2019, Neuron *102*, 120–127
April 3, 2019
https://doi.org/10.1016/j.neuron.2019.01.025

CellPress

CellPress

Neuron
Report

Punishment-Predictive Cues Guide Avoidance through Potentiation of Hypothalamus-to-Habenula Synapses

Massimo Trusel,[1] Alvaro Nuno-Perez,[1] Salvatore Lecca,[1] Harumi Harada,[3] Arnaud L. Lalive,[1] Mauro Congiu,[1] Kiwamu Takemoto,[4] Takuya Takahashi,[4] Francesco Ferraguti,[3] and Manuel Mameli[1,2,5,*]
[1]Department of Fundamental Neuroscience, University of Lausanne, 1005 Lausanne, Switzerland
[2]Inserm, UMR-S 839, 75005 Paris, France
[3]Department of Pharmacology, Medical University of Innsbruck, 6020 Innsbruck, Austria
[4]Department of Physiology, Graduate School of Medicine, Yokohama City University, 236-0004 Yokohama, Japan
[5]Lead Contact
*Correspondence: manuel.mameli@unil.ch
https://doi.org/10.1016/j.neuron.2019.01.025

SUMMARY

Throughout life, individuals learn to predict a punishment via its association with sensory stimuli. This process ultimately prompts goal-directed actions to prevent the danger, a behavior defined as avoidance. Neurons in the lateral habenula (LHb) respond to aversive events as well as to environmental cues predicting them, supporting LHb contribution to cue-punishment association. However, whether synaptic adaptations at discrete habenular circuits underlie such associative learning to instruct avoidance remains elusive. Here, we find that, in mice, contingent association of an auditory cue (tone) with a punishment (foot shock) progressively causes cue-driven LHb neuronal excitation during avoidance learning. This process is concomitant with the strengthening of LHb AMPA receptor-mediated neurotransmission. Such a phenomenon occludes long-term potentiation and occurs specifically at hypothalamus-to-habenula synapses. Silencing hypothalamic-to-habenulainputs or optically inactivating postsynaptic AMPA receptors within the LHb disrupts avoidance learning. Altogether, synaptic strengthening at a discrete habenular circuit transforms neutral stimuli into salient punishment-predictive cues to guide avoidance.

INTRODUCTION

The sound of a fire alarm guides a rapid action to immediately ensure safety. This is an instance where associating environmental cues to aversive events grants individuals to predict and avoid threats, a primary strategy for survival. Neurons in the lateral habenula (LHb) are instrumental in processing aversive events and guide innate escape behaviors. Unexpected punishments or disappointment phasically excite LHb neurons (Lecca et al., 2017; Matsumoto and Hikosaka, 2007; Wang et al., 2017). Importantly, after conditioning, punishment-predictive external cues are also efficient in driving LHb neuronal excitation (Matsumoto and Hikosaka, 2007). This suggests that the LHb may support cue-punishment learning. Such process is instrumental for adaptive behavioral strategies, including avoidance, a cardinal mechanism allowing individuals to prevent the predicted punishment (LeDoux et al., 2017).

Glutamatergic inputs from brain structures, including the lateral hypothalamus (LH), the medial ventral tegmental area (mVTA), and the entopeduncular nucleus of the basal ganglia (EPN) increase LHb neuronal activity and guide aversive behaviors (Root et al., 2014; Stamatakis et al., 2016; Shabel et al., 2012). Importantly, such excitatory synapses can undergo activity-dependent synaptic plasticity (Valentinova and Mameli, 2016). Moreover, in pathological conditions, pre- and postsynaptic modifications of glutamatergic neurotransmission alter LHb neuronal output and ultimately underlie depressive-like states (Lecca et al., 2016; Li et al., 2011; Meye et al., 2015). Altogether, this evidence supports the notion that synaptic plasticity at discrete inputs onto LHb synapses tunes LHb neurons firing and is causal for specific behavioral outcomes.

Long-term potentiation (LTP) of excitatory transmission is crucial for learning processes and enables neuronal networks to represent a memory (Nabavi et al., 2014). Yet, whether synaptic adaptations within habenular circuits represent a cellular substrate for associative learning occurring during avoidance remains poorly understood.

Here, we examined whether cue-punishment associations and the subsequent cue-driven avoidance (1) engage LHb neuronal dynamics and (2) require pathway-specific synaptic plasticity.

RESULTS

Punishment-Predictive Cues Excite LHb Neurons during Avoidance Learning

Aversive events or their predictors lead to a time-locked phasic excitation of LHb neurons (Matsumoto and Hikosaka, 2007). Here, we examined the progression of LHb neuronal dynamics throughout cue-punishment association and avoidance learning.

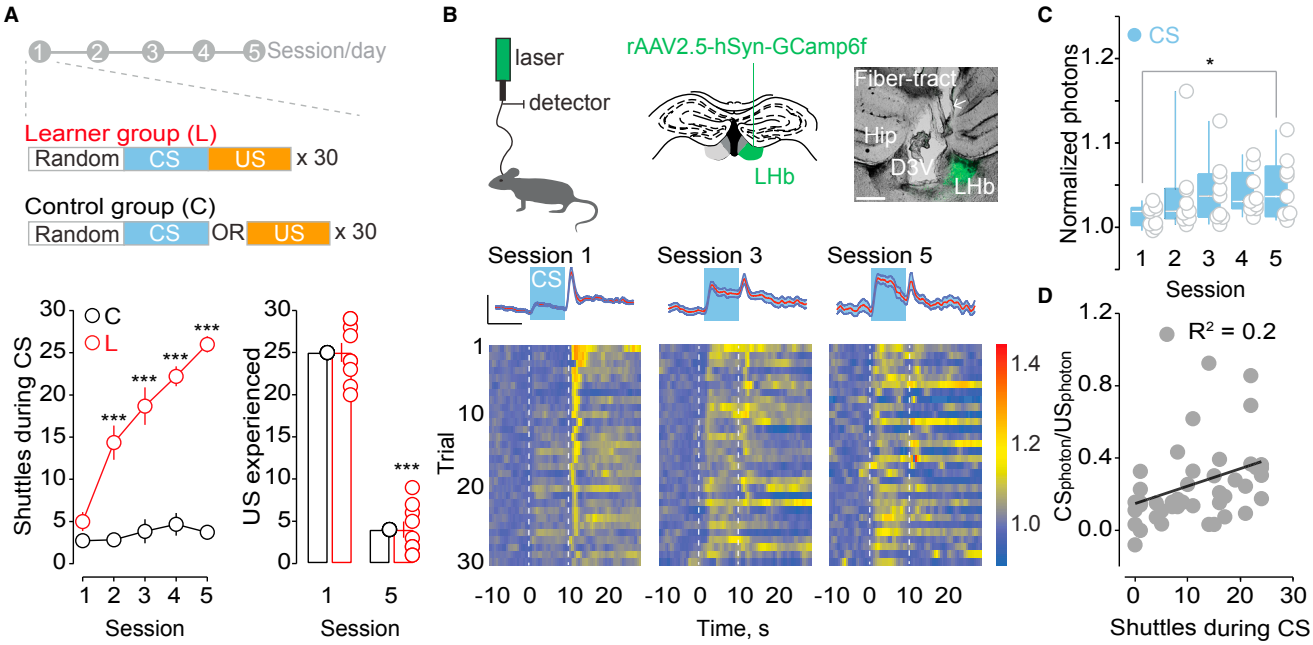

Figure 1. Excitation of LHb Neurons by Aversion-Predictive Cues Develops during Avoidance Learning

(A) Behavioral protocol; time course and bar graph with scatterplot illustrating avoidance rate along 5 sessions (controls [C], [black] $n_{animals}$ = 7, learners [L], [red] $n_{animals}$ = 9; two-way repeated-measures ANOVA, main effect of training protocol, session, and interaction, ***p < 0.001; % US received: session 1, C = 100%, L = 83.4% ± 3.8%; session 5, C = 100% ± 0%, L = 13.3% ± 3.2%, L: session 1 versus session 5, t test, t_{8} = 18.4, ***p < 0.001).

(B) Protocol, injection site, and image illustrating GCamP6f expression in the LHb (500 μm); sample heatmap and traces (100 photons; 10 s) of normalized fluorescence signal after CS (0–10 s, blue) and US (onset 10 s) across the 30 trials on days 1, 3, and 5.

(C) Box and scatterplot summarizing the normalized fluorescence (max photons/baseline) upon CS across sessions (n = 9; repeated measures [RM] one-way ANOVA; Dunnett's D1 versus D5; q_{8} = 3.3; *p = 0.03).

(D) Scatterplot and correlation analysis for avoidance scores and the CS-US fluorescence across the sessions (n = 9; Spearman r = 0.448; *p = 0.047; R^2 represents the goodness of fit).

Data are represented with boxplots (median and quartiles) or mean ± SEM. See also Figure S1.

To model cue-punishment associative learning and subsequent cue-guided avoidance, we employed a two-way active avoidance task (LeDoux et al., 2017). During 5 sessions (1 session/day; 30 trials/session), mice experienced a tone (conditioned stimulus [CS], 10 s) followed by a foot shock (unconditioned stimulus [US]). Foot-shock delivery would stop if mice crossed compartments (shuttles; Figure S1A). We examined avoidance learning by computing goal-directed shuttles during the CS. Mice progressively improve their shuttling performance, thereby preventing shock occurrence (learner group [L]; Figure 1A). In contrast, control mice received similar amount of foot shocks and tones (compared to L-mice), but CS and US were never contingent (control group, [C]; Figure 1A).

To examine LHb neurons' activity during avoidance learning, we employed photometric analysis of calcium-mediated fluorescent transients—used as a proxy for neuronal activity (Lecca et al., 2017). We virally expressed the fluorescent Ca^{2+} sensor GCaMP6f unilaterally in the LHb and implanted a multimodal fiber optic above the injection site to collect the emitted photons (Figures 1B and S1B). Post hoc analysis indicated that ~69% (2,596/3,729 neurons; 4 mice) of the LHb neuronal population expressed GCaMP6f and was glutamatergic (i.e., EAAC1+; Figures S1C and S1D).

During the first training session, calcium fluorescent transients were time locked to foot-shock delivery, with minimal transients evoked during CS presentation (Figures 1A and 1B). During subsequent training days, while cue-punishment association and cue-driven shuttles progressed, fluorescent transients were typically observed in response to both foot shock and CS onset (day 3; Figures 1B, 1C, and S1E). The CS-driven phasic fluorescent responses, measured at the peak, gradually developed over the sessions to become, at day 5, significantly larger than day 1 (Figure 1C). CS-driven fluorescent transients were learning driven and GCamp6f mediated, as they were absent across the five sessions in control mice and GFP-only-expressing learner animals (Figures S1E and S1F). In contrast, the amplitude of US-driven transients remained comparable across training sessions, supporting the stability over time of the photometric signal (Figures S1E and S1G–S1I). Consistently, the ratio $CS_{photons}/US_{photons}$ at each session from individual learner mice correlated with the number of shuttle events during the CS (Figure 1D). Finally, single-unit recordings in awake mice corroborated that CS-driven LHb neurons excitation occurs in learner, but not control, mice (Figure S1J). Altogether, these data indicate that the transition from neutral to punishment-valued cues during avoidance learning associates with cue-evoked LHb neuronal excitation.

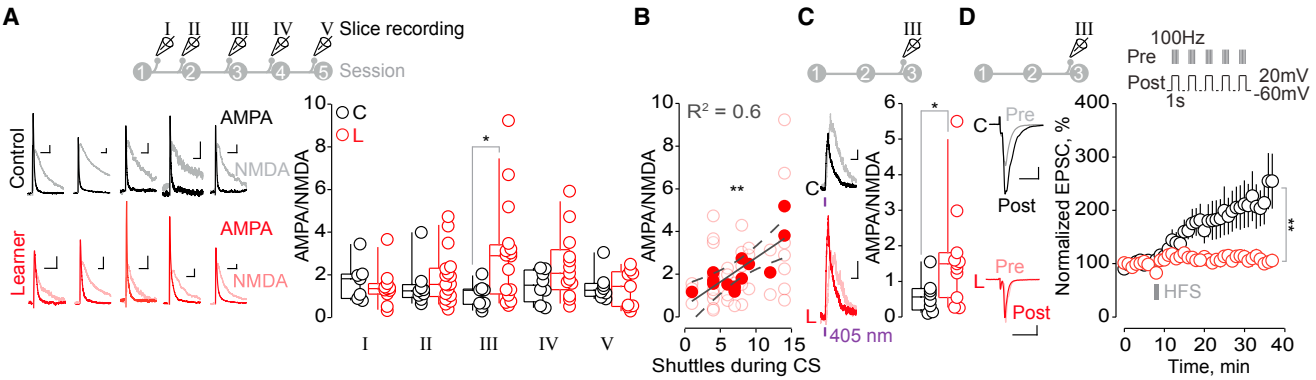

Figure 2. Transient Synaptic Potentiation onto LHb Neurons during Avoidance

(A) Timeline and sample traces (10 pA; 20 ms) representing AMPAR and NMDAR-EPSCs (+40 mV). Box and scatterplot of the AMPAR/NMDAR ratios (session I, 1 h after session 1: C [black] 1.7 ± 0.4, $n_{cells/animals}$ = 7/3; L [red] 1.6 ± 0.4, $n_{cells/animals}$ = 7/3; t test, t_{12} = 0.29, p > 0.05; II, 24 h after session 1: C 1.5 ± 0.3, $n_{cells/animals}$ = 9/3; L 1.8 ± 0.3, $n_{cells/animals}$ = 18/4; t test, t_{25} = 0.87, p > 0.05; III, 24 h after session 2: C 1.1 ± 0.2, $n_{cells/animals}$ = 10/6; L 3.0 ± 0.6, $n_{cells/animals}$ = 16/7; t test, t_{24} = 2.5, *p = 0.02; IV, 24 h after session 3: C 1.5 ± 0.3, $n_{cells/animals}$ = 8/2; L 2.4 ± 0.4, $n_{cells/animals}$ = 13/2; t test, t_{19} = 1.58, p > 0.05; V, 24 h after session 4: C 1.5 ± 0.2, $n_{cells/animals}$ = 8/4; L 1.4 ± 0.3, $n_{cells/animals}$ = 9/4; t test, t_{15} = 0.26, p > 0.05).

(B) Avoidance scores plotted in function of AMPAR/NMDAR ratios (learners, empty circles, single cells; filled circles, average value/mouse; session I, II, and III; correlation value/mouse; Spearman r = 0.766, **p = 0.003, R^2 represents the goodness of fit).

(C) Same as (A) but with MNI-glutamate uncaging (C [black] 0.6 ± 0.2, $n_{cells/animals}$ = 8/2; L [red] 1.7 ± 0.4, $n_{cells/animals}$ = 11/3; Mann-Whitney, U = 19, *p = 0.04).

(D) Amplitude versus time plot and sample traces (50 pA; 10 ms) of EPSCs before (light line) and after (dark line) HFS-pairing protocol (average $EPSC_{34\text{-}36\ min}$: C [black], 208.1 ± 38.4 $n_{cells/animals}$ = 7/3; L [red], 107.5 ± 11.8, $n_{cells/animals}$ = 7/3; t test, t_{12} = 2.5, **p = 0.03).

Data are represented with boxplots (median and quartiles) or mean ± SEM. See also Figure S2.

Avoidance Learning and Synaptic Potentiation in the LHb

Potentiation of excitatory synapses represents a neurobiological substrate underlying the association between cues and salient experiences. Accordingly, LTP may support the emergence of cue-valued excitation of midbrain dopamine neurons during reward-prediction learning (Stuber et al., 2008).

We therefore tested the prediction that synaptic strengthening of excitatory transmission onto LHb neurons represents a core mechanism for cue-driven avoidance learning. To examine excitatory synaptic transmission onto LHb neurons along the progression of avoidance learning, we performed *ex vivo* patch-clamp experiments in LHb-containing acute slices from control and learner mice. Evoked excitatory postsynaptic currents (EPSCs) were recorded at different timings during the training—∼1 h after session one (I) and 24 h after sessions one (II), two (III), three (IV), and four (V; Figure 2A). Bath application of the NMDAR antagonist D-2-amino-5-phosphonopentanoate (AP5) and digital subtraction allowed the isolation of synaptically evoked AMPA- and NMDA-mediated currents (+40 mV; Figure 2A). This permitted computing the NMDAR ratio, a validated proxy for postsynaptic strengthening of excitatory transmission (Meye et al., 2015). The AMPAR/NMDAR ratio significantly, but transiently, augmented in learner mice compared to control mice (Figure 2A). Namely, it was larger 24 h after training session two (III) and positively correlated with avoidance performance (Figures 2A and 2B). However, AMPAR/NMDAR ratios were lower and comparable between experimental groups 24 h after sessions three and four, as well as after session one, indicating the transient nature of this plasticity (Figure 2A).

The increased AMPAR/NMDAR ratio detected 24 h after session two can occur via enhanced AMPAR function and/or number or alternatively via reduction of NMDAR function and/or number (Mameli et al., 2011). To probe the contribution of each glutamate receptor type during avoidance learning, we used uncaging of MNI-glutamate onto LHb dendrites. At +40 mV, a brief (1.5 ms) flash of 405-nm UV light evoked a composite response (AMPAR and NMDAR mediated). Isolation of AMPARs and NMDARs currents unraveled higher AMPAR/NMDAR ratios in learner mice, similarly to the results obtained with extracellular stimulation (Figure 2C). Comparison of AMPAR and NMDAR absolute currents revealed a significant upward shift of AMPAR-EPSCs amplitudes, while NMDAR responses remained comparable across experimental groups (Figure S2A). Avoidance learning (at session III) did not alter EPSCs evoked by high-frequency trains of synaptic stimulation, indicating unaltered presynaptic glutamate release (Figure S2B). Altogether, these data suggest that cue-punishment association, and the consequent development of avoidance, occurs along with a postsynaptic potentiation of AMPAR-dependent transmission onto LHb neurons. We reasoned that, if learning requires such an LTP-like process, animals undergoing avoidance learning would show occluded LTP *in vitro*. Pairing high-frequency extracellular stimulation with postsynaptic depolarization (1 s at 20 mV) led to LTP in slices from control (and naive) mice (Figures 2D and S2C). This phenomenon required NMDARs, as it was abolished by the presence of the NMDAR antagonist AP5 (Figure S2C). The pairing protocol failed, however, to induce LTP in slices obtained from mice undergoing avoidance learning (III; Figure 2D). Altogether, cue-punishment association and avoidance occur along with transient LTP of postsynaptic AMPAR transmission.

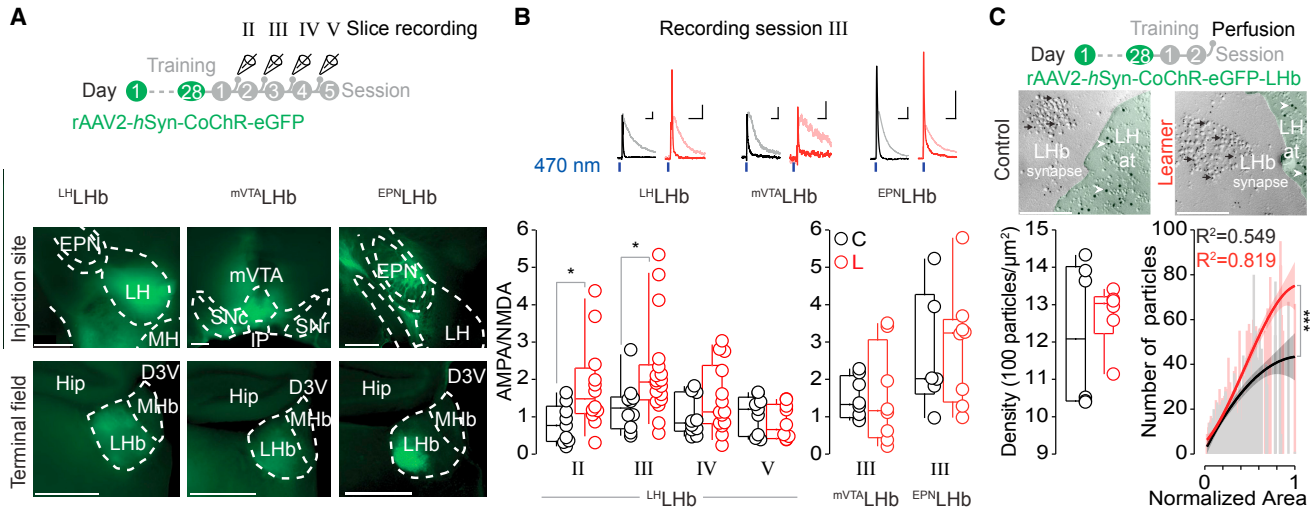

Figure 3. Learning-Driven Potentiation at Hypothalamic-to-Habenula Projections

(A) Timeline and representative images for CoChR expression in LH, mVTA, EPN, and LHb terminals (500 μm).

(B) Sample traces at session III (LH 50 pA, 20 ms, mVTA, 10 pA, 20 ms; EPN 50 pA, 20 ms); box- and scatterplot of the optical AMPA/NMDA ratios (LH, session II: C 0.8 ± 0.2, $n_{cells/animals}$ = 9/2; L 1.8 ± 0.3, $n_{cells/animals}$ = 12/2; $t_{19\ =}$ 2.4, p = 0.03; session III: C 1.3 ± 0.2, $n_{cells/animals}$ = 10/5; L 2.2 ± 0.3, $n_{cells/animals}$ = 18/6; t test, $t_{26\ =}$ 2.2, p = 0.04; session IV: C 1.0 ± 0.2, $n_{cells/animals}$ = 10/2; L 1.5 ± 0.2, $n_{cells/animals}$ = 14/2; t test, $t_{22\ =}$ 1.4, p > 0.05; session V: C 1.1 ± 0.2, $n_{cells/animals}$ = 9/2; L 0.8 ± 0.1, $n_{cells/animals}$ = 10/2; t test, $t_{17\ =}$ 1.0, p > 0.05; mVTA, session III: C [black] 1.5 ± 0.2, $n_{cells/animals}$ = 8/5; L [red] 1.6 ± 0.5, $n_{cells/animals}$ = 8/4; t test, $t_{14\ =}$ 0.13, p > 0.05; EPN, session III: C 2.7 ± 0.7, $n_{cells/animals}$ = 6/3; L 2.9 ± 0.6, $n_{cells/animals}$ = 8/3; t test, $t_{12\ =}$ 0.3, p > 0.05).

(C) Timeline and representative images of freeze-fracture replica immunolabeling for AMPARs at LH-to-LHb synaptic contacts (200 nm). Portion of a LH axon terminal (protoplasmic face in light green, 10 nm gold particle of CoChR-GFP, white arrowheads) apposed to an LHb dendritic shaft. AMPARs (5 nm gold particles, black arrows) were observed in the postsynaptic membrane specialization (PSD). Box and scatterplot of averaged density (5-nm gold particles/μm^2; C [black], 1,220.6 ± 79, $n_{counts/animals}$ = 179/6; L [red], 1,272.3 ± 33.5, $n_{counts/animals}$ = 192/6; Mann-Whitney, U = 18, p > 0.05).

Data are represented with boxplots (median and quartiles). Third-order polynomial fitting of AMPARs number versus normalized PSD area is shown (control versus learners, $n_{animals}$ = 6/group; $F_{4,361\ =}$ 15, p < 0.001, R^2 indicates goodness of fit). See also Figure S2.

Pathway Specificity of Avoidance-Learning-Driven Plasticity

The lateral hypothalamus (LH), the medial VTA (mVTA), and the entopeduncular nucleus (EPN) (1) project glutamate-releasing axons to the LHb, (2) activate AMPARs and NMDARs, and (3) promote LHb neuronal firing to drive aversive behaviors (Root et al., 2014; Shabel et al., 2012; Stamatakis et al., 2016). Importantly, unexpected punishments engage the LH-to-LHb pathway to trigger LHb neuronal excitation (Lecca et al., 2017). We examined the possibility that synaptic potentiation in the LHb during avoidance also presents circuit specificity. To this end, we virally expressed the excitatory opsin CoChR (CoChR-EGFP; Klapoetke et al., 2014) into the LH, mVTA, or the EPN (Figure 3A). Whole-cell recordings within the fluorescent terminal fields in the LHb, from all these inputs, confirmed the excitatory nature of opto-currents (Figures 3B and S2D). 24 h after training session one and two (II and III), AMPAR/NMDAR ratios at LH-LHb synapses were significantly larger in learner compared to control mice, matching the initial progression of avoidance learning. Instead, optically driven mVTA- and EPN-LHb AMPAR/NMDAR ratios were comparable between groups (Figures 3B and S2E). Notably, AMPARs/NMDARs in control condition were highly variable across inputs, indicating pathway-specific postsynaptic properties. In addition, a fear-conditioning protocol, where CS-US association occurs but in an inescapable condition, failed to change LH-LHb AMPAR/NMDAR ratios (Figure S2F).

We find that an optical-high frequency stimulation (HFS) protocol at LH inputs paired with postsynaptic depolarization employing the fast opsins CoChR and Chrimson (Klapoetke et al., 2014) led to LTP in control mice (Figure S2G). This phenomenon was absent at EPN inputs and occluded in learner mice (Figures S2G and S2H). These data support the notion that (1) at LH-LHb synapses, AMPAR/NMDAR ratio increases along with LTP (Figure S2I) and (2) learning-driven AMPAR potentiation is circuit specific.

To corroborate these results and visualize the locus of expression for avoidance-driven AMPAR potentiation, we employed freeze-fracture replica immunolabeling (Schönherr et al., 2016). Combined with infusion of rAAV2-hSyn-CoChR-EGFP, this approach allows the quantification of membrane AMPARs specifically at synapses formed by LH axons to LHb postsynaptic neurons (Figure 3C). AMPARs (GluA1–4) gold immunolabeling showed no overall difference in density between learner and control mice. However, in learner mice (24 h after session 2), a larger fraction of particles (receptors) within the broader postsynaptic membrane specialization (PSD) areas was observed compared to control animals (Figure 3C). Altogether, this suggests that a larger postsynaptic membrane pool of AMPARs underlies the potentiation of LH-to-LHb excitatory synapses during avoidance learning.

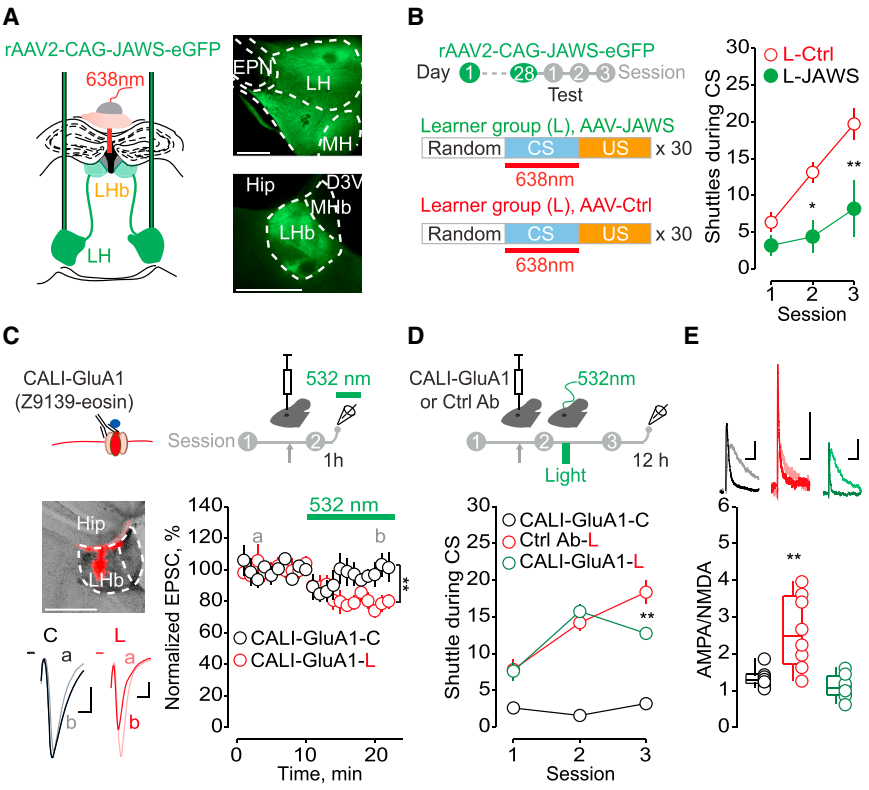

Figure 4. Avoidance Learning Requires LH-to-LHb Projections and AMPARs Potentiation

(A) Fiber implant and infusion of rAAV-CAG-JAWS-EGFP; representative images for JAWS expression (500 μm).

(B) Training protocol and behavioral performance during training (learners-control virus [L-Ctrl] [red, n = 8], learners-JAWS [L-JAWS] [green, n = 5]; two-way repeated-measures ANOVA, main effect of virus, session, and interaction [$F_{2,\ 22} = 3.8$; $p = 0.04$]).

(C) Schematic of CALI approach. Amplitude versus time plot of EPSCs (50 pA, 10 ms) before (light) and after (dark) light exposure (532 nm; average $EPSC1_{8–22\ min}$: CALI-GluA1-C [black] 98.2 ± 3.7 $n_{cells/animals}$ = 6/4; CALI-GluA1-L [red] 79.7 ± 1.9, $n_{cells/animals}$ = 6/4; t test, $t_{10} = 4.4$, **p = 0.01).

(D) Timeline of avoidance performance (infusion 4 h prior session 2; light 1 h post-session 2). Average shuttles during CS at session 3 are as follows: control mice CALI-GluA1 (CALI-GluA1-C) (black) 3.2 ± 0.7; learner mice control antibody (Ctrl-Ab-L) (red) 18.3 ± 1.6; learner mice CALI-GluA1 (CALI-GluA1-L) (green) 12.8 ± 0.7; one-way ANOVA $F_{(2,16)} = 47$, **p < 0.01.

(E) Sample traces (20 pA; 20 ms) representing AMPAR and NMDAR-EPSCs 12 h after behavioral testing. Box- and scatterplot of the AMPAR/NMDAR ratios are shown (CALI-GluA1-C 1.3 ± 0.8, $n_{cells/animals}$ = 8/3; Ctrl-Ab-L 2.6 ± 0.3, $n_{cells/animals}$ = 8/2; CALI-GluA1-L 1.1 ± 0.1, $n_{cells/animals}$ = 8/3; one-way ANOVA $F_{(2,21)} = 13.78$, **p < 0.01).

Data are represented with boxplots (median and quartiles) or mean ± SEM. See also Figure S3.

Required Circuit and Mechanism for Avoidance Learning

We next aimed to probe the necessity of LH inputs for avoidance learning. We tested LH-to-LHb projections requirement by optically reducing their function. We transduced LH neurons with a light-driven chloride pump (orange-red spectrum of activation) via infusion of rAAV2-JAWS-EGFP (Figure 4A). 4 weeks later, we prepared acute brain slices and found that 584-nm light reduced EPSCs within the LHb (Figure S3A). Next, we recorded foot-shock-driven LH-dependent LHb excitation using single units in anesthetized mice (Lecca et al., 2017). Light at 638 nm reduced foot-shock excitation in JAWS-expressing mice, but not in GFP-control animals (Figure S3B). These experiments also revealed that light off failed to induce any rebound excitation (Figure S3B). Thus, JAWS activation efficiently reduces presynaptic function of LH terminals onto the LHb. Next, we chronically implanted JAWS-expressing mice with a single fiber optic directed just above the LHb (Figure S3C). We reasoned that breaking the contingency between CS and US by functionally limiting LH-LHb projections would impair the formation of punishment-predictive cues. Shining light at 638 nm to silence LH-to-LHb terminals during CS presentation reduced avoidance learning (Figure 4B). This highlights the necessary role of the LH-LHb projection for the acquisition of avoidance behavioral strategy.

Although this provides insights for the circuit requirement of avoidance, it leaves open the existence of causality between AMPAR strengthening and behavior. We predicted that synaptic potentiation of AMPARs is an essential mechanism for avoidance learning. To test this, we employed chromophore-assisted light inactivation with eosin (CALI) to inactivate GluA1-containing AMPARs with precise temporal and spatial resolution (Takemoto et al., 2017). Monoclonal antibodies against an extracellular domain of GluA1 (236–286 amino acids [aas]) chemically labeled with eosin produce oxygen singlets in response to 532-nm laser light, thereby damaging synaptic GluA1-AMPARs (CALI-GluA1) (Takemoto et al., 2017). Notably, CALI-GluA1 efficiently targets and impairs newly inserted AMPARs, which represent a receptor pool more labile and less anchored to the scaffolding complex (Malinow and Malenka, 2002; Takemoto et al., 2017). To examine the efficiency of CALI-GluA1 in the LHb, we locally infused the antibody in control and learner mice 4–5 h prior session two (Figure 4C). 1 h after session two, we found that continuous 532-nm laser light onto slices reduced AMPAR currents solely in learner mice (Figure 4C). This suggests that CALI-GluA1 rapidly and efficiently diminishes AMPAR transmission in animals undergoing avoidance learning. Therefore, this intervention offers an opportunity to test causality between strengthened AMPAR transmission and avoidance learning with fine temporal and spatial precision.

In order to achieve this, we initially trained a set of mice during session one. The following day, the same mice underwent infusion of either CALI-GluA1 or a control antibody (anti-Myc-eosin, Ctrl-Ab) into the LHb (Takemoto et al., 2017). Mice were then

implanted with a fiber optic and experienced training session two (Figure S3D). 1 h post-training, we exposed the injected area to 532 nm continuous illumination. The following day, mice were tested on session day three (Figure 4D). All injected animals ("learners") progressively increased avoidance performance during the initial two sessions (Figure 4D). Illumination left the progression of learning intact in mice infused with Ctrl-Ab. In contrast, CALI-GluA1-L mice failed to further improve their avoidance performance and exhibited a significant reduction in cue-driven avoidance compared to Ctrl-Ab-L mice. CALI-GluA1 did not affect the behavior of control mice (Figure 4D). When examining AMPAR/NMDAR ratio in LHb-containing slices from these same animals, we found that Ctrl-Ab-L mice exhibited high AMPAR/NMDAR ratios. In contrast, CALI-GluA1-L mice presented a significantly lower AMPAR/NMDAR, comparable to those from CALI-GluA1 control mice. Altogether, this indicates that GluA1-mediated synaptic potentiation in the LHb is a requirement for proper avoidance.

DISCUSSION

LHb neurons respond to unpredicted punishments. Here, we show that also punishment-predictive cues excite LHb neuronal population during avoidance learning. This phenomenon parallels the expression of an LTP-like process at lateral hypothalamic-to-LHb excitatory synapses, a synaptic substrate necessary for avoidance.

Synaptic Basis of Avoidance

We describe that, during avoidance learning, a transient enhancement of excitatory synaptic transmission onto LHb neurons occurs as a result of AMPAR enrichment at LH-to-LHb synapses. In addition, LHb neurons of learner mice did not show, in contrast to control animals, HFS-LTP in acute brain slices. This suggests that, during the steep initial phase of avoidance learning, LH-to-LHb excitatory synapses undergo potentiation. Such synaptic potentiation, however, does not occur during CS-US association in an inescapable context, an encoding primarily mediated by amygdala neuronal populations (Ciocchi et al., 2010).

Short-term and long-term changes in excitatory transmission within the LHb are also instrumental for punishment-mediated innate escape as well as for behavioral despair in depressive states (Lecca et al., 2017; Li et al., 2013). Altogether, these data highlight the contribution of glutamatergic transmission for precise LHb-dependent neuronal encoding, ultimately leading to avoidance learning.

A feature of this study is the input-specific expression of avoidance learning-induced plasticity. Afferents from the LH, the mVTA, and the EPN onto the LHb contribute to aversion processing and are sufficient to drive aversive behaviors (Root et al., 2014; Shabel et al., 2012; Stamatakis et al., 2016). The avoidance-learning-mediated adaptations, including the increase in AMPAR/NMDAR ratio, occlusion of LTP, and higher AMPARs membrane expression, specifically occur at LH-to-LHb synapses. In addition, silencing LH-to-LHb terminals diminishes avoidance behaviors. What renders the LH-to-LHb an essential substrate for avoidance? cAMP responsive element binding protein (CREB) phosphorylation, crucial for learning processes, occurs during avoidance in the hypothalamus (Saha and Datta, 2005; Won and Silva, 2008). Furthermore, impairment of the orexin signaling in the hypothalamus disrupts taste-aversion learning (Mediavilla et al., 2011). Lastly, LH neurons mediate unpredicted foot-shock-driven LHb neuronal excitation, and their terminal activation in LHb guides real-time place aversion (Lecca et al., 2017). Altogether, LH-driven excitatory transmission onto LHb neurons represents a fundamental substrate contributing to the encoding of both unpredicted aversion and prediction of punishment. Glutamate release onto LHb neurons remains unaffected during progression of learning, suggesting the absence of plastic mechanisms in upstream structures. However, the induction mechanisms (i.e., coincident detection and/or precise firing patterns) endowing LH terminals to establish synaptic potentiation onto LHb synapses remain yet to be clarified. Recent data point to the medial septum as a source of sensory information to the LHb (Zhang et al., 2018). Neuromodulators are released during salient experiences in several brains structures, including the LHb (Lecca et al., 2014). These may represent two potential gating candidates to mechanistically trigger the LTP-like processes that guide avoidance learning. Our data do not rule out a potential contribution of (1) alternative inputs impinging onto the LHb and (2) other types of neurotransmission during discrete phases of avoidance.

The local and temporally restricted inactivation of GluA1-AMPARs resets synaptic strengthening, thereby impairing avoidance behavior. This supports a causal role of AMPAR-mediated potentiation for establishing cue-punishment association and subsequent avoidance learning. Notably, we report that CALI-GluA1 mediates reduction of EPSCs solely in the learner group. This is consistent with previous results suggesting that AMPARs participating to synaptic potentiation during learning are more susceptible to inactivation (Takemoto et al., 2017). This may result from LTP-driven insertion of labile AMPAR pools or unsilencing of silent synapses (Groc et al., 2006; Malinow, 2003). Altogether, these results favor the notion that punishment-predictive memories can form through AMPAR-mediated LTP-like processes.

Evolution of Plasticity during Prediction Learning

A signature of the reported synaptic potentiation during avoidance is its transient nature, as it occurs during a restricted time window, namely during the steepest portion of cue-punishment learning. During this phase, mice exhibited the largest change in number of avoidances compared to the previous session. Therefore, such synaptic plasticity may facilitate cue-punishment association and the consequent acquisition of avoidance. However, the extent of synaptic potentiation, reflected by the AMPAR/NMDAR ratio, returned back to baseline levels at later sessions. This inverted U-shape of learning-driven potentiation suggests that this process may not contribute to the maintenance of the learned avoidance behavior. It is therefore plausible that persistent cue-punishment memories are mediated by different mechanisms within the LHb or stored elsewhere than the LHb (i.e., monoaminergic nuclei; Wenzel et al., 2018). Notably, such phenomenon presents striking similarities with cue-reward

learning in dopamine neurons of the VTA (Stuber et al., 2008). In the midbrain, transient synaptic strengthening of AMPAR neurotransmission has been proposed as a leading substrate to enable reward prediction.

Altogether, these data support that, in the LHb, and more broadly within neuronal circuits of motivation, the transient enhancement in synaptic strength during the acquisition of avoidance (or reward) learning may transform neutral stimuli into punishment- (or reward-) predictive stimuli. This provides insights on how the brain resolves novel cue-stimulus associations.

STAR★METHODS

Detailed methods are provided in the online version of this paper and include the following:

- KEY RESOURCES TABLE
- CONTACT FOR REAGENT AND RESOURCE SHARING
- EXPERIMENTAL MODEL AND SUBJECT DETAILS
- METHOD DETAILS
  - Stereotactic injections
  - Slice electrophysiology
  - *In vivo* electrophysiology
  - Histology and immunofluorescence
  - Freeze fracture replica immunolabeling
  - Immunoparticles quantification
  - Fiber photometry
  - Behavioral testing
  - Drugs
- QUANTIFICATION AND STATISTICAL ANALYSIS

SUPPLEMENTAL INFORMATION

Supplemental Information includes three figures and can be found with this article online at https://doi.org/10.1016/j.neuron.2019.01.025.

ACKNOWLEDGMENTS

We thank M. Carta, D. Dupret, L. Neukomm, F.J. Meye, and the members of the Mameli laboratory for comments on the manuscript. We thank the Bellone and Tan laboratories for viral constructs and technical assistance. This work was supported by the Austrian Science Fund Sonderforschungsbereich grant F44-17 to F.F., ERC StG SalienSy 335333, the Swiss National Funds 31003A, and Vaud Canton to M.M.

AUTHOR CONTRIBUTIONS

M.T. and M.M. conceptualized the project and performed and analyzed the electrophysiological recordings and behavior. M.T. and S.L. performed and analyzed *in vivo* photometry data. A.N.-P. performed electrophysiological recordings. A.L.L. and M.C. performed *in vivo* electrophysiology experiments. H.H. and F.F. performed and analyzed the electron microscopy data. K.T. and T.T. provided tools for CALI. M.M. and M.T. wrote the manuscript with the help of all authors.

DECLARATION OF INTERESTS

The authors declare no competing interests.

Received: July 20, 2018
Revised: November 23, 2018
Accepted: January 14, 2019
Published: February 11, 2019

REFERENCES

Ciocchi, S., Herry, C., Grenier, F., Wolff, S.B., Letzkus, J.J., Vlachos, I., Ehrlich, I., Sprengel, R., Deisseroth, K., Stadler, M.B., et al. (2010). Encoding of conditioned fear in central amygdala inhibitory circuits. Nature *468*, 277–282.

Groc, L., Gustafsson, B., and Hanse, E. (2006). AMPA signalling in nascent glutamatergic synapses: there and not there! Trends Neurosci. *29*, 132–139.

Klapoetke, N.C., Murata, Y., Kim, S.S., Pulver, S.R., Birdsey-Benson, A., Cho, Y.K., Morimoto, T.K., Chuong, A.S., Carpenter, E.J., Tian, Z., et al. (2014). Independent optical excitation of distinct neural populations. Nat. Methods *11*, 338–346.

Lecca, S., Meye, F.J., and Mameli, M. (2014). The lateral habenula in addiction and depression: an anatomical, synaptic and behavioral overview. Eur. J. Neurosci. *39*, 1170–1178.

Lecca, S., Pelosi, A., Tchenio, A., Moutkine, I., Lujan, R., Hervé, D., and Mameli, M. (2016). Rescue of GABAB and GIRK function in the lateral habenula by protein phosphatase 2A inhibition ameliorates depression-like phenotypes in mice. Nat. Med. *22*, 254–261.

Lecca, S., Meye, F.J., Trusel, M., Tchenio, A., Harris, J., Schwarz, M.K., Burdakov, D., Georges, F., and Mameli, M. (2017). Aversive stimuli drive hypothalamus-to-habenula excitation to promote escape behavior. eLife *6*, e30697.

LeDoux, J.E., Moscarello, J., Sears, R., and Campese, V. (2017). The birth, death and resurrection of avoidance: a reconceptualization of a troubled paradigm. Mol. Psychiatry *22*, 24–36.

Li, B., Piriz, J., Mirrione, M., Chung, C., Proulx, C.D., Schulz, D., Henn, F., and Malinow, R. (2011). Synaptic potentiation onto habenula neurons in the learned helplessness model of depression. Nature *470*, 535–539.

Li, K., Zhou, T., Liao, L., Yang, Z., Wong, C., Henn, F., Malinow, R., Yates, J.R., 3rd, and Hu, H. (2013). βCaMKII in lateral habenula mediates core symptoms of depression. Science *341*, 1016–1020.

Malinow, R. (2003). AMPA receptor trafficking and long-term potentiation. Philos. Trans. R. Soc. Lond. B Biol. Sci. *358*, 707–714.

Malinow, R., and Malenka, R.C. (2002). AMPA receptor trafficking and synaptic plasticity. Annu. Rev. Neurosci. *25*, 103–126.

Mameli, M., Bellone, C., Brown, M.T., and Lüscher, C. (2011). Cocaine inverts rules for synaptic plasticity of glutamate transmission in the ventral tegmental area. Nat. Neurosci. *14*, 414–416.

Matsumoto, M., and Hikosaka, O. (2007). Lateral habenula as a source of negative reward signals in dopamine neurons. Nature *447*, 1111–1115.

Mediavilla, C., Cabello, V., and Risco, S. (2011). SB-334867-A, a selective orexin-1 receptor antagonist, enhances taste aversion learning and blocks taste preference learning in rats. Pharmacol. Biochem. Behav. *98*, 385–391.

Meye, F.J., Valentinova, K., Lecca, S., Marion-Poll, L., Maroteaux, M.J., Musardo, S., Moutkine, I., Gardoni, F., Huganir, R.L., Georges, F., and Mameli, M. (2015). Cocaine-evoked negative symptoms require AMPA receptor trafficking in the lateral habenula. Nat. Neurosci. *18*, 376–378.

Nabavi, S., Fox, R., Proulx, C.D., Lin, J.Y., Tsien, R.Y., and Malinow, R. (2014). Engineering a memory with LTD and LTP. Nature *511*, 348–352.

Root, D.H., Mejias-Aponte, C.A., Qi, J., and Morales, M. (2014). Role of glutamatergic projections from ventral tegmental area to lateral habenula in aversive conditioning. J. Neurosci. *34*, 13906–13910.

Saha, S., and Datta, S. (2005). Two-way active avoidance training-specific increases in phosphorylated cAMP response element-binding protein in the dorsal hippocampus, amygdala, and hypothalamus. Eur. J. Neurosci. *21*, 3403–3414.

Schönherr, S., Seewald, A., Kasugai, Y., Bosch, D., Ehrlich, I., and Ferraguti, F. (2016). Combined optogenetic and freeze-fracture replica immunolabeling to examine input-specific arrangement of glutamate receptors in the mouse amygdala. J. Vis. Exp., 53853.

Shabel, S.J., Proulx, C.D., Trias, A., Murphy, R.T., and Malinow, R. (2012). Input to the lateral habenula from the basal ganglia is excitatory, aversive, and suppressed by serotonin. Neuron *74*, 475–481.

Stamatakis, A.M., Van Swieten, M., Basiri, M.L., Blair, G.A., Kantak, P., and Stuber, G.D. (2016). Lateral hypothalamic area glutamatergic neurons and their projections to the lateral habenula regulate feeding and reward. J. Neurosci. *36*, 302–311.

Stuber, G.D., Klanker, M., de Ridder, B., Bowers, M.S., Joosten, R.N., Feenstra, M.G., and Bonci, A. (2008). Reward-predictive cues enhance excitatory synaptic strength onto midbrain dopamine neurons. Science *321*, 1690–1692.

Takemoto, K., Iwanari, H., Tada, H., Suyama, K., Sano, A., Nagai, T., Hamakubo, T., and Takahashi, T. (2017). Optical inactivation of synaptic AMPA receptors erases fear memory. Nat. Biotechnol. *35*, 38–47.

Valentinova, K., and Mameli, M. (2016). mGluR-LTD at excitatory and inhibitory synapses in the lateral habenula tunes neuronal output. Cell Rep. *16*, 2298–2307.

Wang, D., Li, Y., Feng, Q., Guo, Q., Zhou, J., and Luo, M. (2017). Learning shapes the aversion and reward responses of lateral habenula neurons. eLife *6*, e23045.

Wenzel, J.M., Oleson, E.B., Gove, W.N., Cole, A.B., Gyawali, U., Dantrassy, H.M., Bluett, R.J., Dryanovski, D.I., Stuber, G.D., Deisseroth, K., et al. (2018). Phasic dopamine signals in the nucleus accumbens that cause active avoidance require endocannabinoid mobilization in the midbrain. Curr. Biol. *28*, 1392–1404.e5.

Won, J., and Silva, A.J. (2008). Molecular and cellular mechanisms of memory allocation in neuronetworks. Neurobiol. Learn. Mem. *89*, 285–292.

Zhang, G.W., Shen, L., Zhong, W., Xiong, Y., Zhang, L.I., and Tao, H.W. (2018). Transforming sensory cues into aversive emotion via septal-habenular pathway. Neuron *99*, 1016–1028.e5.

STAR★METHODS

KEY RESOURCES TABLE

REAGENT or RESOURCE	SOURCE	IDENTIFIER
Antibodies		
Anti-NeuN mouse	Millipore	Cat# MAB377; RRID: AB_2298772
647-Alexa anti-mouse	Invitrogen	Cat# A-21247; RRID: AB_141778
Anti-GAD67 mouse	Millipore	Cat# MAB5406; RRID: AB_2278725
Anti-EAAC1 goat	Millipore	Cat# MAB1520; RRID: AB_90732
panAMPA	Frontiers Science Company	Cat#: panAMPAR-GP-Af580-1
Anti-GFP Rabbit	Invitrogen	Cat#: A11122; RRID AB_221569
Goat anti-guinea pig IgG-5nm Gold particle	British Biocell International	Cat#: EM.GFAR5
Goat anti-rabbit IgG-10nm Gold particle	British Biocell International	Cat#: EM.GAR10
Bacterial and Virus Strains		
rAAV2.5–*h*Syn–CoChR–eGFP	UNC Vector Core	N/A
AAV5-*h*Syn-Chrimson-tdTomato	Addgene	Cat#: 59171
rAAV2.2–CAG–JAWS–GFP	Vector biolabs	N/A
rAAV2.5–*h*Syn–GCaMP6f	Addgene	Cat#: 100837
rAAV2.1–CAG–tdTomato	Addgene	Cat#: 59462
Chemicals, Peptides, and Recombinant Proteins		
Anti-GluA1-Eosin (Cali-GluA1)	Gift of T. Takahashi	
Anti-Myc-eosin (Control)	Gift of T. Takahashi	
D-AP5	Hello Bio	Cat#: HB0225
Picrotoxin	Hello Bio	Cat#: HB0506
NBQX disodium salt	Hello Bio	Cat#: HB0443

CONTACT FOR REAGENT AND RESOURCE SHARING

Further information and requests for resources and reagents should be directed to and will be fulfilled by the Lead Contact, Manuel Mameli (manuel.mameli@unil.ch).

EXPERIMENTAL MODEL AND SUBJECT DETAILS

Male naive mice (C57Bl6/J; 4–12 weeks) were group-housed (three to five per cage) on a 12:12 h light cycle (lights on at 7 a.m.) with food and water *ad libitum*. All procedures aimed to fulfill the 3R criterion and were approved by the Veterinary Offices of Vaud (Switzerland; License VD3171).

METHOD DETAILS

Stereotactic injections

Mice were anesthetized with ketamine (150 mg kg^{-1}) and xylazine (100 mg kg^{-1}) (Veterinary office University of Lausanne) and were placed on a stereotactic frame (Kopf, Germany). Bilateral injections obtained through a glass needle of 200-400 nL volume were performed at a rate of approximately 100 nL min^{-1}. The injection pipette was withdrawn from the brain 10 min after the infusion. Injections were performed using the following coordinates: lateral hypothalamus (LH: −1.25 mm posterior to bregma, 0.95 mm lateral, −5.1 mm ventral from pia); entopeduncular nucleus (EPN: −1.25 mm posterior to bregma, 1.80 mm lateral, −4.65 mm ventral); medial VTA (mVTA: −2.2 mm posterior to bregma, 0.3 mm lateral, −4.8 mm ventral); lateral habenula (LHb: −1.35 mm posterior to bregma, 0.45 mm lateral, −3.1 mm ventral).

Animals were allowed to recover for a minimum of 3 weeks before the recordings.

Viral constructs employed in the study: rAAV2.5–*h*Syn–CoChR–eGFP (University of North Carolina viral vector core, USA; titer: 1×10^{12} gc/ml); AAV5-*h*Syn-Chrimson-tdTomato (University of Pennsylvania viral vector core; titer: 7×10^{12} gc/ml). rAAV2.2–CAG–JAWS–GFP (Vector biolabs, USA; titer: 7×10^{12} gc/ml); rAAV2.5–*h*Syn–GCaMP6f, rAAV2.1–CAG–tdTomato (University of

Pennsylvania viral vector core; titer: 5×10^{12} gc/ml and 1.19×10^{13} gc/ml). The injection sites were examined for all experiments and only data from animals with correct injections were included.

Slice electrophysiology

The mice were anesthetized (ketamine/xylazine; 150 mg/100 mg kg^{-1}), sacrificed, and their brains were transferred in ice-cold carbogenated (95% O_2/5% CO_2) solution, containing (in mM) choline chloride 110; glucose 25; $NaHCO_3$ 25; $MgCl_2$7; ascorbic acid 11.6; sodium pyruvate 3.1; KCl 2.5; NaH_2PO_4 1.25; $CaCl_2$0.5. Coronal brain slices (250 μm thickness) were prepared and transferred for 10 min to warmed solution (34°C) of identical composition, before they were stored at room temperature in carbogenated artificial cerebrospinal fluid (ACSF) containing (in mM) NaCl 124; $NaHCO_3$ 26.2; glucose 11; KCl 2.5; $CaCl_2$ 2.5; $MgCl_2$ 1.3; NaH_2PO_4 1. During recordings, slices were immersed in ACSF and continuously superfused at a flow rate of 2.5 mL min^{-1} at 30°C. Neurons were patch-clamped using borosilicate glass pipettes (2.7–4 MΩ; Phymep, France) under an Olympus-BX51 microscope (Olympus, France). For voltage or current clamp recordings, signal was amplified, filtered at 5 kHz and digitized at 10 kHz (Multiclamp 200B; Molecular Devices, USA). Data were acquired using Igor Pro with NIDAQ tools (Wavemetrics, USA). Access resistance was continuously monitored with a −4 mV step delivered at 0.1 Hz. Experiments were discarded if the access resistance increased by more than 20% during the recording.

Extracellular stimulation from AMPI ISO-Flex stimulator was delivered through glass electrodes placed in the LHb.

Light stimulation (470 nm 1 ms for CoChR experiments, 584 nm continuous for JAWS experiments) was delivered with a LED (CoolLed, UK) illumination system. We systematically tested for direct optically-driven currents (100 msec light) sporadically observed in regions receiving afferent inputs from the site of injection. In case a direct photo-current was found the cell was discarded.

A 532 nm laser (Integrated Optics, Lithuania) was used in the experiments for the in-vitro validation and in-vivo activation (2 min light exposure) of the CALI strategy. For glutamate uncaging (4-methoxy-7-nitroindolinyl-caged L-glutamate 200μM, Tocris), a single-path photolysis head was connected to a solid-state laser (Rapp Optolectronics, Germany; 405 nm, duration 0.5 ms, diameter 3–5μm).

All recordings were made in voltage-clamp configuration, in picrotoxin-containing ACSF (100 μM). The stimulation intensity (electrical and light) was titered to obtain currents between ± 50-300 pA. AMPAR/NMDAR ratios of evoked EPSC were obtained by AMPAR-EPSC +40 mV/NMDAR-EPSCs at +40 mV. I_{AMPAR} and I_{NMDAR} were pharmacologically isolated by the application of APV (100 μM), NBQX (20 μM), and by subsequent identification of the individual currents via digital subtraction. CALI and JAWS in-vitro validation experiments were performed in voltage clamp mode at −50 mV and light was applied continuously until the end of the experiment. The internal medium consisted of (in mM) cesium methanesulfonate 120, CsCl 10, HEPES 10, EGTA 10, creatine phosphate 5; Na2ATP 4; Na3GTP 0.4.

Long-term plasticity experiments were performed at −60 mV with an internal solution contained the following (in mM): K-gluconate 140; KCl 5; HEPES 10; EGTA 0.2; MgCl2 2; Na2ATP 4; Na3GTP 0.3; and creatine-phosphate 10. For the measurement of AMPAR-$EPSC_{-60\ mV}$/NMDAR-$EPSCs_{+40\ mV}$ before and after the LTP protocol, we used an internal solution containing the following (in mM): cesium methanesulfonate 130; 15 CsCl, 10 HEPES, 0.2 EGTA, 10 Creatine Phosphate, 4 ATP-Mg, 0.3 GTP-Na. The induction protocol for long-term plasticity consisted of 5 trains of 1 s stimulation at 100 Hz, delivered at 0.1Hz, paired with somatic depolarization (+20 mV).

Data collection and analysis for the electrophysiology experiments were not performed blind to the conditions of the experiments.

In vivo electrophysiology

Recordings under anesthesia

For the JAWS validation *in vivo*, mice previously injected in the LH with rAAV2-CAG-JAWS-eGFP were anesthetized using isoflurane (Univentor, Malta. Induction: 2%; maintenance: 1%–1.5%) and placed in the stereotaxic apparatus (Kopf, Germany). Their body temperature was maintained at 36 ± 1°C using a feedback-controlled heating pad (CMA 450 Temperature controller, USA). An optrode was lowered at the coordinates of LHb. Each cell was tested for its response to repetitive (every 5 s) shocks (0.5 s, 1.5 - 2 mA) delivered to the hind paw contralateral to the recording side. If excited the Fs response was re-tested while simultaneously shining the light (638nm, 10mW, 4 s). PSTHs and raster plots were built from 30 to 60 shocks and displayed using 10 ms bin width. A cell was considered excited when the mean number of action potentials/bin (bin length = 10 ms) in at least one of the four epochs (50 ms per epoch) after the shock inset was 2 times the Standard Deviation (SD) higher than baseline levels (the average number of action potentials/bin in the 2 s period before the shock). The duration of the response was calculated from the latency to the first of at least 5 consecutive bins not different than the baseline + 2SD. The magnitude of the response was obtained subtracting the baseline firing rate to the firing during the duration of the shock response.

At the end of each experiment, the electrode placement was determined with an iontophoretic deposit of pontamine sky blue dye (1 mA, continuous current for 5 min). Brains were then rapidly removed and fixed in 4% paraformaldehyde solution. The position of the electrodes was identified with a microscope on coronal section sections (100 μm). Only recordings in the correct area were considered for analysis.

For awake *in vivo* recordings, mice were implanted with a custom stainless steel headbar for head fixation. The scalp was removed and skull scraped clean and dry using a scalpel. LHb sites (AP, lateral, in mm, from bregma: −1.4, 0.45) were marked with sharpie pen

on the skull and covered with a drop of silicone elastomer (Kwik-Cast; WPI). Cyanoacrylate glue (Vetbond, 3M) was lightly dabbed on the skull. Then, the headbar was levelled flat and lowered to touch lambda, covered with dental adhesive (C and B Metabond, Parkell) and secured with dental cement (Jetkit, Lang). Only a thin layer of cement was applied above the marked VM sites.

After at least 3 days of recovery, mice were habituated to head fixation in a 3-cm-wide acrylic cylinder for 10 min twice a day. In parallel, mice were trained for four days in the active avoidance paradigm. After the fourth training session, mice were anesthetized, dental cement and silicone above LHb were removed, and holes were drilled on the marked LHb locations. The craniotomy was then covered *in silico*ne elastomere. The next day, mice were headfixed for recordings, instead of the last behavior session.

After headfixation, the craniotomy was exposed and and electrode was lowered in the LHb (DV 2.3-3.2, from brain, in mm). Single unit activity was recorded extracellularly using glass micropipettes filled with 2% Chicago sky blue dissolved in 0.5 M sodium acetate (impedance 5-15 MΩ). Signal was filtered (band-pass 500–5000 Hz), pre-amplified (DAM80, WPI, Germany), amplified (Neurolog System, Digitimer, UK) and displayed on a digital storage oscilloscope (OX 530, Metrix, USA). Experiments were sampled on- and offline by a computer connected to CED Power 1401 laboratory interface (Cambridge Electronic Design, Cambridge, UK) running the Spike2 software (Cambridge Electronic Design).

Single units were isolated and after recording baseline activity (3 minutes), each cell was tested for its response to CS presentation (25kHz, 80dB, 4 s duration, random interval of 5-30 s, 6 to 12 trials; recordings per single mouse lasted < 90 min) delivered by a speaker placed nearby the mouse. PSTHs and raster plots were built using 100 ms bin normalized to a window of 2 s baseline. For each cell we calculate the modulation index (CS firing – baseline firing / CS firing + baseline firing). A cell was considered excited or inhibited when the modulation index was larger than 0.1 or lower than −0.1, respectively.

Histology and immunofluorescence

Mice were anaesthetized and transcardially perfused with 4% paraformaldehyde (w/v) in 0.1 M phosphate buffered saline (PBS; pH 7.4). Coronal sections (100 μm) were cut with a vibratome. To examine fiber placement and for injection sites examination, we used an epifluorescent microscope (Zeiss) with a 5x and 10x objective. For immunofluorescence, the brain slices were incubated for 48h at 4°C in mouse anti-NeuN antibody (1:500, MAB377 Millipore) in PBS containing 0.3% Triton X and 5% normal goat serum. After extensive washes in PBS, the slices were incubated for 24h at 4°C with 647-Alexa-coupled secondary anti-mouse antibody (1:1000, Invitrogen). Images of the lateral habenula (3 fields/mouse) were acquired using a confocal microscope (TCS SP5 AOBS TANDEM, Leica) with a 20X objective. The number of GCaMP6f and NeuN-positive neurons was counted. To identify the nature of cells expressing GCaMP6f, antigen retrieval was performed by incubating the brain slices in 50mM Na-citrate solution at 80°C for 30 minutes. Slices were rinsed, incubated 1h in a solution containing 0.3% Triton X and 5% normal goat serum, and then for 48h at 4°C in a cocktail of mouse anti-GAD67 antibody (1:250, MAB5406 Millipore) and goat anti-EAAC1 (1:250, MAB1520 Millipore) in PBS containing 5% normal goat serum. After extensive washes in PBS, the slices were incubated for 24h at 4°C with 555-Alexa-coupled secondary anti-goat antibody, and then 647-Alexa-coupled secondary anti-mouse antibody (1:1000, Invitrogen). Images of the LHb were acquired using a confocal microscope (TCS SP5 AOBS TANDEM, Leica) with a 20X and a 63X immersion objective. ImageJ software (version 1.6, https://imagej.nih.gov/ij/) was used for image processing.

Freeze fracture replica immunolabeling

Anesthetized mice were perfused transcardially using a peristaltic pump at a flow rate of 5 ml/min with 25 mM phosphate buffered saline solution (PBS) for 1 min, followed by ice cold 1% paraformaldehyde (PFA) and 15% saturated picric acid in 0.1 M phosphate buffer (PB) for 7 min. Coronal slices (130 mm thick) were cut using a vibrating microslicer (VT1000, Leica, Vienna, Austria) in 0.1 M PB. A region of the LHb was trimmed from the slices and immersed in graded glycerol (10%–30% in 0.1 M PB) at 4°C overnight and frozen by a high pressure freezing machine (HPM 010; BAL-TEC, Balzers, Liechtenstein). Frozen samples were fractured using a double-replica table at −115°C and replicated by carbon deposition (5 nm thick), carbon-platinum (2 nm) and carbon (15 nm) with a freeze-fracture replica machine (BAF060; BAL-TEC). Tissue debris were dissolved with shaking at 80°C for 20 h in a solution containing 15 mM Tris-HCl (pH 8.3), 20% sucrose, and 2.5% SDS. The replicas were washed three times in 50 mM Tris-buffered saline (TBS, pH 7.4) containing 0.05% bovine serum albumin (BSA), 0.1% Tween-20, and 0.05% sodium azide and blocked with 5% BSA in washing buffer for 1 h at room temperature. Subsequently, they were incubated with primary antibodies for 3 overnights at 15°C. The primary antibodies were: guinea pig polyclonal IgG raised against the 717-754 amino acid residues common to all AMPAR subunits (diluted 1:200, Frontier Science Co. Ltd, Hokkaido, Japan, cat. no. panAMPAR-GP-Af580-1) and rabbit polyclonal IgG raised against the green fluorescent protein (GFP) from the jellyfish *Aequorea victoria* (diluted 1:1,000, Molecular Probes-Invitrogen, cat. no. A11122, Lot. no. 1356608). Antigen-antibody complexes were identified using secondary antibodies against the species of the first antibody and conjugated to gold particles of different size: goat anti-guinea pig IgG conjugated with 5 nm gold particles and goat anti-rabbit IgG conjugated with 10 nm gold particles (both diluted 1:30, British Biocell International, Cardiff, UK). Incubation was carried out overnight at 15°C. The labeled replicas were examined using a transmission electron microscope (CM-120; Philips).

Immunoparticles quantification

Images of excitatory postsynaptic specializations (PSD), identified by the presence of intramembrane particle (IMP) clusters on the exoplasmic face (E-face) accompanied by the protoplasmic face (P-face) of the presynaptic plasma membrane labeled by GFP immunoparticles, were captured at a magnification of 88,000 with a digital camera (Morada, Soft Imaging System; SIS). The PSD was

demarcated freehand and the area was measured using the iTEM (SIS) or FIJI software (distributed under the General Public License). Immunoparticles within the PSD and those located outside but within 30 nm from the edge of the PSD were regarded as synaptic labeling, considering possible deviations of the immunoparticle from the antigen. The majority of analysis was performed on dendritic shafts as under our experimental conditions the vast majority of LHb spines were fractured at the neck and the PSD could not be exposed. Sampling and analysis of AMPAR density was performed by an investigator blind of the experimental groups. Data from both full and partial synapses were used since there was no significant difference ($p = 0.31$, unpaired t test) in AMPAR density.

Fiber photometry

The fiber photometry measurements in this study were carried out by the ChiSquare χ^2-200 system (ChiSquare Biomaging, Brookline, MA). Briefly, blue light from a 473-nm picosecond-pulsed laser (at 50 MHz; pulse width ~80 ps FWHM) was delivered to the sample through a single mode fiber. Fluorescence emission from the tissue was collected by a multimode fiber. The singlemode and multimode fibers were arranged side by side in a ferrule that is connected to a detachable multimode fiber implant. The emitted photons collected through the multimode fiber pass through a bandpass filter (FF01-550/88, Semrock) to a single-photon detector. Photons were recorded by the time-correlated single photon counting (TCSPC) module (SPC-130EM, Becker and Hickl, GmbH, Berlin, Germany) in the ChiSquare χ^2-200 system. Online analysis of photon counting was systematically employed to determine whether the fiber probe was correctly placed to detect fluorescent changes (photon count > 300 photons). The experiments were replicated two to three times in the laboratory with different batches of mice.

Behavioral testing

Active avoidance

Behavioral tests were performed during the light phase. The active avoidance procedure (AA) was performed using a modified version of the Ugo Basile shuttle box apparatus. We substituted the door separating the two portions of the apparatus with two separate walls in order to allow the passage of optical fibers reaching the animal's head. The animals were handled daily by the experimenter for 3 days before the start of the behavioral tests. Mice were habituated to the testing room for a minimum of 30 minutes, and then a minimum of 10 minutes to the testing chamber. The training protocol consisted of a maximum of 5 sessions, 30 trials per session, 1 session/day. The protocol consisted in a random inter-trial interval (ITIs, min 20 s max 40 s) followed by a 10 s ≈70dB 5Khz tone (conditioning stimulus, CS), immediately followed by a 0.3 mA footshock (unconditioned stimulus, US) delivered through the metallic floor grid. The foot shock had a maximal duration set to 25 s and was terminated when the animal shuttled to the opposite compartment, or prevented if the animal shuttled during the delivery of the CS. For electrophysiological experiments, the animals exposed to the training were excluded from further testing if they failed to avoid at least 5 trials during session 2. Control animals were subjected to a pattern of US designed to mimick the average experience of the learner group on each specific session (1 to 5). The total duration of foot shock experienced in each session was scattered in episodes of 1, 2 or 3 s, and delivered not contingently to the US. For the control protocol, both CS and US were not-stoppable by shuttling to the opposite compartment.

For experiments employing JAWS *in vivo*, light was provided through a laser-coupled fiber optic at 638 nm. Light was applied during the entire presentation of the CS at a power of 15 mW at the tip of the fiber. For experiments using CALI (site of injection identified with flurobeads), a fiber optic delivered light (532 nm, 60 mW, 2 minutes) above the LHb.

Fear conditioning

Animals underwent a fear conditioning procedure. Briefly, the animals were conditioned in the apparatus used for active avoidance. On the first day, they experienced 4 presentations of the CS (total CS duration of 30 s, 7.5 kHz, 80 dB; inter-trial interval: 20–180 s). On day 2 the CS was paired with a US (1 s foot shock, 0.6 mA, 5 CS+/US pairings; inter-trial interval: 20–180 s) at the offset of the CS. The animals were sacrificed for recordings 24h after the conditioning.

Drugs

The drugs were obtained from Sigma (Switzerland), Tocris (Bristol, UK) and Hellobio (Bristol, UK). With the exception of picrotoxin and NBQX (DMSO, 0.01% final bath concentration), all drugs were dissolved in purified water.

QUANTIFICATION AND STATISTICAL ANALYSIS

Online and offline analysis for electrophysiological data were performed using Igor Pro-6 (Wavemetrics, USA). Sample size was predetermined on the basis of published studies, experimental pilots and in-house expertise. Animals were randomly assigned to experimental groups. Compiled data are always reported and represented as boxplots (median and quartiles) or mean ± SEM, with single data points plotted (single cell for electrophysiology and single animal for behavioral experiments). Animals or data points were not excluded from analyses unless noted. Data distribution was tested for normality. When applicable, statistical tests were one-way ANOVAs, two-way ANOVAs, paired or unpaired t test. In case of not-normally distributed data, we used the Mann-Whitney and Friedman non-parametric test. Curve fitting was statistically tested with Pearson or Spearman tests. Testing was always performed two-tailed with $\alpha = 0.05$.

nature neuroscience

ARTICLES

https://doi.org/10.1038/s41593-019-0512-2

Prenatal THC exposure produces a hyperdopaminergic phenotype rescued by pregnenolone

Roberto Frau[1,6], Vivien Miczán[2,3,6], Francesco Traccis[1], Sonia Aroni[1,4], Csaba I. Pongor[5], Pierluigi Saba[1], Valeria Serra[1], Claudia Sagheddu[1], Silvia Fanni[1], Mauro Congiu[1], Paola Devoto[1], Joseph F. Cheer[4], István Katona[3,6] and Miriam Melis[1]*

The increased legal availability of cannabis has led to a common misconception that it is a safe natural remedy for, among others, pregnancy-related ailments such as morning sickness. Emerging clinical evidence, however, indicates that prenatal cannabis exposure (PCE) predisposes offspring to various neuropsychiatric disorders linked to aberrant dopaminergic function. Yet, our knowledge of how cannabis exposure affects the maturation of this neuromodulatory system remains limited. Here, we show that male, but not female, offspring of Δ⁹-tetrahydrocannabinol (THC)-exposed dams, a rat PCE model, exhibit extensive molecular and synaptic changes in dopaminergic neurons of the ventral tegmental area, including altered excitatory-to-inhibitory balance and switched polarity of long-term synaptic plasticity. The resulting hyperdopaminergic state leads to increased behavioral sensitivity to acute THC exposure during pre-adolescence. The neurosteroid pregnenolone, a US Food and Drug Administration (FDA) approved drug, rescues synaptic defects and normalizes dopaminergic activity and behavior in PCE offspring, thus suggesting a therapeutic approach for offspring exposed to cannabis during pregnancy.

The use of cannabis among pregnant women is increasing, with a prevalence rate of 3–16% in Western societies[1–4]. Together with the boom in cannabis marketing and the increased perception of its safety, cross-sectional analyses indicate that cannabis is often recommended to pregnant women as a treatment for morning sickness[5]. Although the use of medical cannabis for nausea and vomiting is approved in several states and countries, no legal distinction or warning for its use during pregnancy is mentioned[6]. Additionally, doctors or other health-care practitioners seldom advise pregnant women about the risks of taking cannabis during pregnancy[6,7].

The main psychoactive ingredient of cannabis, THC, interferes with the endocannabinoid system, which tightly controls progenitor cell proliferation and neuronal differentiation, axon growth and pathfinding, synapse formation and pruning in the developing brain[3,8–10]. Accordingly, four independent longitudinal clinical studies demonstrated that PCE predisposes individuals to a wide array of behavioral and cognitive deficits, including hyperactivity, enhanced impulsivity, loss of sustained attention, increased sensitivity to drugs of abuse[11–13] and susceptibility to psychosis[14]. Notably, all these neuropsychiatric impairments are tied to a dysfunction of dopaminergic signaling[15,16]. While the effects of acute and chronic cannabis use during adolescence and adulthood have been investigated[17–19], the impact of PCE on dopamine neurons within the ventral tegmental area (VTA), key players in motivation, reward and cognition[20], remains to be elucidated.

The 'two-hit' model of psychiatric disorders posits that genetic background and/or environmental insults act as a first hit, perturbing brain development in a manner that leads to susceptibility to the onset of psychiatric symptoms following a second hit. First hits can also lead to endophenotypes such as neurobehavioral deficits[21,22], and characterizing these may help to elucidate altered trajectories of circuit development that increase susceptibility to subsequent challenges[22,23], which may in turn enable prevention of disease emergence. Notably, PCE was recently suggested to act as a first hit by interfering with the known complex developmental functions of endocannabinoid signaling[3,9,23].

Longitudinal studies evaluating the behavioral effects of PCE on offspring have consistently shown that the offspring exhibit increased impulsivity, increased incidence of risk-taking behaviors and vulnerability to psychosis and enhanced sensitivity to drugs of abuse later in life, which can be detected as early as early infancy and throughout child development[11,12,14]. Furthermore, it is predicted that the ratio of affected children developing prenatal THC-induced endophenotypes is likely to be substantially higher[24,25], but the complexity of uncontrollable genetic, environmental and socioeconomic factors in humans makes the determination of causality very difficult. This highlights the advantage of animal models that mimic specific genetic and environmental factors. Here, we tested the hypothesis that PCE triggers molecular and synaptic changes in the VTA, which lead to aberrant dopaminergic activity and behavioral susceptibility to subsequent challenges. In agreement with evidence that the first clinical neuropsychiatric symptoms manifest as early as infancy in PCE offspring[11,14,24], we find that prenatal THC exposure (a model of PCE, hereafter referred to as PCE) engenders 'silent' functional abnormalities, such as impaired sensorimotor gating,

[1]Department of Biomedical Sciences, University of Cagliari, Cittadella Universitaria, Monserrato, Italy. [2]Momentum Laboratory of Molecular Neurobiology, Institute of Experimental Medicine, Hungarian Academy of Sciences, Budapest, Hungary. [3]Faculty of Information Technology and Bionics, Pázmány Péter Catholic University, Budapest, Hungary. [4]Department of Anatomy and Neurobiology, University of Maryland School of Medicine, Baltimore, MD, USA. [5]Nikon Center of Excellence for Neuronal Imaging, Institute of Experimental Medicine, Hungarian Academy of Sciences, Budapest, Hungary. [6]These authors contributed equally: Roberto Frau, Vivien Miczán, István Katona. *e-mail: myriam@unica.it

increased risk-taking and abnormal locomotor responses to THC in juvenile male offspring, that become overt when acutely challenged with THC. Enhanced excitability of VTA dopamine neurons and larger THC-induced dopamine release accompany the PCE-induced endophenotype. Furthermore, we observe altered excitatory–inhibitory balance of VTA dopamine cells along with switched polarity from long-term depression (LTD) to long-term potentiation (LTP) at afferent excitatory synapses. Postnatal administration of pregnenolone, a federal-drug-agency (FDA)-approved drug, which is currently under investigation in clinical trials for cannabis use disorder (ClinicalTrials.gov identifier: NCT02811939), schizophrenia (NCT00728728 and NCT00615511), autism (NCT01881737 and NCT02627508), and bipolar disorder (NCT00223197 and NCT01409096), normalized dopamine neuron excitability, restored synaptic properties and abnormal polarity of synaptic plasticity, as well as THC-induced dopamine release and deficits of sensorimotor gating functions.

Results

PCE induces a distinct behavioral endophenotype. To test the hypothesis that PCE triggers behavioral dysfunctions by altering midbrain dopaminergic activity, we modeled PCE by administering THC (2 mg per kg, subcutaneously (s.c.) once daily) to rat dams during pregnancy (from gestational day (GD) 5 until GD20). This low THC dose does not recapitulate behavioral responses in the cannabinoid tetrad assay or elicits cannabinoid tolerance after repeated administration[26], hence it represents a mild insult without any substantial direct impact on maternal behavior. We did not detect changes in litter size, in maternal and non-maternal behavior, or in changes in offspring body weight at this dose (Supplementary Fig. 1), which indicates that malnutrition and maternal care did not account for any of the observed behavioral effects in the offspring. In terms of human consumption, this dose is equivalent to THC content in mild cannabis cigarettes (joints) (5%)[27], since the average THC content in illicit cannabis preparations has significantly increased in the last two decades (from ~4% to ~12%)[28].

To assess early signs of altered neurodevelopmental trajectories related to PCE endophenotypes, we tested offspring in a series of behavioral tasks under basal conditions and then following an acute THC (2.5 mg per kg, s.c.) or vehicle challenge during the third and fourth postnatal week (postnatal day (PND) 15–28), corresponding to human pre-adolescence. This is because in the clinical staging model, subclinical symptoms are shown before adolescence and early adulthood[29], and a prominent research goal is the identification of such endophenotypes[22]. Moreover, in healthy human subjects, cannabis induces a wide range of deficits that resemble the phenomenology of schizophrenia spectrum disorders[19,30]. Thus, we first investigated whether PCE alters sensorimotor gating functions by using pre-pulse inhibition (PPI) of the acoustic startle reflex. Measures of sensorimotor gating are among the most widely studied physiological markers used in animal models of schizophrenia, and PPI deficits are present in patients with psychotic disorders[31]. Notably, we found that PCE did not affect PPI per se. However, an acute THC challenge disrupted PPI parameters in the PCE group, but remained ineffective in control offspring (Fig. 1a). Because this effect was sex-dependent and specific for this developmental milestone (Fig. 1b; Supplementary Fig. 2a), all experiments hereafter were carried out in male pre-adolescent rats. To test whether PCE induces an endophenotype associated with altered mesolimbic dopamine transmission, we next performed in vivo cerebral microdialysis experiments in the nucleus accumbens shell (NAcS), one of the major target areas of midbrain VTA dopamine neurons (Supplementary Fig. 2b–d). In accordance with our behavioral observations, we did not detect alterations in basal extracellular dopamine levels, but the response to acute THC administration was significantly larger in the PCE offspring group (Fig. 1c), thus indicating that the mesolimbic dopamine system becomes sensitized following maternal THC use. Moreover, we found that THC-induced disruption of PPI significantly and positively correlated with the levels of dopamine in the NAcS (Fig. 1d) and required enhanced mesolimbic dopamine signaling, because an inhibitor of tyrosine hydroxylase (TH) prevented the PPI deficits (Fig. 1e).

We next used open-field tests to examine the effects of PCE on spontaneous locomotor responses to acute THC exposure. No differences were observed between progenies, unless they were acutely treated with THC, as revealed by increased locomotor parameters (Fig. 1f; Supplementary Fig. 3a,b). These effects on spontaneous locomotion were causally dependent on VTA dopamine neuron function, because chemogenetic silencing of dopaminergic neurons via Gi-coupled DREADD (designer receptors exclusively activated by designer drugs; hM4Di) stimulation counteracted the paradoxical hyperlocomotion elicited by THC in PCE offspring (Fig. 1g; Supplementary Fig. 3c,d). Next, we assessed whether the hyperlocomotion and reduced thigmotaxis observed in PCE after a single exposure to THC were associated with behavioral disinhibition. We tested the progenies in the dopamine-dependent suspended wire-beam bridge task, which measures the proclivity to engage in impulsive risk-taking behaviors. This task is operationally defined as the latency to access and move across an unstable bridge and to display stretched-attend postures, an ethologically relevant rodent behavior that occurs during risk assessment. PCE offspring were more prone to cross the bridge (Fig. 1h) and displayed a markedly impaired evaluation of risk assessment (Fig. 1i). Importantly, the propensity of PCE animals to take risks was not associated with alterations in emotional components, because progenies did not differ in the amount of defensive responses to sudden acoustic stimuli measured by startle amplitudes (Supplementary Fig. 3e). Furthermore, they did not display differences in anxiety-related behavior, as assessed by the number of entries and time spent in open or closed arms, or in the number of transitions in the center on the elevated plus maze (Supplementary Fig. 3f,g).

PCE increases dopamine neuron excitability. We next determined the neurobiological mechanisms underlying the heightened dopamine release associated with the behavioral susceptibility observed in PCE offspring. Because type-1 and type-2 cannabinoid (CB_1 and CB_2, respectively) receptors, molecular targets of THC, regulate progenitor cell proliferation in the developing brain[8], we first investigated via confocal microscopy whether PCE alters the number of TH-positive cells or the intensity of TH-immunostaining in the VTA. Neither TH-positive dopamine neuron density (Supplementary Fig. 4a–e) nor TH levels measured in individual cells (Supplementary Fig. 4f) were different. We next probed the function of dopamine neurons by using whole-cell patch-clamp recordings to assess whether PCE-induced changes in physiological properties of dopaminergic neurons promote enhanced release. We performed current-clamp recordings in the lateral portion of the VTA, where cell bodies of the majority of dopamine neurons projecting to the NAcS reside[32], and we verified the TH-immunopositivity of the recorded neurons by post hoc confocal microscopy. Dopamine neurons obtained from PCE offspring showed a different electrophysiological profile: they spontaneously fired at a higher frequency and displayed depolarized resting membrane potentials (Fig. 2a–c). Moreover, PCE dopamine neurons exhibited an overall increased excitability and high maximum spiking frequencies in response to somatically injected currents (Fig. 2d). We also observed a reduced latency to action potential onset, which is the time needed for the first spike appearance in response to the smallest current injection (Fig. 2e). Moreover, a larger proportion of dopamine neurons fired action potentials (16 out of 20, 80%) compared with control offspring (5 out of 21 cells, ~23%; Fig. 2e) and showed enhanced spike fidelity (Supplementary Fig. 5a–d). This is consistent with a decreased spike

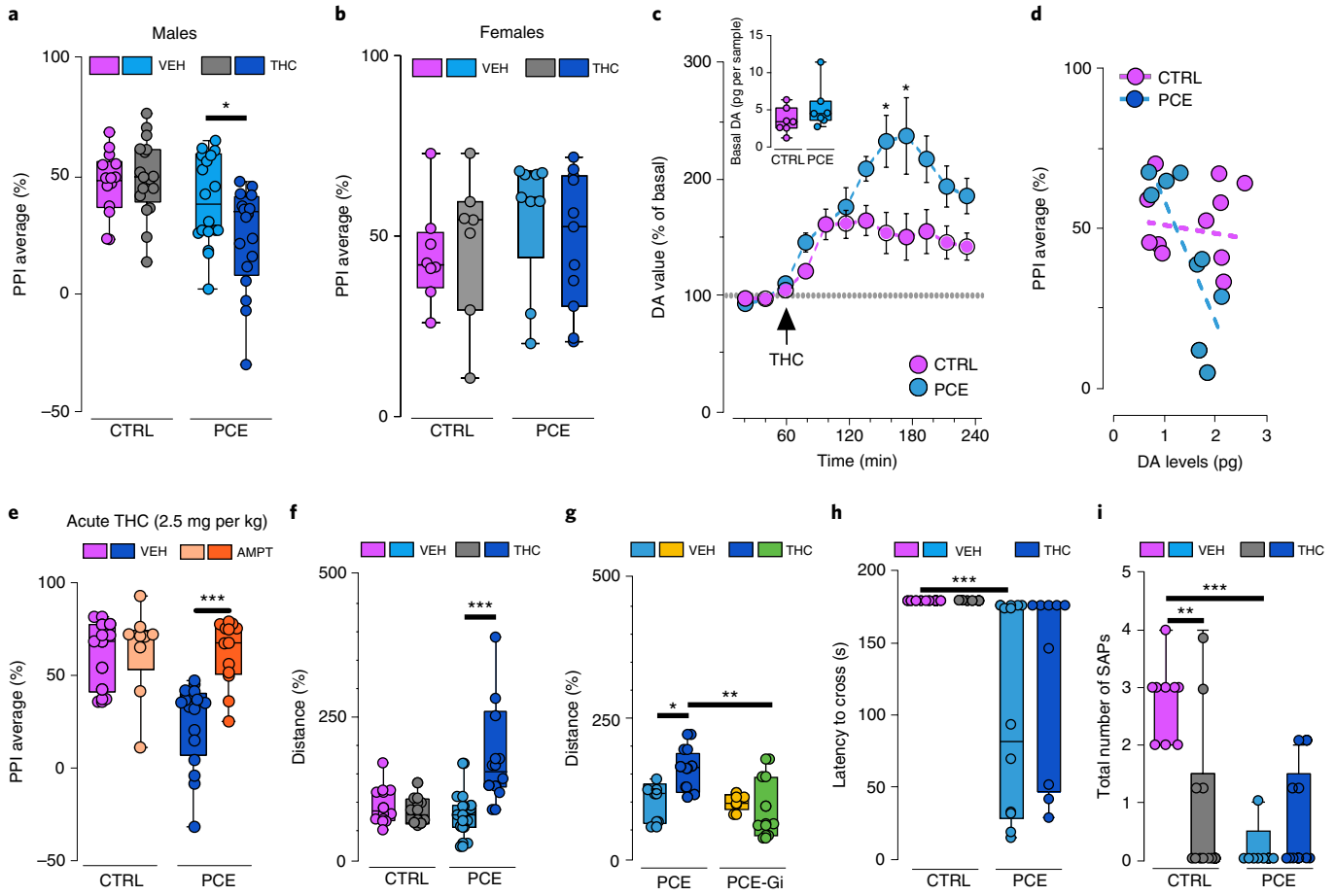

Fig. 1 | PCE elicits behavioral susceptibility to THC in male rat offspring. a,**b**, THC (2.5 mg per kg, s.c.) induces sensorimotor-gating deficits in male (**a**), but not female (**b**), progenies as measured using the PPI index (males, PCE-vehicle (VEH) versus PCE-THC: $^{*}P = 0.037$; control (CTRL)-VEH: $n = 14$; PCE-VEH, PCE-THC: $n = 18$; CTRL-THC: $n = 17$; females: $P = 0.44$ between groups; CTRL-VEH: $n = 8$; PCE-VEH: $n = 9$; CTRL-THC: $n = 7$; PCE-THC: $n = 11$). **c**, THC induces larger dopamine (DA) increase in the NAcS of PCE animals ($^{*}P < 0.05$ between groups; Sidak's test). Data represent the mean ± s.e.m. Inset indicates DA basal values ($P = 0.205$; two-tailed unpaired *t*-test; $n = 7$ per group). **d**, Percentage of PPI values inversely correlates with NAc DA levels of THC-treated PCE offspring. Data are fit by linear regression ($r^2 = 0.62$, $P = 0.01$; CTRL: $n = 11$, PCE: $n = 9$). **e**, DA synthesis inhibition by alpha-methyl-para-tyrosine (AMPT, 200 mg per kg, i.p.) prevents THC-induced PPI deficits in PCE progeny ($^{***}P = 0.0008$, PCE-VEH-THC versus PCE-AMPT-THC; CTRL-VEH-THC, PCE-VEH-THC: $n = 10$ per group; CTRL-AMPT-THC: $n = 9$; PCE-AMPT-THC: $n = 13$). **f**, THC induces hyperlocomotion in PCE offspring ($^{***}P = 0.0008$, CTRL-VEH versus CTRL-THC: $n = 8$ per group; PCE-VEH: $n = 11$, PCE-THC: $n = 10$). **g**, Gi activation prevents THC-induced hyperlocomotion in PCE offspring ($^{*}P < 0.05$, PCE-VEH versus PCE-THC; $^{**}P = 0.003$, PCE-THC versus PCE-Gi-THC; PCE-VEH, PCE-Gi-VEH: $n = 5$ rats per group; PCE-THC: $n = 8$; PCE-Gi-THC: $n = 7$). Distance traveled is the percentage of activity compared with the reference group. **h**,**i**, Crossing latency (**h**; $^{***}P = 0.0006$, PCE versus CTRL) and number of stretched-attend postures (SAPs) (**i**; $^{**}P < 0.01$, CTRL-VEH versus CTRL-THC; $^{***}P < 0.001$, CTRL-VEH versus PCE-VEH) are decreased in PCE offspring. THC does not modify the latency to crossing the bridge (**h**; $P = 0.36$, THC versus VEH group), but reduces SAP number (**i**) only in the CTRL group ($P = 0.02$, THC versus VEH; CTRL-VEH: $n = 8$; CTRL-THC, PCE-THC: $n = 8$ per group; PCE-VEH: $n = 10$). Unless otherwise indicated, graphs depict box-and-whisker plots (including minima, maxima and median values, and lower and upper quartiles) with single values. Data were analyzed using two-way ANOVA followed by Tukey's test.

threshold in response to depolarizing current pulses in neurons from PCE slices (Fig. 2f). In contrast, we did not detect alterations in the after-hyperpolarization period following successive action potentials (Fig. 2g,h), in the membrane capacitance or in inter-spike intervals (Supplementary Fig. 5e,f). Finally, PCE also modified dopamine cell responses to acute THC challenge by increasing spontaneous and evoked activity and enhancing spike fidelity in a dose-dependent and CB_1-receptor-dependent manner (Supplementary Fig. 6). Collectively, these results suggest that PCE biases the dopamine system by changing the intrinsic properties of dopamine neurons and endowing them with a hyper-excitable phenotype, an underlying clinical feature of diverse psychiatric disorders[16,20].

PCE shifts excitatory and inhibitory synaptic weights to dopamine neurons. To further address how PCE affects VTA dopamine neurons, we examined their synaptic properties. First, we observed a robust increase in the excitation-to-inhibition ratio of dopamine neurons from PCE slices (Fig. 3a). To elucidate the underlying mechanisms of this phenomenon, we calculated AMPA/$GABA_A$ and NMDA/$GABA_A$ ratios (Supplementary Fig. 7a–c) and produced input–output curves from the responses measured at different stimulus intensities. A substantial decrease in synaptic inhibition of VTA dopamine cells obtained from PCE rats was revealed (Fig. 3b; Supplementary Fig. 7a–c). To assess whether this change arises from presynaptic mechanisms, we first computed the 1/coefficient of variation^2 ($1/CV^2$) value, which is an independent measure of changes in presynaptic function[33]. We found that PCE markedly decreased the $1/CV^2$ of inhibitory postsynaptic currents (IPSCs) at lower stimulus intensities, which indicated that there was reduced release probability at inhibitory synapses

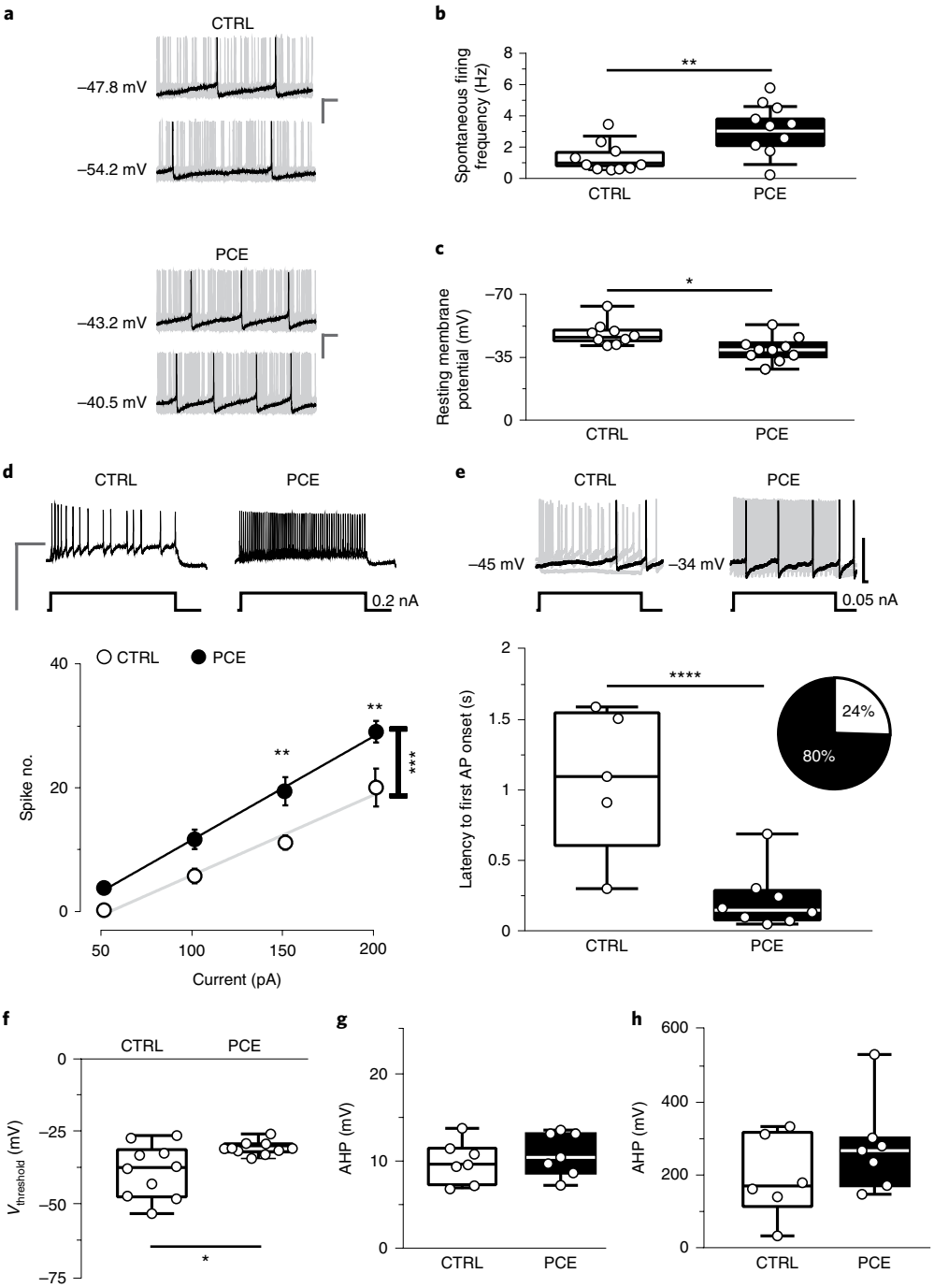

Fig. 2 | PCE enhances pacemaker and evoked activity of VTA dopamine neurons in male rat offspring. a, Representative traces of spontaneous activity of DA neurons in acute slices from CTRL and PCE offspring ($n = 20$ and 21 experiments from PCE and CTRL slices, respectively, were repeated independently with similar results obtained). Calibration bars, 100 ms, 20 mV. **b**,**c**, PCE offspring (n (rat) = 10, n (litter) = 6) show higher spontaneous activity (**b**; $^{**}P = 0.001$ between groups; Welch's correction) and lower resting membrane potentials (**c**; $^{*}P = 0.01$ between groups) compared with CTRL offspring (n (rat) = 10, n (litter) = 6). **d**, PCE DA cells (n (rat) = 10, n (litter) = 6) exhibit increased excitability in response to somatically injected current ($^{***}P = 0.0001$ between groups; two-way repeated-measures ANOVA followed by Bonferroni correction) compared with CTRL cells (n (rat) = 10, n (litter) = 6). Data are represented as average values per animal ± s.e.m. Insets show representative traces of evoked action potentials (APs) in response to maximum current injected. Calibration bar, 400 ms, 100 mV. **e**, Top: representative traces of evoked APs in response to the minimum current injected. Calibration bar, 100 ms, 50 mV. bottom: quantification of the latency of first AP appearance in response to the smallest current injected ($^{***}P < 0.001$ between groups). Inset shows the proportion of cells eliciting APs at 50 pA (CTRL in white, PCE in black). **f**, PCE DA cells exhibit a lower voltage threshold ($^{*}P = 0.015$ between groups). **g**,**h**, PCE does not affect the after-hyperpolarization period (AHP) amplitude (**g**; $P = 0.47$ between groups, not significant (NS)) or AHP duration (**h**; $P = 0.14$ between groups, NS) of DA cells. Unless otherwise indicated, graphs show box-and-whisker plots (including minima, maxima and median values, and lower and upper quartiles) with values averaged per animal and analyzed using two-sided unpaired t-test.

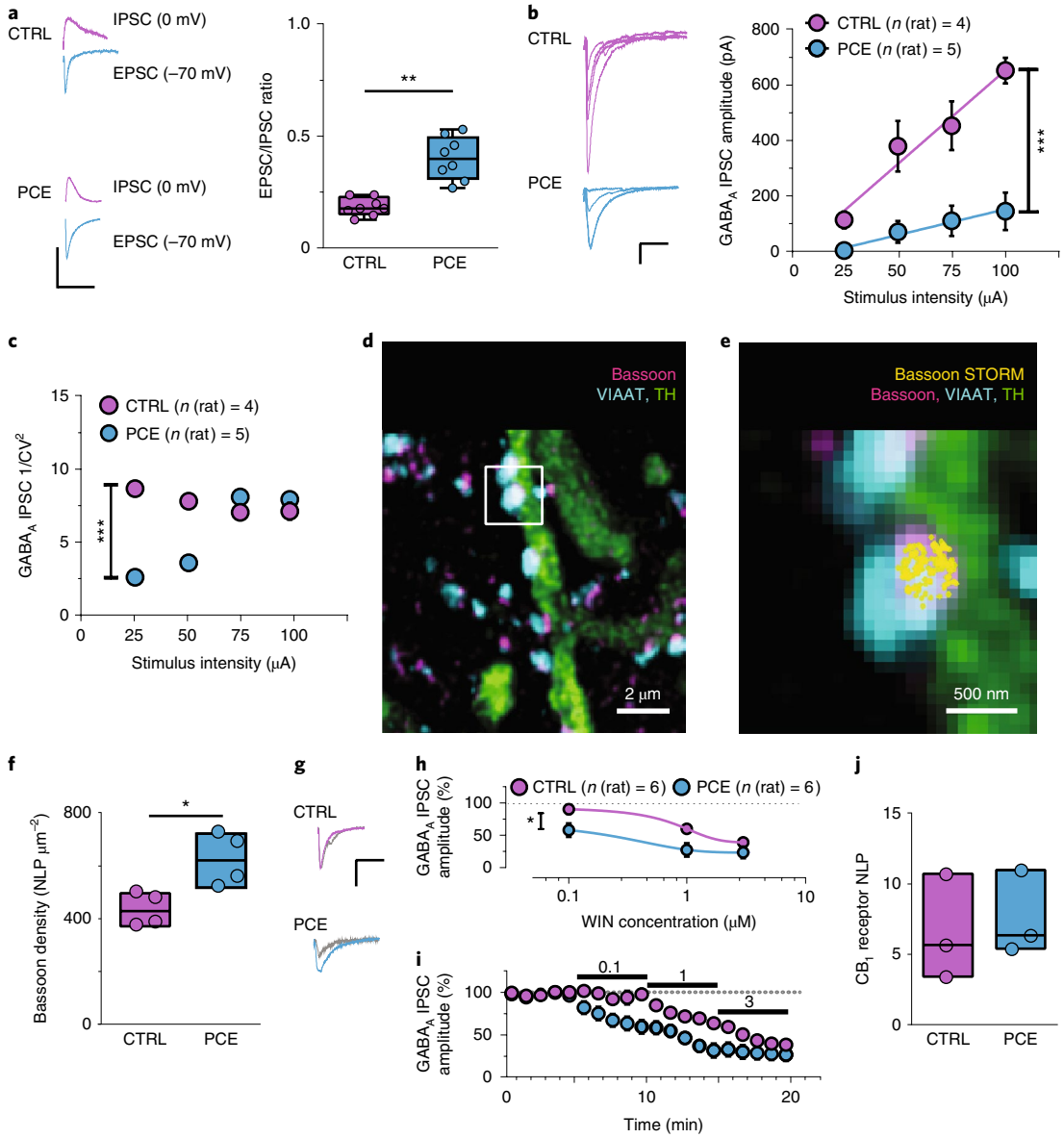

Fig. 3 | PCE reduces synaptic inhibition onto dopamine neurons in male rat offspring. a, Traces (left) and plots (right) of evoked EPSCs and IPSCs recorded from the same DA cells (**$P = 0.002$ between groups; two-sided unpaired *t*-test; *n* (litter) = 5 per group). *n* = 10 experiments from PCE and CTRL slices were repeated independently, with similar results obtained. **b**, Input–output relationships (***$P = 0.0004$ between groups) in CTRL and PCE DA cells. *n* = 5 and 8 experiments from CTRL and PCE slices, respectively, were repeated independently, with similar results obtained. Data represent the mean ± s.e.m. Left panel shows IPSC traces. Calibration bar, 5 ms, 100 pA. **c**, PCE effects on the 1/CV^2 values (***$P = 0.0002$ between groups) from **b**. **d**, Confocal image of VIAAT-containing terminals on a TH$^+$ process. **e**, Enlarged image of an axon terminal (the boxed area in **d)** decorated with bassoon-STORM number of localization points (NLPs) marking the bouton active zone. *n* = 20 images per animal were acquired independently, with similar results obtained. **f**, Bassoon density in VIAAT$^+$ active zones (*$P = 0.030$ between groups; two-sided Mann–Whitney *U*-test; *n* (litter) = 4 per group). **g**, IPSC traces recorded before and after (gray) WIN (0.1 μM) application. Calibration bar, 5 ms, 100 pA. **h**,**i**, Dose–response curves for WIN displaying a larger (**h**; *$P = 0.01$ between groups) and faster effect (**i**; $P = 0.02$ between groups) in PCE versus CTRL groups (*n* (litter) = 4 per group). Numbers on the chart in **i** indicate concentrations of WIN. *n* = 8 and 6 experiments in PCE and CTRL, respectively, were repeated independently, with similar results obtained. Average data per animal ± s.e.m. **j**, CB$_1$ receptor NLPs in VIAAT$^+$ terminals ($P = 0.662$ between groups; two-sided Mann–Whitney *U*-test; *n* (litter) = 3 per group). *n* = 20 images per animal were acquired independently, with similar results obtained. Unless otherwise indicated, graphs show box-and-whisker plots (including minima, maxima and median values, and lower and upper quartiles) with values representing the mean of averaged experiments per animal analyzed with two-way repeated-measures ANOVA followed by Bonferroni's test.

(Fig. 3c). Additionally, PCE increased the paired-pulse ratio (PPR) of GABA$_A$ IPSCs (Supplementary Fig. 7d,e), and decreased the frequency, but not the amplitude, of miniature IPSCs (mIPSCs) (Supplementary Fig. 7f–h).

Recent correlated electrophysiological and super-resolution imaging measurements have uncovered that the clustering of the cytomatrix protein bassoon in the presynaptic active zone is a reliable predictor of presynaptic release probability[34]. This is because an augmented bassoon density inhibits the recruitment of voltage-gated calcium channels required for action-potential-dependent vesicle release[34]. To identify the molecular substrates contributing to the reduced synaptic inhibition of VTA dopamine cells from PCE animals, we combined confocal and stochastic optical reconstruction microscopy (STORM) and quantified bassoon density (measured

with nanometer precision) within identified inhibitory axon terminals impinging on the dendrites of dopamine neurons (Fig. 3d). We observed a substantial increase (by 45%) in the nanoscale density of bassoon at GABAergic synapses obtained from the PCE group (Fig. 3e,f; Supplementary Fig. 8c). In contrast, there was no change in the number and size of inhibitory boutons and their active zones or in vesicular GABA transporter levels (Supplementary Fig. 8). Collectively, these data demonstrate that PCE induces a specific change in the presynaptic nanoarchitecture of inhibitory synapses and suggest that increased molecular crowding at vesicle release sites[34] contributes to the reduced synaptic inhibition of dopamine neurons.

CB_1 receptors are among the most abundant metabotropic regulators of neurotransmitter release probability[35]. Compelling anatomical and electrophysiological evidence shows that CB_1 receptor activation decreases GABA release, thereby sculpting the activity of dopamine signaling[36,37]. Therefore, we tested the hypothesis that enhanced cannabinoid receptor control at inhibitory synapses contributes to reduced synaptic inhibition. The mixed CB_1/CB_2 receptor agonist WIN 55,212-2 (WIN) produced a larger and faster effect on evoked IPSC amplitude recorded from VTA dopamine cells in PCE offspring than in controls (Fig. 3g–i). However, STORM imaging showed no difference in CB_1 receptor levels at GABAergic afferents to dopamine neurons (Fig. 3j). Together, these nanoscale super-resolution data indicate that the ratio of the presynaptic regulatory CB_1 receptors and their molecular effectors in the release machinery complex had shifted so that fewer voltage-gated calcium channels were controlled by a similar number of CB_1 receptors on inhibitory axon terminals in the PCE group compared with the control group. This implies that a saturating dose of the CB_1 receptor agonist WIN should have the same effects on $GABA_A$ IPSC amplitude, and that WIN effects on IPSCs should be faster, which was indeed the case (Fig. 3i). Altogether, these findings demonstrate that PCE induces a molecular reorganization of the active zone that leads to increased presynaptic cannabinoid control along with markedly reduced GABAergic inhibition.

To gain insights into the consequences of PCE on excitatory synaptic transmission, we first measured input–output curves from responses elicited at different stimulus intensities. We found that a larger stimulus intensity is required to recruit the same magnitude of synaptic excitation, which indicates that PCE induces a reduction in the number and/or strength of excitatory inputs terminating on dopamine neurons (Fig. 4a). Indeed, confocal microscopy analysis uncovered a robust (~50%) reduction in the density of type I vesicular glutamate transporter (VGLUT1)-positive excitatory axon terminals contacting TH-positive dopaminergic neurons in the lateral VTA (Supplementary Fig. 9a–c). Conversely, there were no differences in the $1/CV^2$ values of excitatory postsynaptic potentials (EPSCs) (Fig. 4b), in their PPR (Supplementary Fig. 9d,e) or in the frequency of miniature EPSCs (mEPSCs) (Supplementary Fig. 9f,g). In contrast to the lack of presynaptic physiological changes, we observed an increased amplitude of mEPSCs (Supplementary Fig. 9f,h) and longer decay kinetics of postsynaptic AMPA currents in PCE slices compared with control slices (Fig. 4c), which indicates that PCE affected the postsynaptic responsiveness of afferent excitatory synapses of VTA dopamine neurons. Likewise, PCE elicited a larger AMPA/NMDA ratio, with the frequency distribution curve shifted to the right in dopamine cells of PCE offspring, than controls (Fig. 4d–f). Notably, similar increases in the AMPA/NMDA ratio are observed in VTA dopamine neurons of offspring exposed in utero to cocaine or alcohol[38,39]. Thus, potentiated AMPA/NMDA ratios in the postnatal PCE brain directly reflects prenatal drug exposure. We also computed NMDA EPSC decay time kinetics, measured as weighted tau (τ), and found that they were faster in neurons recorded from the PCE progeny (Fig. 5a,b) and were more sensitive to GluN2A blockade (Fig. 5c), which is indicative of an increased ratio of GluN2A/GluN2B subunits in NMDA receptors[38]. Next, we examined the current–voltage relationship (I–V) of AMPA EPSCs. Compared with control animals, the I–V curves of PCE offspring were nonlinear, exhibited inward rectification (Fig. 5d,e) and the GluA2 blocker NASPM reduced AMPA EPSCs to a larger extent (Fig. 5f), thus indicating that there is insertion of calcium permeable (that is, GluA2-lacking) AMPA receptors[38,39]. Taken together, these microscopy and electrophysiological results suggest that PCE delays the molecular and anatomical maturation of excitatory synaptic inputs on VTA dopaminergic neurons, leading to increased postsynaptic responsiveness, a well-known property of developing brain circuits.

A major consequence of reduced inhibitory control of dopamine neurons together with heightened responsiveness to their excitatory inputs might also be a shift in the threshold for synaptic plasticity induction. Pairing low-frequency presynaptic stimulation (LFS; 1 Hz) with postsynaptic membrane depolarization (−40 mV) resulted in the expected LTD of excitatory synapses[40]. In contrast, we found that the very same stimulus protocol elicited a marked LTP in VTA dopamine neurons from PCE animals (Fig. 5g,h), an effect reminiscent of immature glutamatergic synapses.

We next examined whether the synaptic effects of PCE were cell-type-specific in the lateral VTA circuitry. GABA and dopamine neurons, which make up the vast majority of neurons in the lateral VTA[41] (Supplementary Fig. 10a,b), could be reliably distinguished by their morphological and electrophysiological characteristics and by the absence or presence of TH[42] in post hoc immunofluorescence analysis, respectively (Supplementary Fig. 10c–l). While PCE did not affect the excitatory/inhibitory balance, it decreased the AMPA/NMDA ratio (Supplementary Fig. 11a,b). Notably, NMDA EPSC decay times, I–V curves of AMPA EPSCs, PPRs of both AMPA EPSCs and $GABA_A$ IPSCs in putative GABA cells did not differ between progenies (Supplementary Fig. 11c–f). Thus, PCE does not alter the content of GluA2-containing AMPARs or GluN2A-containing NMDARs at these synapses onto VTA putative GABA neurons, but specifically modifies EPSC generation. Collectively, these findings suggest that PCE predominantly affects the synaptic maturation of dopamine cells within the VTA circuitry.

Pregnenolone rescues dopamine function and behavior after PCE. Since preventive strategies to reduce the burden of PCE in offspring are currently not in place[7], the identification of the PCE endophenotype is instrumental in testing therapeutic interventions during the prodromal phases of late-onset psychiatric disorders. In particular, early interventions are needed before the time point at which PCE offspring are of the age of risk for manifesting a disorder to prevent phenoconversion to late-onset disease[14,29,43].

The FDA-approved neurosteroid pregnenolone reverses behaviors such as psychomotor agitation and deficits in PPI that are observed in individuals with schizophrenia[44]. Notably, it also acts as a negative regulator of CB_1 receptor signaling[45]. Therefore, we predicted that a short postnatal treatment of pregnenolone in PCE offspring would be a good candidate for reversing PCE-induced changes in the properties of VTA dopamine neurons and behavior. To assess this, we administered pregnenolone (6 mg per kg, s.c. once daily for 9 days, from PND15 to PND23) or vehicle to PCE offspring, and acute VTA-containing slices were prepared 1 and 2 days following the last administration (Fig. 6a), when pregnenolone is cleared from the brain. Remarkably, pregnenolone rescued LTD at excitatory synapses on dopamine neurons to control levels (Fig. 6b), without affecting synaptic efficacy in control offspring. Moreover, pregnenolone ameliorated PCE-induced dopamine neuron excitability in PCE slices, as assessed by measuring resting membrane potentials (Fig. 6c), and spontaneous (Fig. 6d–f) and evoked firing activity (Fig. 6g,h). Pregnenolone also fully restored the alterations in synaptic properties imposed by PCE on excitatory and

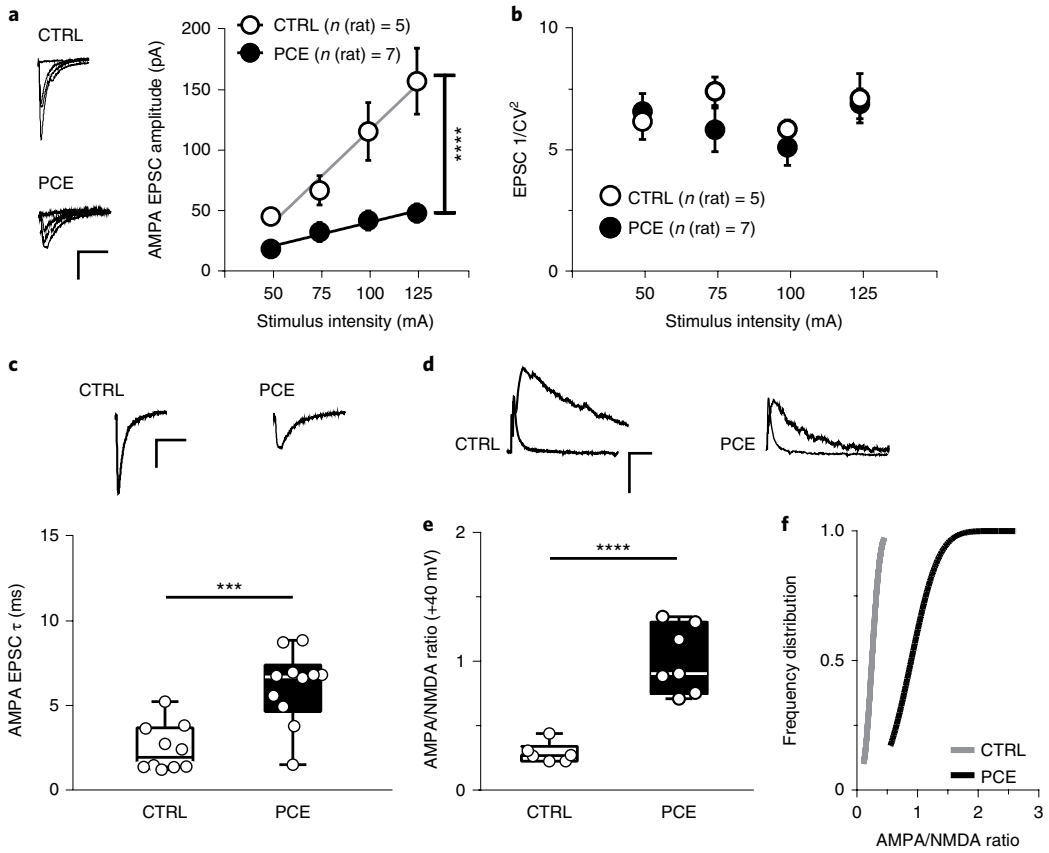

Fig. 4 | Synaptic properties of excitatory inputs onto dopamine neurons are affected by PCE in male rat offspring. a, PCE effects on input–output relationships (****$P < 0.0001$ between groups). $n = 9$ and 7 experiments from PCE and CTRL slices, respectively, were repeated independently with similar results obtained. AMPA EPSC traces are shown on the left. Data represent average values per animal ± s.e.m. **b**, PCE effects on $1/CV^2$ values from **a** ($P = 0.2$ between groups; two-sided Mann Whitney *U*-test). Data represent average values per animal ± s.e.m. **c**, Data from **a** and Fig. 3a (n (litter) = 5 per group) showing that AMPA EPSC decay time kinetic (τ) values differ (***$P = 0.0004$ between groups; two-sided unpaired *t*-test). $n = 15$ and 17 experiments from PCE and CTRL slices, respectively, were repeated independently, with similar results obtained. AMPA EPSC traces (top) were recorded at −70 mV. **d**, AMPA and NMDA EPSC traces recorded from DA neurons held at +40 mV. $n = 9$ and 10 experiments from PCE and CTRL slices, respectively, were repeated independently, with similar results obtained. **e**, PCE effects on the AMPA/NMDA ratio (****$P < 0.0001$ between groups; two-sided unpaired *t*-test). **f**, Cumulative frequency distribution of AMPA/NMDA ratios ($P = 0.0002$ between groups; two-sided Kolmogorov–Smirnov test, $D = 1.0$) recorded from CTRL (n (rat) = 6, n (litter) = 4) and PCE rats (n (rat) = 7, n (litter) = 5). Unless otherwise indicated, graphs show box-and-whisker plots (including minima, maxima and median values, and lower and upper quartiles) with values representing experiments averaged per animal and analyzed with two-way repeated-measures ANOVA. Calibration bars, 10 ms, 50 pA.

inhibitory inputs on dopamine cells (Supplementary Fig. 12). Most importantly, pregnenolone selectively prevented larger acute THC-induced enhancement of dopamine levels in the NAcS (Fig. 6i,j) and THC-induced disruption of somatosensory gating functions in PCE offspring (Fig. 6k). Finally, we found that the mechanism of action of pregnenolone was dissociated from its downstream neurosteroid metabolites (Supplementary Fig. 13). Collectively, these results indicate that pregnenolone prevents PCE-induced hyperdopaminergic states and confers resilience toward heightened acute effects of THC in PCE animals.

Discussion

In the present study, we provide evidence that maternal THC exposure induces multifaceted molecular, cellular and synaptic adaptations that converge into aberrant dopamine function in juvenile male rat offspring. Such persistently enhanced excitability of VTA dopamine neurons is a well-established neurodevelopmental risk factor conferring biased dopamine transmission and vulnerability to discrete psychiatric disorders. This might manifest in aberrant associative learning and abnormal reward processing, and provides an interpretative framework for clinical studies reporting maladaptive behaviors ranging from affective dysregulation to psychosis and addiction vulnerability in the offspring of mothers using cannabis during pregnancy[3,11,14]. It is possible that the decreased expression of dopamine D_2 receptors observed in the amygdala and nucleus accumbens of human PCE offspring[46,47] may be an adaptive response elicited by this hyperdopaminergic state, and may contribute to the vulnerability to psychiatric disorders[15].

We propose that the hyperdopaminergic state and the activity-dependent synapse-specific remodeling identified in the present study are significant neurobiological substrates, which may promote a susceptible endophenotype conferred by maternal cannabis use. This is important because preclinical and clinical studies have also established a prominent and causative role for mesostriatal dopamine dysfunction, in particular elevated dopamine synthesis and release properties, in the pathophysiology of schizophrenia[16]. Notably, positron emission tomography imaging studies have linked a genetic risk for THC-induced psychosis to differential increases of dopamine release by THC[48], a phenomenon exhibiting a high degree of familiarity[49], thus raising the possibility that PCE offspring represent a proportion of cannabis users who are vulnerable to THC-induced psychosis[50]. Hence, PCE might be a risk factor conferring

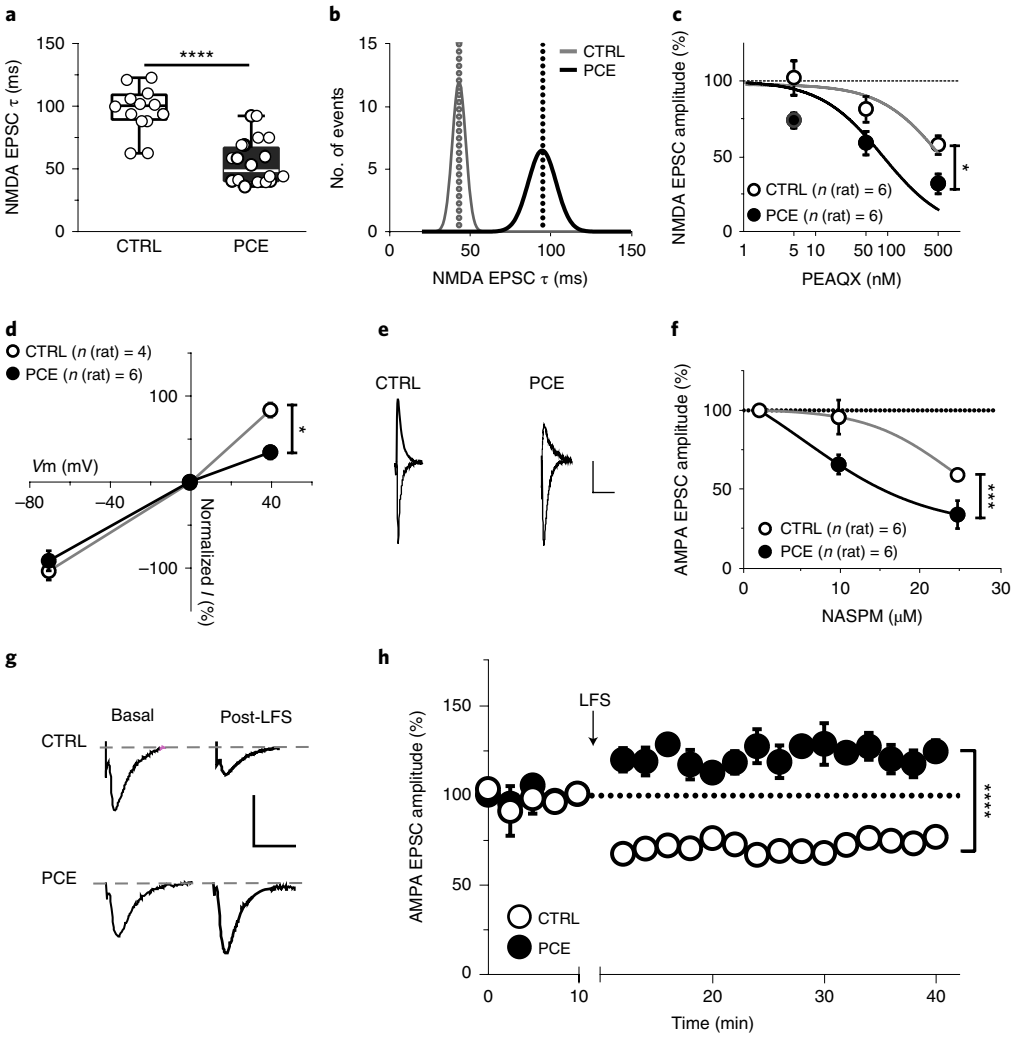

Fig. 5 | PCE enhances postsynaptic responsiveness of dopamine neurons to excitatory stimuli in male rat offspring. a, NMDA receptor EPSC decay time kinetic (weighted tau, τ) values differ (****$P < 0.0001$ between groups; two-sided unpaired *t*-test) between CTRL and PCE slices (*n* (litter) = 6 per group). Box-and-whisker plots (including minima, maxima and median values, and lower and upper quartiles) with circles representing average values per animal. *n* = 18 and 20 experiments from PCE and CTRL slices, respectively, were repeated independently, with similar results obtained. **b**, Bimodal distribution of NMDA receptor EPSC τ values. **c**, Dose–response curves for the GluN2A antagonist PEAQX (*$P = 0.011$ between groups). *n* = 6 experiments per group were repeated independently, with similar results obtained. **d**, Current–voltage relationship (*I*–*V*) plot shows that PCE (*n* (litter) = 4) affects the linearity of *I*–*V* curves (+40 mV; *$P = 0.02$ between groups). **e**, Traces of AMPA EPSCs recorded at −70 and +40 mV from DA neurons in CTRL and PCE offspring. *n* = 11 and 6 experiments from PCE and CTRL slices, respectively, were repeated independently, with similar results obtained. Calibration bar, 10 ms, 50 pA. **f**, Dose–response curves for the GluA2A antagonist NASPM displaying a larger effect (***$P = 0.0002$ between groups) in PCE (*n* (litter) = 2) offspring than in CTRL offspring. *n* = 6 experiments per group were repeated independently, with similar results obtained. **g**, AMPA EPSCs traces recorded at −70 mV before and after pairing low-frequency presynaptic stimulation (LFS; 1 Hz) with postsynaptic membrane depolarization (−40 mV). Calibration bar, 5 ms, 100 pA. **h**, LFS (1 Hz at the arrow) induces LTP (****$P < 0.0001$ between groups) in PCE offspring (*n* (rat) = 5), whereas CTRL DA neurons (*n* (rat) = 4) exhibit LTD. *n* = 7 and 5 experiments from PCE and CTRL slices, respectively, were repeated independently with similar results obtained. Unless otherwise indicated, data are represented as the average of experiments per animal ± s.e.m. analyzed with two-way repeated-measures ANOVA.

increased vulnerability to psychotic experiences as early as childhood[14]. Since PCE-induced dopamine dysregulation may predispose to THC-dependent delusions and hallucinations, PCE may represent a relevant modifiable predictor of transition to a psychotic disorder.

Our findings are consistent with the protective actions of pregnenolone in acute THC intoxication in rodents[45], and in an established mouse model for schizophrenia[44] as a negative regulator of CB_1 receptor signaling. Although pregnenolone metabolites such as progesterone may have direct effects on GABA and NMDA receptors, the observation that inhibition of the converting enzyme 3β-hydroxysteroid dehydrogenase did not modify the protective effects of pregnenolone on PPI disruption induced by acute THC is consistent with the possibility that pregnenolone per se ameliorates PCE-induced physiological and behavioral dysfunctions. Since pregnenolone is a well-tolerated FDA-approved drug, devoid of major side effects[45], our pharmacological treatment has high translational value as a safe and promising therapeutic approach for offspring of mothers who abused marijuana during pregnancy. Our study warrants further investigation into the effects of PCE on other anatomically and functionally heterogeneous dopamine subpopulations with different axonal projections. Indeed, since our recordings were carried out from the lateral portion of the VTA, which largely projects to the lateral NAcS[32], it is likely that these dopamine neurons would mainly project to this region.

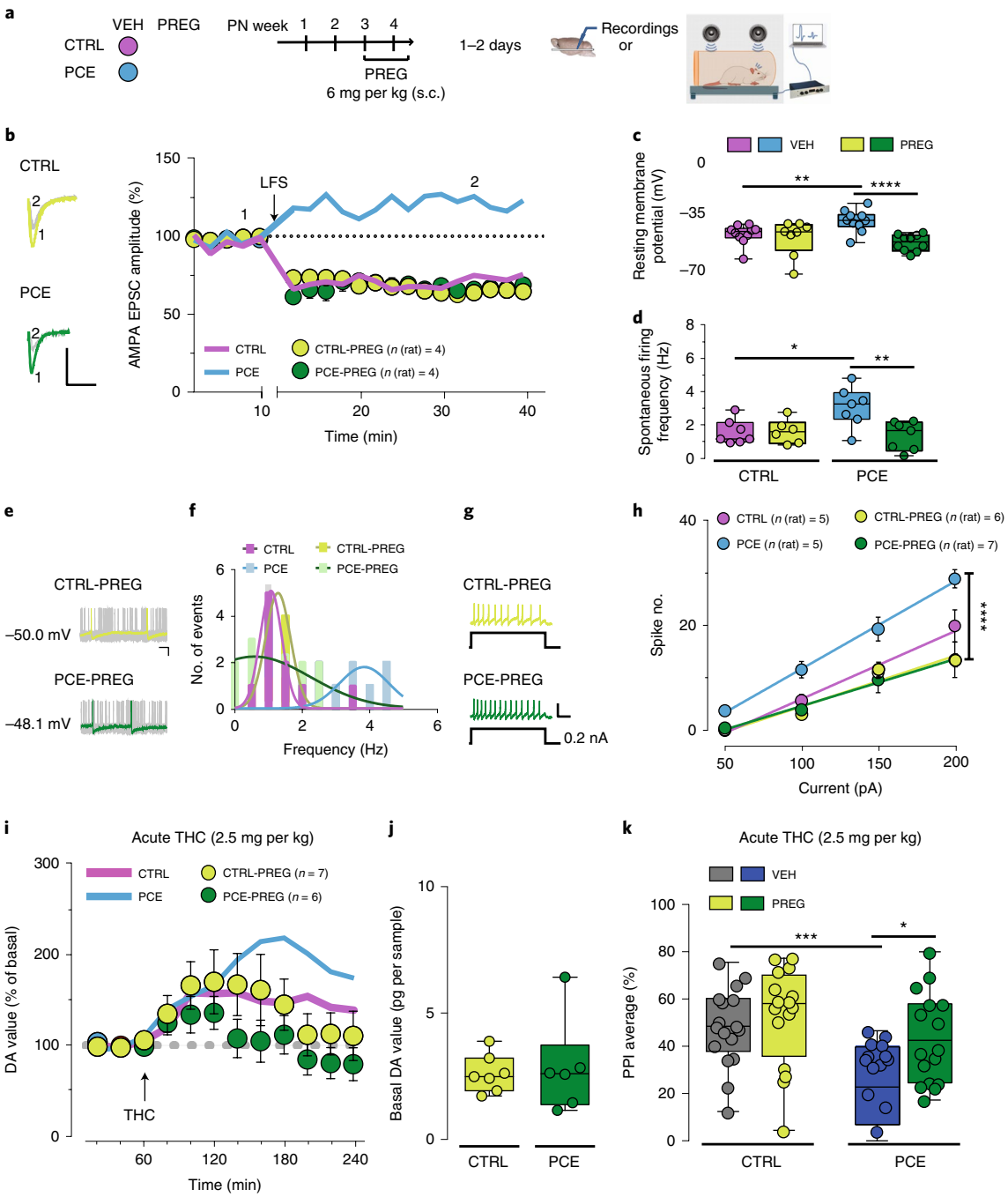

Fig. 6 | Pregnenolone rescues synaptic plasticity, mitigates deficits in dopamine neuron activity and restores behavior in PCE male rat progeny. a, Protocol of pregnenolone (PREG) treatment and analyses. **b**, PREG effects on low-frequency presynaptic stimulation (LFS; 1 Hz at the arrow) ($P = 0.02$, PCE-VEH versus PCE-PREG). Thick lines represent effects from Fig. 5g. Data represent the mean per animal ± s.e.m. Left-hand panel shows traces (−70 mV) from before (1) and after LFS (2). Calibration bar, 5 ms, 100 pA. $n = 6$ experiments per group were repeated independently, with similar results obtained. **c**, Effects of PREG on resting membrane potentials (****$P = 0.0006$, PCE-VEH versus PCE-PREG; **$P < 0.01$, PCE-VEH versus CTRL-VEH; n (litter) = 5 per group). **d**, PREG effects on spontaneous activity (**$P < 0.01$, PCE-VEH versus PCE-PREG; *$P = 0.02$, PCE-VEH versus CTRL-VEH; n (litter) = 5 per group). **e**, Traces from PREG-treated offspring. Calibration bar, 20 ms, 100 pA. $n = 14$ and 12 experiments from PCE and CTRL slices, respectively, were repeated independently, with similar results obtained. **f**, Multimodal distribution of data from **d**. **g**, Traces of evoked firing in PREG-treated offspring. Calibration bar, 400 ms, 100 mV. Numbers of experiments are as in **c**–**h**. **h**, PREG restores evoked firing (****$P < 0.0001$, PCE-VEH versus PCE-PREG; n (litter) = 5 per group). Data represent values averaged per animal ± s.e.m. **i**, PREG attenuates THC effects on NAc DA levels in PCE rats ($P = 0.30$ between groups). Thick lines show data from Fig. 1c. Data represent the mean ± s.e.m. **j**, Basal DA values ($P = 0.768$ between groups; two-sided unpaired t-test). **k**, PREG prevents THC effects on PPI in PCE offspring (*$P = 0.032$, PCE-THC-VEH versus PCE-THC-PREG; ***$P = 0.0004$, CTRL-THC-VEH versus PCE-THC-VEH; Tukey's test; CTRL-THC-VEH: $n = 17$; CTRL-THC-PREG, PCE-THC-VEH, PCE-THC-PREG: $n = 16$; n (litter) = 8 per group). Unless otherwise indicated, box-and-whisker plots (including minima, maxima and median values, and lower and upper quartiles) with circles depicting average data per animal analyzed with two-way repeated-measures ANOVA followed by Sidak's test.

Finally, it is important to emphasize that some of the potentiated state measures of dopamine neurons resemble those described in VTA dopamine neurons of offspring exposed in utero to cocaine or alcohol[38,39]. As physicians caution pregnant women against alcohol and cocaine intake because of their detrimental effects to the fetus, based on our findings, it is our recommendation that they also advise them on the consequences of the use of cannabis during pregnancy. Considering that such preventive strategies do not take place owing to the underestimation of the risks of neurodevelopmental adverse effects associated with maternal cannabis use[6,7], and that cannabis legalization policies move forward worldwide and that conceivably large numbers of children will be prenatally exposed to its ingredients over the next decades, the present findings are critically important for unmasking and highlighting extensive neurobiological maladaptations that increase the vulnerability of at-risk offspring to neuropsychiatric disorders.

Online content

Any methods, additional references, Nature Research reporting summaries, source data, statements of code and data availability and associated accession codes are available at https://doi.org/10.1038/s41593-019-0512-2.

Received: 14 September 2018; Accepted: 11 September 2019;
Published online: 14 October 2019

References

1. *Results from the 2010 National Survey on Drug Use and Health: Summary of National Findings* (Substance Abuse and Mental Health Services Administration, 2011).
2. *Legal Topic Overviews: Possession of Cannabis for Personal Use* (European Monitoring Centre for Drugs and Drug Addiction, 2012).
3. Alpar, A., Di Marzo, V. & Harkany, T. At the tip of an iceberg: prenatal marijuana and its possible relation to neuropsychiatric outcome in the offspring. *Biol. Psychiatry* **79**, e33–e45 (2016).
4. Brown, Q. L. et al. Trends in marijuana use among pregnant and nonpregnant reproductive-aged women, 2002–2014. *JAMA* **317**, 207–209 (2017).
5. Dickson, B. et al. Recommendations from cannabis dispensaries about first-trimester cannabis use. *Obstet. Gynecol.* **131**, 1031–1038 (2018).
6. Volkow, N. D., Compton, W. M. & Wargo, E. M. The risks of marijuana use during Pregnancy. *JAMA* **317**, 129–130 (2017).
7. Jansson, L. M., Jordan, C. J. & Velez, M. L. Perinatal marijuana use and the developing child. *JAMA* **320**, 545–546 (2018).
8. Galve-Roperh, I. et al. Cannabinoid receptor signaling in progenitor/stem cell proliferation and differentiation. *Prog. Lipid Res.* **52**, 633–650 (2013).
9. Maccarrone, M., Guzman, M., Mackie, K., Doherty, P. & Harkany, T. Programming of neural cells by (endo)cannabinoids: from physiological rules to emerging therapies. *Nat. Rev. Neurosci.* **15**, 786–801 (2014).
10. Wu, C. S., Jew, C. P. & Lu, H. C. Lasting impacts of prenatal cannabis exposure and the role of endogenous cannabinoids in the developing brain. *Future Neurol.* **6**, 459–480 (2011).
11. Morris, C. V., DiNieri, J. A., Szutorisz, H. & Hurd, Y. L. Molecular mechanisms of maternal cannabis and cigarette use on human neurodevelopment. *Eur. J. Neurosci.* **34**, 1574–1583 (2011).
12. Huizink, A. C. Prenatal cannabis exposure and infant outcomes: overview of studies. *Prog. Neuropsychopharmacol. Biol. Psychiatry* **52**, 45–52 (2014).
13. De Genna, N. M., Richardson, G. A., Goldschmidt, L., Day, N. L. & Cornelius, M. D. Prenatal exposures to tobacco and cannabis: associations with adult electronic cigarette use. *Drug Alcohol Depend.* **188**, 209–215 (2018).
14. Fine, J. D. et al. Association of prenatal cannabis exposure with psychosis proneness among children in the adolescent brain cognitive development (ABCD) study. *JAMA Psychiatry* **7**, 762–764 (2019).
15. Volkow, N. D., Fowler, J. S., Wang, G. J. & Swanson, J. M. Dopamine in drug abuse and addiction: results from imaging studies and treatment implications. *Mol. Psychiatry* **9**, 557–569 (2004).
16. Grace, A. A. Dysregulation of the dopamine system in the pathophysiology of schizophrenia and depression. *Nat. Rev. Neurosci.* **17**, 524–532 (2016).
17. Bloomfield, M. A., Ashok, A. H., Volkow, N. D. & Howes, O. D. The effects of Δ9-tetrahydrocannabinol on the dopamine system. *Nature* **539**, 369–377 (2016).
18. Bourque, J., Afzali, M. H. & Conrod, P. J. Association of cannabis use with adolescent psychotic symptoms. *JAMA Psychiatry* **75**, 864–866 (2018).
19. Di Forti, M. et al. The contribution of cannabis use to variation in the incidence of psychotic disorder across Europe (EU-GEI): a multicentre case–control study. *Lancet Psychiatry* **6**, 427–436 (2019).
20. Buckholtz, J. W. et al. Mesolimbic dopamine reward system hypersensitivity in individuals with psychopathic traits. *Nat. Neurosci.* **13**, 419–421 (2010).
21. Geschwind, D. H. & Flint, J. Genetics and genomics of psychiatric disease. *Science* **349**, 1489–1494 (2015).
22. Insel, T. R. Rethinking schizophrenia. *Nature* **468**, 187–193 (2010).
23. Heffernan, A. L. & Hare, D. J. Tracing environmental exposure from neurodevelopment to neurodegeneration. *Trends Neurosci.* **41**, 496–501 (2018).
24. Richardson, K. A., Hester, A. K. & McLemore, G. L. Prenatal cannabis exposure—the "first hit" to the endocannabinoid system. *Neurotoxicol. Teratol.* **58**, 5–14 (2016).
25. Young-Wolff, K. C. et al. Trends in self-reported and biochemically tested marijuana use among pregnant females in california from 2009–2016. *JAMA* **318**, 2490–2491 (2017).
26. Wiley, J. L., O'Connell, M. M., Tokarz, M. E. & Wright, M. J. Jr. Pharmacological effects of acute and repeated administration of Δ^9-tetrahydrocannabinol in adolescent and adult rats. *J. Pharm. Exp. Ther.* **320**, 1097–1105 (2007).
27. Mehmedic, Z. et al. Potency trends of Δ9-THC and other cannabinoids in confiscated cannabis preparations from 1993 to 2008. *J. Forensic Sci.* **55**, 1209–1217 (2010).
28. ElSohly, M. A. et al. Changes in cannabis potency over the last 2 decades (1995–2014): analysis of current data in the United States. *Biol. Psychiatry* **79**, 613–619 (2016).
29. McGorry, P. D., Hickie, I. B., Yung, A. R., Pantelis, C. & Jackson, H. J. Clinical staging of psychiatric disorders: a heuristic framework for choosing earlier, safer and more effective interventions. *Aust. NZ J. Psychiatry* **40**, 616–622 (2006).
30. Sherif, M., Radhakrishnan, R., D'Souza, D. C. & Ranganathan, M. Human laboratory studies on cannabinoids and psychosis. *Biol. Psychiatry* **79**, 526–538 (2016).
31. Braff, D. L., Swerdlow, N. R. & Geyer, M. A. Gating and habituation deficits in the schizophrenia disorders. *Clin. Neurosci.* **3**, 131–139 (1995).
32. Lammel, S., Ion, D. I., Roeper, J. & Malenka, R. C. Projection-specific modulation of dopamine neuron synapses by aversive and rewarding stimuli. *Neuron* **70**, 855–862 (2011).
33. Malinow, R. & Tsien, R. W. Presynaptic enhancement shown by whole-cell recordings of long-term potentiation in hippocampal slices. *Nature* **346**, 177–180 (1990).
34. Glebov, O. O. et al. Nanoscale structural plasticity of the active zone matrix modulates presynaptic function. *Cell Rep.* **18**, 2715–2728 (2017).
35. Lovinger, D. M. in *Pharmacology of Neurotransmitter Release* Vol. 184 (eds Südhof, T.C. & Starke, K.) 435–477 (Springer, 2008).
36. Matyas, F. et al. Identification of the sites of 2-arachidonoylglycerol synthesis and action imply retrograde endocannabinoid signaling at both GABAergic and glutamatergic synapses in the ventral tegmental area. *Neuropharmacology* **54**, 95–107 (2008).
37. Melis, M. et al. Enhanced endocannabinoid-mediated modulation of rostromedial tegmental nucleus drive onto dopamine neurons in Sardinian alcohol-preferring rats. *J. Neurosci.* **34**, 12716–12724 (2014).
38. Bellone, C., Mameli, M. & Luscher, C. In utero exposure to cocaine delays postnatal synaptic maturation of glutamatergic transmission in the VTA. *Nat. Neurosci.* **14**, 1439–1446 (2011).
39. Hausknecht, K. et al. Excitatory synaptic function and plasticity is persistently altered in ventral tegmental area dopamine neurons after prenatal ethanol exposure. *Neuropsychopharmacology* **40**, 893–905 (2015).
40. Thomas, M. J., Malenka, R. C. & Bonci, A. Modulation of long-term depression by dopamine in the mesolimbic system. *J. Neurosci.* **20**, 5581–5586 (2000).
41. Yamaguchi, T., Sheen, W. & Morales, M. Glutamatergic neurons are present in the rat ventral tegmental area. *Eur. J. Neurosci.* **25**, 106–118 (2007).
42. Chieng, B., Azriel, Y., Mohammadi, S. & Christie, M. J. Distinct cellular properties of identified dopaminergic and GABAergic neurons in the mouse ventral tegmental area. *J. Physiol.* **589**, 3775–3787 (2011).
43. Marin, O. Developmental timing and critical windows for the treatment of psychiatric disorders. *Nat. Med.* **22**, 1229–1238 (2016).
44. Wong, P., Sze, Y., Chang, C. C., Lee, J. & Zhang, X. Pregnenolone sulfate normalizes schizophrenia-like behaviors in dopamine transporter knockout mice through the AKT/GSK3beta pathway. *Transl Psychiatry* **5**, e528 (2015).
45. Vallee, M. et al. Pregnenolone can protect the brain from cannabis intoxication. *Science* **343**, 94–98 (2014).
46. Wang, X., Dow-Edwards, D., Anderson, V., Minkoff, H. & Hurd, Y. L. In utero marijuana exposure associated with abnormal amygdala dopamine *D2* gene expression in the human fetus. *Biol. Psychiatry* **56**, 909–915 (2004).
47. DiNieri, J. A. et al. Maternal cannabis use alters ventral striatal dopamine D2 gene regulation in the offspring. *Biol. Psychiatry* **70**, 763–769 (2011).
48. Kuepper, R. et al. Delta-9-tetrahydrocannabinol-induced dopamine release as a function of psychosis risk: 18F-fallypride positron emission tomography study. *PLoS One* **8**, e70378 (2013).

49. McGrath, J. et al. Association between cannabis use and psychosis-related outcomes using sibling pair analysis in a cohort of young adults. *Arch. Gen. Psychiatry* **67**, 440–447 (2010).
50. Compton, M. T. et al. Association of pre-onset cannabis, alcohol, and tobacco use with age at onset of prodrome and age at onset of psychosis in first-episode patients. *Am. J. Psychiatry* **166**, 1251–1257 (2009).

Acknowledgements

The authors thank R. Tonini and O. J. Manzoni for discussions and comments on the manuscript, and G. Talani, M. Pignatelli, M. Tuveri, S. Aramo, G. Giua and B. Tuveri for their skillful assistance. The authors are also grateful to L. Barna for his help with STORM microscopy images, and thank Nikon Europe, Nikon Austria and Auro-Science Consulting for kindly providing microscopy support. The present study was supported by the University of Cagliari (RICCAR 2017 and 2018 to M.M.), the Region of Sardinia (RASSR32909 to M.M. and F72F16002850002 to R.F.), the Fondazione Banco di Sardegna (F71I17000200002 to R.F.), the European Molecular Biology Organization (ASTF 371-2016 to C.S.), the Fondazione Zardi Gori (to C.S.), the National Institutes of Health (R01DA022340 to J.F.C., R01NS099457 to I.K. and R01DA044925 to J.F.C., M.M. and I.K.), the Hungarian Academy of Sciences Momentum Program (LP-54/2013 to I.K.), and the National Research, Development and Innovation Office of Hungary (VKSZ-14-1-2015-0155 to I.K.). The project was also funded by the Ministry of National Economy for STORM super-resolution microscopy (VEKOP-2.3.3-15-2016-00013 to I.K.).

Author contributions

R.F. and F.T. designed and performed the behavioral experiments and analyzed the data. S.F. and V.S. carried out behavioral observations. F.T. and V.S. prepared the figures. V.M. and C.I.P. carried out the confocal imaging and STORM experiments, the corresponding data analyses and prepared the figures. P.S. and P.D. carried out the cerebral microdialysis experiments and analyzed the data. M.C. and V.S. designed and performed the maternal observation experiments. C.S., V.S. and S.A. performed the chronic drug administration treatment. S.A. performed the DREADD experiments. J.F.C. designed the DREADD experiments and contributed to manuscript preparation. I.K. designed the confocal and STORM experiments, analyzed and supervised the imaging data and wrote the manuscript. M.M. conceived, designed and supervised the project, performed patch-clamp recordings, analyzed the data, prepared the figures and wrote the manuscript.

Competing interests

The authors declare no competing interests.

Additional information

Supplementary information is available for this paper at https://doi.org/10.1038/s41593-019-0512-2.

Correspondence and requests for materials should be addressed to M.M.

Peer review information *Nature Neuroscience* thanks Camilla Bellone, Paul Kenny, and the other, anonymous, reviewer(s) for their contribution to the peer review of this work.

Methods

Animals. All procedures were performed in accordance with the European legislation EU Directive 2010/63 and the National Institutes of Health Guide for the Care and Use of Laboratory Animals and were approved by the Animal Ethics Committees of the University of Cagliari and by the Italian Ministry of Health (authorization numbers: 659/2015-PR and 725/2019-PR) and by the Institutional Animal Use and Care Committee at the University of Maryland (0617002). We made all efforts to minimize pain and suffering and to reduce the number of animals used. Primiparous female Sprague–Dawley (Envigo) rats (bred with males) were used as mothers and single housed during pregnancy. Long–Evans dams expressing Cre recombinase under the control of the *TH* promoter (*TH*::Cre) were used for the DREADD experiments. THC or vehicle was administered (2 mg per kg, 2 ml per kg, s.c. once per day) from GD5 until GD20. Offspring were weaned at ~PND21 and maintained without any further manipulation in standard conditions of temperature (21 ± 1 °C) and humidity (60%) on a normal 12-h light–dark cycle with access to food and water until the experimental day (PND15–28). We did not use more than two males from each litter for the same experiment to control for litter effects. All the additional male pups in each litter were used for other experiments (that is, cerebral microdialysis, behavioral paradigms, STORM analysis and different electrophysiological protocols) to minimize the total number of animals used for the study.

Surgical procedures. *TH*::Cre-positive offspring were stereotaxically injected under isoflurane (3% induction, 1–2% maintenance) with a Cre-dependent adeno-associated virus expressing an inhibitory DREADD construct (AAV5-DIO-hM4D(Gi)-mCherry (PCE-Gi)) or control virus (AAV5-DIO-mCherry (PCE)) to target dopamine neurons in the VTA at PND7. Viruses were injected at a volume of 0.5 µl per side and a rate of 0.1 µl min^{-1} in the VTA (anterior–posterior: −4.2, medial–lateral: ± 0.6 mm from bregma, and dorsal–ventral: −5.25 mm from the cortical surface) with a Hamilton syringe. Injection needles were left in place for 5 min after the injection to ensure adequate viral delivery.

Behavioral analyses. *Maternal behavior observation.* The behavior of each dam was assessed from PND1 to PND20 by an observer blinded to the experimental groups until the analyses of data. The observation was performed five times per day at 9:00, 11:30, 13:30, 15:00 and 17:00 during the light phase (lights on at 7:00) and consisted of 3 trials of instantaneous observation for a total of 15 observations per day and a total 300 observations per dam. Behavioral parameters such as retrieval, arched-back, blanket and passive nursing, pup licking (regarded as maternal behaviors), self-grooming, eating, drinking, rearing, moving, resting, standing out of the nest (considered as non-maternal behaviors) were scored. Observations strictly followed a previously published detailed analysis protocol[51]. Briefly, the behaviors were recorded using dichotomous scores of 0 and 1, where 0 was assigned when the behavior was not present, and 1 was assigned when it was present. Data were expressed as a percentage of observations of maternal or non-maternal behavior.

Startle reflex and PPI. Startle reflex and PPI were tested as previously described[52]. Briefly, the apparatus (Med Associates) consisted of four standard cages placed in sound-attenuated chambers with fan ventilation. Each cage consisted of a Plexiglas cylinder 5 cm in diameter, mounted on a piezoelectric accelerometric platform connected to an analog–digital converter. Two separate speakers conveyed background noise and acoustic bursts, each one properly placed so as to produce a variation of sound within 1 dB across the startle cage. Both speakers and startle cages were connected to a main personal computer, which detected and analyzed all chamber variables using specific software. Before each testing session, acoustic stimuli and mechanical responses were calibrated via specific devices supplied by Med Associates. The testing session featured a background noise of 70 dB and consisted of an acclimatization period of 5 min, followed by three consecutive sequences of trials (blocks). Unlike the first and the third block, during which rats were presented with only five pulse-alone trials of 115 dB, the second block consisted of a pseudorandom sequence of 50 trials, including 12 pulse-alone trials, 30 trials of pulse preceded by 74, 78 or 86 dB pre-pulses (10 for each level of pre-pulse loudness), and 8 no-stimulus trials, where only the background noise was delivered. Inter-trial intervals were selected randomly between 10 and 15 s. The percentage PPI value was calculated using the following formula: 100 − ((mean startle amplitude for pre-pulse pulse trials/mean startle amplitude for pulse alone trials) × 100). PPI values related to different pre-pulse levels were collapsed, given that no interactions were found between pre-pulse levels throughout the study.

Locomotor activity. Locomotor behaviors of Sprague–Dawley rats and Long–Evans *TH*::Cre rats were tested in two different facilities at the University of Cagliari and at the University of Maryland School of Medicine, respectively. Rats were placed in the center of a novel, square open-field (dimensions of 42-cm long × 42-cm wide × 30-cm high) and their behavior was monitored for 40 min and collected every 10 min. Analysis of locomotor activity of Sprague–Dawley rats and Long–Evans *TH*::Cre rats were performed using an Omnitech Digiscan monitoring system (Omnitech Digiscan cages) and Ethovision (Noldus Instruments), respectively. Behavioral measurements included the assessment of the total distance traveled (in cm), and the periphery and center time, respectively, calculated as the durations of time spent along the perimeter of the walls (a 20-cm-wide external square frame) or in the center of the arena (an internal square measuring 20 × 20 cm). To minimize differences in baseline spontaneous locomotor activity (that is, distance traveled), we normalized the data to their reference group (for example, control-vehicle and PCE-vehicle). For the DREADD experiments, open-field testing was performed 30 min following a systemic administration of clozapine-*N*-oxide (3 mg per kg, 2 ml intraperitoneally (i.p.)) to engage VTA Gi-DREADDs.

Elevated plus maze. The test was performed as previously described[53]. Briefly, we used a black Plexiglas apparatus consisting of two opposing open arms (length of 40 cm, width of 9 cm) and two closed arms (wall height of 15 cm), which extended from a central square platform (9 × 9 cm), positioned 70 cm from the ground. Rats were individually placed on the central platform facing the open arm. Behavior was recorded for 5 min. Measures included the number of entries and duration in the open and closed arms and in the central platform, frequencies of stretch-attend postures and head dips (defined as previously described).

Wire-beam bridge test. Testing was performed using a variant of a previously detailed protocol[54,55], specifically adapted for rats. The apparatus consists of two 156-cm high Plexiglas platforms connected by a horizontal, flexible wire-beam (100-cm long). A 52-cm high Plexiglas wall was placed 3 cm from the edge of one platform to make the starting position uncomfortable and to promote movement. The bridge consisted of 2 parallel beams (0.1-cm thick) perpendicularly connected by 34 equally distanced cross-ties (3-cm long). It was modestly flexible, with a downward deflection of 2 cm per 100-g load at the center point. Rats were individually placed in the start position, and the latency to cross and reach the other platform was recorded. The duration of overall immobility and number of crossings on ties were also monitored.

Cerebral microdialysis. Rats were anesthetized with Equithesin and placed in a Kopf stereotaxic apparatus. In-house constructed vertical microdialysis probes (AN 69-HF membrane, Hospal-Dasco; cut-off 40,000 Dalton, 3-mm dialyzing membrane length) were implanted in the NAcS (from bregma: anterior–posterior: + 1.5; lateral: ± 0.7; ventral: −7.0) according to atlas coordinates[56], which were empirically corrected after a pilot experiment. Rats were given antibiotic therapy (enrofloxacin, Bayer HealthCare) and allowed to recover in their home cages before testing. The day after probe implantation, artificial cerebrospinal fluid solution (ACSF; 147 mM NaCl, 4 mM KCl, 1.5 mM $CaCl_2$, 1 mM $MgCl_2$, pH 6–6.5) was pumped through the dialysis probes at a constant rate of 1.1 µl min^{-1} via a CMA/100 microinjection pump (Carnegie Medicine). Samples were collected every 20 min and immediately analyzed for dopamine content by high-performance liquid chromatography with electrochemical detection, as previously described[57]. When a stable baseline was obtained (three consecutive samples with a variance not exceeding 15%), THC (2.5 mg per kg, 2 ml per kg) was i.p. administered, and sample collection continued for 2 h. On completion of the testing, rats were killed via an Equithesin overdose, the brains were removed and sectioned using a cryostat (Leica CM3050 S) into 40-µm thick coronal slices to verify the anatomical locations of dialysis probes.

Electrophysiological recordings. The preparation of posterior VTA slices was performed as previously described[58]. Briefly, a block of tissue containing the midbrain was obtained from male offspring deeply anesthetized with isoflurane and the tissue sliced in the horizontal plane (300 µm) with a vibratome (Leica) in ice-cold low-Ca^{2+} solution containing the following (in mM): 126 NaCl, 1.6 KCl, 1.2 NaH_2PO_4, 1.2 $MgCl_2$, 0.625 $CaCl_2$, 18 $NaHCO_3$ and 11 glucose. Slices were transferred to a holding chamber with ACSF (37 °C) saturated with 95% O_2 and 5% CO_2 containing the following (in mM): 126 NaCl, 1.6 KCl, 1.2 NaH_2PO_4, 1.2 $MgCl_2$, 2.4 $CaCl_2$, 18 $NaHCO_3$ and 11 glucose. Slices were allowed to recover for at least 1 h before being placed, as hemislices, in the recording chamber and superfused with ACSF (36–37 °C) saturated with 95% O_2 and 5% CO_2. Cells were visualized using an upright microscope with infrared illumination (Axioskop FS 2 plus, Zeiss), and whole-cell patch-clamp recordings were made using an Axopatch 200B amplifier (Molecular Devices). Recordings were carried out in the lateral portion of the posterior VTA (Supplementary Fig. 10a,b). Voltage-clamp recordings of evoked IPSCs and current-clamp recordings were made with electrodes filled with a solution containing the following (in mM): 144 KCl, 10 HEPES buffer, 3.45 BAPTA, 1 $CaCl_2$, 2.5 Mg_2ATP and 0.25 Mg_2GTP, pH 7.2–7.4, 275–285 mOsm. All $GABA_A$ IPSCs were recorded in the presence of 2-amino-5-phosphonopentanoic acid (AP5; 100 µM), 6-cyano-2,3-dihydroxy-7-nitro-quinoxaline (10 µM), strychnine (1 µM) and eticlopride (100 nM) to block NMDA, AMPA, glycine and dopamine-D_2-receptor-mediated synaptic currents, respectively. As previously described[58], this solution had no effect on the holding current of the dopamine cells. Current-clamp experiments were performed in the absence of any pharmacological blocker, that is, in regular ACSF. Experiments were begun only after series resistance had stabilized (typically 10–30 MΩ), which was monitored by a hyperpolarizing step of −4 mV at each sweep every 10 s. Data were excluded when the resistance changed >20%. Voltage-clamp recordings of

evoked EPSCs were made with electrodes filled with a solution containing the following (in mM): 117 caesium methanesulfonic acid, 20 HEPES, 0.4 EGTA, 2.8 NaCl, 5 TEA-Cl, 0.1 mM spermine, 2.5 Mg_2ATP and 0.25 Mg_2GTP, pH 7.2–7.4, 275–285 mOsm. Picrotoxin (100 µM) was added to the ACSF to block $GABA_A$-receptor-mediated IPSCs. In addition, random experiments were performed with an internal solution that contained biocytin (0.2%) to allow for subsequent immunocytochemical detection of TH[37] (Supplementary Fig. 10e–g). Series and input resistance were monitored continuously online with a 5-mV depolarizing step (25 ms). Data were filtered at 2 kHz, digitized at 10 kHz and collected online with acquisition software (pClamp 10.2, Molecular Devices). Dopamine neurons from the lateral portion of the posterior VTA were identified according to previously published criteria[58] as follows: cell morphology and anatomical location (that is, medial to the medial terminal nucleus of the accessory optic tract; Supplementary Fig. 10a,b); slow pacemaker-like firing rate (<5 Hz); long action potential duration (>2 ms; Supplementary Fig. 10d); and the presence of a large hyperpolarization-activated current (I_h > 150 pA)[59], which was assayed immediately after break-in using 13 incremental 10-mV hyperpolarizing steps (250 ms) from a holding potential of −70 mV (Supplementary Fig. 10c). Putative GABA neurons of the lateral posterior VTA were identified by their morphology, the absence of I_h and a short action potential duration (<2 ms) (Supplementary Fig. 10h,i). In addition, random experiments were performed with an internal solution containing biocytin (0.2%) to allow for subsequent immunocytochemical detection of TH[37], since GABA cells are negative for TH (Supplementary Fig. 10j–l).

Spike fidelity was measured as the reliability of eliciting an action potential in response to somatically injected current (50–200 pA); the jitter, which is equal to the standard deviation of the latency to elicit the first action potential, inversely correlates with the spike fidelity, as the smaller the jitter the higher degree of temporal precision exhibited by the cell. A bipolar, stainless steel stimulating electrode (FHC) was placed ~100–200 µm rostral to the recording electrode and was used to stimulate at a frequency of 0.1 Hz. Paired stimuli were given with an interstimulus interval of 50 ms, and the ratio between the second and the first postsynaptic currents (PSC2/PSC1) was calculated and averaged for a 5-min baseline[58]. NMDA EPSCs were evoked while holding cells at +40 mV. The AMPA EPSC was isolated after bath application of the NMDA antagonist D-AP5 (100 µM). The NMDA EPSC was obtained by digital subtraction of the AMPA EPSC from the dual (AMPA + NMDA-mediated) EPSC[60]. The values of the AMPA/NMDA ratio might be underestimated, since the experiments were performed in the presence of spermine in the recording pipette. The spontaneous mEPSCs and mIPSCs were collected in the presence of lidocaine (500 µM) or tetrodotoxin (1 µM) and analyzed (120 sweeps for each condition, 1 s per sweep) using Mini Analysis (Synaptosoft). To accurately determine the miniature PSC amplitude, only events that were >8 pA were accepted for analysis (rise time <1 ms, decay time <3 ms). The choice of this cut-off amplitude for acceptance of miniature PSCs was made to obtain a high signal-to-noise ratio. Then, each event was also visually inspected to prevent noise affecting the analysis. Experiments were performed blinded to the experimental group.

Immunostaining. For a detailed protocol, see a previous study[61]. Rats were transcardially perfused with 4% (m/v) paraformaldehyde (PFA) or immersion-fixed in 4% PFA overnight, and 20, 40 or 50 µm-thick sections of the midbrain were cut using a Leica VT-1000S Vibratome in phosphate buffer (PB). Immunostaining was performed in a free-floating manner. After extensive washing in PB and 0.05 M Tris-buffered saline (TBS, pH 7.4), slices were blocked and permeabilized with 5% (v/v) normal donkey serum (Sigma) and 0.3% (v/v) Triton X-100 (Sigma) in TBS for 45 min, then they were incubated in primary antibodies (see Supplementary Table 1) in TBS while rinsed on an orbital shaker. Sections were then washed in TBS and incubated with the appropriate secondary antibodies (see Supplementary Table 1) supplemented with 4,6-diamidino-2-phenylindole (DAPI; 1:1,000), if needed, then extensively washed in TBS and PB.

For confocal imaging, sections were mounted in VectaShield (Vector Laboratories) or Prolong Diamond Antifade Mounting Medium (Invitrogen). Confocal imaging was performed on the samples, and TH-positive cell density and TH-immunofluorescence intensity were calculated on the images within the region of interest (ROI). VGLUT1 and VIAAT inputs of the filled dopaminergic cells were counted in a ~1-µm neighborhood of the cells, and input density was calculated based on the surface of the processes. Objects with a volume lower than 0.02 μm^3 were considered as noise and excluded from the analysis.

For STORM imaging, sections were post-fixed in 4% PFA for 10 min and washed in PB. Samples were then mounted and dried on acetone-cleaned no. 1.5 borosilicate coverslips.

Correlated confocal and STORM imaging. Samples were covered with freshly prepared STORM imaging medium as previously described[62] and contained 0.1 M mercaptoethylamine, 5% (m/v) glucose, 1 mg ml^{-1} glucose oxidase and catalase (2.5 µl ml^{-1} of aqueous solution from Sigma, approximately 1,500 U ml^{-1} final concentration) in Dulbecco's PBS (Sigma). Coverslips were sealed with nail polish. Imaging started after 10 min and was performed for up to 3 h. Images were acquired using a Nikon Ti-E inverted microscope equipped with a Nikon N-STORM system, CFI Apo TIRF ×100 objective (1.49 numerical aperture), a Nikon C2 confocal scan head and an Andor iXon Ultra 897 EMCCD (with a cylindrical lens for astigmatic 3D-STORM imaging[63]). Nikon NIS-Elements AR software with the N-STORM module was used to control the imaging process. A 300-mW laser (VFL-P-300-647, MPB Communications) fiber-coupled to the laser board of the microscope setup was used for STORM imaging. The field of view was selected using the live EMCCD image with a 488-nm illumination, and VIAAT-positive axon terminals impinging on TH-positive cell bodies and dendrites were selected. A three-channel confocal stack (512 × 512 × 15 pixels, 78 × 78 × 150 nm resolution) was then collected using 488-nm, 561-nm and 647-nm excitations. After brief bleaching, direct STORM imaging was performed with 10,000 cycles of 30 ms of exposure, with continuous low-power activator laser (405 nm) and maximal power reporter laser (647 nm) using a STORM filter cube (Nikon) and the EMCCD camera.

Correlated confocal and STORM image processing. Confocal image stacks were deconvolved with 100 iterations of the classic maximum likelihood estimation algorithm in Huygens software (SVI). STORM image processing was performed using the N-STORM module of the NIS-Elements AR. The peak detection threshold was set to 1,000 gray levels. Correlated confocal and STORM image analysis was performed using the software VividSTORM[61]. The data from the two imaging modalities were manually aligned based on the correlated STORM and confocal channels. One axon terminal was selected per image from the center of the field of view. The borders of the axon terminals and the outline of the active zones (for CB1 STORM and bassoon STORM, respectively) were delineated using the Morphological Active Contour Without Edges (MACWE) algorithm[61] with the appropriate confocal channels. STORM localization points (LPs) belonging to the ROI were stored and counted and were normalized to the overall density of LPs per image. The size of the active zone was determined from the active contour ROIs, and the density of bassoon staining in the active zone was calculated by dividing the bassoon number of LPs and the active zone size. The size of the axon terminals was also determined with the MACWE method using the VIAAT confocal channel, and the sum intensity of the VIAAT confocal staining was calculated in the ROIs to estimate transporter levels. Figures were prepared using Photoshop CS5 (Adobe Systems). All images were modified in the same way for all treatment groups during preparation of the figures to ensure equal comparison.

Statistical analyses. No statistical methods were used to predetermine the number of animals and cells required. Sample sizes were estimated based on previous experience and are similar to those reported in previous publications[37,64,65] and generally employed in the field. The animals were randomly assigned to each group for the prenatal pharmacological treatment or behavioral tests. Statistical analyses were conducted using GraphPad Prism 6. Statistical outliers were identified using Grubb's test ($\alpha = 0.05$) and excluded from analyses. Datasets were tested for normality using the Kolmogorov–Smirnov test, and differences between animals within a treatment group were calculated using the Kruskal–Wallis test to determine the appropriate statistical method. For STORM imaging, the mean values of each animals were used in the statistical analyses, differences between the groups were determined using Mann–Whitney *U*-tests. Data always met the assumptions of the applied statistical probes. Electrophysiological data were analyzed using two-way ANOVA for repeated measures (treatment × time) or one-way ANOVA or Student's *t*-test when appropriate, followed by Sidak's, Dunnett's or Bonferroni's post hoc test. Behavioral parameters were analyzed using one-way or multiway ANOVAs followed by Tukey's or Fisher's least significant difference test for post hoc comparisons. Correlation analyses were conducted using Pearson correlation coefficients. The significance threshold was set at 0.05. Data collection and analyses were performed blinded to the conditions of the experiments.

Reporting Summary. Further information on research design is available in the Nature Research Reporting Summary linked to this article.

Data availability

The datasets generated and analyzed during the current study are available from the corresponding author upon reasonable request.

References

51. Capone, F., Bonsignore, L. T. & Cirulli, F. Methods in the analysis of maternal behavior in the rodent. *Curr. Protoc. Toxicol.* **Chapter 13**, Unit13.19 (2005).
52. Frau, R. et al. Sleep deprivation disrupts prepulse inhibition of the startle reflex: reversal by antipsychotic drugs. *Int. J. Neuropsychopharmacol.* **11**, 947–955 (2008).
53. Godar, S. C. et al. Maladaptive defensive behaviours in monoamine oxidase A-deficient mice. *Int. J. Neuropsychopharmacol.* **14**, 1195–1207 (2011).
54. Frau, R. et al. The neurosteroidogenic enzyme 5α-reductase mediates psychotic-like complications of sleep deprivation. *Neuropsychopharmacology* **42**, 2196–2205 (2017).
55. Bortolato, M., Godar, S. C., Davarian, S., Chen, K. & Shih, J. C. Behavioral disinhibition and reduced anxiety-like behaviors in monoamine oxidase B-deficient mice. *Neuropsychopharmacology* **34**, 2746–2757 (2009).

56. Paxinos, G. & Watson, C. *The Rat Brain in Stereotaxic Coordinates* (Academic, 2007).
57. Devoto, P., Flore, G., Longu, G., Pira, L. & Gessa, G. L. Origin of extracellular dopamine from dopamine and noradrenaline neurons in the medial prefrontal and occipital cortex. *Synapse* **50**, 200–205 (2003).
58. Melis, M., Camarini, R., Ungless, M. A. & Bonci, A. Long-lasting potentiation of GABAergic synapses in dopamine neurons after a single in vivo ethanol exposure. *J. Neurosci.* **22**, 2074–2082 (2002).
59. Johnson, S.W. & North, R. A. Two types of neurone in the rat ventral tegmental area and their synaptic inputs. *J. Physiol.* **450**, 455–468 (1992).
60. Ungless, M. A., Whistler, J. L., Malenka, R. C. & Bonci, A. Single cocaine exposure in vivo induces long-term potentiation in dopamine neurons. *Nature* **411**, 583–587 (2001).
61. Barna, L. et al. Correlated confocal and super-resolution imaging by VividSTORM. *Nat. Protoc.* **11**, 163–183 (2016).
62. Dani, A., Huang, B., Bergan, J., Dulac, C. & Zhuang, X. Superresolution imaging of chemical synapses in the brain. *Neuron* **68**, 843–856 (2010).
63. Huang, B., Jones, S. A., Brandenburg, B. & Zhuang, X. Whole-cell 3D STORM reveals interactions between cellular structures with nanometer-scale resolution. *Nat. Methods* **5**, 1047–1052 (2008).
64. Dudok, B. et al. Cell-specific STORM super-resolution imaging reveals nanoscale organization of cannabinoid signaling. *Nat. Neurosci.* **18**, 75–86 (2015).
65. Melis, M. et al. PPARα regulates cholinergic-driven activity of midbrain dopamine neurons via a novel mechanism involving α7 nicotinic acetylcholine receptors. *J. Neurosci.* **33**, 6203–6211 (2013).